REFERENCE ONLY

UNIVERSITY OF LONDON THESIS

Degree PhD Year 2005 Name of Author EAST E-C

COPYRIGHT

This is a thesis accepted for a Higher Degree of the University of London. It is an unpublished typescript and the copyright is held by the author. All persons consulting the thesis must read and abide by the Copyright Declaration below.

COPYRIGHT DECLARATION

I recognise that the copyright of the above-described thesis rests with the author and that no quotation from it or information derived from it may be published without the prior written consent of the author.

LOANS

Theses may not be lent to individuals, but the Senate House Library may lend a copy to approved libraries within the United Kingdom, for consultation solely on the premises of those libraries. Application should be made to: Inter-Library Loans, Senate House Library, Senate House, Malet Street, London WC1E 7HU.

REPRODUCTION

University of London theses may not be reproduced without explicit written permission from the Senate House Library. Enquiries should be addressed to the Theses Section of the Library. Regulations concerning reproduction vary according to the date of acceptance of the thesis and are listed below as guidelines.

A. Before 1962. Permission granted only upon the prior written consent of the author. (The Senate House Library will provide addresses where possible).

B. 1962 - 1974. In many cases the author has agreed to permit copying upon completion of a Copyright Declaration.

C. 1975 - 1988. Most theses may be copied upon completion of a Copyright Declaration.

D. 1989 onwards. Most theses may be copied.

This thesis comes within category D.

☑ This copy has been deposited in the Library of UCL

☐ This copy has been deposited in the Senate House Library, Senate House, Malet Street, London WC1E 7HU.

The Role of the Fibrinolytic System in Experimental Allergic Encephalomyelitis.

A thesis submitted for the degree of Doctor of Philosophy.

By

Emma East

Department of Neuroinflammation

Institute of Neurology

University College London

ProQuest LLC
789 East Eisenhower Parkway
P.O. Box 1346
Ann Arbor, MI 48106-1346

Abstract

The immunopathology of multiple sclerosis (MS), a disease of the central nervous system (CNS), is characterised by widespread inflammation, focal demyelination and axonal degeneration. As a result of early disturbances in the blood brain barrier (BBB), serum proteins, including fibrin(ogen) enter into the CNS. Up-regulation of components of the plasminogen activator (fibrinolytic) system correlates with onset of inflammation and migration of leucocytes into the brain parenchyma.

Significant upregulation of plasminogen and plasminogen activator inhibitor-1 (PAI-1), and an accumulation of fibrin D-dimer was found during neuroinflammation, in the established mouse model of MS, chronic relapsing experimental allergic encephalomyelitis (CREAE) induced with spinal cord homogenate (SCH). Onset and progression of disease correlated with a reduction in dendritic markers, supporting evidence of early neuronal/axonal dysfunction. Furthermore an impairment of fibrinolysis in these mice ensured that fibrin entering the CNS was not effectively removed, suggesting a role for the PA system in the pathogenesis of CREAE.

Initially, using mice deficient in tissue-type plasminogen activator ($tPA^{-/-}$) and myelin oligodendrocyte glycoprotein (MOG)-induced EAE, animals displayed an early and a more severe acute disease characterised by incomplete recovery when compared to wild-type controls, with significantly higher CNS levels of PAI-1. This correlated with fibrin accumulation, which co-localised with non-phosphorylated neurofilament on thickened axons in EAE tissue. In contrast, urokinase plasminogen activator receptor knockout mice ($uPAR^{-/-}$) had a delayed, less acute disease reflected in delayed infiltration of inflammatory cells. However, these animals developed chronic disease as a result of steadily increasing inflammation, high levels of urokinase-type plasminogen activator (uPA) and greater degree of demyelination. Due to low rates of EAE susceptibility, mice deficient for PAI-1 were backcrossed onto the ABH strain for 4

generations. Induction of SCH-CREAE in PAI-$1^{-/-}$ mice resulted in a lower incidence of disease, with mice developing clinical signs of EAE significantly later than WT littermates. A delay in cellular entry into the CNS accompanied by a higher capacity for fibrinolysis resulted in a milder disease in PAI-$1^{-/-}$ mice with no clinical relapses and less axonal damage.

Thus, the plasminogen activator system can modulate both inflammatory and degenerative events in the CNS through the respective effects of tPA, PAI-1 and uPAR on fibrinolysis and cell adhesion/migration, manipulation of which may be of therapeutic importance in multiple sclerosis.

CONTENTS

List of Figures

List of Tables

Abbreviations

ABC	Avidin-biotinylated enzyme complex
ABH	Biozzi antibody high
AD	Alzheimer's disease
AIC	Adjuvant injected controls
AMPA	alpha-amino-3-hydroxy-5-methyl-4-isoxazolepropionic acid
APC	Antigen presenting cell
APP	Amyloid precursor protein
BBB	Blood brain barrier
BM	Basement membrane
BSA	Bovine serum albumin
Ca^{2+}	Calcium ion
CNS	Central nervous system
CREAE	Chronic relapsing EAE
CSF	Cerebrospinal fluid
DAB	Diaminobenzadine tetrahydrochloride
DEPC	Diethylpyrocarbonate
DNA	Deoxyribonuleic acid
dNTP	Deoxyribonucleoside triphosphate
DPI	Days post EAE induction
EAE	Experimental allergic encephalomyelitis
EC	Endothelial cell
ECM	Extracellular matrix
EGF	Epidermal growth factor
ELISA	Enzyme-linked immunosorbant assay
FITC	Fluorescein isothiocyanate
GAP	Growth associated protein
GM	Grey matter
h	Hour(s)
HLA	Human leukocyte antigen
HRP	Horseradish peroxidase
ICAM	Intracellular adhesion molecule
Ig	Immunoglobulin
iNOS	Inducible nitric oxide synthase

IL	Interleukin
K^+	Potassium ion
kDa	Kilo Daltons (molecular weight)
KSP	Lysine-serine-proline
LDL	Low density lipoprotein
LRP	Low density lipoprotein receptor-related protein
LFA-1	Leucocye function-associated antigen 1
mAb	Monoclonal antibody
MAP	Microtubule associated protein
MBP	Myelin basic protein
MCAO	Middle cerebral artery occlusion
MHC	Major histocompatibility complex
min	minute(s)
MMP	Matrix metalloproteinases
MOG	Myelin oligodendrocyte glycoprotein
MOG-EAE	EAE induced with MOG peptide
MRI	Magnetic resonance imaging
mRNA	Messenger ribonucleic acid
MS	Multiple sclerosis
Na^+	Sodium ion
NAWM	Normal-appearing white matter
NF	Neurofilament
NfH	Neurofilament heavy
NfL	Neurofilament light
NfM	Neurofilament medium
NMDA	N-methyl D-aspartate
NO	Nitric oxide
OD	Optical density
PAI	Plasminogen activator inhibitor
PBS	Phosphate-buffered saline
PCR	Polymerase chain reaction
PLP	Proteolipid protein
PNS	Peripheral nervous system
PP	Primary progressive
PSD	Postsynaptic density

RR	Relapsing remitting
RT	Room temperature
SCH	Spinal cord homogenate
SDS	Sodium dodecyl sulphate
sec	seconds
SP	Secondary progressive
Taq	*Thermus aquaticus*
TBE	Tris boric acid-EDTA
TCR	T-cell receptor
TGF-β	Transforming growth factor beta
TJ	Tight junction
TMB	Tetramethlybenzidine
TMEV	Theiler's murine encephalomyelitis viruses
TNF-α	Tumour necrosis factor alpha
TRITC	Tetramethylrhodamine isothiocyanate
tPA	Tissue Plasminogen Activator
Tris	Tris (hydroxymethyl) aminomethane
TTBS	Tween 20 – Tris buffered saline
uPA	Urokinase Plasminogen Activator
uPAR	Urokinase Plasminogen Activator Receptor
VCAM	Vascular cell adhesion molecule
VLA-4	Very late antigen 4
VN	Vitronectin
v/v	Volume per volume
WM	White matter
WT	Wildtype
w/v	Weight per volume

Acknowledgements

I would like to thank my supervisors Dr. Djordje Gveric and Professor David Baker for their support and guidance throughout my PhD. A special thanks also to Professor Louise Cuzner who despite her retirement never faltered in her help, advice and interest in my work. I am indebted to my collegues in the lab for providing humour and motivation throughout my time in the department.

I would like to acknowledge my collaborators Dr Arie Reijerkerk and Professor Roger Lijnen, who gave me the opportunity to work in his laboratory in Leuven, Belgium, for their enthusiasm and help with this project.

Finally I would like to thank AIMS2Cure for their generous funding this project.

This thesis is dedicated to Richard and my family.

1. Introduction.

1.1. Thesis introduction.

Serine proteases have a central role in the pathogenesis of multiple sclerosis (MS), both in the neuroinflammatory process and in demyelination. As a result of disturbances in the blood-brain barrier (BBB), serum proteins such as fibrin, together with leucocytes, enter the central nervous system (CNS) with resultant upregulation of the plasminogen activator (PA) cascade as one of the earliest pathological signs. Concentrations of free active tissue plasminogen activator (tPA), the key fibrinolytic enzyme, associated with a significant increase in its inhibitor PAI-1, ensure that fibrin entering the CNS is not efficiently removed. The proteolytic activity of urokinase PA (uPA), dependent on binding with its receptor uPAR, is involved in the migration and adhesion of inflammatory cells. Further investigation into the role and effects of the plasminogen activator system during inflammatory demyelination could lead to the development of more effective therapies, the need for which is great in patients with MS.

1.2. Multiple Sclerosis; an overview.

MS is thought to be an autoimmune disease of the CNS characterised by widespread inflammation, focal demyelination and a varying degree of axonal loss (Conlon *et al.,* 1999). MS affects approximately 2.5 million people world wide, in countries of Caucasian prevalence. The disease onset usually occurs in young adulthood, ages 29-33, affecting twice as many women as men (Steinman, 1996). In the majority of cases, MS begins with a relapsing-remitting (RR) course. The time between the relapses can vary greatly however most patients will go on to develop a secondary progressive (SP) phase where the number of relapses decreases but a persistent accumulation of neurological deficits over time leads to an increase in disability (Bjartmar and Trapp, 2001). In approximately 10% of patients, MS begins with a

primary progressive (PP) phase (Zamvil and Steinman, 2003) which, like SPMS, is characterised by less inflammation but acute neurodegeneration. Much research has been carried out into the genetics, immunology and neurobiology of MS in an attempt to uncover the mechanisms that underlie the disease cause, susceptibility, onset and progression.

1.2.1. Genetics and epidemiology.

There is a genetic association with MS as the concordance rate for disease among genetically identical twins is approximately 25% (Conlon *et al.,* 1999). This observation prompted a large number of linkage studies to identify disease associated alleles (GAMES and Transatlantic Multiple Sclerosis Genetics Cooperative, 2003; Kellar-Wood *et al.,* 1995). To date there is one key region of the genome that has been consistently shown to contain a gene conferring susceptibility to MS. This is the region of the major histocompatibility complex (MHC) located on chromosome 6, which contains the human leucocyte antigen (HLA) genes (Compston *et al.,* 1998). The MHC gene products are involved in the processing and presentation of antigenic peptides to T-cells. However genetics are not solely responsible for the development of MS (Willer *et al.,* 2003). Environmental factors are also proposed to play a role as MS affects people predominantly in geographically restricted areas such as the northern hemisphere and it is a disease particularly of the western world. Studies have revealed that migration from a high risk to a low risk area before adolescence can reduce the risk of developing MS (Gale and Martyn, 1995). Although the cause of MS is still unknown, it is likely to be a number of factors, both genetic and environmental, which when combined act synergistically towards the manifestations and progression of MS (Hemmer *et al.,* 2002).

1.2.2. Diagnosis of MS.

The symptoms of MS are notoriously variable but in general reflect the involvement of those parts of the CNS that are demyelinated (Compston *et al.*, 1998). The most common presenting symptoms include weakness of one or more limbs, optic neuritis, paraesthesiae, diplopia, vertigo and disturbance of micturition (Compston and Coles, 2002). There are many additional symptoms of MS that have been documented; however problems arise with diagnosis due to the overlapping nature of many of these signs with other primary, neurological and systemic autoimmune diseases. The disease usually manifests itself in either two or more episodes each lasting more than 24h and at least one month apart or as a stepwise progression over a minimum of six months (Compston *et al.*, 1998). Oligoclonal immunoglobulin G bands in the CSF are found in >95% of patients with clinically definite MS (Andersson *et al.*, 1994) and the absence of these bands in a patient with suspected MS should lead to a careful reassessment of the diagnosis (Compston and Coles, 2002). The introduction of magnetic resonance imaging (MRI) in the 1980's (Young *et al.*, 1981) has greatly improved the diagnosis of MS. MRI is a highly sensitive technique which can detect changes in the white matter with respect to the identification of the development of lesions in space and time. However MRI also aids detection of CNS abnormalities and changes associated with many other disorders, many of which have similarities with the MRI of MS patients. Thus MRI can be used as a tool to confirm the diagnosis of MS, which is supported by other clinical and laboratory investigations. Once a diagnosis is confirmed, a decision is made on how to manage and possibly treat the MS patient.

1.2.3. Pathology of MS.

Early studies on the macroscopic pathology of MS were carried out by Carswell and Cruveilhier in the mid 19th century (Compston *et al.*, 1998), however Jean Martin

Charcot, in the late 19th century, gathered together many clinical and pathological observations and identified the destruction of myelin sheaths as the key pathological feature of MS (Compston *et al.,* 1998). Today the pathology of MS is well documented. On a macroscopic level, plaques or lesions are seen in the white matter of the brain and spinal cord of MS patients. These lesions tend to occur around blood vessels and correspond to areas of focal myelin destruction or demyelination (Conlon *et al.,* 1999). Microscopically there is complete loss of the myelin sheaths surrounding axons in the lesion and infiltration of inflammatory lymphocytes and macrophages (Adams, 1989). Characteristic of demyelinating lesions is the presence of macrophages and activated microglial containing lipid filled vesicles of myelin debris followed by the development of a dense astrocytic scar (Adams, 1989); lesions are sharply demarcated with evident inflammation and relative axonal preservation. Also observed are shadow plaques, areas of previously demyelinated white matter which are spontaneously partially remyelinated by oligodendrocytes, the specialised myelinating cells of the CNS (Compston *et al.,* 1998). However with PP or SPMS, inflammation becomes less evident and axonal degeneration more apparent (Lassmann, 1998). There is a great deal of heterogeneity of multiple sclerosis lesions, suggesting that MS may be a disease with heterogeneous pathogenetic mechanisms. A detailed pathological study of MS lesions by Lucchinetti *et al.,* (2000) assessed extent of demyelination, plaque geography and extension, oligodendrocyte destruction and evidence of complement activation and found that most lesions can be categorised into two large groups. One in which lesions are of a typical nature, with a high number of inflammatory cells including macrophages and microglia (Li *et al.,* 1993), and the other in which lesions have features of primary oligodendrocyte loss rather than of autoimmunity. Furthermore, recent findings of widespread oligodendrocyte apoptosis in the absence of a clear cellular immune response (Barnett and Prineas, 2004) suggest a mechanism of pathogenesis that has not

yet been fully explored. Oligodendrocyte apoptosis as a result of a viral infection or excitotoxicity could contribute to the inflammatory response in MS.

1.2.4. Current treatment of MS.

Although the pathogenesis of MS is not yet fully understood, the evidence that immunological mechanisms are involved has prompted the development of immunological therapies acting on the inflammatory stages of disease. Drug treatments which alter the duration and frequency of relapse in MS include oral and intravenous (i.v.) steroids, Interferon beta (IFN-β), Glatiramer acetate and mitoxantrone (Compston and Coles, 2002). These therapies are more beneficial in patients with relapsing remitting MS rather than in progressive MS as they act on the inflammatory elements of disease. The therapeutic mechanism of IFN-β is unknown (Arnason *et al.,* 1997). It has an anti-inflammatory action, reduces evidence of BBB dysfunction and is thought to act by restoring suppressor T cell functioning and also by inhibiting the release of the pro-inflammatory cytokines; lymphotoxin, TNF and IFN-γ, which are all cytotoxic to oligodendrocytes (Arnason *et al.,* 1997). Glatiramer acetate, a synthetic mixture of four amino acid copolymers ranging from 40 to 90 amino acids in length, was originally synthesised to evoke a model of MS in animals, as it resembles the structure of myelin basic protein (Dhib-Jalbut, 2003). However it was actually found to have anti-inflammatory properties and in addition to actions on the immune system, Glatiramer acetate is also neuroprotective (Gilgun-Sherki *et al.,* 2003a). Mitoxantrone suppresses T and B cell immunity by intercalating with DNA and inhibiting DNA and RNA synthesis, thus preventing cell replication and inducing immunosuppression (Compston *et al.,* 1998). More recently two humanised antibodies, Natalizumab and Campath-1H, which target the antigens α_4 integrins and CD52 respectively, have been in clinical trials for the treatment of MS. These surface antigens have a central role in lymphocyte

adhesion and migration into the CNS, and in MS patients both antibodies reduce relapses and formation of new lesions (Coles *et al.,* 2005; Miller *et al.,* 2003). However, natalizumab has now been withdrawn after three cases of progressive multifocal leukoencephalopathy in MS patients taking the drug (Engelhardt and Ransohoff, 2005). Additionally, campath-1H causes prolonged immunosupression, and in patients with SPMS failed to prevent sustained accumulation of disability attributable to ongoing axonal loss (Coles *et al.,* 2005).

No existing therapy is ideal and although all these drugs have some beneficial actions, there are still a large number of MS patients who don't respond to these treatments and/or whose disease is too advanced. Furthermore, despite inhibition of new MRI lesion formation and inhibition of relapses, secondary progressive disease continues. With the increasing recognition of MS as a neurodegenerative disorder future therapies are likely to focus on neuroprotection in addition to anti-inflammatory strategies.

1.3. Myelin and autoimmunity.

Although the autoimmune nature of MS has not yet been proven, the importance of immunopathological events is extensively documented (Hemmer *et al.,* 2002; Lassmann, 1998; Neumann *et al.,* 2002). The presence of blood-derived myelin specific T cells, and B cells that secrete antibodies to myelin components in MS lesions (Martino *et al.,* 2002), may contribute to the autoimmune hypothesis, although these are also found in normal individuals (Steinman, 1996). Although the primary event leading to the manifestation of MS is still unknown, a pro-inflammatory environment leads to an antigen driven immune response whereby CNS antigens are released (Hemmer *et al.,* 2002). The main candidate CNS autoantigens are thought to be myelin proteins (Zamvil and Steinman, 2003). The myelin sheath is a lipid rich multilamellar

membrane, which both insulates and enhances conduction in nerve axons (Cuzner and Norton, 1996). It is synthesised by specialised myelinating glial cells called oligodendrocytes. Myelin is composed of many proteins, the main ones proteolipid protein (PLP) and myelin basic protein (MBP), and smaller proteins including myelin oligodendrocyte glycoprotein (MOG), are highly susceptible to proteolytic activity and are exceptionally encephalitogenic (Cuzner and Norton, 1996). T-lymphocytes with receptors for CNS myelin components recognise their antigen presented by the MHC on antigen presenting cells, notably dendritic cells, and enter tissues, including the brain in search of their target antigen. Additionally, in the complete collection of proteins extracted from MS-affected myelin, there was one protein that appeared to be a dominant antigen for $CD4^+$ T cells, which was a small heat-shock protein, called αB-crystallin (van Noort *et al.,* 1995). αB-crystallin is present at enhanced levels in the cytosol of oligodendrocytes and astrocytes in MS lesions, and increased expression is closely correlate with immunological activity of the lesion (Bajramovic *et al.,* 1997). Thus αB-crystallin is a potential autoantigen in MS.

Entry of T cells into the brain is an active process requiring the breakdown of BBB components, the surrounding extracellular matrix (ECM) (Owens, 2003) and endothelial cell remodelling (Etienne-Manneville *et al.,* 2000). On re-encountering their antigen, T-cells can activate and undergo further clonal expansion thus targeting local cells and triggering an inflammatory cascade (Compston *et al.,* 1998). One hypothesis states that MS is a disease which is initially targeted against one myelin antigen (Lehmann *et al.,* 1992). T cells specific for the antigen are activated upon recognition of the antigenic peptides presented on MHC class II and release cytokines to recruit non-specific circulating lymphocytes, microglia and astrocytes. As the disease progresses and demyelination occurs, new myelin epitopes are thought to appear, which recruit more T cells, leading to an exacerbation of inflammation (Figure 1.1). This is

known as the Epitope spread theory by which "diversification of epitope specificity from the initial focused, dominant epitope-specific immune response spreads to subdominant (cryptic) epitopes on that protein" (Vanderlugt and Miller, 2002). Another hypothesis describing possible mechanisms of the pathogenesis of MS is the molecular mimicry theory. This postulates that there is an infectious aspect involved which triggers the autoimmune response leading to MS. This is based on structural similarities in protein sequence between infectious pathogens and self-antigens (Conlon *et al.*, 1999).

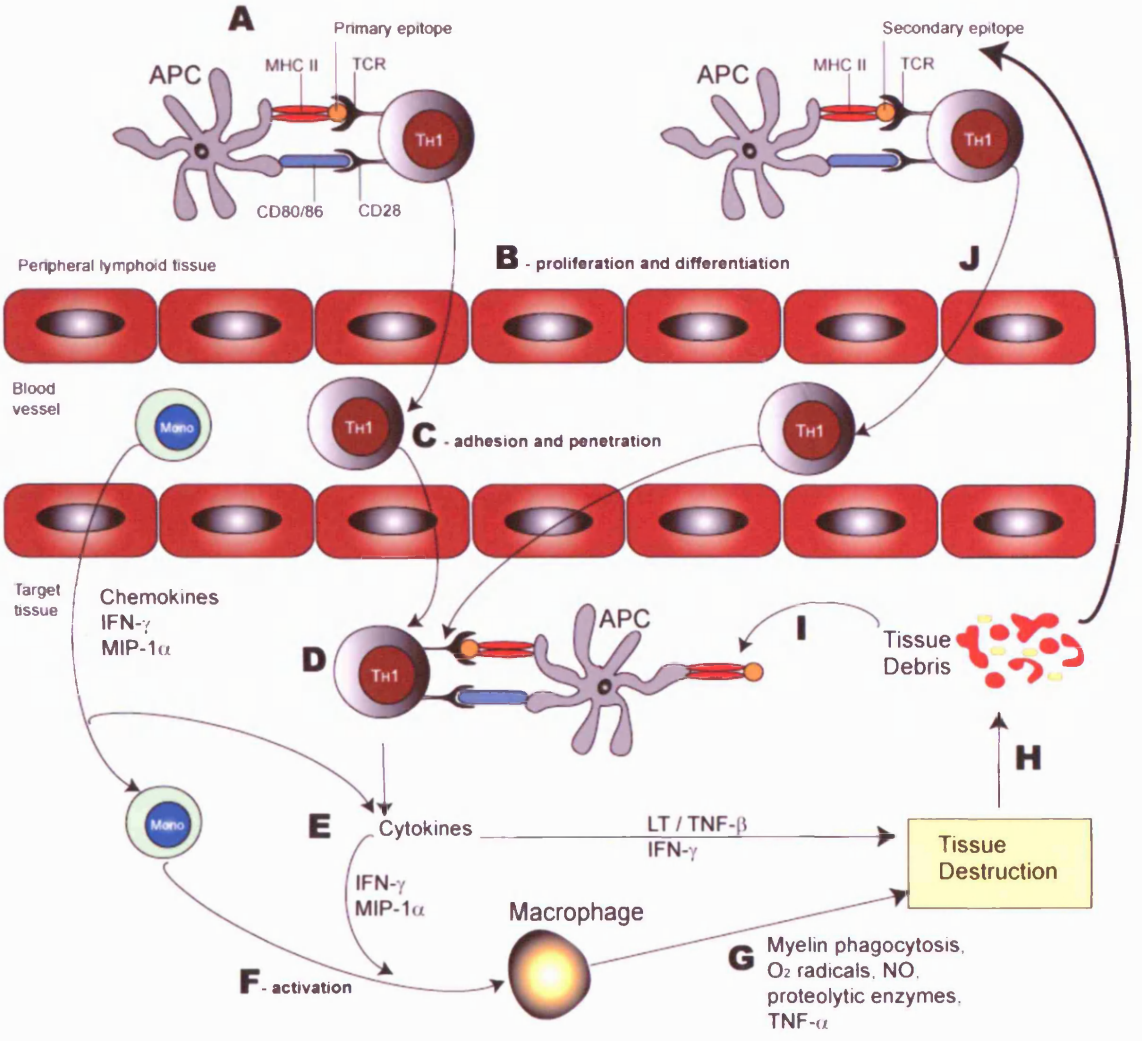

Figure 1.1. *Onset of neuroinflammation and the epitope spread hypothesis.* **A** Presentation of the primary epitope by the MHC class II on antigen presenting cells (APC) in the peripheral lymphoid tissue (self antigen, or viral/bacterial antigen mimicking self). **B** Upon presentation to a T-cell with the correct T-cell receptor (TCR), these Th1 autoreactive T cells undergo activation and differentiation and enter the vasculature to circulate through the tissues. **C** Entry into the target tissue, in this case the CNS, requires adhesion and migration through the BBB endothelium. **D** Upon re-encountering the antigen presented on resident APC, T-cells release a host of cytokines and chemokines, **E**, which leads to further recruitment of additional mononuclear phagocytes and T-cells from the periphery. **F** Locally produced cytokines are capable of activating macrophages and microglia leading to, **G**, myelin phagocytosis and the release of cytotoxic substances. **H** Resulting tissue debris is, **I**, processed and presented on peripheral and resident APCs, leading to activation and differentiation of a second wave of Th1 cells, **J**, which can re-enter the CNS and cause additional tissue destruction. Adapted from Vanderlugt and Miller, (2002).

1.4. Animal models of MS.

A number of animal models have been developed, which over the years have aided understanding of neuroimmunology and allowed investigation into the pathogenesis of inflammatory demyelination, in addition to providing models for preclinical analysis of new drug compounds. It is important to note that no existing model exactly mimics all the features of MS, but that each model represents specific features of inflammation and/or demyelination, which aid in the attempt to investigate the underlying mechanisms involved in the onset and progression of the disease. These models are grouped into three main categories according to their aetiology and include; immune-mediated, viral-induced and toxic demyelinative disorders (Glabinski *et al.,* 1997). There are a number of viruses that can induce demyelinating syndromes in mammals, the most commonly studied are Theiler's murine encephalomyelitis viruses (TMEV) and Semliki forest virus (SFV), which can induce demyelination and encephalitis in susceptible mouse strains (Fazakerley, 2004; Lipton and Dal Canto, 1979). TMEV are single stranded RNA picornaviruses and are natural mouse pathogens. There are two main groups of TMEV viruses characterised by the degree of CNS infection in which they cause (Dal Canto *et al.,* 1996). One group produces a fatal encephalomyelitis whilst the other produces a chronic persistent infection, which is more reminiscent of MS, thus virus strains from the second group are more commonly used in experimental demyelination. Onset of disease occurs typically 4 weeks after infection and clinical signs include waddling gait, spasm and incontinence and upon histological analysis, perivascular inflammatory cell infiltrates and primary demyelination are evident in the spinal cord (Lehrich *et al.,* 1976). SFV inoculation in mice leads to infection of neurons and oligodendrcotyes, with resulting variable mild – fatal encephalitis, with a predominantly $CD8^+$ T-cell response (Fazakerley, 2004). In both TMEV and SFV, viral-induced demyelination seems to be immune-mediated. The

disease course and susceptibility depends on the ability of the mouse to mount a delayed-type hypersensitivity response to the viral antigens. The method of toxic demyelination is particularly useful when investigating a precise area of the CNS and requires a focal area or lesion of demyelination to study. It can be induced by intracerebral or intraspinal injection of lysolecithin or ethidium bromide and by dietary administration of cuprizone (Blakemore, 1973; Blakemore, 1978; Blakemore, 1982). Mechanisms of demyelination are due to toxic effects on oligodendrocytes and are not related to inflammatory attack, although there is macrophage recruitment which remove myelin debris. This model can provide a useful method for studying the mechanisms involved in the process of remyelination (Woodruff and Franklin, 1999).

1.4.1 Experimental Allergic Encephalomyelitis.

EAE is the most commonly used immune-mediated model and is also the leading model of MS. It was first developed at the end of the 19th century after complications were observed with the rabies vaccination in man (Compston *et al.*, 1998). The inactivated virus was cultured in rabbit CNS tissue and inoculation occasionally and unpredictably resulted in fever, paralysis, and even death. Post-mortem tissue of these patients showed perivenular demyelination and acute inflammation reminiscent of MS (Compston *et al.*, 1998). This lead to the conclusion that autoimmunity targeted against nervous tissue elements can induce brain inflammation. Rivers *et al.*, (1933) formally proved this theory by immunising monkeys with brain tissue to induce inflammatory demyelination. EAE can be induced in virtually all mammalian species, including man; the most commonly used include mice, rats, guinea pigs and primates. Active induction of EAE involves immunisation with nervous tissue from an animal of the same or different species. Spinal cord is usually employed for disease induction as it is more encephalitogenic, as it contains

more myelin than brain tissue, mixed with Freund's adjuvant and injected subcutaneously (Mullay-Eberhard and Miescher, 1976). Injection in this way ensures that encephalitogenic antigen plus adjuvant are delivered to draining lymph nodes to initiate an immune response. Freund's adjuvant, which contains killed mycobacterium, paraffin oil and emulsifier is important for manifestation of EAE (Lee and Schneider, 1962). In addition to killed *Mycobacterium tuberculosis*, other bacteria, for example *Bordetella pertussis* vaccine, can be substituted or given in addition to the other adjuvants (Goverman *et al.,* 1993). *B. pertussis* has a potentiating effect on EAE possibly by increasing BBB permeability to cell trafficking, enhancing the production of cytokines by T cells and by induction of lymphocytosis (Hofstetter *et al.,* 2002). EAE onset usually occurs 10-20 days after injection in rodents, and clinical signs include tail paralysis, ataxic gait and paresis or paralysis of hind limbs (Mullay-Eberhard and Miescher, 1976). Histopathologically there are many similarities with MS. EAE is characterised by BBB breakdown/damage, subsequent entry of plasma proteins, namely fibrinogen, followed by infiltration of inflammatory mononuclear cells. There are varying degrees of demyelination and axonal damage depending on the particular model used but the presence of macrophages and activated microglia are common of most forms of EAE (Kornek *et al.,* 2000). The type and dose of encephalitogenic antigen, type of adjuvant, route of sensitisation, and species and strain of animal all influence the onset and course of disease in EAE (Mullay-Eberhard and Miescher, 1976). Studies with various inbred and outbred strains of rodents showed that the susceptibility to EAE varied greatly (Levine and Sowinski, 1973). Through extensive backcrossing experiments it became clear that resistance or susceptibility to myelin protein induced EAE in inbred rodent strains of mice, rats and guinea pigs was primarily associated with their MHC-class II antigen haplotypes (Fritz and McFarlin, 1989). This can account for the differences in disease course observed with different

strains and species, for example immunisation of the Lewis rat with MBP induces a monophasic EAE characterised by acute inflammation but notably little demyelination or axonal damage (Stepaniak *et al.,* 1995). After injection of spinal cord into the DA rat, they develop a relapsing remitting disease which is more reminiscent of MS with evident axonal pathology and demyelination (Lorentzen *et al.,* 1995). In addition chronic relapsing EAE (CREAE) can be induced in strain 13 guinea pigs and in susceptible mouse strains such as SJL and ABH (Baker *et al.,* 1990; Fallis *et al.,* 1989). However, the differences in clinical course observed are not solely due to differences in genetics. Chronic disease in mouse EAE, characterised by axonal loss, is associated with $CD8^+$ MOG specific T cell activation (Sun *et al.,* 2001), described in detail in section 1.5, whereas classic-remitting EAE is mediated by $CD4^+$ T cells (O'Neill *et al.,* 1993). Different strains of mice are susceptible to induction of EAE with different proteins (summarised in Table 1.1) (Levine and Sowinski, 1973). C57BL/6 mice, the strain commonly used for making genetic knockouts, are amongst the most resistant to MBP or whole myelin induced disease, are only susceptible to EAE induced with MOG whilst SJL mice are susceptible to all antigenic peptides (Levine and Sowinski, 1973; Tuohy *et al.,* 1988).

	EAE inducing antigen			
Strain	MBP[1]	PLP[2]	MOG[3]	SCH[4]
C57BL/6	-	-	+	-
BALB/c	-	-	-	-
SJL	+	+	+	+
ABH	-	+	+	+

Table 1.1. *The susceptibility of different mouse strains to actively induced EAE with different antigens.* Myelin basic protein (MBP), proteolipid protein (PLP), myelin oligodendrocyte glycoprotein (MOG) or whole spinal cord homogenate (SCH). [1] (Bernard and Carnegie, 1975), [2] (Tuohy *et al.,* 1988), [3] (Mendel *et al.,* 1995); (Amor *et al.,* 1994), [4] (Raine *et al.,* 1980).

As it is widely accepted that the incidence of MS in females is twice that of males, it is understandably of importance and interest to determine whether the same is true for EAE. While it was thought that sex hormones play a role in the susceptibility of humans to MS (Soldan *et al.,* 2003) and animals to EAE, the mechanisms by which this occurs are poorly understood (Voskuhl *et al.,* 1996). Several reports have shown that female SJL mice are more susceptible to induction of EAE with either MBP (Cua *et al.,* 1995) or PLP (Bebo *et al.,* 1998; Papenfuss *et al.,* 2004). However little work has been carried out on gender differences in MOG-induced EAE. One recent study demonstrated no differences in EAE development between male and female C57BL/6 when the mice were immunised with MOG_{35-55} peptide (Okuda *et al.,* 2002). This highlights that the gender difference influencing susceptibility of mice to EAE depends on the strain of animals used and/or the encephalitogenic substance employed for disease induction (Okuda *et al.,* 2002).

EAE can also be induced by a procedure known as "adoptive transfer" in which activated encephalitogenic T cells, obtained from sensitised animals or propagated *in vitro*, are injected intravenously into immunologically compromised or naïve recipients, with resulting disease that is similar to actively induced EAE (Lafaille *et al.,* 1997). Adoptive transfer in the rat was the first demonstration that EAE was mediated by T cells and that the response was initiated and generated in the lymph nodes (Paterson, 1960). Many people categorise EAE as a delayed, type IV, hypersensitivity reaction. Reactions of this type are mediated by T cells in response to soluble or cell-associated antigens. Injected cells then migrate to the CNS where they initiate an immune response resulting in the recruitment of additional lymphocytes and monocytes from the blood. Monocyte recruitment is an essential step in EAE as disease development is suppressed in animals after elimination of monocytes/macrophages (Brosnan *et al.,* 1981; Huitinga *et al.,* 1990). As with MS, perivascular accumulation of leucocytes is

evident. More recently, aided by molecular biology techniques, transgenic mice which can spontaneously develop autoimmunity in the CNS have been developed. Mice that express a MBP-specific TCR spontaneously develop EAE when kept in a non-sterile animal housing facility (Goverman *et al.,* 1993). Additionally, TCR transgenic mice for $PLP_{139-151}$ also spontaneously develop CNS inflammation, and are also highly susceptible to EAE induction with PLP peptide indicating that these T cells were not tolerised in the thymus (Waldner *et al.,* 2000).

Whilst no single EAE model exactly mimics MS it is important to note that there are models which give a better representation of the underlying pathological mechanisms involved in MS than others. It may be useful to use a MOG-induced or chronic relapsing EAE model in mice when investigating neurodegeneration, in which neurological damage is evident, as opposed to MBP induced acute Lewis rat EAE, which is a monophasic disease with no axonal pathology. However this monophasic EAE may be more suitable to investigate earlier stages of the disease.

1.5. Neuroinflammation and neurodegeneration.

There are varying degrees of axonal loss in MS lesions, correlating to the permanent disability characterising the chronic progressive stage of the disease (Bjartmar *et al.,* 2003; Siva *et al.,* 1999). Damage to CNS axons has important clinical consequences because they are normally unable to regenerate (Neumann, 2003). Focal damage to axons leads to Wallerian degeneration of the distal segment, and possible death of the cell body due to lack of connections with other neurons (Coleman and Perry, 2002). It is increasingly evident that neuronal and axonal damage and degeneration takes place early on in MS (Bjartmar *et al.,* 2003). Studies into axonal pathology in MS have used various markers to assess axonal damage and degeneration. Work by Trapp *et al.,* (1998) using an antibody against nonphosphorylated

neurofilaments (SMI32), found that although rarely detected in normal white matter from control patients, a large increase in SMI32 immunoreactivity was found within areas of demyelination in MS patients. The pattern of staining depended on the activity of the lesion, as in active lesions, axonal swellings and ovoids were found throughout the plagues consistent with axonal transaction. Additionally, antibodies directed to neurofilaments are detected in the CSF of MS patients, which could aid in neurodegeneration through the guidance of macrophages to their targets. Ferguson *et al.,* (1997) studied the immunoreactivity of amyloid precursor protein (APP), a marker for axonal injury, in acute, active chronic and chronic MS lesions. The study revealed that axonal damage was evident in areas coinciding with inflammation and demyelination. Axonal loss appears to remain clinically silent for many years, and irreversible neurological disability develops when a threshold of axonal loss is reached and compensatory CNS resources are exhausted (Bjartmar *et al.,* 2003). In the EAE model of MS axonal degeneration is also an early pathological feature of disease, which increases in severity with relapses (Onuki *et al.,* 2001; Wujek *et al.,* 2002). Ultimately the degree of axonal loss in mice with EAE determines the permanent neurological disability (Wujek *et al.,* 2002). The actual mechanisms of axonal injury are not known, and whether axons degenerate purely in response to demyelination, or together with other factors involved is still the focus of much research (Summarised in Figure 1.2). Axonal injury correlates with the number of macrophages and CD8 positive T-cells but not with the expression of tumour necrosis factor-alpha (TNF-α) or inducible nitric oxide synthase (iNOS), two potential mediators of demyelination (Bitsch *et al.,* 2000). This suggests that axonal damage is closely associated with inflammation and demyelination (Ferguson *et al.,* 1997) but can also occur independently of demyelination.

Due to their unusual shape and high level of metabolic activity, axons are highly vulnerable to toxic inflammatory mediators, oxidative stress and changes in protein turnover (Neumann, 2003). There is evidence to suggest that excitotoxicity may play a role in neuronal and oligodendrocyte damage and degeneration in MS and EAE (Groom *et al.,* 2003; Matute *et al.,* 2001; Smith *et al.,* 2000; Werner *et al.,* 2000; Werner *et al.,* 2001). Macrophages and activated microglia produce glutamate in large quantities (Werner *et al.,* 2001). Furthermore alterations in glutamate transporters on glia (Werner *et al.,* 2000) affects cellular glutamate/glutamine homeostasis leading to overactivation of the glutamate receptors, N-methyl-D-aspartate and alpha-amino-3-hydroxy-5-methyl-4-isoxazolepropionic acid (NMDA, AMPA) and Kainate. This in turn produces an increase in the cell's permeability to calcium. Excessive calcium influx via this route can lead to free radical formation (Traynelis and Lipton, 2001) and ultimately injury and death to axons and oligodendrocytes (Matute *et al.,* 2001). Using magnetic resonance spectroscopy techniques levels of glutamate are found to be significantly higher in acute MS lesions and in NAWM when compared to control subjects (Srinivasan *et al.,* 2005). Antagonists to glutamate receptors NMDA and AMPA/kainate ameliorate EAE disease (Achiron *et al.,* 2000; Bolton and Paul, 1997; Pitt *et al.,* 2000; Smith *et al.,* 2000) with increased oligodendrocyte survival and reduced axonal damage. Furthermore, the NMDA antagonists, MK801 and memantine are capable of modulating the neurological course of EAE disease, and are particularly effective in reducing BBB breakdown (Bolton and Paul, 1997; Paul and Bolton, 2002). Additionally, Riluzole, a glutamate receptor antagonist and sodium channel blocker suppresses inflammation and demyelination in EAE (Gilgun-Sherki *et al.,* 2003b) and appears to slow the progression of CNS atrophy in PPMS (Killestein *et al.,* 2005).

There has also been much interest in the role of nitric oxide (NO) in MS and its contribution to axonal injury and degeneration. In MS lesions, levels of NO are

increased due to upregulation of iNOS by cytokines and production by activated macrophages/microglia and reactive astrocytes (Oleszak *et al.,* 1998). NO alone is capable of causing vasodilation in the cerebral vessels which may aid in the migration of lymphocytes into the CNS by reducing the velocity of the surrounding blood flow (Smith and Lassmann, 2002). As NO is a highly reactive molecule, it readily combines with other molecules to form several related compounds including peroxynitrite ($ONOO^-$). This reactive nitrogen species is potentially capable of exacerbating demyelination through damage of oligodendrocytes (Mitrovic *et al.,* 1996) and contributing to neuronal degeneration by impairment of mitochondrial energy metabolism and depletion of ATP (Bolanos *et al.,* 1995). Axons exposed to NO *in vivo* can undergo persistent conduction block, particularly if they are electrically active during NO exposure, due to axonal degeneration (Smith *et al.,* 2001). Sodium and calcium channel blockers are effective in ameliorating EAE (Bechtold *et al.,* 2004) and preventing NO- mediated axonal degeneration (Kapoor *et al.,* 2003). These effects are thought to be mediated by blocking deleterious accumulations of Na^+ and Ca^{2+} at sites of inflammation as a result of Na^+ / K^+ ATPase failure and reversal of the Na^+ / Ca^{2+} exchanger (Bechtold *et al.,* 2004; Kapoor *et al.,* 2003). It is possible that detrimental accumulation of these ions is due to NO-mediated impairment of mitochondrial ATP generation. Therapies limiting Na^+ and Ca^{2+} entry into axons might have beneficial effects treating axonal injury and degeneration associated with MS.

The presence of cytotoxic lymphocytes with a CD8 positive phenotype in MS lesions has been recently indicated in the pathogenesis of axonal injury. Inflammatory infiltrates into the brains of MS patients include both $CD4^+$ and $CD8^+$ T cells (Steinman, 2001). Much research has focused on the role of $CD4^+$ T cells in MS since the observation that the genetic susceptibility to MS lies within the region encoding for the MHC class II molecules (Haines *et al.,* 1996). The MHC class II molecules are

expressed in the CNS by microglia, and infiltrating macrophages and B cells and are recognised by $CD4^+$ T cells. In contrast, all CNS cells including neurons and oligodendrocytes can express MHC class I molecules (Neumann *et al.*, 2002), which are recognised by $CD8^+$ T cells (Janeway *et al.*, 2001). In MBP and MOG induced EAE there is a consistently higher activation of $CD8^+$ than $CD4^+$ T cells (Huseby *et al.*, 2001; Sun *et al.*, 2001). When these cells were adoptively transferred they induced a much more severe and permanent disease characterised by more progressive and destructive lesions (Sun *et al.*, 2001). In addition, demyelination and inflammation are reduced in MOG induced EAE in $CD8^{-/-}$ mice (Abdul-Majid *et al.*, 2003). The degree of axonal injury correlates with the number of macrophages and $CD8^+$ T-cells (Bitsch *et al.*, 2000). It is therefore a possible theory that $CD8^+$ T cells are contributing to the destruction of axons in MS. Possible mechanisms include release of proteases contained in cytotoxic granules by $CD8^+$ cells and/or activation of the Fas (CD95) receptors both leading to apoptosis of the target cells (Neumann *et al.*, 2002) which could include neurons and oligodendrocytes, thus having an effect on remyelination in addition to neurodegeneration.

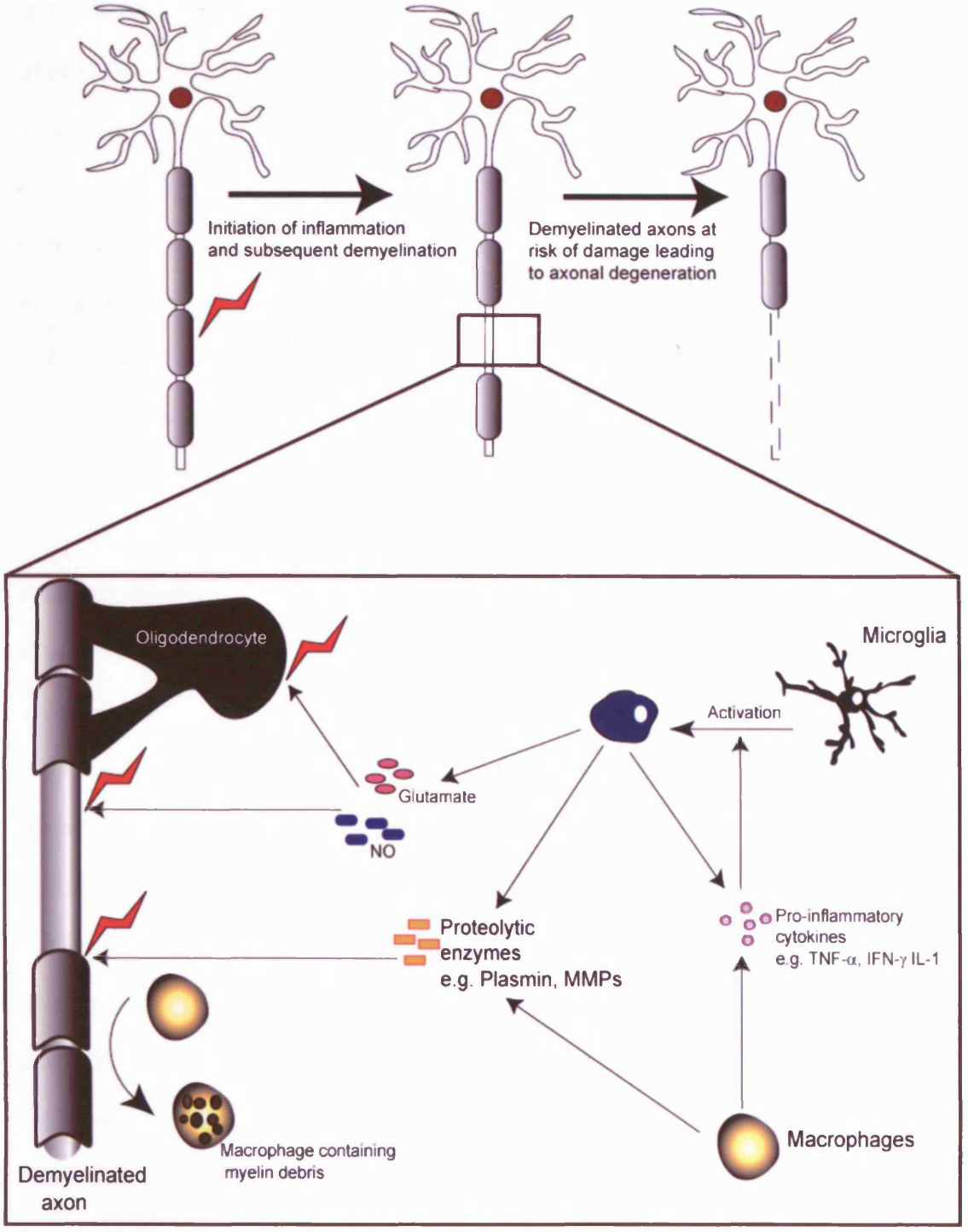

Figure 1.2. *Putative mechanisms of neurodegeneration during neuroinflammation.* T-cells re-encountering their antigen in the CNS activate local cells triggering an inflammatory cascade, releasing cytokines into the parenchyma. Activation of microglia and recruitment of monocytes/macrophages leads to myelin phagocytosis, thus promoting demyelination. Microglia and macrophages are also capable of releasing a number of other potentially cytotoxic substances, and demyelinated axons are particularly at risk from these molecules. Proteolytic enzymes are capable of further degrading the myelin sheath, in addition to causing further microglial activation, and promoting leucocyte migration into the CNS. Furthermore, NO can cause axonal conduction block, and excessive glutamate can potentially cause excitotoxic cell death to oligodendrocytes and neurons.

1.5.1. Neurofilaments.

Neurofilaments are one of the major protein components of the neuronal cytoskeleton. They are classified as intermediate filaments (~10nm in diameter) and are responsible for maintaining the calibre of axons (Al-Chalabi and Miller, 2003). This is important as the speed of conductivity of an impulse down the axon is proportional to its calibre (Miller *et al.,* 2002). As neurofilaments are CNS cell-type specific proteins they can qualify as potential surrogate markers of axonal and neuronal damage (Petzold, 2005). Neurofilaments are heteropolymers and are composed of three subunits termed light (NfL), medium (NfM) and heavy (NfH) chain which are 68, 150 and 200 kDa respectively (Petzold, 2005). Each subunit is composed of a head, rod and a hypervariable C-terminal tail domain. These three subunits form heterodimeric tetramers, combine into protofilaments, eight of which join together, resulting in neurofilament formation (Petzold, 2005). NfL is essential for correct assembly of neurofilaments as each tetramer contains at least two NfL subunits (Al-Chalabi and Miller, 2003). These filamentous structures can run the entire distance of axons which can be over a metre in length. Diversity in NF subunits resides primarily in the length and sequence of the tail domain, with NfH exhibiting the longest (Grant and Pant, 2000). The most distinct feature of this domain is a number of lysine-serine-proline (KSP) repeats which are highly phosphorylated. The function of neurofilaments is intimately related to their phosphorylation state and phosphorylation of the C-terminal tail domain is thought to occur at the side arms protruding from the assembled filaments (Grant and Pant, 2000). The side arm domains of NfM and NfH form cross bridges which stabilises the filament network by interacting with neighbouring structures and other filaments. Additionally, neurofilaments are also phosphorylated at the amino-terminal head domain, which is a possible mechanism by which neurofilament assembly is regulated (Miller *et al.,* 2002).

Neurofilaments are synthesised in neuronal cell bodies and transported down the axon. It was originally thought that this was by slow axonal transport processes, at a rate of between 0.1 and 3mm per day, much slower than fast transport by molecular motors such as kynesin and dynein (Miller *et al.,* 2002). However more recent studies suggest that neurofilaments are transported by conventional fast rates of movement which is interrupted by periods of extended pausing, giving the appearance of slow movement (Wang *et al.,* 2000). This intermittent movement points to a mechanism by which neurofilaments are capable of controlling their attachment and release to motor proteins (Miller *et al.,* 2002). Side arm phosphorylation of NfM and NfH may be a regulating factor in this process, as degree of phosphorylation correlates inversely with the velocity of axonal transport (Grant and Pant, 2000).

Disruption of neurofilament phosphorylation and transport are common features of many neurodegenerative conditions. Staining for phosphorylated neurofilaments (SMI34 or SMI35) is increased in Alzheimer's disease (AD), amyotrophic lateral sclerosis (ALS) and MS (Petzold, 2005). However, increased staining for non-phosphorylated neurofilaments have also been related to axonal injury in MS (Trapp *et al.,* 1998), and neurofilament dephosphorylation has been shown to precede excitotoxicity in a cell culture model of ALS (Vartiainen *et al.,* 1999).

1.5.2. Synaptic and dendritic proteins.

Neuronal dendrites are basic but essential functional units, which integrate neuronal circuits and are sites of structural and functional synaptic plasticity. More than 90% of dendrites in the mammalian CNS are contacted by excitatory synapses (Harris and Kater, 1994), which renders them highly vulnerable and sensitive to excitotoxic insult. Following NMDA or kainate treatment, cultured neurons show dramatic dendritic beading, however dendrites recover and pre- and post-synaptic elements

remain in physical proximity, suggesting that dendritic beading is not necessarily associated with loss of synaptic contacts (Hasbani *et al.,* 2001). By using markers for synapses and dendrites, it is possible to detect early changes in these structures following insult to the nervous system, as a possible indication of underlying excitotoxicity. Recently the localisation and expression of microtubule-associated protein (MAP)-2, synaptophysin, postsynaptic density protein (PSD)-95 and synapsin I was investigated in EAE to assess synaptic and dendritic pathology (Zhu *et al.,* 2003). MAP-2 is the most abundant MAP in the brain where it is expressed in the neuronal somata and dendrites (Johnson and Jope, 1992). It has dynamic functions in the growth, differentiation and plasticity of neurons and has key roles in neuronal responses to growth factors, neurotransmitters, synaptic activity and neurotoxins (Johnson and Jope, 1992). Loss of MAP-2 is an early feature of neuronal dysfunction following transient ischaemia in a guinea pig model of stroke, indicating that this is an important marker of changes in dendritic pathology and that dendritic breakdown may be a first sign of neurodegeneration (Matesic and Lin, 1994). In the normal rat spinal cord, antibodies against MAP-2 stain large motorneurons and the intricate dendritic network in the grey matter (GM), which extends heavily into the white matter (WM) (Zhu *et al.,* 2003). At peak of disease in EAE, most dendrites in the WM show a beaded morphology, which return to normal following clinical recovery from EAE (Zhu *et al.,* 2003). From this the authors concluded that MAP-2 loss may be induced by excitotoxicity, however other inflammatory components may contribute including reactive oxygen species, cytokines and/or proteases. Thus, it appears that MAP-2 represents a sensitive marker for early changes in dendritic pathology, however it does not provide a marker for permanent neurological damage.

Synaptophysin is a pre-synaptic protein, which is localised in the membrane of synaptic vesicles where it is thought to have a role in neurotransmitter vesicle

exocytosis (Valtorta *et al.,* 2004). In AD, early progression correlates with alterations synaptophysin and growth associated protein (GAP)-43 (Masliah *et al.,* 2001). Additionally, synaptophysin loss in the midfrontal cortex is associated with a reduction in local glutamate uptake (Masliah *et al.,* 1996). Post-synaptic density protein (PSD)-95 is an important protein which is associated with NMDA glutamate receptors at excitatory synapses. It contributes to both synaptic targeting of receptors and to their signalling functions (Kim and Sheng, 2004). Disruption of PSD-95/NMDA receptor interactions attenuates NMDA receptor-mediated neurotoxicity (Aarts and Tymianski, 2003). Although PSD-95 is continuously turned over as a result of synaptic activity, NMDA receptor activation leads to PSD-95 degradation by the calcium-dependent protease, calpain (Lu *et al.,* 2000), thus PSD-95 can be used as a marker of excessive NMDA receptor activation as occurs under excitotoxic conditions. In control rat spinal cord, the GM matter showed punctuated staining for synaptophysin and PSD-95 which encircled large motorneurons. At the peak of EAE disease, staining for synaptophysin and PSD95 were greatly reduced, although levels partially recovered following EAE remission (Zhu *et al.,* 2003).

GAP-43 is an axonal phosphoprotein which is involved in regulating the growth state of axon terminals, in combination with other molecules, including c-jun (Benowitz and Routtenberg, 1997). GAP-43 is expressed at high levels during development and is re-induced by regeneration in the PNS (Benowitz and Routtenberg, 1997). However, injury to the CNS does not result in significant regeneration and this has been suggested to correlate with a failure of central neurons to up-regulate GAP-43 after axotomy (Kerschensteiner *et al.,* 2004). Following a targeted EAE lesion, GAP-43 staining is decreased, and only a small proportion of c-jun positive cells also express GAP43 and are thus unlikely to initiate growth (Kerschensteiner *et al.,* 2004). However a negative correlation exists between levels of GAP-43 and myelination in the adult CNS, thus in

animals with a targeted EAE lesion, resulting in extensive demyelination, it would be expected to lead to a reduced effect of myelin inhibition on neurite outgrowth in and around the lesion area.

Investigating different synaptic and dendritic proteins in disease states, including EAE and MS, could provide clues about the degree of axonal pathology, and point to early changes that precede neurodegeneration.

1.6. Immunology of Neuroinflammation.

All tissues in the body contain a resident population of immune cells, namely macrophages and dendritic cells, which play key roles in a variety of immune responses. Macrophages are part of the innate immune repertoire and are responsible for pathogen recognition, clearance and phagocytosis (Janeway *et al.,* 2001). Dendritic cells have the ability to capture antigen, migrate to lymphoid tissue and present it to T cells, initiating T cell responses (Janeway *et al.,* 2001). The CNS has evolved to protect its functioning from damaging immune-mediated inflammation by shielding itself with the BBB (Aloisi, 2001). The BBB is a dynamic, complex cellular system capable of rapid modulation, comprising of cerebral endothelial cells (EC) resting on the basal lamina (Huber *et al.,* 2001). These specialised EC line the cerebral capillaries containing tight intercellular junctions, which seclude the CNS parenchyma. The function of these cells is to regulate the entry of blood-borne molecules into the brain and to preserve metabolic and immunoregulatory homeostasis within the brain microenvironment (Tepass, 2003). The cerebral capillaries are also surrounded by astrocytic foot processes and perivascular macrophages/microglia that exert a regulatory effect on BBB tightness (Aloisi, 2001). Small lipophilic molecules such as oxygen can freely diffuse across the lipid membranes of the endothelial cells whereas small polar molecules, such as glucose, require special transporters. The CNS lacks any obvious lymphatic vessels

and the BBB prevents entry of any plasma proteins or immune cells into the nervous tissue. However the CNS is routinely and efficiently surveyed by the immune system (Hickey, 2001) by perivascular microglial and astrocytic cells which scrutinise all portals of entry for blood-derived pathogens and immune cells (Aloisi, 2001). MS is associated with a disruption to the BBB, and opening of the BBB is necessary but not sufficient for establishing the cascade of events which culminates in demyelination (Compston *et al.,* 1998). Inflammatory changes of the BBB are characterised by increased permeability to serum proteins (Kwon and Prineas, 1994) and infiltration of mononuclear cells into the perivascular space and brain parenchyma. Breakdown of the BBB and subsequent lymphocyte entry into the CNS depends on a variety of mechanisms including increases in the expression components of the plasminogen activator (PA) - matrix metalloproteinases (MMPs) cascade, adhesion molecules, cytokines and chemokines (Cuzner and Woodroofe, 2002). Perivascular astrocytes and microglial cells, as well as the cerebral ECs, are thought to locally produce inflammatory cytokines that increase BBB permeability which subsequently increase the expression of adhesion molecules (Chavarria and Alcocer-Varela, 2004).

1.6.1. Migration of lymphocytes across the BBB.

Trafficking of inflammatory T-cells into the CNS is a crucial step during neuroinflammation and begins with weak adhesion and rolling of cells on the endothelium of the BBB, followed by firm arrest on the luminal side of the endothelium and subsequent diapedesis across the BBB, cells then finally penetrate the basement membrane (Languino *et al.,* 1995; van-Horssen *et al.,* 2005). Cell migration is a complex process which is regulated by cytokines, chemokines and growth factors acting through multiple pathways (Brown, 2001). Much of the work carried out to investigate how lymphocytes cross the BBB has been carried out in an animal model of MS, EAE.

A distinct feature of MS and EAE is the presence of cuffs of lymphocytes around small blood vessels. Infiltrating T lymphocytes can be $CD4^+$ and $CD8^+$, and the $CD4^+$ cells mostly express the phenotype of Th1 lymphocytes in that they produce pro-inflammatory cytokines, in contrast to Th2 cells which secrete anti-inflammatory and B lymphocyte differentiation cytokines (Janeway *et al.,* 2001). The leucocyte migration patterns observed in EAE are thought to also be relevant to the pathogenesis of MS. Lymphocyte binding to blood vessel walls depends upon the interaction of adhesion molecules, expressed on its surface, with corresponding ligands on ECs, as migration does not occur without adhesion (Pryce *et al.,* 1997). Integrins, intracellular adhesion molecule 1 (ICAM-1/CD54) and vascular cell adhesion molecule-1 (VCAM-1/CD106) are thought to be involved in the passage of lymphocytes though the BBB prior to demyelination. VCAM-1 is expressed on endothelial cells and is a ligand for the integrin $\alpha_4\beta_1$, also called very late antigen 4 (VLA-4), which is expressed on the surface of activated leucocytes. It plays a crucial role in adhesion of leucocytes to the vascular endothelium and migration into the parenchyma (Miller *et al.,* 2003). ICAM-1 is constitutively expressed at low levels on BBB endothelial cells however, in the presence of pro-inflammatory cytokines, specifically tumour necrosis factor alpha (TNF-α) (Brown, 2001; Cannella and Raine, 1995; Zameer and Hoffman, 2003), the expression of ICAM-1 is rapidly increased on the luminal surface. Levels of ICAM-1 are increased in EAE and in active MS lesions (Ahmed *et al.,* 2003; Cannella and Raine, 1995), indicating that ICAM-1 plays an important role in leucocyte infiltration into the CNS (Pryce *et al.,* 1997). There are two receptors for ICAM-1, namely the integrin leucocyte function-associated antigen-1 (LFA-1 or CD11a/CD18, $\alpha_L\beta_2$) and also Mac-1 (CD11b/CD18, $\alpha_M\beta_2$) (Lee and Benveniste, 1999). It was initially though that cell migration of leucocytes occurs through the tight junctions (Bianchi *et al.,* 1997), however it has become evident that this migration could in fact occur through the

endothelial cells, keeping the tight junction "tight" (Figure 1.3) (Wolburg *et al.,* 2005). To enable leucocytes to migrate through endothelial cells, a rearrangement of the actin cytoskeleton is required. ICAM-1 cross-linking induces calcium signalling which, via protein kinase C, mediates phosphorylation of actin associated proteins, activation of Rho and cytoskeletal rearrangement in brain endothelial cell lines (Etienne-Manneville *et al.,* 2000; Walters *et al.,* 2002; Wolburg *et al.,* 2005).

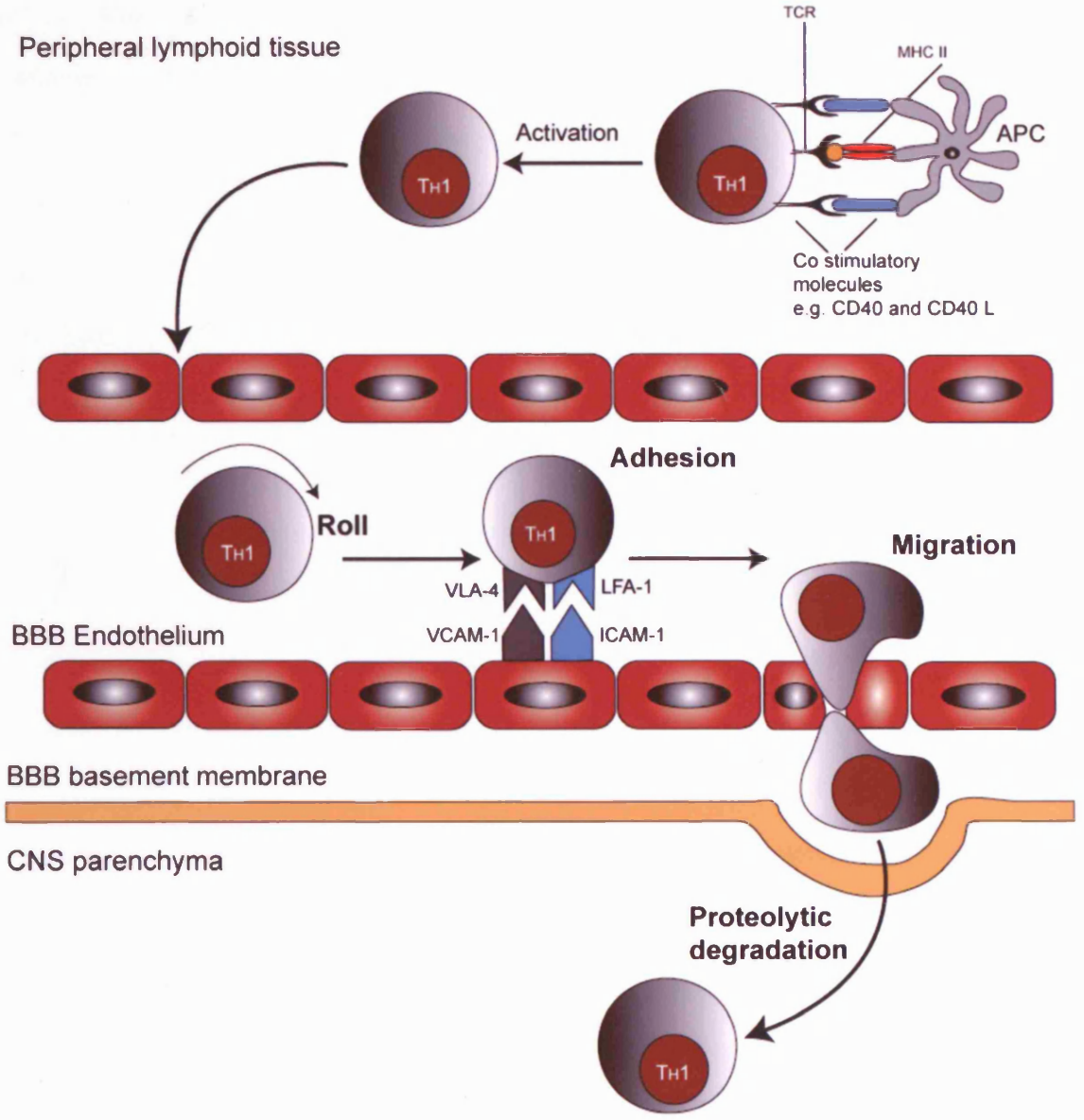

Figure 1.3. *T-lymphocyte migration through the BBB and into the CNS during inflammatory demyelination.* Following activation of Th1 T cells in the peripheral lymphoid tissue, they enter the blood stream and circulate through the tissues in search of their target antigen. Increased levels of cytokines and chemokines, released from activated microglia, macrophages, APCs and T cells, leads to the upregulation of adhesion molecules such as ICAM-1 and VCAM-1 on the endothelial cell surface. Adhesion of the T-lymphocytes to the endothelium occurs when ICAM-1 or VCAM-1 bind to their corresponding receptors on the T-cells, leucocyte function associated antigen-1 (LFA-1) and very late antigen-4 (VLA-4). This brings about ICAM-1 cross-linking, ultimately leading to activation of Rho and cytoskeletal rearrangement, enabling migration through the endothelial cell by a transcellular pathway. Cells must then degrade the basement membrane to enter into the CNS parenchyma.

1.6.2. BBB Tight junctions.

Tight and adheren junctions together form the junction complex between adjacent endothelial cells, which line the vascular walls. Tight junctions (TJs) are located in the most apical section of the plasma membrane of adjacent cells where they form a seal to prevent solutes from diffusing through the intracellular (paracellular) space (Tepass, 2003), thus mediating the gate function of the BBB. Tight junctions at the BBB are composed of an intricate combination of transmembrane and cytoplasmic proteins, linked to an actin cytoskeleton, which allows the junction to form a seal (Figure 1.4) (Huber *et al.,* 2001). Claudins are considered to be the core components of the TJ strands as they can mediate adhesion between opposing plasma membranes. Claudins are small proteins about 20-22 kDa that span the membrane four times (Petty and Lo, 2002). They form dimers and bind to claudins on adjacent cells to form the primary junction seal. In mice deficient for claudin 5 the development and morphology of brain blood vessels were not altered (Nitta *et al.,* 2003). However, the BBB TJs in these knockouts showed a peculiar abnormality. Tracer experiments and MRI have revealed that the BBB permeability is severely affected against small molecules (< 800 D), but not larger molecules, thus concluding that there is a size-selective loosening of the tight junctions in these mice. Additionally it is possible that removal of claudin 5 would be harmful to CNS activity as claudin-5 knockout mice died within 10 hours of birth (Nitta *et al.,* 2003). Another integral protein of TJs is occludin. Occludin is a ~60 kDa protein with four transmembrane segments. Its presence at the BBB is correlated with increased electrical resistance across the barrier and decreased permeability (McCarthy *et al.,* 1996). In mice deficient for occludin, most tissues bear TJ morphologically indistinguishable from those of the wild type controls (Saitou *et al.,* 2002), indicating that occludin is not required for the formation of TJs. However occludin knockout mice do bear some puzzling phenotypes. Their sexual behaviour is

affected, and they suffer severe postnatal growth retardation. Furthermore, histological abnormalities are found in several tissue including chronic inflammation and hyperplasia in the gastric epithelium and progressive accumulation of mineral deposits in the cerebellum and basal ganglia (Saitou *et al.,* 2000). These deposits were composed almost entirely of calcium suggesting that lack of occludin does in fact alter some aspect of TJs and that this barrier dysfunction could affect the absorption of calcium.

Alterations in the permeability of the BBB are thought to precede or accompany inflammation in the CNS during MS. As demonstrated by gadolinium-enhanced MRI, BBB breakdown is characteristic of new and expanding lesions; however the anatomical route of leakage has not been established. It is possible that brain endothelial TJs play a role in increasing the permeability of the BBB and that increased leucocyte migration alters the molecular organisation of the junctional complex (Bolton *et al.,* 1998). By examining TJ proteins in blood vessels in MS lesions using immunofluorescence, Plumb *et al.,* (2000) discovered changes in staining for occludin and a junctional cytoplasmic accessory protein called zona occludens 1 (ZO-1). Tight junction abnormalities manifested as beading, interruption or diffuse cytoplasmic localisation of immunofluorescent staining, and were most common in active MS lesions with perivascular inflammation and microglial activation. The absence of these disruptions in chronic plaques suggests a mechanism of reversible junction disturbance, related to the involvement of such vessels in the diapedesis of inflammatory cells (Plumb *et al.,* 2000). Using fibrinogen as a marker of BBB leakage, further work revealed that blood vessels with the highest degree of TJ alterations showed severe fibrinogen leakage (Kirk *et al.,* 2003). Additionally, Kirk *et al.,* (2003) discovered that TJ abnormalities were independent of blood vessel size and lesion activity. Had changes in tight junctions resulted solely from infiltration of inflammatory cells, post-capillary venules and veins

would have been expected to bear the brunt of pathological changes (Kirk *et al.,* 2003), however the involvement of all blood vessels suggests that TJ alterations are partly mediated by alterations within the CNS.

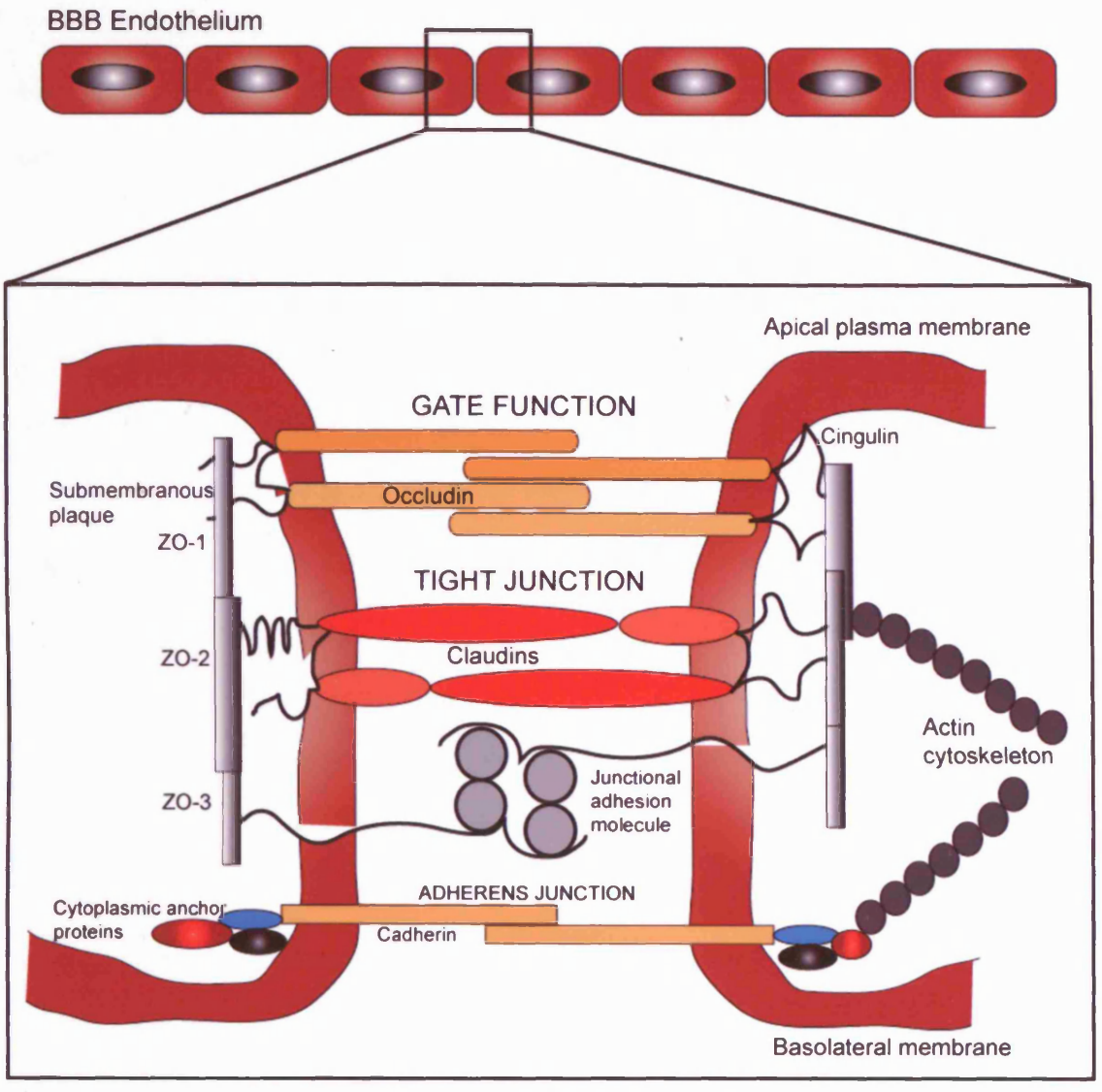

Figure 1.4. *Proposed interactions of the major proteins associated with BBB endothelial tight junctions.* Claudins are the proposed backbone of the junctions which form dimers by binding to claudins on adjacent cells. Claudins 1 and 5 have been identified at BBB TJs. Claudins can also bind to occludins which act as regulatory proteins. The presence of occludins at the BBB TJ is associated with increased electrical resistance across the membrane and decreased permeability. Junctional adhesion molecule (JAM) is involved in cell-cell adhesion, and also contributes to permeability control. There are several cytoplasmic accessory proteins, such as the zono occludens (ZO) and cingulin which anchor the proteins to the actin cytoskeleton and aid in signal transduction. Adapted from Petty and Lo, (2002).

1.6.3. Basement membrane penetration and BBB disruption.

Once past the EC barrier, leucocytes are faced with the complex hurdle of the basement membrane (BM) (van-Horssen *et al.,* 2005). The BM is a subendothelial 3D network of ECM proteins, e.g. laminins, collagens and proteoglycans, and underlying connective tissue. Given the complexity of the BM it is likely that there are many different proteolytic systems involved in the degradation of matrix components. It is possible that the cytokines TNF-α, interleukins (IL) -1β (IL-1β) and IL-6, released from activated microglia and astrocytes, lead to the early disruption of the BBB via release of prostaglandins (De Vries *et al.,* 1996). In addition, microglia and astrocytes have been shown to release elevated levels of MMPs in response to inflammation (Rosenberg, 2002). MMPs are a group of tightly regulated neutral proteases which have important functions in the CNS including remodelling of the ECM. They are generally secreted as inactive pro-forms, or zymogens, that are extracellularly activated by other MMPs or other proteinases such as plasmin (Lo *et al.,* 2002). The synthesis and activity of MMPs is tightly regulated at several levels by transcription, secretion, activation or by endogenous tissue inhibitors of MPs (TIMPs) and by α_2-macrogloblin (Rosenberg, 2002). The balance of these processes prevents excessive proteolysis or inhibition. However under neuroinflammatory conditions where excessive amounts of MMPs are produced, the balance is disrupted and increased ECM breakdown occurs. There are four main categories of MMPs, several of which are upregulated in MS (Bar-Or *et al.,* 2003). The expression of MMP-9 or gelatinase B, so called because it breaks down gelatin, is markedly increased during inflammation and is thought to have a critical destructive role during the multiple phases of neuroinflammation. MMP-9 is elevated in the cerebrospinal fluid (CSF) of MS patients (Gijbels *et al.,* 1992; Leppert *et al.,* 2003) and in lesions and normal appearing white matter (NAWM) of MS tissue (Cuzner *et al.,* 1996; Lindberg *et al.,* 2001). MMPs 2, 3 and 7 have also been linked to

inflammation (Rosenberg, 2002). Activated T cells and monocytes express MMPs at a higher levels which facilitates their entry into the CNS through breakdown of the basement membrane ECM (Leppert *et al.,* 1992). In addition to BBB breakdown, MMPs have a number of other potentially harmful actions which could play a role in the pathogenesis of MS. Myelin proteins, such as MBP, and ECM molecules are vulnerable to proteolysis by MMP-9 and plasmin which could be implicated with demyelination (Cammer *et al.,* 1978). That cleavage of MBP by MMP-9 can release encephalitogenic peptides (Gijbels *et al.,* 1993) has lead to the "remnant epitopes generate autoimmunity" (REGA) theory. This postulates that myelin proteins, after proteolysis, can take on a very different conformations and additional alterations in the local CNS environment may render these peptides immune to degradation thus increasing the opportunity for MHC presentation (Cuzner and Opdenakker, 1999; Descamps *et al.,* 2003). Investigations into MMPs in EAE has had varied results. A number of MMPs and their inhibitors are upregulated in EAE correlating with disease progression (Nygardas and Hinkkanen, 2002) and synthetic inhibitors of MMPs can alleviate and suppress severity of EAE (Hewson *et al.,* 1995). Treatment of mice with minocycline, an inhibitor of MMP activity, reduces disease severity in both mild and severe EAE (Brundula *et al.,* 2002). Young MMP-9 knockout mice are less susceptible to the onset of EAE (Dubois *et al.,* 2002), however knockout mice older than 4 weeks were equally susceptible as wild types. More dramatic were the effects of a combined MMP and TNF-α inhibitor which markedly suppressed EAE signs in the Lewis rat and dramatically reversed the weight loss characteristic of this disease (Clements *et al.,* 1997)

In addition to the action of MMPs, there is a unique mechanism by which leucocytes can focally degrade the ECM proteins of the BM. This is via the urokinase plasminogen activator (uPA) system. This is discussed in detail in section 1.7.3.

1.6.4. Microglia and macrophages – effector cells of neuroinflammation.

Microglia constitute 5–15% of the total brain cell population (Carson, 2002) and are the resident macrophages and primary immune cells of the central nervous system. In their resting state microglia are present in a ramified, downregulated form characterised by a small elongated cell body and highly branched processes which extend along myelinated nerve fibres. Their exact role in the normal CNS is still unknown but they are involved in glial-neuron signalling and supporting neuronal survival (Cuzner and Woodroofe, 2002). They are the first cells to respond to neural insults sensing changes in their microenvironment and rapidly migrate to sites of injury where they undergo a series of changes that characterise their activation (Kreutzberg, 1996). They become more amoeboid in morphology and begin to express a number of cell surface markers, including CD45 (and F4/80 in mice), which are key to induce the macrophage-like functions and phagocytic capabilities. Activated microglia are known to release a number of substances that contribute to both neuroprotection and neurotoxicity (Zhang and Fedoroff, 1996) and whether they exert cytotoxic or protective effects depends on the nature of the tissue and the presence or absence of other immune cells (Diemel *et al.,* 1998). Activated microglia accumulate in many CNS diseases and are thought to be involved in the pathogenesis of MS. In addition to microglia-derived macrophages, blood-borne monocyte-derived macrophages are also identified in MS lesions, they both play a role in myelin phagocytosis and debris clearance and are an indicator of lesion activity (Li *et al.,* 1996). Upregulation of MHC class I and II molecule expression and therefore the acquisition of antigen presenting properties are also features of microglial activation (Bo *et al.,* 1994; Matsumoto *et al.,* 1992). Activated microglia are thought to aid in the initiation of demyelination following phagocytosis of myelin by presenting the autoantigen to T cells. Macrophages and microglia are thought to contribute to demyelination by secreting a variety of soluble

factors, including cytokines, proteolytic enzymes, reactive oxygen species and nitric oxide, which can be cytotoxic to oligodendrocytes and neurons (Cuzner and Woodroofe, 2002; Diemel *et al.,* 1998). Cytokines are key regulators of immune responses and are released by tissue infiltrating immune cells, CNS-associated macrophages, microglia and astrocytes in conditions of CNS inflammation (Imitola *et al.,* 2005). To maintain homeostasis, a dynamic balance between pro- and anti-inflammatory cytokines is required. Microglia are a major source of the pro-inflammatory cytokines TNF-α and IL-1 which in turn have been implicated in the facilitation of leucocyte entry into the CNS via upregulation of adhesion molecules and chemokines (Sedgewick *et al.,* 2000). Other cytokines considered to have an active role in demyelination include Interferon gamma (IFN-γ), IL-2 and IL-12. Additionally, chemokines, released from microglia and macrophages also play a central role in the inflammatory recruitment of leucocytes and other cell types. Chemokines induce and activate leucocyte adhesion molecules and establish a chemotactic gradient that results in their migration across the endothelial barrier (Sellebjerg and Sørensen, 2003). Whilst past research has focused on glial-derived pro-inflammatory cytokines it is becoming increasing evident that microglia also secrete cytokines with anti-inflammatory properties such as TGF-β and IL-10 which are thought to be potential mediators of remyelination or MS disease remission (Diemel *et al.,* 1998; Ledeen and Chakraborty, 1998).

1.7. The fibrinolytic system.

1.7.1. Plasminogen and fibrinolysis.

The final stage in the blood clotting cascade is the activation of thrombin by factor Xa, thus enabling thrombin to convert soluble fibrinogen into the insoluble mesh-like substance fibrin (Adams *et al.,* 2004). In order to breakdown fibrin, another

cascade or series of enzymes is involved. The central component of the fibrinolytic system is the glycoprotein plasminogen, which is a 92 kDa proenzyme. It is composed of 5 kringle-like domains which facilitate binding to fibrin, with a C-terminal domain that is homologous to other trypsin-like proteases (Dobrovolsky and Titaeva, 2002). Plasminogen is secreted by the liver in its inactive form, which circulates in the vasculature and is converted into the active two-chain structure of plasmin by proteolytic cleavage of a single peptide bond (Castellino and Ploplis, 2005). There are two main plasminogen activators (PA) namely tissue-type and urokinase-type (tPA and uPA). Proteolytic cleavage of plasminogen can result in different conformations, Glu-plasminogen and Lys-plasminogen, and dramatic differences exist in these conformations that are highly influential to their functions (Castellino and Ploplis, 2005). Lys-plasminogen has a more open conformation that is highly activatable compared to Glu-plasminogen, which is severely attenuated in its activation (Castellino and Ploplis, 2005). The main plasmin inhibitor is α_2-antiplasmin (α_2-AP), but its activity can also be inhibited by α_2-macroglobulin (α_2-MG) and by thrombin-activated fibrinolysis inhibitor (TAFI) (Lijnen H.R., 2002). Although the primary target of plasmin is fibrin, it is also capable of binding to and degrading several other constituents of the extracellular matrix, such as laminin and fibronectin (Dobrovolsky and Titaeva, 2002), and activating cytokine precursors and other proteolytic enzymes into their active forms (Liu *et al.,* 2005). The generation of plasmin occurs preferentially on the fibrin surface, which offers binding sites for plasminogen and its main activator tPA (Kamath and Lip, 2003). Localisation of plasmin to sites of fibrin formation promotes efficient clot lysis where fibrin is digested into soluble degradation products (FDP) (Figure 1.5). Fibrinogen has a symmetrical structure formed by three pairs of non-identical polypeptide chains called Aα, Bβ and γ chains. When

fibrin(ogen) is sequentially digested by plasmin, the resulting degredation products are designated as X-, Y-, D- and E- fragments (Kamath and Lip, 2003).

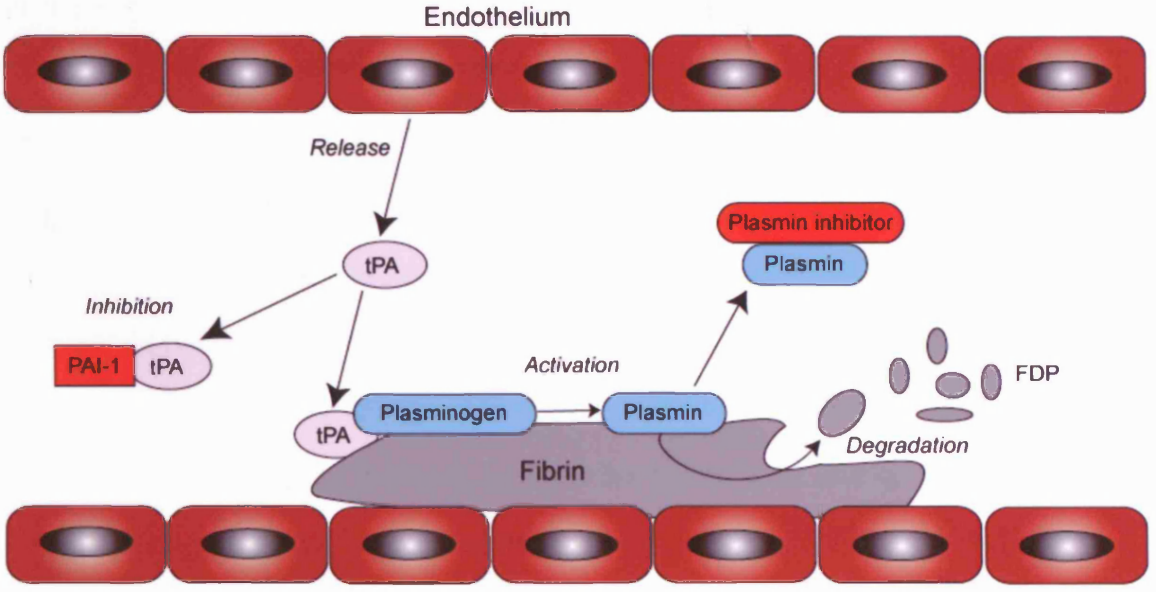

Figure 1.5. *Illustration of fibrinolysis in the vasculature*. The key plasminogen activator, tPA is released from the endothelium into the blood stream where it can bind to plasminogen, converting it to the active enzyme plasmin. The proteolytic activity of tPA is greatly increased in the presence of fibrin. Plasmin catalysed digestion of fibrin leads to the release of soluble fibrin degradation products (FDP). tPA activity is inhibited by plasminogen activator inhibitor-1 (PAI-1) and plasmin can be inhibited by α_2-antiplasmin or by α_2-macroglobulin. Adapted from www.chromogenix.com.

1.7.2. Plasminogen activators - structure and function.

Tissue plasminogen activator (tPA) and urokinase plasminogen activator (uPA) are the major proteins in the group of plasminogen activators (Castellino and Ploplis, 2005). The primary action of tPA is in the periphery where it is responsible for the dissolution of fibrin at sites of vascular injury via the conversion of the zymogen plasminogen to its active protease form plasmin to release soluble fibrin products. tPA is synthesised and secreted by ECs as a single chain active enzyme of 70 kDa (Lijnen H.R., 2002). It is composed of 5 domains and bears distinct homology to trypsin like proteases, plasminogen, epidermal growth factor (EGF) and fibronectin (Dobrovolsky and Titaeva, 2002) (Figure 1.6). In physiological conditions tPA activates plasminogen at a very low rate, however in the presence of fibrin, a ternary complex of plasminogen, tPA and fibrin is formed which increases the catalytic activity of tPA by 1000 fold (Dobrovolsky and Titaeva, 2002). Whilst tPA can act in a single form, formation of two chain tPA by plasmin, kallikrein or factor Xa increases its activity (Lijnen H.R., 2002). The main site of clearance for tPA is in the liver, where it binds to one of its many receptors, low density lipoprotein (LDL) receptor-related protein (LRP) (Dobrovolsky and Titaeva, 2002). LRP is a multifunctional receptor that binds to several structurally and functionally unrelated ligands and endocytoses them.

uPA is a 53 kDa trypsin-like protease which is secreted by many cells in the body (Lijnen, 2002). It is produced as an inactive single chain that is activated into two chain uPA by plasmin, cathepsin, plasma kallikrein or mast cell tryptase (Lijnen, 2002). It is composed of three domains and like tPA has homology to EGF (Figure 1.6). It is found at much lower plasma concentrations than tPA, although synthesis is highly upregulated during inflammation (Gabay and Kushner, 1999). Urokinase PA requires binding to a cell surface receptor (uPAR) via its EGF-like domain before it can initiate activation of plasmin (Dobrovolsky and Titaeva, 2002), and due to this receptor bound

nature of uPA, its major role is in cell-mediated proteolysis (Blasi and Carmeliet P., 2002). The specific receptor for uPA, uPAR, is expressed on many cell types as a 65 kDa cell surface bound glycosyl phosphatidylinositol (GPI)-linked protein (Lijnen H.R., 2002). It consists of three domains (D1, D2 and D3) and cleavage of the GPI anchor can release soluble uPAR (suPAR) from the plasma membrane (Castellino and Ploplis, 2005) (Figure 1.6). The amino terminal fragment of uPA, is essential and sufficient for uPAR binding (Bu *et al.,* 1994). This results in the exposure of the catalytic, carboxy-terminal domain and subsequent plasminogen activation. Binding of uPA to uPAR controls uPA activity through endocytosis (Section 1.7.3.) and also activates local proteolysis and intracellular signalling transduction, which is as a result of uPAR interactions with neighbouring integrins (Myöhänen and Vaheri, 2004). Recycling and endocytosis of the uPA:uPAR complex also involves intereaction with LRP and the key PA inhibitor, PAI-1 (Binder *et al.,* 2002).

Endogenous inhibitors of PA's exist, which form part of the family of the serine protease inhibitors (SERPINS). This family includes plasminogen activator inhibitor-1 (PAI-1), 2 and 3, α_2-antiplasmin and antithrombin III. PAI-1, a 45-50 kDa protein, is the major inhibitor of tPA and uPA (Figure 1.6), thus is capable of inhibiting vascular fibrinolysis and cell-associated proteolysis (Lijnen H.R., 2002). PAI-1 is produced by ECs, smooth muscle cells, macrophages and in liver, spleen and adipose tissue (Huber, 2001), however 90% of the inhibitor is stored in platelets from where it can be released locally at sights of thrombus formation (Dobrovolsky and Titaeva, 2002). In plasma, PAI-1 is present in 2 forms; active and latent. The active form specifically interacts with vitronectin, an extracellular matrix protein which stabilises PAI-1 in its active conformation (Loskutoff *et al.,* 1999). The involvement of PAI-1, vitronectin, uPAR, uPA and LRP is given in more detail in section 1.7.3. The synthesis of PAI-1 is markedly increased by a large number of substances including pro-inflammatory

cytokines, insulin, TGF-β and thrombin. PAI-1 is regarded as an acute phase protein, as it is rapidly increased several fold during the acute phase of disease (Dobrovolsky and Titaeva, 2002) and thus may be regarded as a marker for an ongoing inflammatory process (Binder *et al.,* 2002). Interaction of tPA, uPA, uPAR and PAI-1 is illustrated in Figure 1.7, which also depicts the link between the PA and MMP cascades.

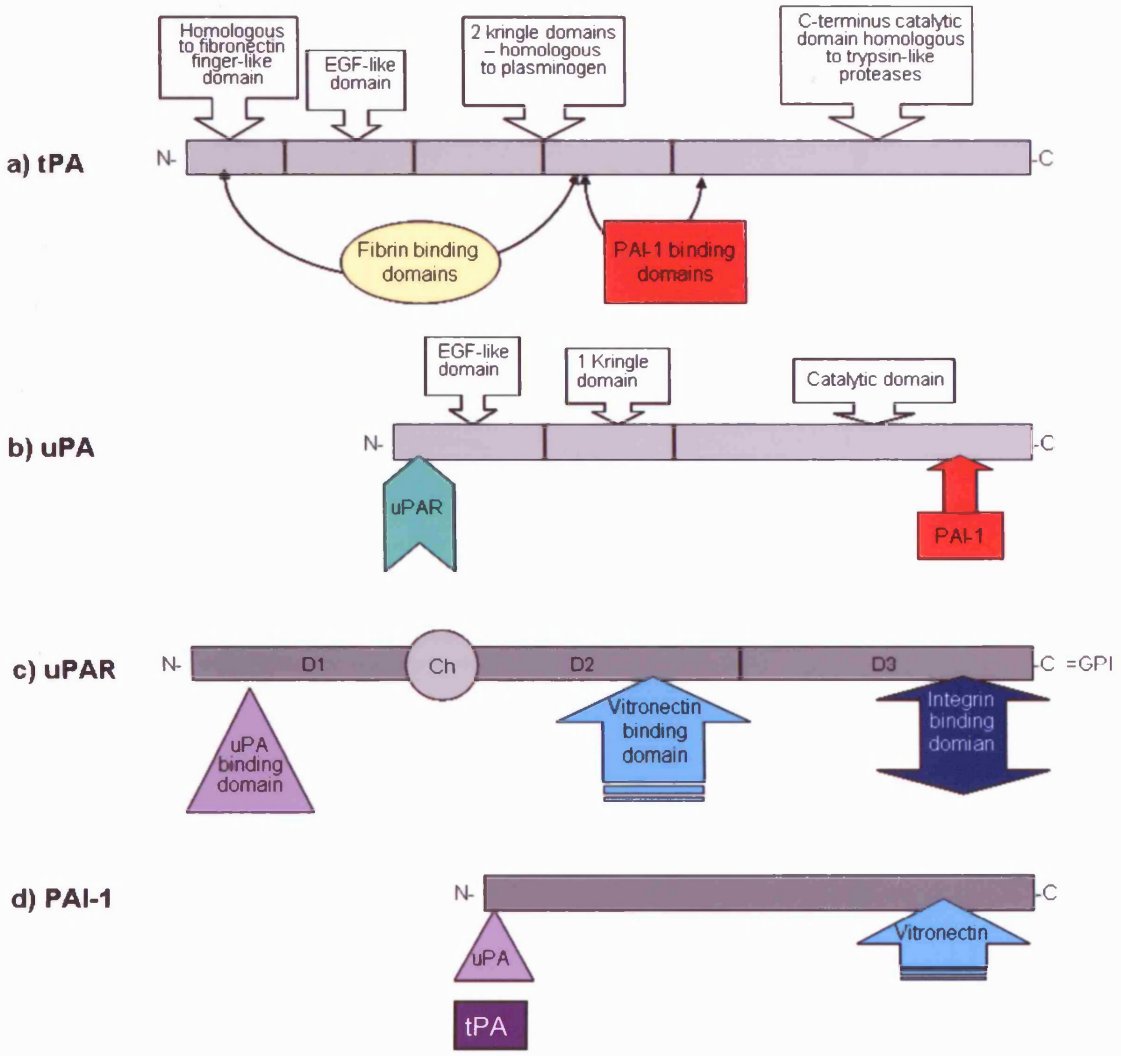

Figure 1.6. *A schematic representation of the structure of tPA, uPA, uPAR and PAI-1.* (a) tPA protein is composed of a fibronectin-like domain, an epidermal growth factor (EGF)-like domain, 2 kringle domains and a catalytic C-terminal domain. The fibrin binding sites are located in the fibronectin-like domain and the second of the kringle domains. PAI-1 binding also occurs at two sites in the second kringle domain and at the catalytic domain. (b) uPA, a smaller protein than tPA, also has an EGF-like domain, only one kringle domain and a C-terminal catalytic domain. uPAR binding occurs at the N-terminal EGF domain and PAI-1 interaction occurs in the catalytic domain indicating that interaction of uPA with its receptor and inhibitor can occur at the same time. (c) uPAR protein is composed of three domains. The chemotactic region (Ch) is activated upon splicing of the protein between domains 1 and 2. Domain 1 contains the uPA binding site, domain 2, the vitronectin binding region and domain 3, the interaction site for integrins. (d) PAI-1 protein has a region for vitronectin interaction at the C-terminus and interactions with uPA and tPA occur near the N-terminal domain of the protein.

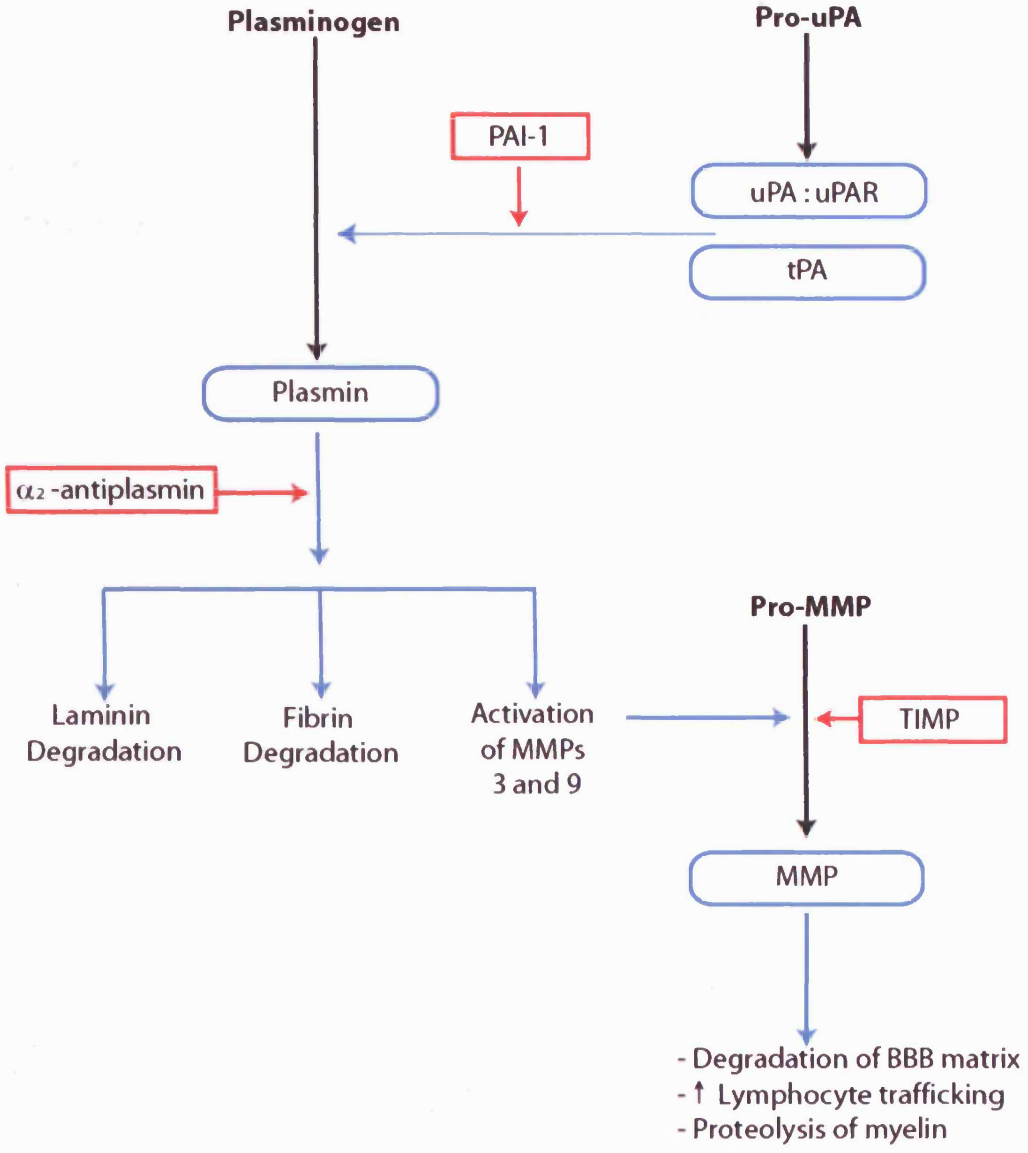

Figure 1.7. *Schematic representation of the PA cascade; functions and interactions.* A number of effects, both beneficial and deleterious, can occur as a result of the activation of these systems. Active enzymes and their interactions are indicated in blue, inhibitors are indicated in red and enzymes precursors in bold text.

Plasminogen activators are not solely expressed in tissues that are associated with fibrinolysis suggesting that this group of proteins have additional roles. The expression of tPA has been described both in the developing and the adult mouse brain where it plays a role in development, synaptic plasticity and remodelling (Sappino *et al.,* 1993). High levels are found particularly in the thalamus, amygdala and hippocampal pyramidal neurons (Teesalu *et al.,* 2002), an area associated with learning and memory. Neurons and glial cells are the key tPA producing cells in the CNS where it is stored intracellularly and released upon depolarisation of the neuronal cell membrane in a calcium dependent manner (Gualandris *et al.,* 1996). In line with this, a brain specific inhibitor of tPA, neuroserpin has been identified (Hastings *et al.,* 1997). Unlike other PA inhibitors, neuroserpin is a more effective inhibitor of tPA than uPA (Yepes and Lawrence, 2004). It is a 44kDa protein which is expressed primarily in neuronal cells in areas of the brain also associated with tPA expression, such as the hippocampus (Hastings *et al.,* 1997).

In the last decade the introduction of methods of gene inactivation have enabled in depth study of the components of the fibrinolytic system. Disruption of the tPA gene involved the replacement of a section of the gene encoding for the kringle 2 domain and part of the proteolytic domain with a neomycin-resistance gene (Carmeliet P. *et al.,* 1994). Litter size, frequency of birth and body weights are normal in these homozygous knockout animals. Mice deficient for tPA suffer impaired clot lysis (Carmeliet P. *et al.,* 1994) although no histological or macroscopic abnormalities are observed in mice aged up to 14 months (Ploplis and Castellino, 2002). Mice deficient for uPAR were created by replacing a large part of the genomic sequence, exons 2–5, with the neomycin resistance gene (Dewerchin *et al.,* 1996). None of the homozygous knockout offspring demonstrate abnormal growth or fertility, and histologically there are no pathological lesions or fibrin deposits (Ploplis and Castellino, 2002). Clot lysis in these animals is

normal, although uPA mediated plasminogen activation is reduced (Dewerchin *et al.*, 1996). PAI-1 deficient mice were generated by homologous recombination in embryonic stem cells resulting in the deletion of the entire coding region of PAI-1 (Carmeliet P. *et al.*, 1993). PAI-1 knockout mice are viable, litter and offspring sizes are similar to wild type animals, with no apparent macroscopic or microscopic histological abnormalities. Use of these knockouts in a wide variety of experiments has enabled in-depth exploration into the roles of the components of the PA system in a number of pathological models.

1.7.3. uPAR, PAI-1 and cell migration.

Binding of the serine protease enzyme uPA to its cell surface bound receptor, uPAR, activates local proteolysis via the conversion of the zymogen plasminogen to plasmin. However, the role of uPAR is not limited to cell associated proteolysis, as interaction of uPAR with uPA, PAI-1, LRP, vitronectin and integrins provide a novel mechanism for cell chemotaxis, adhesion and migration (Binder *et al.*, 2002). Leucocytes including monocytes, macrophages and activated T-cells all constitutively express uPAR (Garcia-Monco *et al.*, 2002) which plays an important role in adhesion and migration to sites of inflammation via interactions with vitronectin and numerous integrins (Chapman, 1997; May *et al.*, 1998; Tarui *et al.*, 2001). The function of PAI-1 in modulating cell adhesion and migration is somewhat complex. The key modulatory effect of PAI-1 occurs through its capacity to bind to vitronectin (Hertig and Rondeau, 2004). Vitronectin (VN) is an adhesive glycoprotein present in plasma and tissues which, once deposited, binds many ligands including uPAR, PAI-1 and integrins. Binding of PAI-1 to VN stabilises the inhibitor in its active conformation thus enabling PAI-1 to competitively inhibit the uPAR-dependent attachment of cell to VN (Waltz *et al.*, 1997). In this way PAI-1 acts as a molecular switch interfering with the uPAR-VN

link, leading to detachment of cells from the substrate (Deng *et al.,* 1996). Binding of PAI-1 to VN not only directly blocks uPAR mediated adhesion, but also sterically hinders $\alpha_v\beta_3$ integrin binding to VN (Loskutoff *et al.,* 1999). Waltz *et al.,* (1997) discovered that by promoting detachment of uPAR bearing cells from VN, PAI-1 increased cellular migration on this matrix. The effect of PAI-1 on cell migration is particularly evident in cancer whereby high levels of this inhibitor are associated with tumour metastasis and a poor prognosis (Dellas and Loskutoff, 2005). A summary of the molecules capable of interacting with components of the PA system and their effects on cell migration/ adhesion is given in Table 1.2.

uPAR bound uPA is polarised at the leading edge of migrating leucocytes (Estreicher *et al.,* 1990) where it can remain for some time, unless complexed with an inhibitor (PAI), whilst also increasing the affinity of uPAR for association with integrins (Blasi, 1997). In addition to competitively binding to VN, PAI-1 can also complex with uPAR bound uPA, and the inhibitor-proteinase-receptor complex are removed from the cell surface via members of the scavenger receptor family such LRP (Nykjaer *et al.,* 1997). In this case the complex is then endocytosed and the uPA-PAI-1 complex is targeted for lysosomal degradation whilst uPAR is recycled and reappears at the cell surface (Figure 1.8). This unique tool enables the cell to recycle uPAR in a ligand-free form promoting the adhesion/chemotaxis state of the cell in favour of the proteolytic state (Bianchi *et al.,* 1997). uPAR also interacts with integrins, cell surface receptors that anchor cells to the ECM, and this model provides the attachment, detachment and reattachment of integrins necessary for cell migration.

PA components	Interacting molecules	Adhesive/deadhesive funtions
uPAR	VN	Adhesion
uPAR + PAI-1	VN	Detachment
uPAR + uPA	VN, FN, $\alpha_V\beta_3$, $\alpha_5\beta_1$, $\alpha_V\beta_1$	Adhesion
uPAR + uPA + PAI-1	VN, FN, $\alpha_V\beta_3$, $\alpha_V\beta_1$	Detachment
uPAR + uPA + PAI-1	VN, FN, $\alpha_V\beta_3$, $\alpha_V\beta_1$, LRP	Detachment, integrin inactivation, endocytosis
uPAR (uPA?)	$\alpha_4\beta_1$, $\alpha_V\beta_3$, $\alpha_9\beta_1$	Cell-cell adhesion
uPA	uPAR, $L_m\beta_2$	Adhesion

Table 1.2. *Components of the PA cascade, their interactions and functions.* VN = vitronectin, FN = fibronectin. From Myöhänen and Vaheri, (2004).

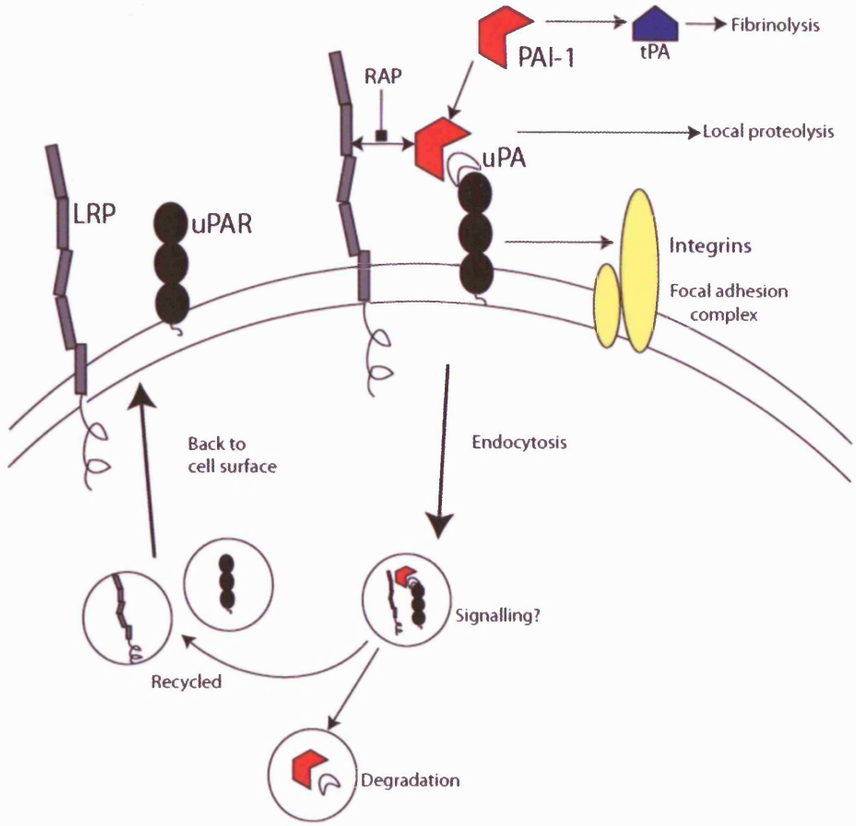

Figure 1.8. *Schematic to illustrate the interactions between uPAR, uPA, PAI-1, LRP and integrins.* The interaction of uPAR, uPA and PAI-1 with LRP is inhibited by receptor associated protein (RAP) which will prevent the recycling of uPAR back to the cell surface. The interaction of uPA with its receptor promotes local proteolysis whilst PAI-1 forms the bridging element between the uPA:uPAR complex and LRP, promoting cell migration. Endocytosis of the uPAR is thought to lead to intracellular signalling events via the Janus-kinase and signal transducer and activator of transcription (JAK-STAT) pathway, Src-like protein-tyrosine kinases and extracellular signal-regulated protein kinases (ERKs). uPA interaction with uPAR increases the affinity of the receptor for vitronectin and a variety of integrins also promoting cell adhesion and migration. Adapted from Binder *et al.*, (2002).

Generation of uPAR deficient mice (Dewerchin *et al.,* 1996) has enabled detailed study of the role of uPAR on cell adhesion / migration in response to infection, injury and inflammation (Busso *et al.,* 1998; Gyetko *et al.,* 2001; Ploplis and Castellino, 2002). Mice deficient for uPAR have impaired neutrophil recruitment in response to *Pseudomonas aeruginosa* pneumonia when compared to the wild type (Gyetko *et al.,* 2000). In addition, this mechanism appears to be dependent on β_2 integrins confirming the required interaction of uPAR with integrins for cell migration. Increase in uPAR expression has been linked to numerous human diseases (Blasi and Carmeliet P., 2002), including cancer where increased levels of uPAR are strongly correlated with tumour invasiveness and metastasis and poor prognosis (Blasi and Carmeliet P., 2002). Several approaches at inhibiting the uPA:uPAR interaction in preclinical studies of cancer treatment with small peptide molecules, monoclonal antibodies or using antisense technology have shown promising results (Choong and Nadesapillai, 2003). In addition, amplified uPAR expression has also been indicated in cerebral malaria (Fauser *et al.,* 2000), traumatic brain injury and focal cerebral ischaemia (Beschorner *et al.,* 2000). Although uPAR is found in the serum and CSF of patients with various neurological diseases (Garcia-Monco *et al.,* 2002), little research has been carried out into the roles of uPAR in inflammatory diseases of the CNS.

1.7.4. PAs and Neuropathology.

Over the last decade much interest has been invested into exploring the role of the PAs, particularly tPA, in various neuropathologies (summarise in Table 1.2). tPA was found to be expressed as an early gene induced after seizures (Qian *et al.,* 1993). Following on from this discovery, Tsirka *et al.,* (1995) discovered that tPA knockout mice were less susceptible to pharmacologically induced seizures. In addition, they also observed that tPA deficient mice, and plasminogen deficient mice, were resistant to

excitotoxin-induced neuronal degeneration following intracerebral administration of NMDA, AMPA or kainate into the hippocampus, indicating that the tPA/plasmin cascade is in involved in the mechanisms underlying excitotoxic cell death (Tsirka *et al.,* 1997b). Further work revealed that the critical event in this cascade appeared to be plasmin mediated degradation of laminin matrix in the hippocampus which precedes the onset of neuronal death (Chen and Strickland, 1997; Tsirka *et al.,* 1997a). Mechanisms of excitotoxicty are thought to be involved in the underlying pathology of many conditions such as AD and stroke (Hynd *et al.,* 2004), thus these findings understandably led to the investigation of the role of the PA cascade in ischaemia. This was of particular interest as tPA is used as a clot busting drug clinically, administered to people who have suffered an acute stroke. The expression of all components of the PA system are increased in response to ischaemia and traumatic brain injury (Dietzmann *et al.,* 2000). Investigating the role of tPA in various animal models of stroke has however led to conflicting results and these differences appear generally due to the model of ischaemia employed in the studies. Using a permanent middle cerebral artery occlusion (MCAO) model of stroke, Wang *et al.,* (1998) discovered that tPA deficient mice had 50% smaller infarcts that the wild type. In addition, intravenous injection of tPA increase the infarct size in $tPA^{-/-}$ and wild type mice indicating that tPA can increase stroke-induced injury. In the same model it has also been shown that transgenic mice over-expressing neuroserpin, the brain specific tPA inhibitor, have smaller infarcts after MCAO (Cinelli *et al.,* 2001). Injection of neuroserpin directly into the brain of rats shortly after MCAO reduced stroke volume by 64% at 72h compared with untreated animals (Yepes *et al.,* 2000). In both of these studies, the thrombolytic effect of tPA is not assessed as the model used does not involve microvascular thrombus formation. Experiments using a transient model of ischaemia by MCAO with an unsiliconised thread, leading to cerebrovascular thrombosis indicate that tPA has beneficial effects

where $tPA^{-/-}$ mice suffer exacerbated ischaemic insult (Tabrizi *et al.,* 1999). In conclusion, it is still not entirely clear of the role of tPA in ischaemia, however it is clear that differences in experimental design can yield different results and that tPA can have beneficial and deleterious effects within the same and different neuropathologies.

More recently the PA system has been linked to AD. AD is a common form of dementia in aged individuals, the cause of which is unknown. A characteristic pathology includes plaques in the brains of AD patients largely composed of amyloid-β (Aβ) peptide (Hynd *et al.,* 2004). It has been documented that the activation of plasmin by tPA can degrade Aβ (Tucker *et al.,* 2000), as can uPA (Tucker *et al.,* 2002), however neither of the PA enzymes can degrade Aβ in culture without the presence of plasminogen. Aβ peptide injected into the brains of mice deficient for either tPA or plasminogen revealed persistent Aβ immunoreactivity which completely disappeared in the wild type (Melchor *et al.,* 2003). Increases in uPAR expression have also been documented in the post mortem tissue from the brains of AD patients (Walker *et al.,* 2002). It is becoming increasingly evident that AD has an inflammatory component to the pathology, and here, uPAR upregulation is a marker of microglia and macrophage activation.

The actions of tPA and the PA cascade in the CNS led to investigations of their effects in models of peripheral nervous system injury. Axonal outgrowth during peripheral nerve regeneration relies on the ability of growth cones to migrate through ECM components utilising the actions of the PA proteases (Seeds *et al.,* 1996). After peripheral nerve injury, expression of the PA system is rapidly induced (Siconolfi and Seeds, 2001a), thus to investigate the functional consequences of the absence of various components of the PA system on peripheral nerve regeneration, a model of sciatic nerve crush was employed in mice deficient for tPA, uPA or plasminogen (Siconolfi and Seeds, 2001b). The results indicated that the PA system facilitates recovery after sciatic

nerve injury. Knockout animals suffered delayed recovery of sensor and motor functions in the hindlimb after injury, possibly due to impaired nerve outgrowth. Another study of sciatic nerve injury also showed a protective role for tPA and plasminogen in this model and, focusing on the mechanisms behind this particular effect, demonstrated that fibrin deposition on axons correlates to the degree of nerve damage observed (Akassoglou *et al.,* 2000). Mice deficient for tPA or plasminogen showed exacerbated axonal loss after injury and pharmacological depletion of fibrin ameliorated the axonal degeneration in the knockout animals (Akassoglou *et al.,* 2000). In addition, double knockout mice for plasminogen and fibrinogen showed similar levels of axonal loss and demyelination to wild type (Akassoglou *et al.,* 2000). This was the first example of how the fibrinolytic capacity of tPA can have beneficial effects other than its role in the vascular system.

Neuropathology	Findings	References
Normal CNS tissue		
Human	tPA expressed in neurones and microglia, high levels in the hippocampus. Involved in axonal growth cone migration and neurite outgrowth.	(Seeds *et al.*, 1996)
Rodent		
Traumatic brain injury and ischaemia		
Mouse model of TBI	tPA amplified cortical brain damage and oedema in TBI	(Mori *et al.*, 2001)
Acute stoke - humans	tPA used as a treatment because of its thrombolytic activity.	
Mouse model of focal ischaemia	tPA can increase stroke-induced injury.	(Wang *et al.*, 1998)
Inflammatory demyelinating disease		
Multiple sclerosis	tPA activity increased in CSF of MS patients and correlates with disease progression. Decreased tPA activity in MS brains due to increased PAI-1. Increased uPAR expression on inflammatory cells in lesions.	(Akenami *et al.*, 1996) (Gveric *et al.*, 2001)
EAE	Increased severity of EAE and delayed recovery in tPA ko mice.	(Lu *et al.*, 2002)
Neurodegenerative disease		
Excitotoxin-induced neurodegeneration	tPA ko mice resistant to neurodegeneration after injection of excitotoxin.	(Tsirka *et al.*, 1995)
Alzheimer's disease	Increased uPAR expression in AD brain.	(Walker *et al.*, 2002)
Mouse model of AD	tPA-plasmin proteolytic system accelerates Aβ degeneration.	(Melchor *et al.*, 2003)
Spinal cord and peripheral nerve injury		
Sciatic nerve crush	tPA and uPA aid recovery and peripheral nerve regeneration after SNC.	(Akassoglou *et al.*, 2000) (Siconolfi and Seeds, 2001b)
Spinal cord contusion	tPA increases secondary injury after spinal cord contusion and is involved in the activation of microglia and macrophages after injury.	(Abe *et al.*, 2003)

Table 1.3. *Alterations/involvement of the PA system in different neuropathological conditions.*

1.7.5. tPA and microglia.

Microglial activation is known to have an important role in the progression of neuroinflammation via release of a number of neurotrophic and particularly neurotoxic substances, which are thought to promote disease development (Kreutzberg, 1996). In recent years activation of microglia has been documented in a number of neuropathologies, including stroke, MS and AD. As tPA is stored and released from

microglia, it was of some interest to investigate its role in their activation. As previously discussed, $tPA^{-/-}$ mice are resistant to excitotoxin induced neuronal degeneration, in addition the same study revealed that microglia in these animals showed attenuated activation (Tsirka *et al.,* 1995). Microglia isolated from $tPA^{-/-}$ mice show attenuated activation in response to lipopolysaccharide (LPS) in culture, determined by morphological changes and upregulated expression of the surface antigen F4/80, and this effect of tPA on microglia appears to be independent of its proteolytic action (Rogove *et al.,* 1999). LPS-activated microglia produce conditioned medium which results in neuronal death, *in vitro.* This effect is inhibited by PAI-1 or by incubation with an anti-tPA antibody (Flavin *et al.,* 2000), suggesting that microglial tPA contributes significantly to hippocampal neuronal death. Under pathological conditions *in vivo*, it appears that injured neurones are the primary source of tPA, which acts as a cytokine to activate microglia, that in turn secrete additional tPA, promoting ECM degradation and neurodegeneration (Siao *et al.,* 2003). In EAE, although $tPA^{-/-}$ mice suffered worse clinical disease, they showed delayed and attenuated microglial activation when compared to the wild type (Lu *et al.,* 2002), indicating that in this situation microglia are releasing potentially beneficial substances such as growth factors and anti-inflammatory cytokines (Diemel *et al.,* 1998). High levels of NO are considered to be toxic to neurons and oligodendrocytes and are thought to play a role in a number of diseases, including MS. It has been shown that tPA derived from astrocytes can inhibit NO produced from activated microglia (Vincent *et al.,* 1998) providing a possible beneficial mechanism for tPA.

1.7.6. Plasminogen activators and Neuroinflammation.

Activation of serine proteases in inflammatory CNS lesions in MS is considered to play a major role in the disturbance of the BBB and subsequent leucocyte entry leading to inflammation and demyelination (Lo *et al.,* 2002; Teesalu *et al.,* 2001). Studies on human brain tissue homogenates (Gveric *et al.,* 2001) has revealed that antigen levels of uPA, uPAR and PAI-1 are significantly increased in normal appearing white matter (NAWM) and MS lesions compared to control brains. However, tPA, although being the most abundant plasminogen activator in normal control brains, was reduced in both MS white (WM) and grey matter (GM). tPA is immunolocalised on thick and damaged axons in active MS lesion borders but was confined to blood vessel walls in chronic lesions. In contrast, in a relapsing model of EAE in the Lewis rat induced by IL-12, tPA antigen and activity levels were found to rise during the acute phase and subsequent two relapses and the enzyme was primarily localised in inflammatory cells in perivascular infiltrates (Ahmed *et al.,* 2001). However, during the third relapse, a small decrease in tPA antigen levels was coupled with tPA immunolocalisation on axons overlapping with the areas of axonal death. Levels of PAI-1 and particularly tPA are increased in the CSF of MS patients (Akenami *et al.,* 1996; Akenami *et al.,* 1997). Although levels of tPA antigen have been shown to decrease in MS tissue, other studies have suggested expression levels are actually increased (Cuzner *et al.,* 1996). Akenami *et al.,* (1999) demonstrated an increase in tPA mRNA, particularly in neuronal cells, however whether tissue damage in MS is the cause or effect of increased tPA is not known.

Fibrin(ogen), a protein of the extracellular matrix with a broad range of biological functions, is not present physiologically in the nervous tissue. However in neuroinflammatory disease such as MS, there is evidence of fibrin exudation through a damaged BBB (Claudio *et al.,* 1995) followed by deposition on axons, which precedes

clinical symptoms of MS (Kermode *et al.,* 1990) and occurs prior to demyelination (Wakefield *et al.,* 1994). Co-localisation of tPA on demyelinated damaged axons stained with non-phosphorylated neurofilament and fibrin may indicate a role for tPA in axonal damage (Gveric *et al.,* 2001), paradoxically it may also indicate a protective role for tPA, via fibrin removal. Significant upregulation of the tPA inhibitor PAI-1 in MS tissue decreases the amount of enzyme thus affecting fibrin removal and axonal integrity (Gveric *et al.,* 2003). Fibrin deposition has been shown to hinder axonal regeneration in a model of peripheral nerve damage, (Akassaglou et al 2000), thus it is possible that the same applies in the CNS. Indeed more recently it has been proven that MS tissue, and in part NAWM, has impaired fibrinolytic capacity, leading to accumulation of fibrin products on axons (Gveric *et al.,* 2003). Under conditions of neuroinflammation it also appears that there are conflicting data proving an unclear message as to whether tPA is harmful or protective in this situation. A recent experiment investigated the role of tPA in EAE by using mice tPA knockout mice (Lu *et al.,* 2002). In these animals, the disease progression of EAE was significantly different to the wild type, and knockout mice had a delayed onset of disease which was more severe than the wild type. In addition, axonal degeneration and demyelination were delayed, but prolonged in the $tPA^{-/-}$ mice.

The role of fibrin in EAE has previously been investigated in the rat. Early studies by Paterson, (1976) demonstrated that perivascular fibrin deposits correlated to the occurrence of clinical paralytic signs, however neither paralytic signs nor fibrin deposition related to the development of perivascular cellular infiltrates. In addition, rats treated with ancrod, a defibrinogenating agent, showed a marked inhibition of fibrin deposits and exhibited no paralytic signs (Paterson, 1976). It has been shown more recently that increased BBB permeability and activation of the coagulation cascade occur one day before clinical signs of EAE and maximal fibrin deposition (Koh *et al.,*

1993). Recovery of BBB permeability and return of fibrin deposition to normal levels were demonstrated prior to complete remission of neurological signs (Koh *et al.*, 1993). Defibrination with batroxobin suppresses cell transferred EAE in Lewis rats (Inoue *et al.*, 1996) and in TMEV-induced demyelinating disease (Inoue *et al.*, 1997). Fibrin entry into the CNS during neuroinflammation occurs as a result of increased BBB permeability. Although the role of tPA on BBB breakdown has not been investigated in neuroinflammation, in a model of cerebral ischaemia tPA has been shown to induce increases in vascular permeability and opening of the BBB, via plasminogen and MMP-9 independent mechanisms, through LRP (Yepes *et al.*, 2003). This occurs possibly by a receptor-mediated cell signalling event although the exact mechanism has not yet been elucidated (Yepes *et al.*, 2003).

Although uPAR is largely undetectable in the normal brain, a significant increase in its expression is seen in MS tissue and NAWM. uPA-uPAR complexes are immunolocalised on inflammatory cells (monocytes and foamy macrophages) in the perivascular zone of evolving lesions (Gveric *et al.*, 2001), suggesting that uPAR may facilitate cellular infiltration into the CNS via proteolysis and ECM breakdown. This increase in uPAR may also initiate adhesion of inflammatory cells to blood vessel walls, thus amplifying focal uPA activity (Gveric *et al.*, 2001). uPAR expression on monocytes is increased in patients with CPMS and SPMS and also moderately in RRMS (Balabanov *et al.*, 2001). Expression of uPAR on peripheral monocytes markedly increases prior to onset of an exacerbation, and subsequently decreases (Balabanov *et al.*, 2001) suggesting that $uPAR^{+}$ cells are migrating into the CNS. Microglia isolated from MS patients display an increase in uPAR on the cell surface (Washington *et al.*, 1996) as uPAR is a marker for microglial activation (Beschorner *et al.*, 2000).

1.8. Aims of the thesis

Tissue plasminogen activator is thought to play a role in contributing to increased BBB permeability and neurodegeneration during the course of MS. Paradoxically, it can also promote neuronal survival through removal of fibrin deposits. Therefore, depending on the stimulus and surrounding microenvironment, tPA has the potential to be either a destructive or a beneficial agent in CNS injury and disease. In addition to roles in fibrinolysis, uPAR and PAI-1 are involved in cell migration and adhesion.

The aims of this project were to determine the role of the PA system on fibrinolysis and cell migration in an established chronic relapsing model of MS. Furthermore, these studies aimed to shed light on the endogenous fibrinolytic pathway as a potential therapeutic target by examining the disease pathology in a mouse model of MS, in the absence of this system. By developing EAE in tPA, uPAR and PAI-1 knockout mice, characterising inflammation, and investigating demyelination and axonal pathology, the functions of these molecules could be determined. Finally, in order to explain the variations observed in the different knockout genotypes of mice, the known functions of the PA molecules were studied to uncover how they act during neuroinflammation and neurodegeneration. Enzyme-linked immunosorbant assays (ELISAs) for tPA, PAI-1 and uPA, and Western blotting for plasminogen and fibrin, in addition to *in vitro* and *in situ* assays, were used to analyse the fibrinolytic capactity of control and diseased CNS tissue.

2. Materials and methods.

2.1. Mice.

$tPA^{-/-}$, $uPAR^{-/-}$, $PAI\text{-}1^{-/-}$ mice (Carmeliet P. *et al.,* 1993; Carmeliet P. *et al.,* 1994; Carmeliet P. *et al.,* 1995; Dewerchin *et al.,* 1996) and their respective wild type littermates (C57BL/6 x 129) (obtained from Professor H.R. Lijnen, Centre for Molecular and Vascular Biology, University of Leuven, Belgium) were bred in-house at the Institute of Neurology and screened by polymerase chain reaction (PCR). Biozzi ABH mice (Baker *et al.,* 1990) were from stock bred in-house. All mice were fed RM-1(E) diet and water *ad libitum*. All experiments were ethically performed according to the UK Animals (Scientific Procedures) Act (1984).

2.1.1 ABH Backcrosses.

Induction of MOG-EAE in $PAI\text{-}1^{-/-}$ and PAI-1 WT littermate mice on the C57BL/6 background revealed a very low incidence of disease (36 % and 25 % respectively). As it is important to have a true comparison of knockouts with WT littermates, mice deficient for PAI-1 were backcrossed for 4 generations into the ABH strain of mice. This yielded PAI-1 heterozygote ($PAI\text{-}1^{-/+}$) mice. By backcrossing the mice susceptibility rates are increased, as the C57BL/6 background is relatively resistant to EAE induction (Levine and Sowinski, 1973). Heterozygote animals were then paired up and resulting offspring produced $PAI\text{-}1^{-/-}$, $PAI\text{-}1^{-/+}$ and $PAI\text{-}1^{+/+}$ mice. The genotypes of mice were assessed using PCR to establish correct mice for breeding. To produce both knockout and WT littermate counterparts $PAI\text{-}1^{-/-}$ x $PAI\text{-}1^{-/-}$ and $PAI\text{-}1^{+/+}$ x $PAI\text{-}1^{+/+}$ breeding pairs were established. Following on from the homozygous breeding pairs, mice were routinely screened by PCR to confirm the integrity of the strain.

2.2. Polymerase Chain Reaction (PCR).

In order to ascertain the correct genotype of the mice, it was necessary to set up polymerase chain reaction (PCR) methods, which could be routinely performed on DNA extracted from tail snip samples. PCR is a technique for amplifying areas of DNA using complimentary fragments of DNA flanking the region of interest (oligonucleotide primers). Primer design requires knowledge of the DNA sequence of a gene. Complementary sequences are chosen at sites on the DNA, which are most unique to reduce the chance of primers binding to other regions on the template DNA. A primer length of 17-28 bp is required to ensure uniqueness and is usually composed of 50-60% G + C content. The first stage in PCR is whereby the DNA double helix is separated to single strand segments using a high temperature, usually between 91 and 97°C for 1 min, following which primers anneal to the single stranded DNA at specific temperatures related to their basic structure. The melting temperature (T_m) of primers depends on their length and composition of bases. The annealing temperature (T_a) is directly related to the Tm. These parameters are calculated by the following formulae:

$T_m = 4\ (G + C) + 2\ (A + T)\ °C$

$T_a = T_m - 4\ °C$

Most annealing temperature are in the range of about 50-65 °C. A higher temperature means the reaction is more stringent, with less chance of primer mismatch, however if the temperature is too high, then less product will be made. When using a combination of primers, the annealing temperature should be optimised to ensure the formation of non-specific low molecular weight products are minimised. After the annealing stage the temperature is then changed to allow activation of a heat-tolerant DNA polymerase, which extends the primer in a 5' to 3' direction using surplus free

deoxyribonucleoside triphosphates (dNTPs). A third temperature change denatures the DNA strands and the cycle can repeat, allowing the number of cycles to determine the degree of DNA amplification. The amplification is exponential up to a point then plateaus out, with DNA polymerase being the rate limiting factor. Taq DNA polymerase (from *Thermus aquaticus* bacteria) is heat stable and therefore ideal for this application. It has a half life of 30 min at 95 °C thus the number of amplification cycles shouldn't exceed 30 cycles without reducing the denaturation time. Taq polymerase requires the presence of free magnesium ions to function, with the magnesium acting as a cofactor. Lower concentrations of magnesium chloride ($MgCl_2$) increase the stringency of the reaction, thus $MgCl_2$ titrations should be performed with each new primer combination.

2.2.1. DNA Extraction.

Genomic DNA was prepared from the tails of mice that required screening. Tail snips (0.5 cm) were taken using Ethyl Chloride local anaesthetic (Roche, Ireland) and were digested by incubation overnight in 50µl 2mg/ml proteinase K (Invitrogen, Paisley, UK) and 450µl lysis buffer (400mM Tris/HCl, 60mM EDTA, 150mM NaCl and 1% sodium dodecyl sulphate (SDS), adjusted to pH 8 with 40% NaOH) in a heating block at 60°C (Techne-Dri block DB-2B, Cambridge, UK). The following day 188µl 5M sodium perchlorate was added and samples were incubated for a further 30min at 60°C. 750µl chloroform (VWR, Lutterworth, Leicestershire, UK), was then added and samples vortexed and centrifuged at 15,000 g (Eppendorf centrifuge 5425R, Eppendorf UK Ltd, Cambridge, UK) for 5 min. The upper aqueous phase was removed and transferred to fresh tubes containing 1ml absolute ethanol (VWR). These samples were incubated at 4°C overnight to precipitate the DNA. The following day samples were spun at 15,000 g in a centrifuge (Eppendorf) to pellet the DNA, the ethanol was

removed and the DNA was resuspended in 50μl diethyl pyrocarbonate -treated water (DEPC; Sigma, Poole, Dorset, UK).

2.2.2. PCR protocol.

PCR was set up in sterile PCR reaction tubes (Perkin-Elmer Applied Biosystems, Norwalk, USA; 8 tubes per strip) using a mastermix consisting of; 10 x PCR reaction buffer (200mM Tris-HCL pH 8.4, 500mM KCl; Invitrogen) 2mM dNTPs, 1.5 – 2mM $MgCl_2$ final concentration, 2.5 units of Taq DNA polymerase (Invitrogen) and 1mM forward and reverse primers. 4μl DNA was added per sample and the total volume made up to 50μl with DEPC-treated water. Primers were custom made (Qiagen, Crawley, Sussex, UK) (Table 2.1); and samples were cycled in PCR machine (GeneAmp 9700, Applied Biosystems) according to the protocols indicated in Table 2.2.

Primer name	Sequence
tPAfwd	5'-CGCTGTGTAACTCTTGCCCATGAGGAC-3'
tPArev	5'-GGAAAGGTGTGACTTACCGTGGCACCCAC-3'
PAIfwd	5'-GAGTGGCCTGCTA GGAAATTCATTC-3'
PAIrev	5'-GACCTTGCCAAGGTGATGCTTGGCAAC-3'
uPARko	5'-TTGATGAGACGCCTCTTCGGAGGAAC-3'
uPARwtfwd	5'-GTTACCTCGAGTGTGCGTCCT GCAC-3'
uPARwtrev	5'-CCACCATTGCAGTGGGTGTAGTTGC-3'
insert PgKpA cassette	5'-AATGTGTCAGTTTCATAGCC-3'

Table 2.1. *Oligonucleotide primers and their sequences used for genotyping knockout mice by PCR.*

Stage		tPA genotyping	PAI-1 genotyping	uPAR genotyping
Denaturing		94°C – 4 min	94°C – 4 min	94°C – 4 min
Denaturing	x 30	94°C – 1 min	94°C – 1 min	94°C – 1 min
Annealing		55°C – 1 min	57°C – 1 min	57°C – 1 min
Extension		72°C – 1 min	72°C – 1 min	72°C – 1 min
Extension		72°C – 10 min	72°C – 10 min	72°C – 10 min
HOLD		4°C	4°C	4°C

Table 2.2. *Cycling programs for genotyping of $tPA^{-/-}$, $uPAR^{-/-}$ and $PAI\text{-}1^{-/-}$ mice.*

Magnesium chloride titrations were performed to determine to optimum concentration for each reaction (Figure 2.1 A - C). Lower concentrations of $MgCl_2$ increase the stringency of the reaction. Following this it was found that 1.5 mM $MgCl_2$ most favourable for tPA primers, whilst 2 mM $MgCl_2$ was optimal for PAI-1 and uPAR primers. Primer annealing temperatures were used according to the melting temperatures of individual primer pairs.

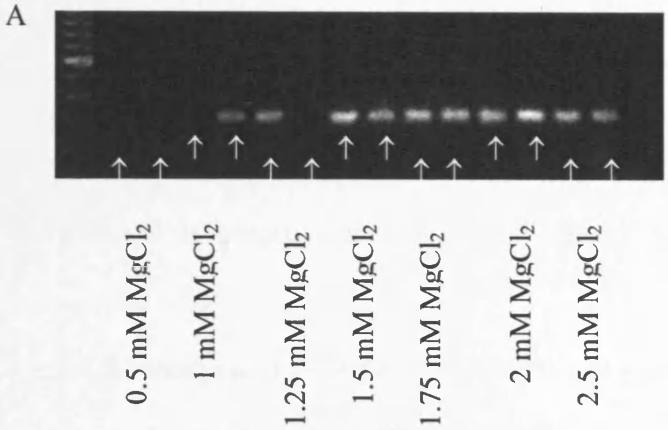

$MgCl_2$ titrations for tPA primers.

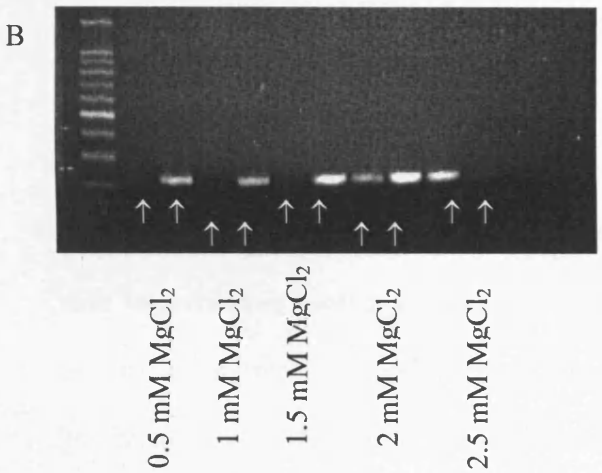

$MgCl_2$ titrations for PAI-1 primers.

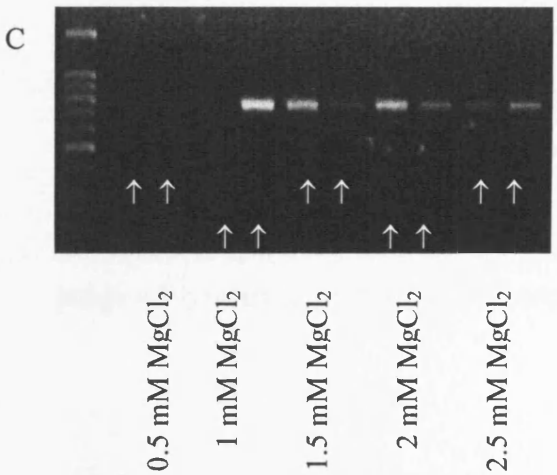

$MgCl_2$ titrations for uPAR primers.

Figure 2.1. *Magnesium chloride titrations for tPA, PAI-1 and uPAR primers.* Various concentrations of $MgCl_2$ (between 0.5 and 2.5 mM) were tested to investigate which were optimal for each set of primers. Optimal $MgCl_2$ concentrations were found to be 1.5mM for tPA primers and 2mM for PAI-1 and uPAR primers.

For tPA and PAI-1 reactions a multiplex system was used whereby three primers were added in one reaction to detect knockout and wild type DNA samples (Figure 2.2 and 2.3). For uPAR, two separate reactions were carried out, one to detect the knockout gene and the other to detect the wild type gene (Figure 2.4).

2.2.3. Analysis of PCR products by 1% agarose gel electrophoresis.

Separation of DNA fragments was performed on a 1% agarose gel, and visualised under ultra violet light using ethidium bromide. The sizes of PCR products were determined by comparison with a DNA ladder. Agarose (Sigma) in 1 x Tris-boric acid-EDTA (TBE) buffer (10 x solution; 1M tris, 0.1M boric acid, 0.01M EDTA; Invitrogen) with 0.5μg/ml ethidium bromide was prepared and poured into a gel box with well-forming combs, and allowed to set for 45 min. Once set, the combs and barriers were removed, and the gel was mounted in an electrophoresis box and immersed in 1 x TBE buffer. Samples and a 100 base pair DNA ladder (Promega, Southampton, UK) were prepared by diluting 5μl of PCR product/ladder with 5μl dH_2O and 2μl loading dye (Promega). Samples were loaded into separate wells, flanked by wells containing DNA ladder, and the gel was run at 110 volts for 1 hr and 30 min. After running, the gel was destained in dH_2O under agitation for 15 min, photographed using dedicated CoolSnapPro-cf monochrome camera and analysed using the GelPro image analysis package (Media Cybernectics, Berkshire, UK).

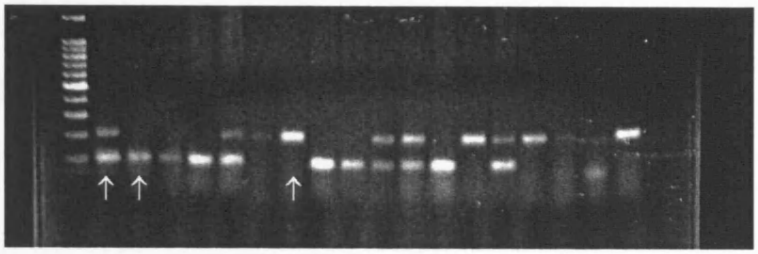

Figure 2.2. *PCR for tPA homozygous knockouts, heterozygotes and homozygous wild types.* DNA was extracted from tail snips samples with proteinase K and lysis buffer. Chloroform extracted DNA was precipitated in ethanol and resuspended in water. The DNA was amplified using PCR and subject to agarose gel electrophoresis. Lane one indicates a heterozygote, with two bands present at 200 and 100 base pairs (bp). Lane 2 shows a homozygote tPA wild type with one band at 100bp and lane 7 shows a homozygote tPA knockout with one band at 200bp.

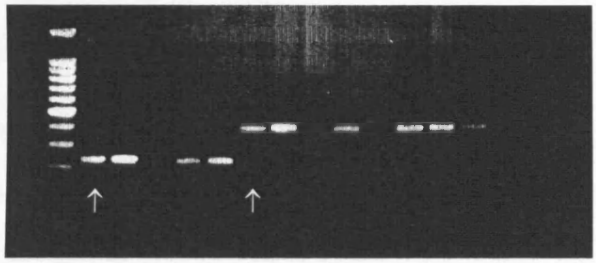

Figure 2.3. *PCR for PAI-1 homozygous knockouts, heterozygotes and homozygous wild types.* DNA was extracted as described above. The DNA was amplified using PCR and subject to agarose gel electrophoresis. Lane 1 indicates a PAI-1 homozygous knockout with one band at 190bp and lane 6 shows a PAI-1 homozygous wild type with one band at 400bp. This gel shows no heterozygous DNA, but this would be seen as two bands in the same lane, one at 190bp and the other at 400bp.

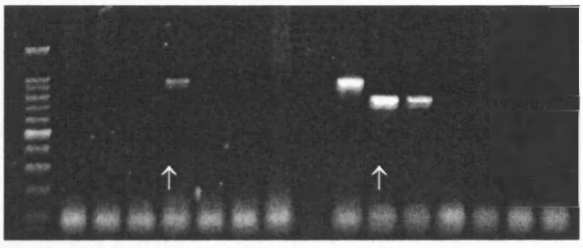

Figure 2.4. *PCR for uPAR homozygous knockouts, heterozygotes and homozygous wild types.* DNA was extracted as described above. The DNA was amplified using PCR and subject to agarose gel electrophoresis. Lane 4 indicates a uPAR homozygous knockout with one band at 970bp and lane 10 show a uPAR homozygous wild type with one band at 780bp.

2.3. Myelin Oligodendrocyte Glycoprotein (MOG) induced EAE.

Mice (6-8 weeks) received 300μg MOG peptide $_{35-55}$ (Met –Glu –Val –Gly –Trp -Tyr –Arg –Ser –Pro –Phe –Ser –Arg –Val –Val –His –Leu –Tyr – Arg – Asn –Gly - Lys; Advanced Biotechnology Centre, Imperial College, London) (Bernard *et al.,* 1997) injected into the flanks on day 0 and day 7. The peptide was emulsified in 300μl Incomplete Freund's adjuvant (IFA) (Difco, Beckton Dickenson, Oxford, UK) supplemented with 4mg/ml of *Mycobacterium tuberculosis* (H37Ra) (Difco). Mice were injected intraperitoneally with 300ng of reconstituted lyophilised *Bordetella pertussis* toxin (Sigma) in 200μl PBS on day 0. The pertussis toxin injection was repeated after 48 h. Mice were monitored and weighed daily.

2.4. Spinal cord homogenate induced EAE.

2.4.1. Making of spinal cord homogenate.

Spinal cords were removed from ABH mice under hydrostatic pressure. This involved decapitation of the mouse followed by an incision into the lumbar spinal column in the pelvic region. A syringe filled with 1 x PBS with a 20 gauge needle was wedged into the spinal column and the spinal cord expelled from the cervical column using hydrostatic pressure. Spinal cords were homogenised by hand using a glass homogeniser. The container was covered with parafilm with small holes in the top to allow water to sublimate. This was frozen overnight at -20°C, and freeze dried for 48 hours (Edwards Freeze drier, Crawley, Sussex, UK). Finally, the spinal cord homogenate was diced into a fine powder with a single edged razor blade and stored at -20°C until used.

2.4.2. EAE induction.

ABH and backcrossed ABH/PAI-$1^{-/-}$ and ABH/PAI-$1^{+/+}$ mice each received 1mg freeze dried spinal cord homogenate injected into the flanks on day 0 and day 7. The homogenate was emulsified in 300µl IFA (Difco) supplemented with 4mg/ml of *M. tuberculosis* (H37Ra) (Difco) and 1mg/ml *M. butyricum* (Difco). Mice were monitored and weighed daily.

2.5 Assessment of functional deficit in EAE mice.

2.5.1. Clinical scoring of mice.

Clinical disease was assessed and scored: 0 = normal, 1 = limp tail, 2 = impaired righting reflex, 3 = partial paralysis of hindlimbs, 4 = complete paralysis of hindlimbs and 5 = moribund/death. In addition, intermediate scores were given when appropriate. 0.5 = loss of tail tonicity, 1.5 = slower than normal righting reflex, 2.5 = hindlimb weakness, 3.5 = paralysis of one hindlimb and paresis in the other. The mean day of onset, mean maximal score, mean score at experiment termination and the incidence of relapse were calculated from the data. Accompanying these signs in ABH and ABH backcrossed mice, weight loss occurred 1 – 2 days prior to onset of disease and is an accurate predictor of changes in disease, with animals regaining weight prior to recovery in remission (Baker *et al.,* 1990). Weight loss in the C57BL/6 strain of mice is not that apparent therefore not used as a predictor of disease onset. Signs of tail spasticity included stiffness, curling and flicking and was visually assessed as being either present or absent. For specimen collection, mice were killed with carbon dioxide and immediately perfused intracardially with PBS. Spinal cords were removed under hydrostatic pressure and brains were dissected out. Once removed, the tissue was immediately snap frozen on dry ice, wrapped in foil and stored at -70°C until used.

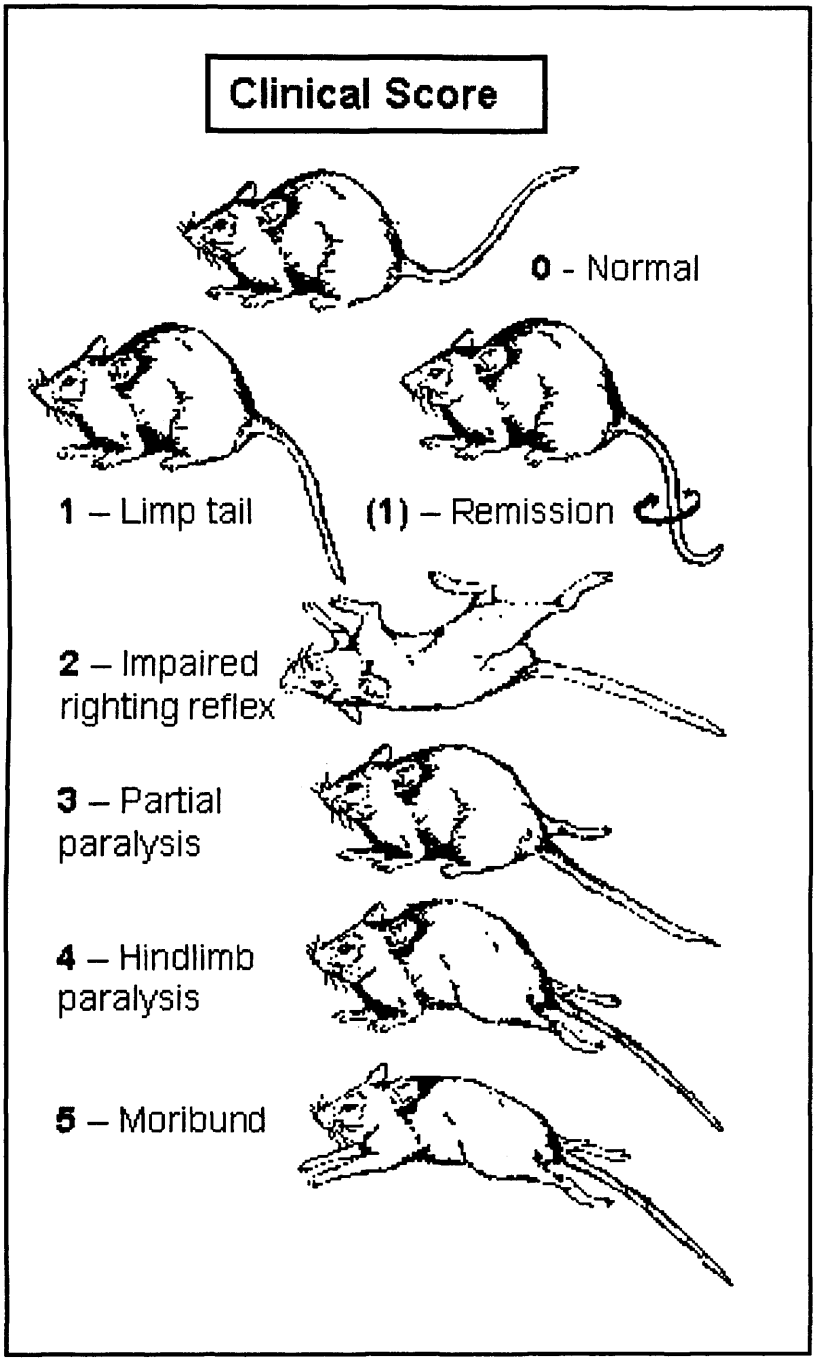

Figure 2.5. *The clinical scoring criteria in MOG_{35-55} or spinal cord homogenate induced EAE.* Signs become more severe as the disease course progresses. Used with permission of David Baker.

2.5.2. Movement in an open-field activity chamber.

Movement activity of mice was carried out to investigate motor dysfunction and the degree of neurological impairment, which was found in previous studies to be closely correlated with axonal damage (Pryce *et al.*, 2003). Mice were placed in a 27 x 27 cm open-field activity chamber (Med Associates, Georgia, VT, USA) at 35 days post EAE induction (dpi) for all groups of mice and at 60 dpi for MOG-induced EAE. The movement around the chamber was recorded over a 5 min period and the total distance travelled (cm) per mouse was noted. Non-injected mice of each genotype were used as controls as mice injected with MOG or SCH which developed no EAE disease had comparable levels of activity to non-injected mice. Control $tPA^{-/-}$ mice were significantly more active than control WT mice thus all data for EAE mice was normalised to the appropriate control and expressed as a percentage of that control.

2.6. Immunohistochemistry.

2.6.1. Slide preparation.

Super premium twin frost glass slides (VWR) for immunocytochemical staining were coated with Vectabond reagent (Vector Laboratories, Peterborough, UK) according to manufacturer's instruction. Briefly, 2% Vectabond solution was prepared by mixing 7ml of Vectabond with 350ml of acetone (VWR). Slides were thoroughly washed in soapy water followed by distilled water, before being left to air dry. Slides were then immersed in acetone for 5 min. A coating solution of 2% Vectabond in acetone was applied for another 5 min. Slides were briefly washed in distilled water and dried at 37°C overnight.

2.6.2. Haematoxylin and eosin staining.

Haematoxylin and eosin (H & E) staining was used to assess the extent of inflammatory infiltration and cellularity in EAE sections. Unfixed sections mounted on glass slides were placed in Harris haemotoxylin (Sigma) for 3 min and then blued briefly with running tap water. Slides were dipped into acid alcohol (1% v/v HCl in 70% ethanol) 10 times and then washed again for 2 min in cold running water. Finally, slides were counterstained in eosin (VWR) for 30 s, dehydrated through graded ethanol solutions (95% followed by 2 x 100% solution) and xylene (VWR) for 45 sec each, followed by a further 3 min in xylene. Finally slides were mounted in DPX (VWR) and left to dry overnight.

2.6.3. Histopathological evaluation.

To assess the extent and degree of infiltration of inflammatory mononuclear cells into the spinal cord during EAE, the total number of perivascular cuffs was counted in a spinal cord longitudinal section area of $4cm^2$. Each cuff was given a score according to the degree of cellular infiltration, to gain a semi-quantitative measure of inflammation as follows; 1, perivascular inflammation three or fewer cells deep; 2, more than three cells deep; 3, parenchymal infiltrate. The average cuff count and score was taken from a total of three slides from different mice per time point.

2.6.4. Preparative techniques: choice of tissue fixative and antibody titration.

Adequate and complete fixation forms the foundation of all good histological preparations and its aim is to preserve the tissue antigens as far as possible in their native structure. Four protocols were tested to assess the effects of different fixatives on antigen-antibody reaction. Each reagent was initially tested under three different temperature conditions with antibody markers for neurofilament, and MBP as internal

controls (Table 2.3). Based on the clarity of cellular staining, tissue structure preservation, low background signal and suitability for both single and double immunocytochemisty, methanol at -20°C for 5 min was adopted as the protocol of choice. Aldehydes were typically not used as they are known to reduce antibody detection of many antigens (Baker *et al.*, 1990).

Fixative	RT	4°C	-20°C
Ethanol	++	+	-
Methanol	++	+++	+++
Acetone	-	+	-

Table 2.3. *Assessment of different fixation protocols.* Key: - poor, + good, ++ satisfactory and +++ excellent.

Optimal binding conditions for primary antibodies were established by applying a range of dilutions to sections of normal and EAE CNS tissue. Initial dilutions for monoclonal antibodies were 1:20, 1:50, 1:100 and 1:200 and for polyclonal antibodies 1:200, 1:500, 1:1000 and 1:2000. Further titrations after these initial dilutions were carried out if necessary. The optimum dilution was considered to be the antibody concentration which gives a clear staining pattern and a low background signal (Table 2.4).

Antibody	Cell specificity	Isotype	Dilution	Source and reference
mAb SMI-35	Phosphorylated neurofilament	IgG1	1 in 10000	Sternberger monoclonals
mAb SMI-32	Non-phosphorylated neurofilament	IgG1	1 in 2000	Sternberger monoclonals
Rabbit ∝-MBP	Myelin basic protein	Polyclonal	1 in 2000	Chemicon (Chandlers Ford, Hampshire, UK)
Rat ∝-CD45	All haemopoietic cells, leucocyte common antigen	IgG2b	1 in 2000	Serotec (Kidlington, Oxford, UK)
Rat ∝-CD8	Cytotoxic T cells and macrophages	IgG2b	1 in 500	(Cobbold *et al.*, 1984)
Rat ∝-CD4	Th1 and Th2 cells	IgG2b	1 in 1000	(Cobbold *et al.*, 1984)
Rat ∝-F4/80	Microglia and macrophages	IgG2b	1 in 50	Serotec
Goat ∝-Fibrinogen	Fibrin(ogen)	Polyclonal	1 in 10000	Sigma
Rabbit ∝-uPA	Urokinase plasminogen activator	Polyclonal	1 in 1000	Prof. H.R. Lijnen
mAb ∝-PAI	Plasminogen activator inhibitor	IgG	1 in 100	(Declerck *et al.*, 1995)
mAb ∝-uPAR	Urokinase plasminogen activator receptor	IgG1	1 in 100	Axis Shield Diagnostics (Dundee, UK)
Rabbit ∝-GAP43	Growth-associated protein	IgG	1 in 5000	Abcam (Cambridge, UK)
Rabbit ∝-MAP2	Microtubule-associated protein	Polyclonal	1 in 1000	Santa Cruz (Insight Biotech, Wembley, UK)
Goat ∝-PSD-95	Post-synaptic density protein -95	Polyclonal	1 in 100	Santa Cruz
mAb ∝-synaptophysin	Synaptophysin	IgG1	1 in 200	Sigma

Table 2.4. *Characteristics and source of antibodies used in immunohistochemistry.*

2.6.5. Single immunocytochemical staining.

A three step peroxidase method was employed for single immunohistochemical staining. Cryostat sections (10-μm) cut onto Vectabond-coated slides, were fixed in methanol (-20°C, 5 min) and blocked with 2.5% normal serum diluted in phosphate buffered saline (PBS, 0.15M NaCl, 100mM $K_2HPO_4.3H_2O$ and 20mM KH_2PO_4, pH 7.4) for 1 hour at room temperature (RT). The blocking serum used was dependent on the animal in which the secondary antibody was raised. Blocking serum was tipped off and sections were incubated overnight at 4°C with primary antibodies in PBS. The following day slides were washed 3 x 5 min in PBS on a magnetic stirrer and sections were incubated with biotinylated secondary antibodies (1:100, Vector) for 1 h at RT. Peroxidase-labelled avidin and biotin reagents (ABC; Vector) were mixed at 1:100 in PBS and pre-incubated for 30 min according to the manufacturer's instructions to ensure formation of complexes. After a further three washes in PBS, the avidin-biotin solution was incubated on slides for 1 h at RT. The peroxidase substrate was prepared by mixing 0.05% (w/v) 3,3'-diaminobenzidine tetrahydrochloride (DAB, Sigma), 0.04% (w/v) $NiCl_2$ and 0.02% (v/v) hydrogen peroxide in 400 ml PBS immediately before use. Sections were incubated in the nickel-enhanced peroxidase substrate for 5 min giving a black colour where antigen was immunolocalised. Slides were washed in tap water for 5 min, dehydrated through graded ethanol solutions (95% followed by 2 x 100% solution) and xylene for 45 s each, followed by a further 3 min in xylene. Finally slides were mounted in DPX (VWR) and left to dry overnight. Omission of primary antibody, secondary antibody or ABC complex was routinely used as controls. Isotype matched controls were also used as controls and failed to show any staining, as previously shown by (Baker *et al.,* 1990).

2.6.6. Semi-quantitative analysis of demyelination and axonal pathology.

For semi-quantitative analysis of demyelination, sections stained with anti-MBP antibody were examined using a Quantimet 500 image analyzer (Leica Microsystems Imaging Solutions Ltd, Cambridge, UK) attached to a Zeiss microscope (Zeiss, Hertfordshire, UK). Four random fields per section were studied with three or four sections per group. The results were expressed as the amount of light transmittance through a stained portion of section normalized to a non-stained area of the slide. Axonal pathology was assessed by counting the number of SMI32 positive axons in randomly selected areas of spinal cord white matter from control and EAE mice at x 400 magnification. Four areas were counted by two independent observers per section with three sections per group. In all instances the results were consistent between the different observers.

2.6.7. Single immunocytochemistry for CD45, CD8, CD4 and F4/80.

For immunohistochemical staining for CD45, CD8, CD4 and F4/80 a slightly different method was employed (Baker *et al.,* 1990). Primary antibodies were diluted in 5% normal mouse serum to eliminate the blocking stage, and incubated on the sections for 1 h at RT. Following 3 x 5 min in PBS, a rabbit $\propto$ rat biotinylated secondary antibody was diluted 1 in 100 in 5% normal mouse serum and incubated on the sections for 1 h at RT. Peroxidase-labelled avidin and biotin elite reagents (Vector) were mixed at 1:50 in 5% normal mouse serum and pre-incubated for 30 min according to the manufacturer's instructions to ensure formation of complexes. After a further three washes in PBS, the avidin-biotin solution was incubated on slides for 30 min at RT. Finally a swine $\propto$ rabbit horse radish peroxidase (HRP) labelled antibody was diluted 1 in 50 in 5% normal mouse serum and incubated on the sections for 30 min at RT. This was used to enhance and amplify the signal from the primary antibody. The peroxidase

substrate was prepared as described above, however DAB substrate without nickel was used for CD45, CD8, CD4 and F4/80 staining and slides were counterstained in Mayer's haematoxylin (HD scientific supplies, Aylesbury, UK) for 30 s. Slides were dehydrated and mounted as described in section 2.6.5.

2.6.8. Double immunocytochemical staining.

Double immunocytochemical staining was performed using immunofluorescence. Sections were fixed in the same way as described for single staining and blocked with 2.5% normal horse serum for 1 h at RT. A mixture of two antibodies (SMI32, 1:2000 and goat ∝ fibrinogen, 1:5000) in PBS were added to the sections and incubated overnight at 4°C. The following day after 3 x 5min wash in PBS, sections were incubated with horse ∝ mouse biotinylated secondary antibody (1:200, Vector) in PBS for 1h at RT. Following another washing stage a mixture of fluorescent antibodies were added to the sections for 1h at RT, avidin fluorescein isothiocyanate (FITC) DCS (1:200, Vector) and rabbit ∝ goat IgG tetramethylrhodamine isothiocyanate (TRITC) (1:20, Sigma) in sodium bicarbonate buffer (100mM NaH_2CO_3, pH 8.5). After a final wash sections were mounted in Citifluor® anti-fade reagent (Citifluor Ltd, London, UK). Sections were examined under a fluorescent microscope. Single fluorescent staining with each primary antibody was carried out as a control. Omissions of primary, secondary and fluorescent antibodies were also routinely employed as controls.

2.6.9. Immunofluorescent staining for tight junction proteins.

Double staining for tight junction proteins using immunofluorescence was performed by Dr. Arie Reijerkerk of the Department of Molecular Biology and Immunology, VU medical Centre, Amsterdam, to investigate changes in the BBB

before and during EAE onset. Cryostat sections (10-μm) cut onto Vectabond-coated slides, were fixed in acetone (RT, 15 min) and blocked with 20% normal goat serum diluted in 1 x PBS containing 1% bovine serum albumin (BSA) for 20 min at room temperature (RT). Primary antibodies, mouse ∝ claudin-5 (Zymed, Sam Fransisco, CA, USA), or mouse ∝ occludin (Zymed) were diluted 1 in 100 in PBS-1% BSA, and incubated on the sections overnight at 4°C. Following 3 x 5 min washes in PBS-1% BSA a biotinylated goat ∝ mouse secondary antibody was diluted 1 in 500 in PBS-1% BSA and incubated for 1 h at RT. Following another washing stage, a 1 in 500 dilution of the fluorescent antibody ∝ goat Alexa 546 (Molecular Probes, Leiden, Netherlands) was added to the sections for 1 h at RT. Following 3 x 5 min washes in PBS-1% BSA a rabbit ∝ laminin antibody (MP Biochemical Inc., Eschwege, Germany) was diluted 1 in 100 in PBS-1% BSA and incubated on sections for 1 h at RT. After a further washing stage, a 1 in 500 dilution of a second fluorescent antibody, ∝ rabbit Alexa 488 (Molecular Probes) was added to the sections for 1 h at RT. After a final washing stage, slides were mounted in Citifluor and examined under a fluorescent microscope.

2.7. Protein Extraction.

Snap frozen samples of spinal cord from EAE and control mice were weighed, finely cut and resuspended at 1:10g wet weight/ml in Tris-HCl buffer pH7.4 (100mM Tris, 5mM EDTA, 150mM NaCl, with 1% Triton X-100). Samples were homogenised using a high-intensity ultrasonic processor (Jencons Scientific Ltd, Leighton Buzzard, UK) and incubated on ice for 30 min. The tissue suspensions were spun at 15,000 g in an Eppendorf centrifuge for 60 min at 4°C and the supernatants collected at stored in aliquots at -70°C.

2.7.1. Protein measurement.

The total protein concentration of spinal cord homogenates was determined by the Folin phenol method (Lowry *et al.,* 1951), which is based on a two-step colour reaction. In an alkaline solution copper associates with protein and subsequently reduces the Folin reagent to form a blue coloured product. To maximise the colour resulting from the reduction, 0.4M sodium hydroxide is present to neutralise any acid released on addition of the Folin's solution and sodium carbonate is added to buffer the reagents to an optimal pH of 10. The optical density, read at 750nm, is proportional to the copper bound protein.

For protein analysis an aliquot of each sample was thawed on ice and diluted to 1 in 30 using 0.05M NaOH. Standards of bovine serum albumin (BSA) fraction V (Sigma) were prepared (0, 5, 10, 15, 20 and 30 μg/ml) in a volume of 150μl. Samples and standards were assayed in duplicate. 50μl of each diluted sample was placed in a 10ml conical tube (Fisher Scientific, Loughborough, UK) with 100μl distilled water. 50μl 0.4M NaOH was added to each tube (standards and samples), followed by 1ml of freshly prepared solution X (2% Na_2CO_3, 0.02% K_2 Tartrate in 0.1M NaOH added to 1% $CuSO_4.5H_2O$ in a ratio of 99:1). All tubes were vortexed, and left for 15min. 100μl of Folin and Ciocalteu's reagent (Lowry *et al.,* 1951) (diluted 1:1 with water; VWR) was added to each tube. After vortex mixing the tubes, they were incubated in the dark for a further 30 min. The absorbance of each sample was read on an Ultraspec 2000 spectrophotometer (Amersham Pharmacia Biotech UK Ltd., Little Chalfont, Buckinghamshire, UK), with water as a reference reading repeated in between samples. The generation of a linear standard curve allowed conversion of optical density to μg of protein per sample, any samples with concentrations above the level of the standard curve were re-assayed with a 1:50 dilution.

2.8. Western blotting.

Western blotting is a technique for quantifying specific protein levels in a given sample. This technique entails running the protein in a sample through a gel under high electrical current to separate protein by molecular weight – smaller proteins will travel further than large proteins in a given time. These are then transferred on to a membrane and probed with antibodies raised against the protein of interest. Bands on an autoradiograph can then be quantified using computer imaging techniques.

40μg of supernatant proteins (3-6 μl) were diluted in reducing or non-reducing sample buffer (Reducing; 2% sodium dodecyl sulphate (SDS), 10% glycerol, 2.5% β-mercaptoethanol, 125M Tris-HCl pH 6.8, 0.02% bromophenol blue, Non-reducing; same as before, expect without β-mercaptoethanol), denatured at 100°C and loaded onto a 5% stack, 5 or 10% resolve sodium dodecyl sulphate-polyacrilamide gel (Bio-Rad, Hemel Hempstead, Hertfordshire, UK) which were placed in a Biorad Mini-Protean 3 gel-electrophoresis tank. The chamber and wells were filled with 1 x running buffer (0.25M Tris base, 1.92M glycine, 1% SDS). The gel was then run at 180 volts for ~ 45min until the bromophenol blue dye front had reached the bottom of the gel. Following removal of the gel, it was equilibrated in transfer buffer (0.25M Tris base, 1.92M glycine, 20% methanol and 0.1% SDS) for 20 min along with a piece of Immobilon-P polyvinylidene difluoride membrane (Millipore, Bedford, UK) which had previously been activated in ice cold methanol for 1 min. Mini Protean 3 fibre pads and 3mm blotting paper were also soaked in transfer buffer. The transfer sandwich was constructed according to the manufacturer's instructions, and loaded into the transfer block. This was then immersed in transfer buffer in the Mini Protean 3 chamber and proteins transferred to the membrane for 1 hour at 80 volts for 5 % gels or overnight at 22 volts for 10 % gels. When using an overnight transfer, an ice block was added into the transfer chamber to reduce heat production from the electric current. Following

removal of the membrane and a 1 x 10 minute wash in Tris-buffered saline with Tween-20 (T-TBS; 0.01M Tris-HCl, pH 7.4, 0.15M sodium chloride, 0.05% tween-20 (Sigma)), non specific binding sites on the membrane were blocked with 5% Marvel ® dried fat free milk (Premier International Food (UK) Ltd, Lincolnshire, UK) dissolved in T-TBS for 1 h at RT. Following 1 x 10 min wash in T-TBS, the primary antibody of interest was diluted in 5% Marvel in T-TBS and incubated with the membrane for 2 h at RT (Table 2.5). After washing 3 x 10 min in T-TBS, the membrane was incubated with the secondary antibody which was coupled to horseradish peroxidase (HRP); ∝ mouse IgG HRP (1:1000, Affinity Bioreagents, Cambridge, UK), ∝ rabbit IgG HRP (1:1000; Amersham Biosciences) or ∝ goat IgG HRP (1:1000, Santa Cruz) for 1 h at RT. After 3 x 10 min washes in T-TBS, the blots were developed by enhanced chemiluminescence (ECL, Amersham Biosciences) for 1 min according to the manufacturers instructions. The blot was the visualised using ECL x-ray film (Amersham Biosciences) with exposures of 1, 2, 5, 8 or 10 min. Film was placed in Kodak developer solution (Sigma) until there was a good contrast between the bands and the background (~2 min), and fixed in Kodak reagent (Sigma) for 5 min. Blots were analysed using the GelPro software package and the density measured in arbitrary units. Blots probed with secondary antibody only were used as control to check for non-specific binding (Figure 2.6).

Antibody	Specificity	Dilution	Source	Conditions
mAb ∝ fibrinogen Clone 85D4	Fibrinogen, fibrin monomers, D-dimer and D-fragment.	1 in 1000	Sigma	Non-reducing 5 % gel
Rabbit ∝-Plasminogen	Plasminogen, pre-activation.	1 in 1000	Dako	Non-reducing 10 % gel
Rabbit ∝-laminin	Laminin – component of basement membranes.	1 in 1000	Sigma	Reducing 5 % gel
mAb ∝-synaptophysin Clone SVP-38	Synaptophysin, a synaptic vesicle protein.	1 in 1000	Sigma	Reducing 10 % gel
Rabbit ∝-GAP43	Growth associated protein expressed by regenerating neurons.	1 in 1000	Abcam	Reducing 10 % gel
Rabbit ∝-MAP-2	Microtubule associated protein 2.	1 in 1000	Santa Cruz	Reducing 10 % gel
Rabbit ∝-Neuroserpin	Neuroserpin	1 in 1000	Dr. DA Lawrence	Reducing 10 % gel
Goat ∝-annexin II	Annexin II	1 in 2000	Santa Cruz	Reducing 10% gel
mAb ∝-LRP	LRP heavy chain	1 in 1000	Calbiochem, VWR.	Non-reducing 5% gel
mAb ∝-β-actin Clone AC-15	β isoform of actin (nonmuscle).	1 in 1000	Sigma	N/A

Table 2.5. *Antibodies used in Western blotting*; their specificity, dilution and conditions for investigation.

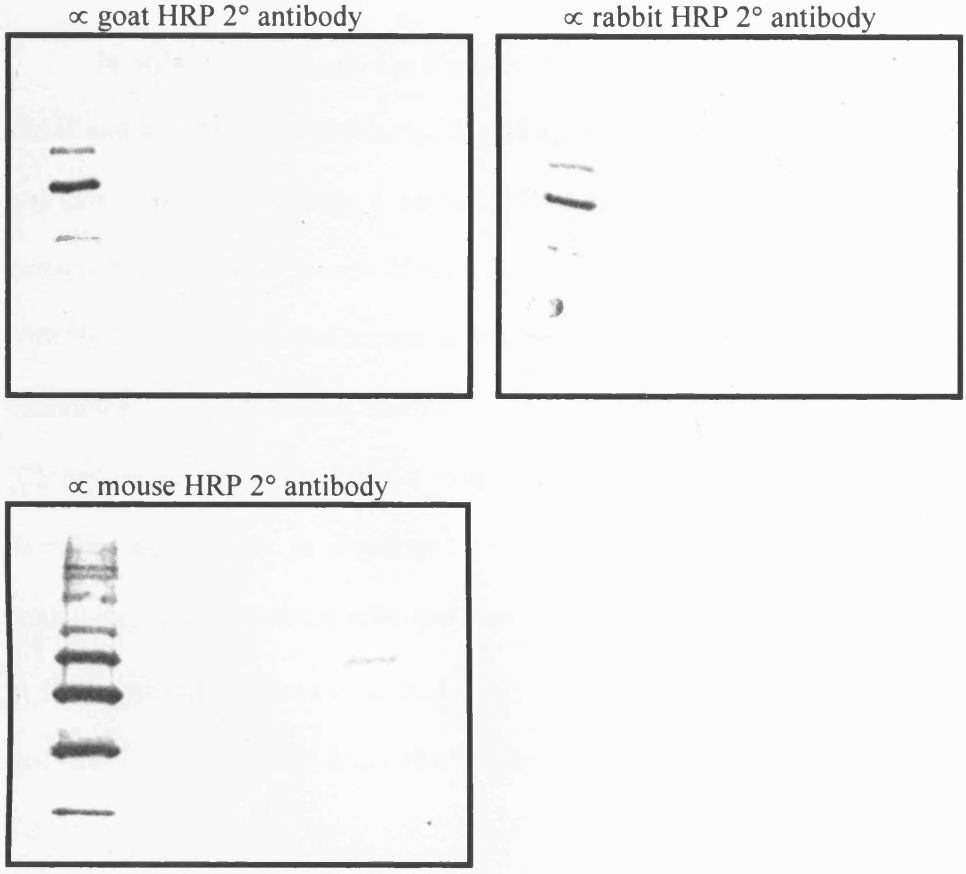

Figure 2.6. *Secondary antibody controls for Western blotting.* Protein samples were run on 10 % Tris-HCL gels under reducing conditions and transferred overnight onto PVDF membranes. The following day blots were blocked with 5% Marvel in T-TBS for 1 h at RT. After washing, membranes were incubated with an ∝-goat, ∝-rabbit or ∝-mouse secondary antibody conjugate to HRP. Following washing, blots were developed using ECL solution and exposed to photographic film under safe light. Secondary antibodies bound in a specific manner and produced no non-specific bands.

2.9. Clot Lysis Assay.

In order to investigate the fibrinolytic capacity of different CNS tissue extracts, and if and how this changed during experimental neuroinflammation, a clot lysis assay was carried out as previously described (Urano *et al.,* 1996). Spinal cord tissue protein extracts were mixed 1:10 with dilution buffer (50 mM Tris, 0.2% Triton X-100, pH 7.4 with HCl). 40 µl of diluted sample or standard was mixed with 360 µl of dilution buffer containing 7.3 µM human fibrinogen (Sigma), 0.25 µM human lys-plasminogen (Chromogenix, Milan, Italy), 1.7 mM $CaCl_2$, 0.7 mM $MgCl_2$ and 12.5 mM NaCl. Samples were added in duplicate (180 µl per well) to 96-well microtitre plates containing 20 µl human thrombin per well (100U/ml, Sigma, Dorset, UK) and incubated at 37°C. Absorbance was measured at 405 nm in 15/30 min intervals for 4 h and at 17, and 24 h for samples from $tPA^{-/-}$ mice. Human recombinant tPA (2 mg/ml; Technoclone, Dorking, Surry, UK) mixed with dilution buffer was used as a positive control, whilst omission of sample or plasminogen in the buffer was used as a negative control.

2.10. Neurofilament enzyme-linked immunosorbant assay (ELISA).

Disruption of neurofilament phosphorylation and transport are common features of many neurological conditions. Staining for phosphorylated neurofilaments (SMI34 or SMI35) is increased in MS, however total neurofilaments are decreased in CREAE (Pryce *et al.,* 2003), correlating with neurological impairment. In order to quantify phosphorylated neurofilament an ELISA was carried out as described by (Petzold *et al.,* 2003b). A 96-well microtitre plate (Maxisorp, Nunc, Rochester, NY, USA) was coated overnight at 4°C with SMI35 anti-heavy chain neurofilament antibody (1:1000, Sternberger Monoclonals Inc., Lutherville, MD, USA) in sodium carbonate buffer (0.025M sodium carbonate, 0.025M sodium bicarbonate, pH 9.7 with 1N HCl or 1N

NaOH). After bringing the plate up to RT, non-specific binding was blocked by incubation with 200µl of 1% BSA in barbitone buffer (63mM sodium barbital, 11mM barbital and 1.2mM EDTA) to each well for 1 h at RT. Following blocking, the plate was washed in barbitone buffer containing 0.2% BSA and 0.05% Tween-20. Spinal cord protein extracts were serially diluted from neat to 1:100,000 in barbitone buffer and a standard curve was prepared from serially diluting porcine neurofilament (Chemicon) (0.16 – 10 ng/ml). The final standard concentration was zero, using diluent alone to control for background activity. Samples and standards were incubated at RT for 2 h under gentle agitation. After washing 4 times as above, the detect antibody (rabbit polyclonal anti-neurofilament H antibody, Sigma) was diluted 1:1000 and then added at 100µl per well for 1 h at RT under gentle agitation. Following 4 further washes, horseradish peroxidase-conjugated anti-rabbit immunoglobulin (Amersham Biosciences) was diluted 1:1000 in diluent as before and 100µl added to each well before incubating for 1 h under gentle agitation at RT. Tetramethylbenzidine (TMB) chromogenic substrate reagent (R&D Systems UK Ltd., Abingdon, UK) was removed from refrigeration and prepared in a light-excluded 50 ml centrifuge tube to allow it to rise to room temperature. Following 4 final washes, 100µl of substrate was added to each well before stopping the reaction with 1M phosphoric acid. The plate was read on a 96-well spectrophotometer (Anthos Labtec Instruments, Salzburg, Austria) with the absorbance set at 450 nm, and a reference reading at 620 nm. All samples were analysed in duplicate.

Using Microsoft Excel, an equation representing the standard curve was determined, and used to predict the concentration of NF in each sample from the optical density reading. This figure was then divided by the total protein for that sample, as determined by the Folin phenol method, to give the concentration of NF per mg protein.

In this way differences in protein concentration caused by non-identical samples were normalised, allowing direct comparison of samples.

2.11. ELISAs for PAI-1, tPA and uPA.

In order to investigate levels of tPA, PAI-1 and uPA, under control and experimental neuroinflammatory conditions, ELISAs were performed in collaboration with Professor Roger Lijnen, Centre for Molecular and Cardiovascular Biology, KU Leuven, Belgium. For ELISAs Costar 96-well plates were coated with mouse antibodies against PAI-1, tPA or uPA at 4μg/ml for 48h at 4°C (Declerck *et al.,* 1995). The wells were blocked with 1% BSA in 1 x PBS overnight at 4°C and plates were then washed with 1 x PBS tween 80 (0.004%). Protein extract samples and standards were diluted in 1 x PBS containing 0.004% tween 80, 0.1% BSA and 5mM EDTA, and were added 180μl/well and incubated overnight at 4°C. Samples were diluted 1 in 7.2 and standard curves range from 0.023 - 3 ng/ml (PAI-1), 0.078 - 10 ng/ml (tPA) and 0.156 - 20ng/ml (uPA). After washing a biotinylated secondary antibody (PAI-1, tPA or uPA) was added for 1 hour at 37°C. After addition of the avidin-biotin peroxidase complex (ABC; Vector) for 1 hour at room temp, plates were developed using *o*-phenylenediamine, and the reaction was stopped using 4M sulphuric acid. Absorbance was read at 490nm with a reference reading at 650nm.

2.12. *In situ* zymography on fibrin overlay.

In situ zymography was carried out on 10μm cryosections of normal and EAE spinal cords as previously described (Lijnen *et al.,* 1998), in order to investigate the *in situ* fibrinolytic capacity of spinal cord tissue from different genotypes of mice at various time points of EAE disease. A gel was prepared by clotting a mixture of human fibrinogen (final concentration 4 mg/ml), plasminogen (final concentration 10μg/ml),

and agarose (final concentration 0.5%) with thrombin (final concentration 0.3NIHU/ml). A thin overlay of gel was added onto cryostat sections of control and EAE spinal cord and allowed to set. Zymography was performed in a wet box at 37°C for 2 hours. The lysis of substrate was quantified using computer-assisted image analysis (Zeiss, Axioplan 2). The lysis area was normalised to the total section area.

2.13. Statistical analysis.

Data was analysed with the GraphPad Prism computer package (GraphPad Software, San Diego California, USA). A normality and quality of variance test was carried out on all data to determine which test was appropriate. A t-test, for normally distributed data sets, or a Mann-Whitney U test, for non-parametric data, was used with significance level set at 95 %. If variances of data sets were significantly different, then Welch's correction was applied to correct for this. All values are indicated as the mean ± standard error of the mean (SEM). P-values were taken as an indicator of statistical significance with the following nomenclature: * - $P < 0.05$, ** - $P < 0.01$ and *** - $P < 0.001$. The parametric Pearson's correlation test was used for the regression analysis and the r value given where appropriate. Individual n-numbers are given in each results chapter.

3. Fibrinolysis and the plasminogen activator system in ABH mice during chronic relapsing EAE.

3.1. Introduction.

Chronic relapsing EAE (CREAE) in Biozzi antibody high (ABH) mice is a well established experimental neuroinflammatory disease model, induced by sensitisation to CNS homogenate. It is highly reproducible, with pronounced periods of relapse and remission. Mice in the acute and relapse stages of disease have a high number of inflammatory mononuclear cells present in the spinal cords, but rarely in the brains, which resolve during periods of remission (Baker *et al.,* 1990). The histology of CREAE in ABH mice, the mononuclear cell trafficking, BBB permeability and cytokine profile are all well characterised (Allen *et al.,* 1993; Baker *et al.,* 1990; Butter *et al.,* 1991). The role of the fibrinolytic system in EAE has been previously investigated in BALB/c mice, a strain relatively resistant to EAE induction, where clinical disease is typically short, acute and monophasic (Teesalu *et al.,* 2001). In that study, upregulation of tPA, PAI-1 and uPAR and accumulation of fibrin correlated to the peak of paralytic disease (Teesalu *et al.,* 2001). However, the role of the plasminogen activator system in CREAE in ABH mice has not been investigated. It is becoming increasingly evident that neuronal and axonal loss are characteristic of MS, thus it was important to utilise a model where neurodegeneration is a key feature of disease, to fully elucidate the mechanisms and involvement of the PA system during all stages of EAE. Following induction of CREAE, spinal cords were taken at different time points, during the acute phase of disease, remission and finally in the chronic phase of disease. Levels of tPA, PAI-1, uPA, plasminogen and fibrin D-dimer were measured in spinal cord homogenate protein extract samples. In addition the fibrinolytic capacity of the tissue was measured using a clot lysis assay.

3.2 Results.

3.2.1. Clinical features of CREAE disease in ABH mice.

Induction of CREAE in ABH mice by injection with spinal cord homogenate on day 0 and day 7 resulted in the development of an acute disease around 14-15 days post disease induction (dpi), with peak disease score on 18 – 20 dpi (Figure 3.1 A). This was followed by a period of almost complete remission (26 – 30 dpi). With each subsequent relapse, the capacity for recovery diminished due to an accumulation of neurological deficit leading to the development of clinical signs of spasticity and tremor. Significant weight loss preceded the onset of disease ($P < 0.001$ versus pre-disease onset weights) and persisted for approximately 5 days (Figure 3.1 B). Mean weight of animals prior to EAE onset was 23.9g ± 1.1, and mean maximal weight loss was 7.3g ± 0.3 (31%) which occurs concurrently with maximum clinical score. It has been found from previous studies that Freund's alone injected ABH mice develop no EAE disease (Allen *et al.*, 1993).

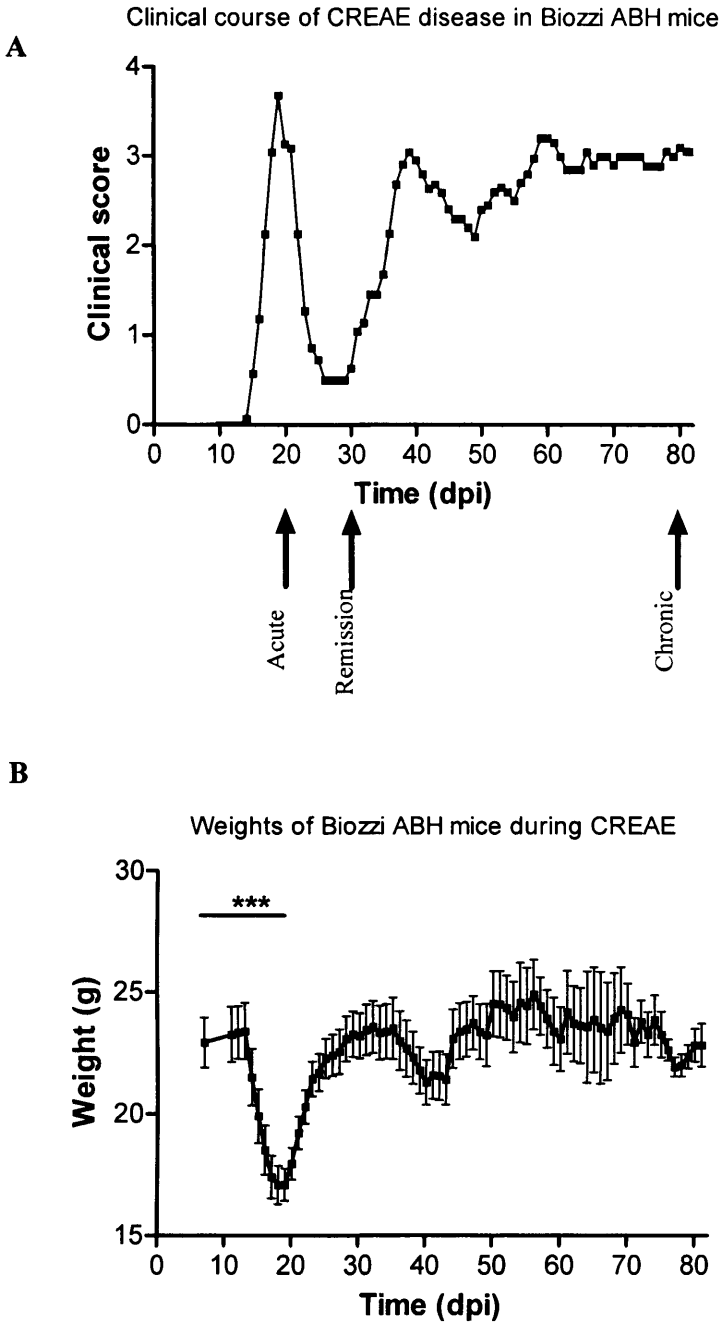

Figure 3.1. *CREAE - disease progression and weight loss in ABH mice injected with spinal cord homogenate.* **A.** Mice were injected with spinal cord homogenate in IFA supplemented with *M. tuberculosis* and *M. butyricum* on day 0 and day 7 and disease developed around 14 dpi. Mice were scored on a scale of 0 – 5 and the mean clinical score was calculated, n = 18. An acute phase of disease was followed by a period of remission and at least two separate relapse phases. Chronic disease developed due to an accumulation of deficits and was characterised by incomplete recovery, and the development of additional signs such as spasticity and tremor. **B.** Mice were weighed daily, data expressed as mean weights ± SEM. Disease onset was preceded by significant weight loss. n = 18, *** $P < 0.001$ day 7 versus day 19.

3.2.2. Upregulation of the PA system during CREAE in ABH mice.

To investigate the expression of components of the PA system during CREAE, mice were killed at various time points throughout the disease (acute – 20 dpi, first remission – 30 dpi and chronic - 80 dpi, indicated by the arrows Figure 3.1 A) and levels of tPA, PAI-1 and uPA were measured in spinal cord homogenate protein extracts by ELISA. Levels of tPA did not change significantly throughout the course of EAE, (Figure 3.2 A). uPA antigen was slightly increased in all samples from CREAE mice (Figure 3.2 B) but this was not significant until 80 dpi of EAE ($P < 0.01$). Interestingly, levels of uPA did not return to control values during disease remission at 30 dpi. PAI-1 was significantly increased during the acute phase of disease at 20 dpi ($P < 0.01$, Figure 3.2 C), correlating with inflammation. Levels of PAI-1 returned to those of control animals during EAE disease remission at 30 dpi. Additionally, whilst PAI-1 was significantly ($P < 0.05$) increased at 80 dpi during chronic EAE when compared to amounts from controls and mice in disease remission, levels were still a third lower than during the acute phase at 20 dpi ($P < 0.01$). To investigate what these changes meant in the *in vivo* situation, calculating ratios of enzyme to inhibitor are useful (Table 3.1). Under physiological conditions, in control mice the ratio of tPA to PAI-1 was approximately 56:1, and the ratio of uPA to PAI-1 was approximately 8:1. This ensured that at all times enzyme was present in much greater amounts than inhibitor. Ratios of enzyme to inhibitor during the acute phase of CREAE, at 20 dpi fell dramatically when compared to controls ($P < 0.05$). This would indicate that levels of PAI-1 were higher than uPA or tPA during the inflammatory stages of the disease, thus inhibiting the majority of plasminogen activation by these enzymes during acute EAE. Ratios were not significantly different during remission at 30 dpi, and were much nearer normal levels. Interestingly, the ratio levels of tPA enzyme to inhibitor fell significantly again

during chronic EAE ($P < 0.05$), and although ratios of uPA were decreased, this was not significant due to increased uPA at 80 dpi.

Ratio (ng/mg)	Control	20 dpi	30 dpi	80 dpi
tPA:PAI-1	56.3 ± 19.4	1.7 ± 0.3*	34.2 ± 1.6	7.7 ± 1.3*
uPA:PAI-1	8.2 ± 2.8	0.5 ± 0.1*	8.3 ± 0.4	2.6 ± 0.4

Table 3.1. *Ratios of tPA and uPA to the inhibitor PAI-1 during different phases of CREAE.* Results expressed as mean ± SEM, * $P < 0.05$ versus control.

Levels of tPA, uPA and PAI-1 in spinal cords from ABH mice during CREAE

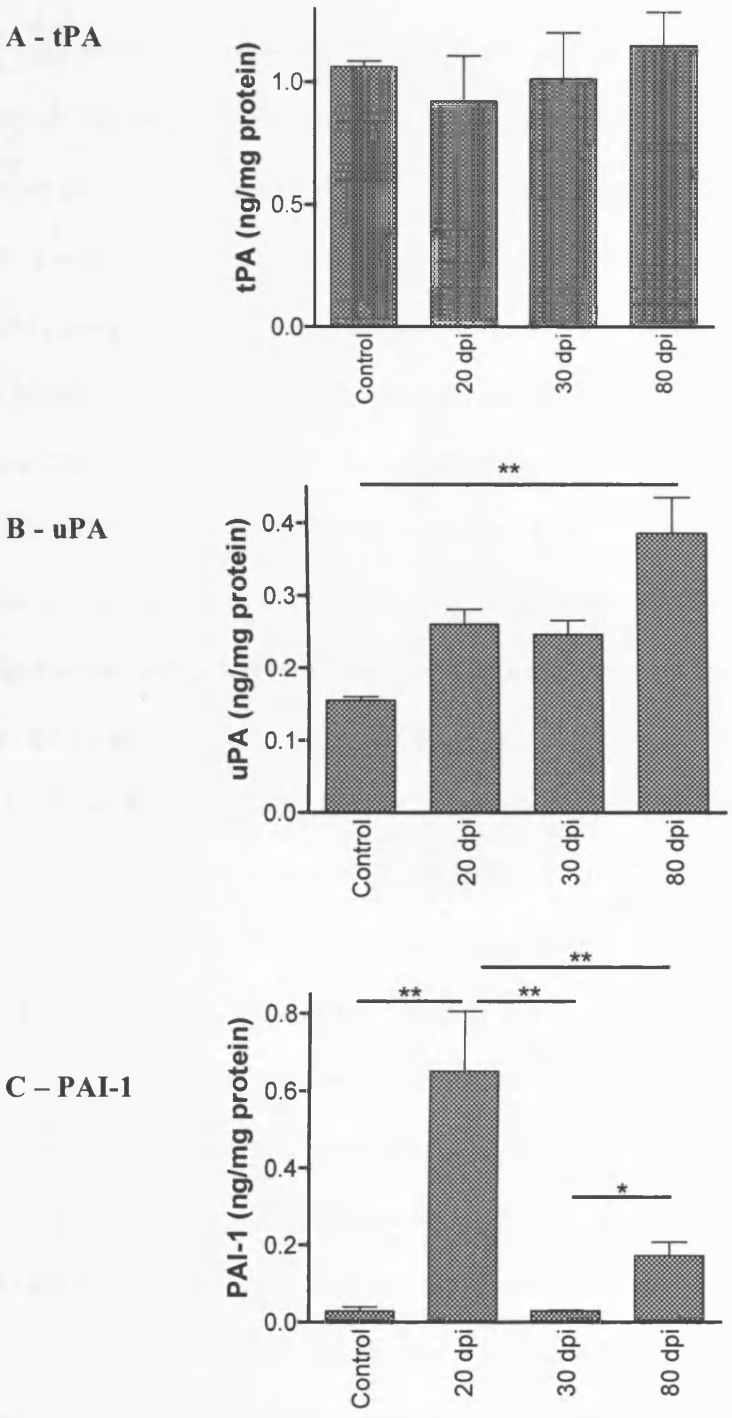

Figure 3.2. *Levels of tPA, uPA and PAI-1 during CREAE in ABH mice.* Levels of tPA, uPA and PAI-1 were detected in spinal cord homogenate samples from ABH mice at various time points during CREAE. **(A)** Levels of tPA did not change throughout CREAE disease. **(B)** A significant increase in uPA was observed during chronic EAE (80 dpi) and **(C)** a dramatic increase in PAI-1 was seen at 20 dpi of CREAE. Data is presented as the mean ± SEM, n = 4 or 5 per group. * $P < 0.05$, ** $P < 0.01$. .

3.2.3. Plasminogen and fibrin D-dimer are significantly increased in ABH mice during CREAE.

As levels and therefore activity of tPA and uPA are changed throughout the course of CREAE, due to increased PAI-1, it was of interest to investigate how this had an effect on levels and activation of plasminogen. Western blotting was performed on spinal cord protein extract samples from ABH mice taken at specific time points during CREAE, using an antibody against plasminogen. Plasminogen migrated as an 85 kDa band which corresponds to cell-bound pre-activation form, called lysine-plasminogen (Figure 3.3 A). Plasminogen was significantly increased during the acute phase of CREAE at 20 dpi ($P < 0.001$) when compared to levels in control mice (Figure 3.3 B). Levels returned to those in control non-injected mice during disease remission at 30 dpi. Whilst lys-plasminogen protein levels were slightly increased again during chronic EAE at 80 dpi, these were not significantly different to controls, and were significantly lower than levels at 20 dpi ($P < 0.001$). It is possible to measure activity of plasmin indirectly by measuring levels of its substrate fibrin(ogen), and the fibrin degradation product, fibrin D-dimer. This was also done by Western blotting. A very small amount of fibrin D-dimer was detected in the spinal cords of control mice (Figure 3.4 A), as expected, because under physiological conditions the BBB ensures that high molecular weight plasma proteins are excluded from the CNS. A significant increase of fibrin D-dimer was found in the spinal cords of mice during the acute phase of CREAE (20 dpi) when compared to control mice (Figure 3.4 B) and mice at 30 dpi, the remission phase of CREAE ($P < 0.01$ and $P < 0.05$ respectively). Furthermore, fibrin D-dimer was also found to accumulate during the chronic phase, at 80 dpi of CREAE ($P < 0.05$).

A

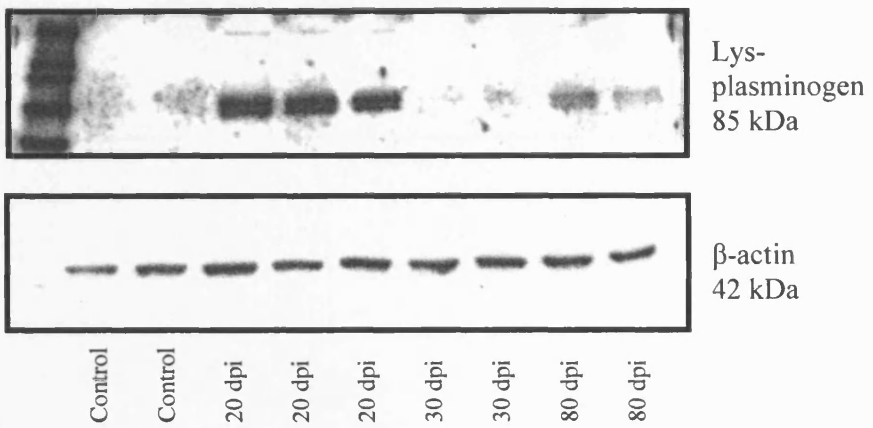

B Levels of plasminogen in the spinal cord of ABH mice during CREAE

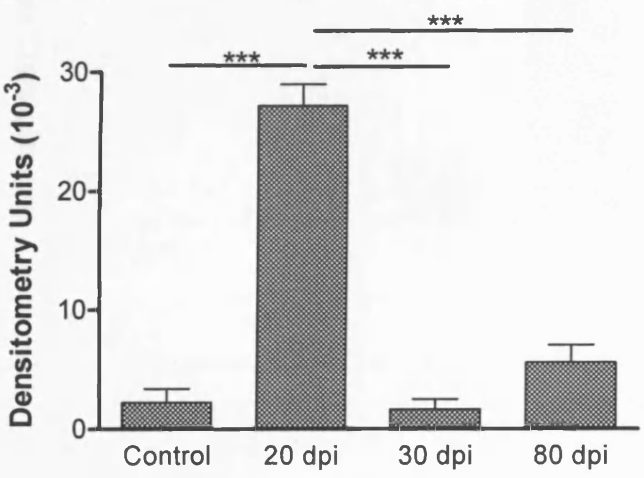

Figure 3.3. *Accumulation of plasminogen in ABH mice during the acute phase of CREAE.* Spinal cords from control and CREAE mice were homogenised for protein extraction. **A.** Levels of plasminogen were detected by Western blotting and were quantitatively measured by densitometry scanning. Results are shown as arbitrary densitometry units ± SEM. Blots were re-probed with anti-actin to ensure equal loading of proteins. **B.** Plasminogen was significantly increased during the acute phase of CREAE in ABH mice at 20dpi. n = 4 or 5 per category, *** $P < 0.001$.

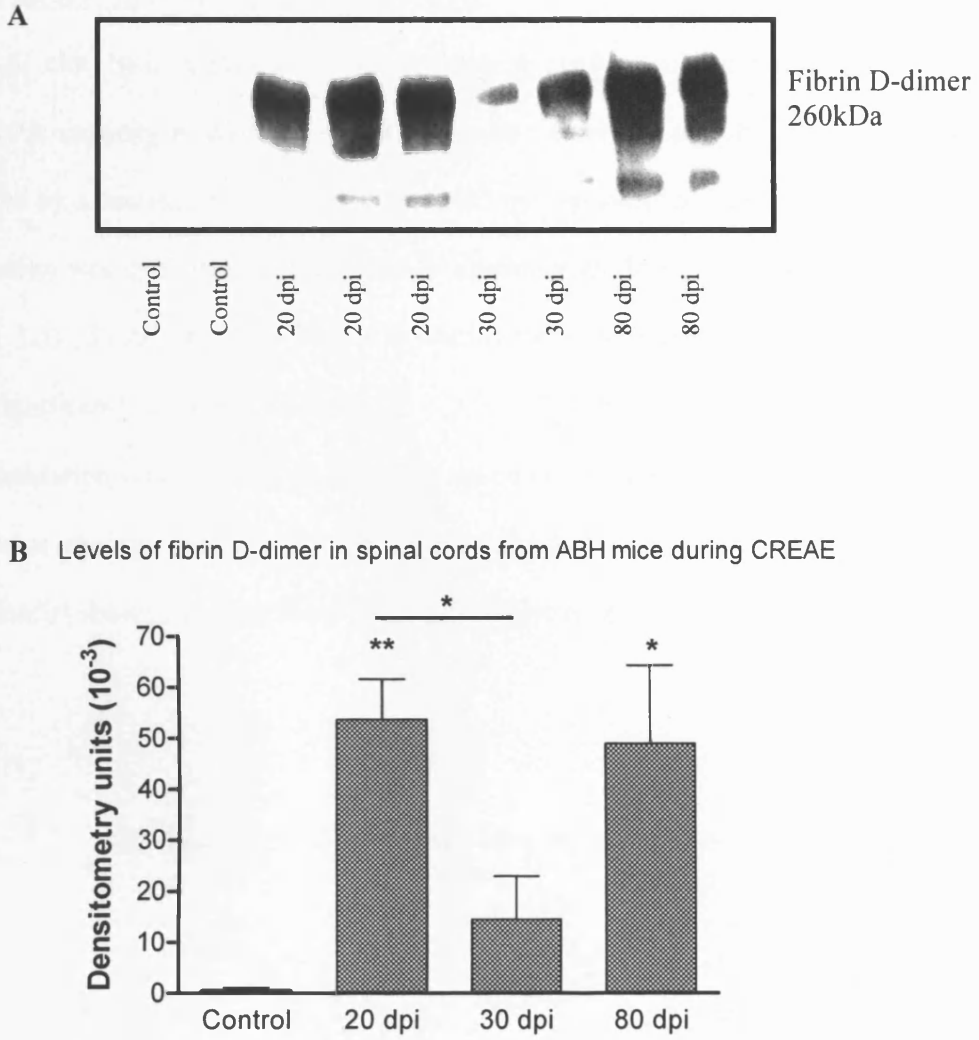

Figure 3.4. *Accumulation of fibrin D-dimer in ABH mice during CREAE.* Spinal cords from control and CREAE mice were homogenised for protein extraction. Levels of fibrin D-dimer were detected by Western blotting and were quantitatively measured by densitometry scanning; results are shown as arbitrary densitometry units ± SEM. Fibrin D-dimer was significantly increased during the acute and chronic phase of CREAE in ABH mice at 20 and 80 dpi respectively. n = 4 or 5 per category, * $P < 0.05$, ** $P < 0.01$ versus control unless indicated by bar.

3.2.4. Fibrinolysis in ABH mice during CREAE.

A clot lysis assay was used for spinal cord protein extracts to examine fibrinolytic capacity in control and CREAE mice. Over 5 h the clot degradation was measured by a decrease in optical density at 405 nm. In samples from control mice, clot degradation was complete after 2.5 h of incubation with thrombin to start the reaction (Figure 3.5). Protein extracts from mice during the acute phase of CREAE at 20 dpi, had a significantly impaired clot lysis, ($P < 0.05$ at 2 h) when compared to controls and clot degradation was complete an hour later than controls at 3.5 h (Figure 3.5). Samples from mice during remission or the chronic phase of CREAE (30 dpi or 80 dpi respectively) showed no significant difference in clot lysis when compared to controls.

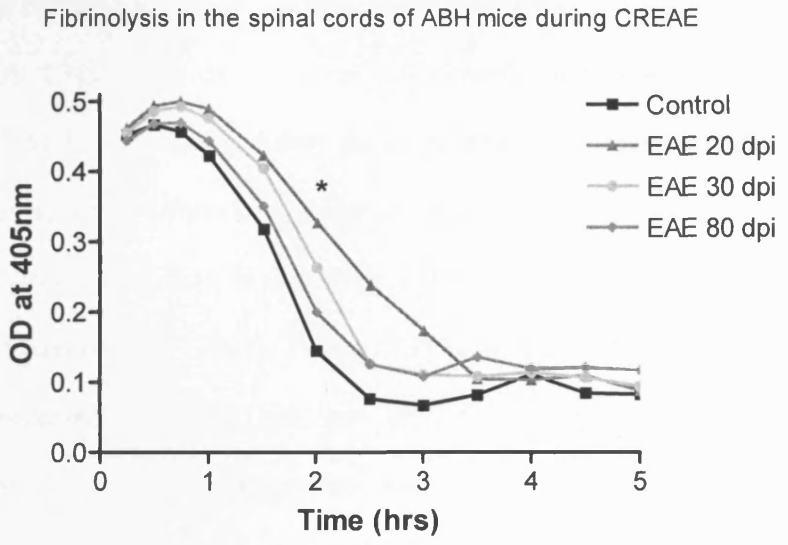

Figure 3.5. *Fibrinolysis in the ABH mouse CNS during CREAE.* Spinal cords from control and CREAE mice at specific time points were homogenised for protein extraction. The fibrinolytic capacity was investigated using a clot lysis assay which measures the degradation of an *in vitro* formed clot using spectrophotometry. Results are presented as the mean clot degradation over time as measured by optical density (OD) at 405 nm. Clot degradation was significantly impaired in samples from mice at 20 dpi when compared to controls. n = 4 or 5 per category. * $P < 0.05$.

3.3. Discussion.

The CREAE model in Biozzi ABH mice was used as an initial tool to investigate the changes in the expression of components of the PA system during different phases of disease. This model, induced by immunisation with spinal cord homogenate, has been well characterised, by pathological investigations (Baker *et al.*, 1990; Butter *et al.*, 1991; Allen *et al.*, 1993) particularly of the neurodegeneration (Petzold *et al.*, 2003a; Pryce *et al.*, 2003). As this model enabled separation of easily-recognisable distinct phases of EAE, samples could be taken during the initial acute, remission and chronic stages of disease in order to elucidate the involvement of the PA / fibrinolytic system during the inflammatory and neurodegenerative components of the disease. A significant increase in PAI-1, lys-plasminogen, an accumulation of fibrin D-dimer and slower clot lysis points to an involvement of the PA system in the pathogenesis of CREAE, and an impairment of fibrinolysis.

Whilst CNS levels of tPA were not altered during CREAE, the significant increase in PAI-1, particularly during the acute phase of disease, correlated with the peak clinical score and therefore a high degree of inflammation. Studies on post mortem MS brain tissue showed that levels of PAI-1 are also significantly increased in acute lesions (Gveric *et al.*, 2001). As the ELISAs measure antigen levels, the knock on effect of increased PAI-1 on tPA and uPA activity were not directly assessed. However, the decreased enzyme:inhibitor ratios during the acute and chronic stages of disease, could be an indicator of decreased activity. PAI-1 is an acute phase protein and its expression is known to be upregulated in response to pro-inflammatory cytokines such as TNF-α and IL-1 (Kasza *et al.*, 2001) thus it is likely that the increases in PAI-1 and possible decreased tPA and uPA activity are a consequence, rather than the cause, of inflammation. A surprising observation was that PAI-1 protein was also increased during chronic disease, thus indicating that although the key pathological feature of this

phase of CREAE is neurodegeneration, there was still some ongoing inflammation to account for this, as was evidenced in histological assessment of such tissues (Pryce *et al.,* 2003; Pryce *et al.,* 2005). Another feature of chronicity was the significantly increased levels of uPA, however this would probably be equilibrated by the higher levels of PAI-1 as the ratio of uPA:PAI-1 was not significantly different to that of controls.

Increased amounts of plasminogen in the spinal cord of ABH mice at the peak of acute disease reflect its accumulation resulting from decreased activation of the zymogen into its active form, plasmin. This reduction in plasminogen activation by tPA or uPA, was probably due to increased enzyme-inhibitor complex formation, as a result of increased PAI-1, thus reducing enzyme activity. As an indicator of this, lys-plasminogen, the pre-activation form of plasmin, and fibrin D-dimer were increased during CREAE particularly at the acute stage of disease and impaired fibrin clot lysis correlated with these increases. This correlates well with observations in MS tissue. Fibrinolysis was markedly reduced in NAWM, acute and chronic lesions due to increase complex formation of tPA with PAI-1 and resulting decrease of tPA activity (Gveric *et al.,* 2003). Increased PAI-1 and complex formation with tPA is also a key feature of disease pathology in rheumatoid arthritis. As a result, fibrinolysis is decreased, which correlates with disease severity (Kopeikina *et al.,* 1997).

Fibrin D-dimer is a large molecular weight fibrin degradation product (FDP), and its accumulation reflects an impairment of fibrinolysis, as under control conditions, fibrinolysis occurs rapidly, thus FDPs are not present in large amounts. Elevated levels of fibrinogen and chronically elevated levels of fibrin derivatives are well established risk indicators of vascular disease (Koenig *et al.,* 2001; Koenig, 2003), and they may be linked to a variety of inflammatory mechanisms as well (Kamath and Lip, 2003). Surprisingly increased fibrin D dimer during chronic EAE disease at 80 dpi was not

accompanied by increased lys-plasminogen levels, nor was a significant impairment of fibrinolysis, thus this finding was somewhat puzzling. However during chronic disease, the ratio of tPA to PAI-1 is still significantly lower than normal thus there would be less tPA activity, which could account for the fibrin accumulation. It appears that this system is under tight control and balance, and that slight alterations in the homeostasis have significant effects. Perhaps the clot lysis assay was not sensitive enough to detect the small reduction in fibrinolysis in samples from mice at 80 dpi of CREAE, even though it resulted in a large fibrin deposition in the spinal cords. The observation of persisting fibrin during chronic EAE disease follows on from the findings of Claudio *et al.,* (1995) who demonstrated that chronic silent MS lesions show persistent BBB abnormalities and fibrin deposition even in the absence of active inflammation. Additionally, at 80 dpi of CREAE, ABH mice have considerable neurological deficits, indicating underlying neurodegeneration Pryce *et al.,* (2003) demonstrated that decreased phosphorylated neurofilaments correlated with reduced movement activity of ABH mice during CREAE. Increased fibrin during chronic disease also correlates with neurological deficits and could point to a role for fibrin in contributing to axonal/neuronal loss (Akassoglou *et al.,* 2000; East *et al.,* 2005).

Investigation into the PA system during CREAE has revealed key roles for components of this cascade during inflammatory demyelination. Additionally, many similarities were found between the CREAE model and that observed in studies using MS tissue, thus further supporting the use of SCH-induced CREAE in ABH as a close model of MS. Persisting impairment of fibrinolysis, resulting in accumulation of fibrin correlates with neurodegeneration and thus could provide a useful target for therapeutic intervention.

4. Characterisation of EAE in tPA and uPAR deficient mice.

4.1. Introduction.

Components of the plasminogen activator cascade are postulated to have detrimental effects contributing to the onset and progression of inflammatory demyelination. To investigate the role of tPA and uPAR in experimental neuroinflammation, EAE was induced with myelin oligodendrocyte glycoprotein (MOG) in $tPA^{-/-}$ and $uPAR^{-/-}$ mice and their wildtype (WT) counterparts. Transgenic mice on the C57BL/6 background are resistant to CREAE induction with spinal cord homogenate, but are susceptible to EAE induced with MOG_{35-55} peptide. The clinical and histopathological characteristics of the disease were examined in order to identify any similarities and differences between the genotypes and to isolate possible mechanisms of action.

4.2. Results.

4.2.1. Clinical features of MOG-EAE disease in $tPA^{-/-}$ and $uPAR^{-/-}$ mice.

To study the role of tPA and uPAR during experimental neuroinflammation $tPA^{-/-}$ and $uPAR^{-/-}$ mice were used in the MOG_{35-55} peptide induced EAE model. After induction of MOG-EAE, WT animals exhibited signs of disease at 11.0 ± 0.5 days post disease induction (dpi) (Figure 4.1 A; Table 4.1), with peak of disease at 17.6 ± 0.5 dpi. The acute phase of disease lasted for approximately 15 days with an average mean maximal score of 2.0 ± 0.2. Animals recovered from the attack with little residual deficit (Figure 4.1 A) and a mean score at 60 dpi of 0.3 ± 0.1. In contrast, $tPA^{-/-}$ mice (Figure 4.1 A) had a significantly earlier onset of disease, 8.9 ± 0.4 dpi (Table 4.1; $P < 0.01$) with a more severe acute phase lasting approximately 22 days reaching a peak significantly earlier at 14.4 ± 0.7 dpi ($P < 0.01$) than in the WT and with a significantly higher mean maximal score of 3.3 ± 0.2 ($P < 0.001$). Disease course in $tPA^{-/-}$ animals was characterised by an incomplete recovery (Figure 4.1 A) with signs of residual

deficit including hindlimb paresis (82 %) and occasional tail spasticity (18 %). Mean scores at 40 and 60 dpi were 2.2 ± 0.2 and 1.6 ± 0.2 respectively, both significantly higher than WT mice ($P < 0.001$) at comparable time points. Following induction of EAE, uPAR$^{-/-}$ mice (Figure 4.1 B), developed signs of disease significantly later than WT mice, on 17.4 ± 1.1 dpi ($P < 0.001$), with peak disease occurring at 34.4 ± 3.3 dpi ($P < 0.001$). uPAR$^{-/-}$ mice developed a more chronic disease than WT mice which was characterised by incomplete recovery and a significantly higher clinical score at 60 dpi than WT (1.9 ± 0.4; $P < 0.01$).

Clinical course of MOG-EAE disease in $tPA^{-/-}$, $uPAR^{-/-}$ and WT mice

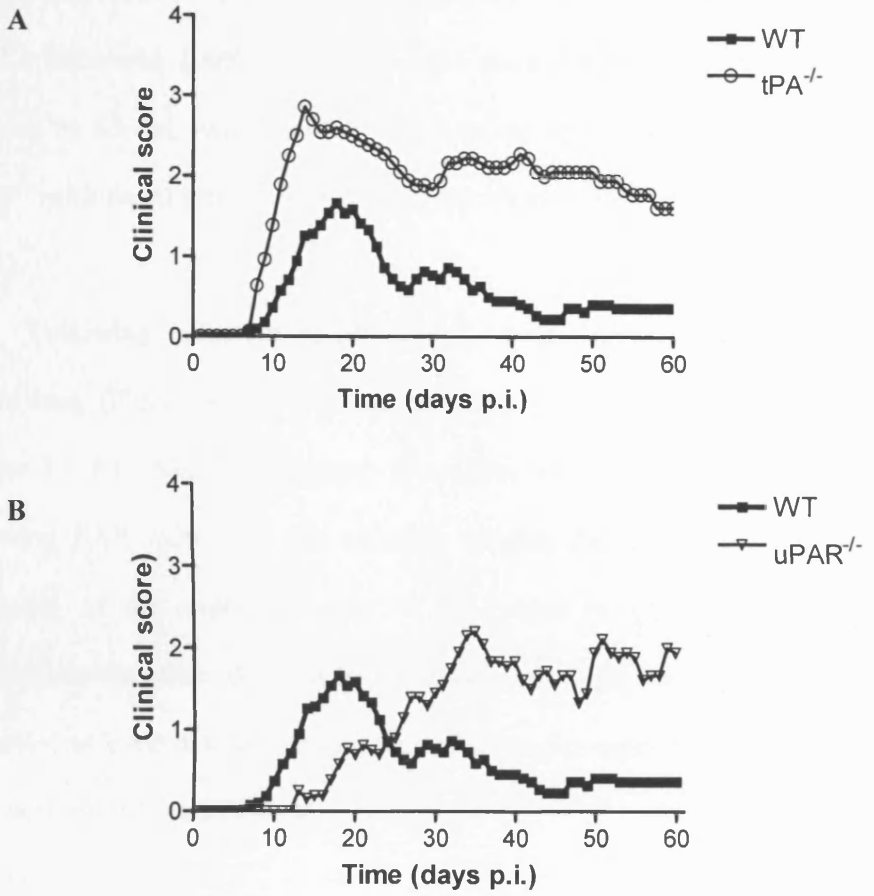

Figure 4.1. *MOG-EAE disease course in $tPA^{-/-}$, $uPAR^{-/-}$ and WT mice.* All mice were injected with MOG_{35-55} peptide in IFA supplemented with *M. tuberculosis* on day 0 and 7 and *B. pertussis* toxin on day 0 and day 2. Adjuvant injected mice (AIC) were used as negative controls and developed no disease. Mice were scored daily on a scale of 0 – 5 and the daily mean score was calculated. **(A)** n = 19 for WT, n = 14 for $tPA^{-/-}$ and **(B)** n = 14 for $uPAR^{-/-}$.

Strain	EAE incidence	Onset (dpi)	Peak of disease (dpi)	Mean Maximal Score	Mean Score at 60 dpi
WT	16/19	11.0 ± 0.5	17.6 ± 0.5	2.0 ± 0.2	0.3 ± 0.1
$tPA^{-/-}$	14/14	$8.9 \pm 0.4^{**}$	$14.4 \pm 0.7^{**}$	$3.3 \pm 0.2^{***}$	$1.6 \pm 0.2^{***}$
$uPAR^{-/-}$	14/14	$17.4 \pm 1.1^{***}$	$34.4 \pm 3.3^{***}$	2.4 ± 0.3	$1.9 \pm 0.4^{**}$

Table 4.1. *Summary of the EAE data for wildtype (WT), $tPA^{-/-}$ and $uPAR^{-/-}$ mice.* ** $P < 0.01$ and *** $P < 0.001$ versus WT. All values shown as mean ± SEM.

The incidence and timing of onset of MOG-EAE disease is illustrated in Figure 4.2. Whilst 84% of WT mice developed EAE, the incidence of EAE in $tPA^{-/-}$ and $uPAR^{-/-}$ mice was 100%. All $tPA^{-/-}$ mice showed signs of EAE disease by 12 dpi, however by 15 dpi, two WT mice had failed to develop any clinical signs. 100% of $uPAR^{-/-}$ mice developed EAE by 30 dpi, significantly later than WT or $tPA^{-/-}$ mice ($P < 0.001$).

Following induction of MOG-EAE, mice were weighed daily to check for weight loss, (Figure 4.3), which can be an early sign of disease onset in ABH mice (Figure 3.1 B). Slight fluctuations in weights were observed over the first 20 days following EAE induction, and although weights did not significantly differ at the beginning of the experiment, by 18 dpi, mean weights of $tPA^{-/-}$ animals were significantly less than WT and $uPAR^{-/-}$ mice ($P < 0.001$ and $P < 0.01$ respectively). However, as EAE diseased progressed, all three genotypes of mice gained weight and there were no differences between the groups.

4.2.2. Adjuvant injected controls developed no EAE disease.

Mice injected with Freund's adjuvant supplemented with *M. tuberculosis*, without MOG peptide were used as controls. These mice also received an intraperitoneal injection of *B. pertussis* toxin on day 0 and day 2. Adjuvant injected mice failed to develop any clinical EAE signs (Figure 4.4 A), and all genotypes had a clinical score of 0 for the duration of the experiment. Additionally, there was no significant weight loss in any of the three groups of mice (Figure 4.4 B). Upon histological examination of the spinal cords from adjuvant injected control (AIC) mice taken at different time points, there was no evidence of infiltration of inflammatory mononuclear cells in any of the sections (Figure 4.4 C). As a consequence of this result, all subsequent controls were taken as normal-non-injected mice from each genotype.

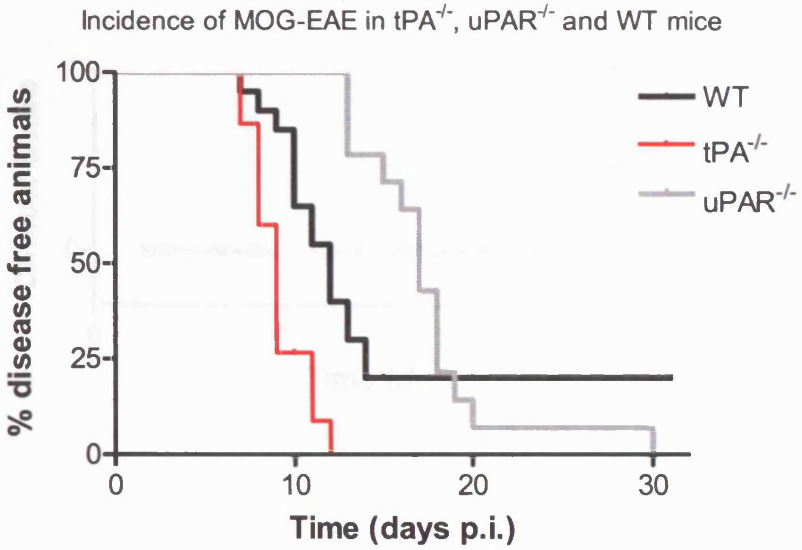

Figure 4.2. *Incidence and time course of MOG-EAE onset in WT, tPA$^{-/-}$ and uPAR$^{-/-}$ mice.* All tPA$^{-/-}$ mice showed signs of EAE disease by 12 dpi, however by 15 dpi, two WT mice had failed to develop any clinical signs. 100% of uPAR$^{-/-}$ mice developed EAE by 30 dpi, significantly later than WT or tPA$^{-/-}$ mice ($P < 0.001$).

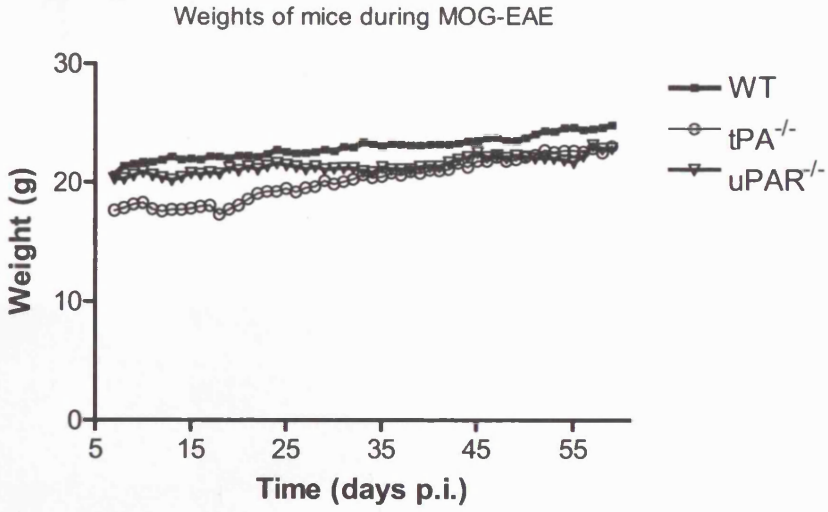

Figure 4.3. *Weights of WT, tPA$^{-/-}$ and uPAR$^{-/-}$ mice during MOG-EAE.* Following induction of EAE, mice were weighed daily to check for any significant weight loss. Although weights did not significantly differ at the beginning of the experiment, by 18 dpi, mean weights of tPA$^{-/-}$ animals were significantly less than WT and uPAR$^{-/-}$ mice ($P < 0.001$ and $P < 0.01$ respectively). As EAE progressed there were no significant differences in weights between the three genotypes.

Clinical course of EAE disease and weights of adjuvant injected control mice

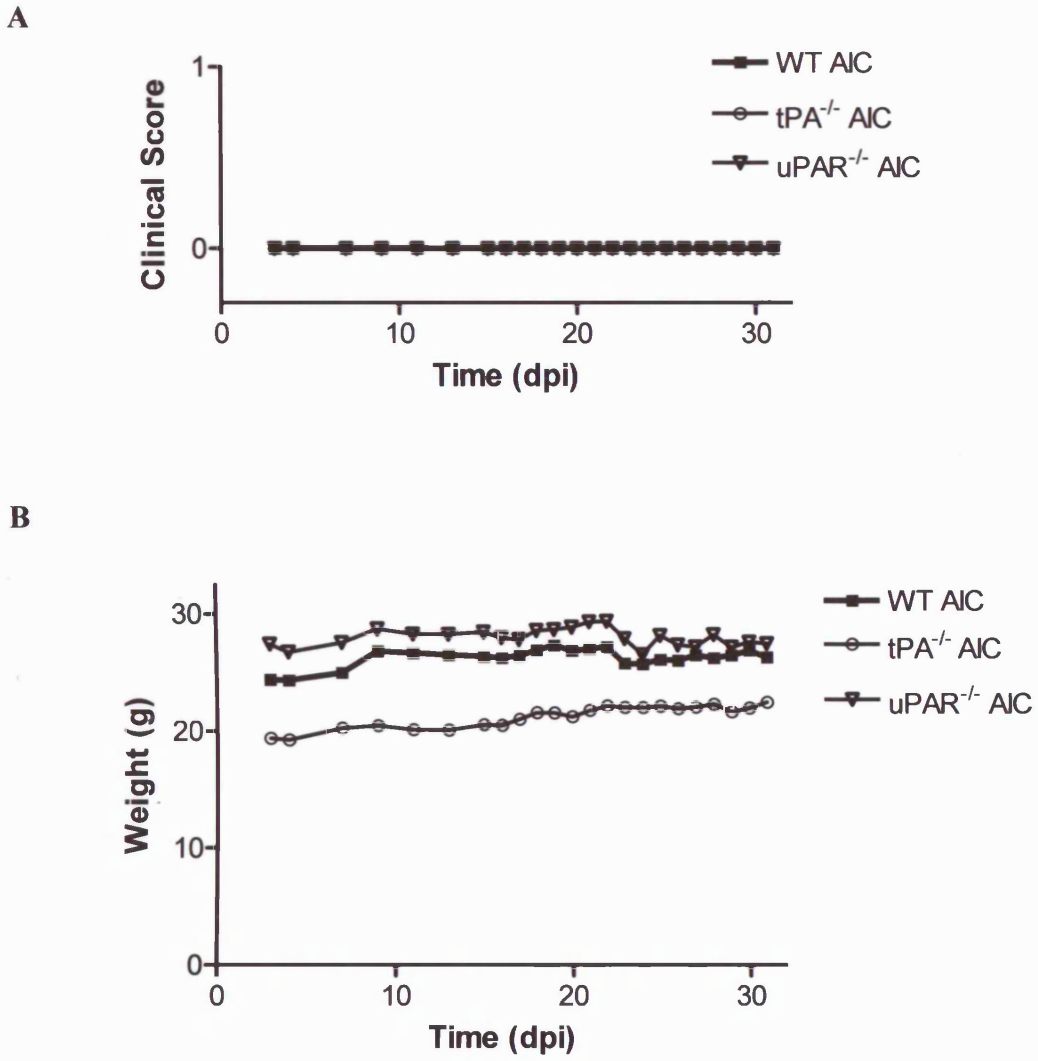

Figure 4.4. *Adjuvant injected controls (AIC) developed no signs of EAE disease, weight loss or CNS inflammation.* Mice were injected with Freund's adjuvant supplemented with *M. tuberculosis* on day 0 and day 7 and received an intraperitoneal injection of *B. pertussis* toxin on day 0 and day 2. **A**. In the absence of MOG, adjuvant injected mice developed no clinical EAE disease. **B**. There was no significant weight loss and **C**. histological examination revealed no inflammatory infiltrates in the spinal cord of these mice (Original magnification x100). n = 6 per genotype.

4.2.3. Activity of WT, tPA$^{-/-}$ and uPAR$^{-/-}$ mice during MOG-EAE.

Movement activity of mice was performed to investigate motor dysfunction and the degree of neurological impairment (Pryce *et al.,* 2003). Mice were placed in an open field activity chamber and the total distance travelled in 5 min was recorded. Control tPA$^{-/-}$ mice were significantly more active than control WT mice ($P < 0.05$, Table 4.2), thus all data was normalised to the appropriate controls, i.e. WT EAE against WT controls, tPA EAE against tPA controls etc. Following EAE induction all mice had a significant reduction in activity when compared to the relevant control groups ($P < 0.001$). tPA$^{-/-}$ mice at 35 and 60 dpi were significantly less active than WT animals at 35 and 60 dpi of MOG-EAE ($P < 0.05$; Figure 4.5). Movement of uPAR$^{-/-}$ mice at 35 dpi was also significantly reduced compared to WT mice at 35 dpi ($P < 0.001$), however by 60 dpi, although uPAR$^{-/-}$ animals had a higher mean score than WT ($P < 0.05$) the activity of the two groups was not significantly different (Figure 4.5).

Baseline activity data Distanced travelled (cm) in 5 min		
WT	tPA$^{-/-}$	uPAR$^{-/-}$
679.3 ± 30.7	928.2 ± 92.6 *	674.1 ± 99.9

Table 4.2. *Baseline activity data for control WT, tPA$^{-/-}$ and uPAR$^{-/-}$ mice.* * $P < 0.05$. Control tPA$^{-/-}$ mice were significantly more active than control WT mice, thus all data was normalised to the appropriate controls.

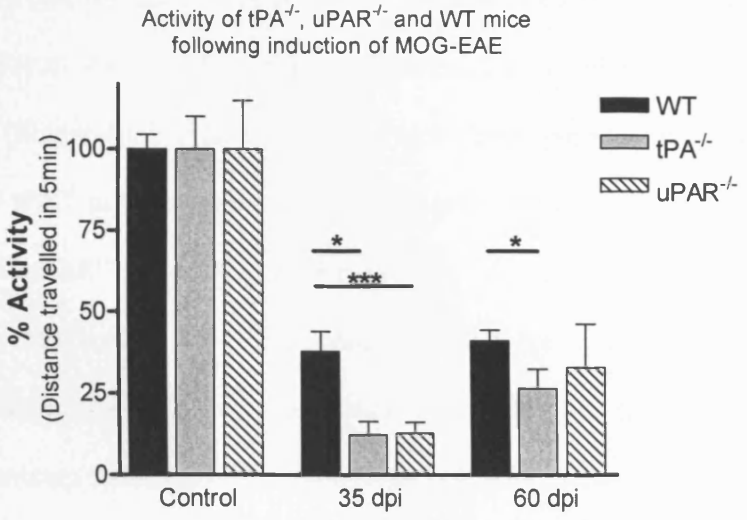

Figure 4.5. *Activity of WT, $tPA^{-/-}$ and $uPAR^{-/-}$ before and after induction of MOG-EAE.* The motor function of control and EAE mice (35 and 60 dpi) was assessed using an open field activity chamber, and total distance travelled in 5 min was recorded for each mouse. The data represents the average activity of each group of mice normalised to the relevant control ± SEM. $tPA^{-/-}$ and $uPAR^{-/-}$ mice were less active than WT mice at 35 dpi, and $tPA^{-/-}$ mice were still significantly less active than WT animals at 60 dpi. For control groups; WT n = 11, $tPA^{-/-}$ n = 13, $uPAR^{-/-}$ n = 7. For EAE groups; WT n = 19, $tPA^{-/-}$ n = 9, $uPAR^{-/-}$ n = 9. * $P < 0.05$, *** $P < 0.001$.

4.2.4. Histological evaluation of spinal cords from MOG-EAE mice.

Histological staining, with haematoxylin and eosin, of spinal cord sections taken at 20, 35 and 60 dpi, revealed differences in the degree of infiltration of inflammatory cells into the CNS between the three genotypes (Figure 4.6). No mononuclear cells were found in the spinal cords of control mice (Figure 4.6 A – C), however a large number of perivascular cuffs were evident in sections from WT and $tPA^{-/-}$ mice at 20 dpi of EAE (Figure 4.6 D and E), but no infiltrating mononuclear cells in the cords of $uPAR^{-/-}$ mice (Figure 4.6 F). At 35 dpi, there were fewer perivascular cuffs in sections from WT and $tPA^{-/-}$ mice, however a number of perivascular cuffs were identifiable in sections from $uPAR^{-/-}$ mice (Figure 4.6 G - I). By 60 dpi, a higher degree of inflammation was evident in $uPAR^{-/-}$ mice whilst there appeared to be very few infiltrating cells remaining in the spinal cords of WT and $tPA^{-/-}$ (Figure 4.6 J – L). To quantify the amount and degree of mononuclear cell infiltration, cuff counts and scores were assessed in the three genotypes of mice at 20, 35 and 60 dpi of EAE. The total number of perivascular cuffs was counted in a spinal cord longitudinal section area of $4cm^2$, and each cuff was given a score according to the degree of cellular infiltration; 1, perivascular inflammation three or fewer cells deep; 2, more than three cells deep; 3, parenchymal infiltrate. The average total cuff count and score was taken from a total of three slides from three different mice per time point. Cuff count and score were significantly higher in $tPA^{-/-}$ mice than WT at 35 dpi ($P < 0.01$), but at 20 and 60 dpi, these were comparable (Figure 4.7). Cuff count and score in $uPAR^{-/-}$ mice at 35 dpi were comparable with those at the peak of acute disease in WT and $tPA^{-/-}$ (20 dpi, Figure 4.7). Persistent inflammation in $uPAR^{-/-}$ mice at 60 dpi was reflected in high numbers of mononuclear cells in perivascular cuffs (Figure 4.6 L), and a higher cuff score in comparison with WT and $tPA^{-/-}$ mice at 60 dpi (Figure 4.7) in accord with the clinical data.

H & E

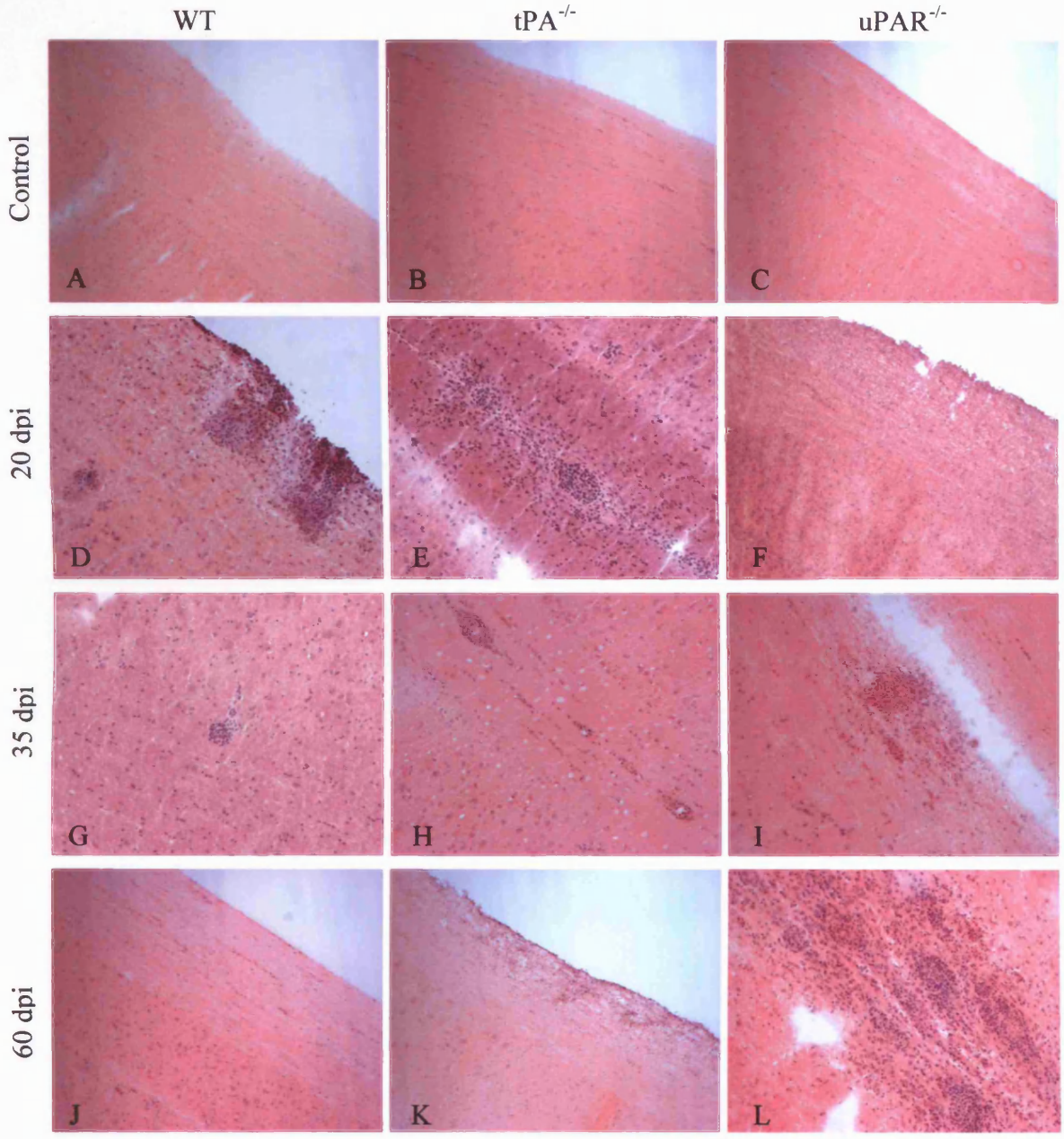

Figure 4.6. *Haematoxylin and eosin staining of spinal cord sections from WT, tPA$^{-/-}$ and uPAR$^{-/-}$ mice during acute and chronic phases of MOG-EAE.* Spinal cords were removed from mice at 20 (D – F), 35 (G – I) and 60 (J – L) dpi of EAE and cut longitudinally. H & E was performed on frozen sections to detect nuclei distinct from other tissue components. Normal sections (A - C) showed no clustering of nuclei. Whilst perivascular cuffs, indicative of inflammation, were identified in sections from WT (D and G) and tPA$^{-/-}$ (E and H) mice during acute EAE, there were few additional nuclei in sections from uPAR$^{-/-}$ animals before the peak of disease at 35 dpi (F and I). During chronic EAE there was evidence persistent inflammation in uPAR$^{-/-}$ mice (L). Original magnification x 100.

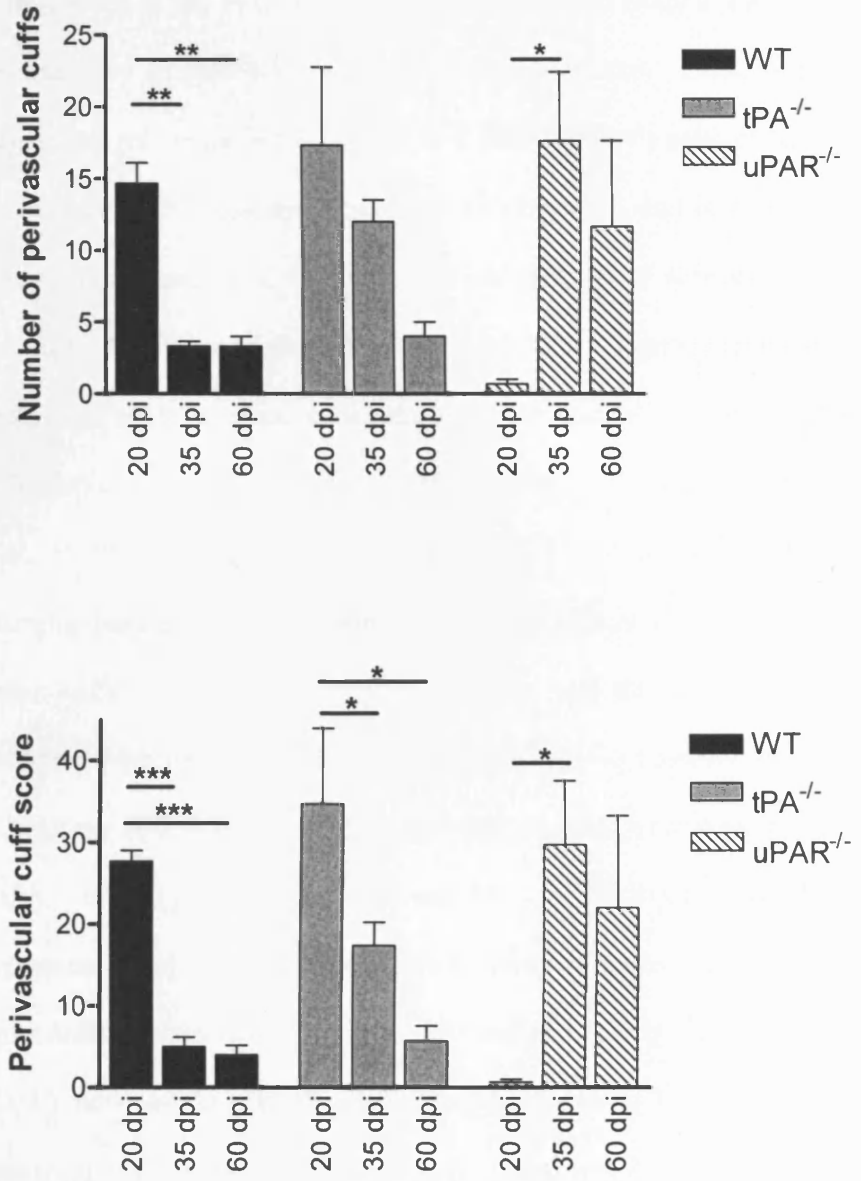

Figure 4.7. *Perivascular cuff counts and scores for WT, tPA$^{-/-}$ and uPAR$^{-/-}$ EAE mice.* Spinal cords from EAE mice at 20, 35 and 60 dpi were sectioned longitudinally and stained with an antibody against CD45. The total number of cuffs were counted in a section area of 4cm^2, and each cuff was given a score according to the degree of infiltration; 1, perivascular inflammation fewer three or fewer cells deep; 2, more than three cells deep; 3, parenchymal infiltrate. The total cuff score was calculated for each slide and the average of three slides from three different mice per time point was calculated. The data is shown as the mean total number of cuffs or mean total cuff score ± SEM; n = 3, * $P < 0.05$, ** $P < 0.01$ and *** $P < 0.001$.

4.2.5. Participation of macrophages, microglia and T-lymphocytes in MOG-EAE.

Immunohistochemical staining was performed on sections of spinal cords removed from mice at 20, 35 and 60 dpi, comparing CD45 (Figure 4.8), F4/80 (Figure 4.9) CD8 and CD4 (Figure 4.10) staining on serial sections. F4/80 is a marker for macrophages and microglia, whilst CD45 is a marker for all cells of haematopoietic origin including lymphocytes, monocytes and macrophages, and is a general indicator of the entry of immune cells, inflammation and microglial activation in the CNS. Antibodies against CD8 and CD4 detect $CD8^+$ and $CD4^+$ T-lymphocytes respectively. No staining was seen in spinal cord sections from control (non-injected) mice nor adjuvant injected animals (Figure 4.4 C) as previously observed (Amor *et al.*, 1993; Baker *et al.*, 1990). Staining of serial sections for CD45, F4/80 and T-cells showed that both microglia/macrophages and lymphocytes were present in large numbers in the perivascular cuffs in all three genotypes of mice, and that microglia/macrophages contributed to a high proportion of the CD45 positive cells observed in the CNS. As observed with the H & E histology, high numbers of cuffs were seen in sections from WT and $tPA^{-/-}$ mice at 20 dpi (Figures 4.8 and 4.9 A, Ai, B, Bi), but essentially no cells or cuffs were observed in sections from $uPAR^{-/-}$ mice (Figures 4.8 and 4.9 C). A few perivascular cuffs were evident at 35 dpi in WT and particularly $tPA^{-/-}$ mice (Figures 4.8 and 4.9 D, E), however the peak of disease in $uPAR^{-/-}$ mice at 35 dpi, corresponded to a high number of infiltrating mononuclear cells (Figures 4.8 and 4.9 F, Fi). A few residual stained microglia/macrophages were still present in $tPA^{-/-}$ mice at 60 dpi, but not in the WT animals (Figure 4.9 G and H). Furthermore, inflammation was still ongoing at 60 dpi in $uPAR^{-/-}$ mice with a high number of perivascular cuffs and a large amount of infiltrating inflammatory cells (Figure 4.8 I).

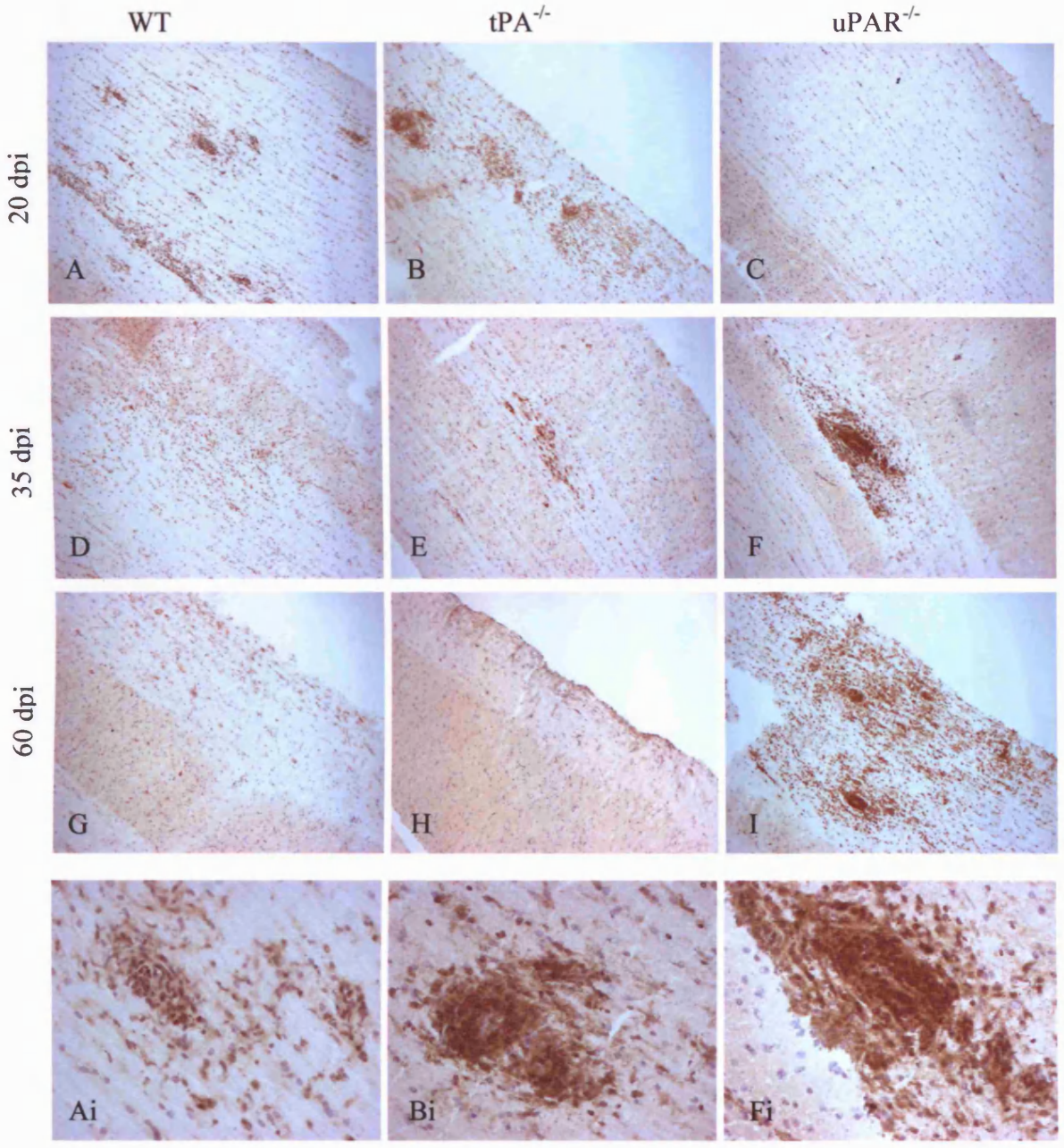

Figure 4.8. *Total leucocyte population in MOG-EAE.* Spinal cords were removed at 20 (A – C), 35 (D – F) and 60 (G – I) dpi of MOG-EAE and cut longitudinally. Frozen sections were stained with an antibody against CD45 and counterstained with Mayer's haematoxylin to assess the infiltration/migration of inflammatory mononuclear cells. In control animals there were no mononuclear cells in the spinal cord tissue (not shown). There was a delay in microglial migration and infiltration of macrophages and lymphocytes in uPAR$^{-/-}$ mice (C) when compared to WT and tPA$^{-/-}$animals at 20 dpi (A and B). However, perivascular cuffs containing mononuclear cells were evident in uPAR$^{-/-}$ mice at the peak of disease, 35 dpi (F). A high degree of persisting inflammation was evident in uPAR$^{-/-}$ at 60 dpi (I) although not in WT animals (G). Ai, Bi and Fi are high power images of A, B and F respectively. Original magnification x 100, inserts (i); original magnification x 400.

F4/80

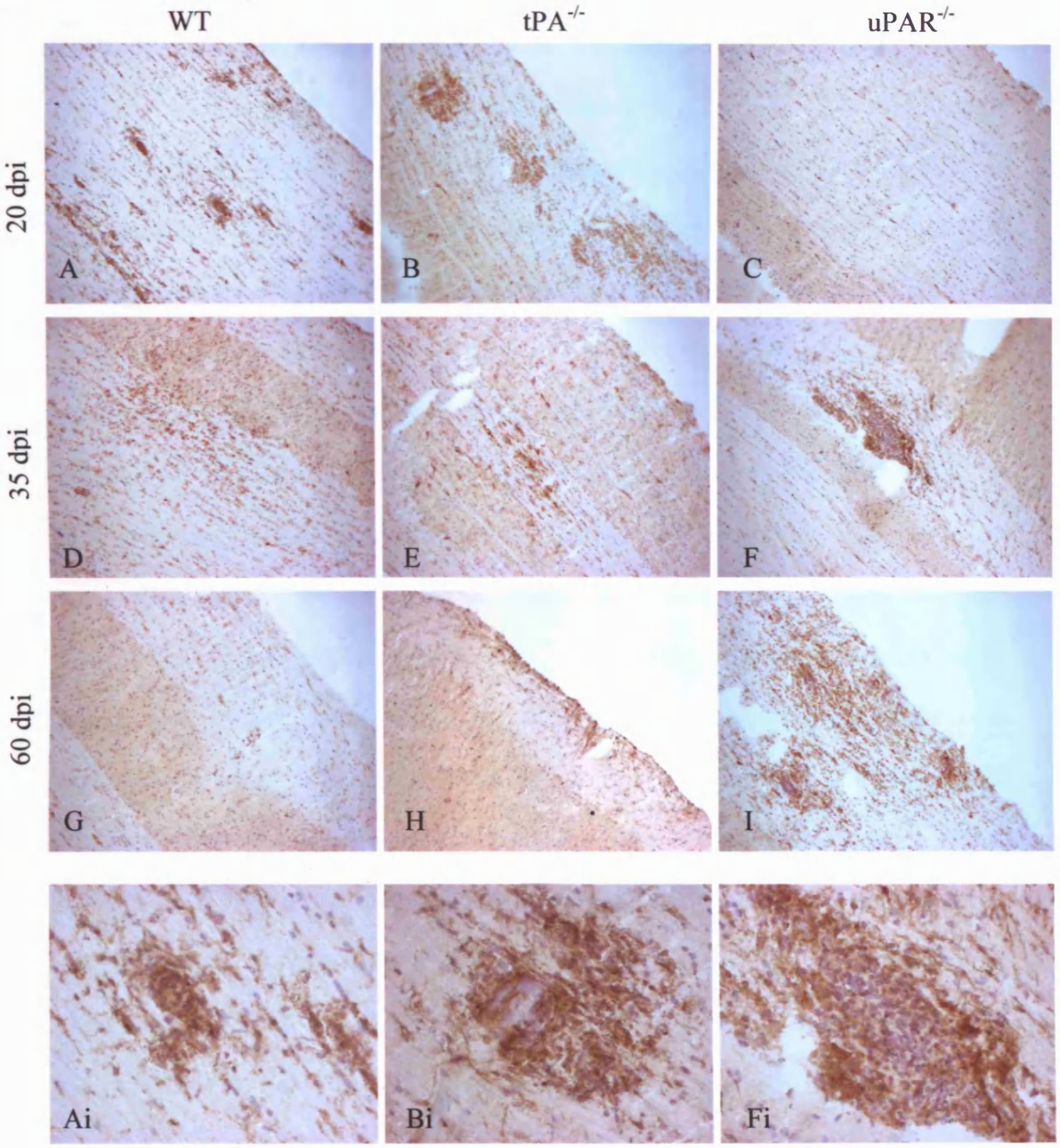

Figure 4.9. *Infiltration of macrophages/microglia in MOG-EAE.* Spinal cords were removed at 20 (A – C), 35 (D – F) and 60 (G – I) dpi of MOG EAE and cut longitudinally. Frozen sections were stained with an antibody against F4/80 and counterstained with Mayer's haematoxylin to assess the infiltration/migration of macrophages and microglia. In control animals there were no mononuclear cells in the spinal cord tissue (not shown). F4/80 staining on serial sections showed a very similar pattern to CD45 (Figure 4.8). Ai, Bi and Fi are high power images of A, B and F respectively. Original magnification x 100, inserts (i); original magnification x 400.

Immunohistochemical analysis of CD8 and CD4 positive lymphocytes on serial sections of spinal cord (Figure 4.10), revealed a high number of both these cell types, which showed a similar pattern to the CD45 and F4/80 staining. More staining of CD4 and CD8 positive cells was seen in the sections from $tPA^{-/-}$ and WT mice than in $uPAR^{-/-}$ at 20 dpi (Figure 4.10 A – C). An interesting observation is that there was a high number of CD8 positive cells in all sections (Figure 4.10 J, K and L), which suggests that the MOG-induced EAE in these animals has a strong component of disease mediated by $CD8^+$ cells in addition to $CD4^+$ cells (Schroeter *et al.,* 2003; Sun *et al.,* 2001). To quantify the number of different cell types in perivascular cuffs, the total number of $CD45^+$ cells in a cuff were counted, then the total number of $CD4^+$ and $CD8^+$ cells were counted in the same cuff on serial sections. A total of three cuffs per section were counted, with three slides per time point. The number of $CD4^+$ and $CD8^+$ cells were subtracted from the total number of $CD45^+$ cells to give a representation of cells which were probably either macrophages/microglia or B lymphocytes; these cells accounted for the majority of cells in spinal cords during MOG-EAE. The total number of inflammatory cells decreased as EAE disease progressed (Figure 4.11). $CD4^+$ T cells were the predominant type of lymphocytes, although $CD8^+$ cells were present in nearly equal numbers. Total number of cells ($CD45^+$, $CD4^+$ and $CD8^+$) were significantly higher in $uPAR^{-/-}$ mice at 35dpi than WT and $tPA^{-/-}$ mice at the same stage of EAE disease ($P < 0.01$ and $P < 0.05$ respectively), but were comparable to the number of cells in WT and $tPA^{-/-}$ mice at the peak of disease, 20 dpi (Figure 4.11). Additionally, the number of cells at 60 dpi of MOG-EAE in $uPAR^{-/-}$ mice was significantly higher than WT at the same stage of EAE ($P < 0.01$); however there was no significant difference between $uPAR^{-/-}$ and $tPA^{-/-}$ mice at 60 dpi (Figure 4.11). Although the total number of cells changed throughout the course of MOG-EAE disease, there were no

apparent differences in different cell types between the genotypes. There were similar numbers of $CD4^+$, $CD8^+$ and $CD45^+$ cells at the peak of disease in all groups of mice.

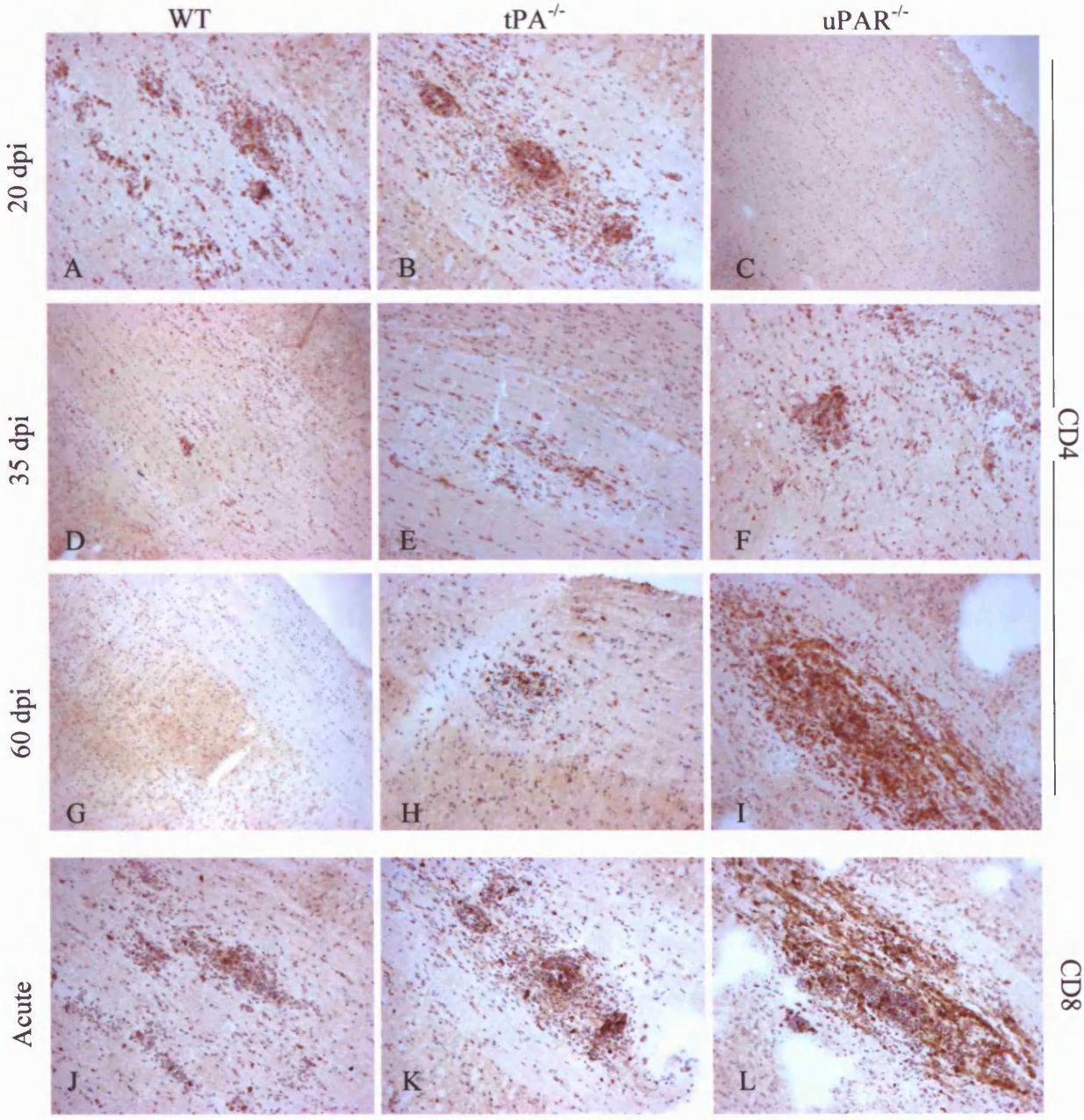

Figure 4.10. *Infiltration of CD4$^+$ and CD8$^+$ cells in MOG-EAE.* Spinal cords were removed at 20 (A – C), 35 (D – F) and 60 (G – I) dpi of EAE and cut longitudinally. Frozen sections were stained with an antibody against CD4 and counterstained with Mayer's haematoxylin to assess the proportion of CD4$^+$ and CD8$^+$ T cells in the perivascular cuffs. In control animals there were no CD4$^+$ or CD8$^+$ cells detected in the spinal cord tissue (not shown). There was a delay in infiltration of lymphocytes in uPAR$^{-/-}$ mice (C) when compared to WT and tPA$^{-/-}$animals at 20 dpi (A and B). However, perivascular cuffs containing CD4$^+$ T cells were evident in uPAR$^{-/-}$ mice at the peak of disease, 35 dpi (F). A high degree of persisting inflammation was evident in uPAR$^{-/-}$ at 60 dpi (I) although not in WT animals (G). CD4 and CD8 showed similar patterns of staining; J, K and L are staining for CD8 on serial sections corresponding to images A, B and I respectively. Original magnification x 200.

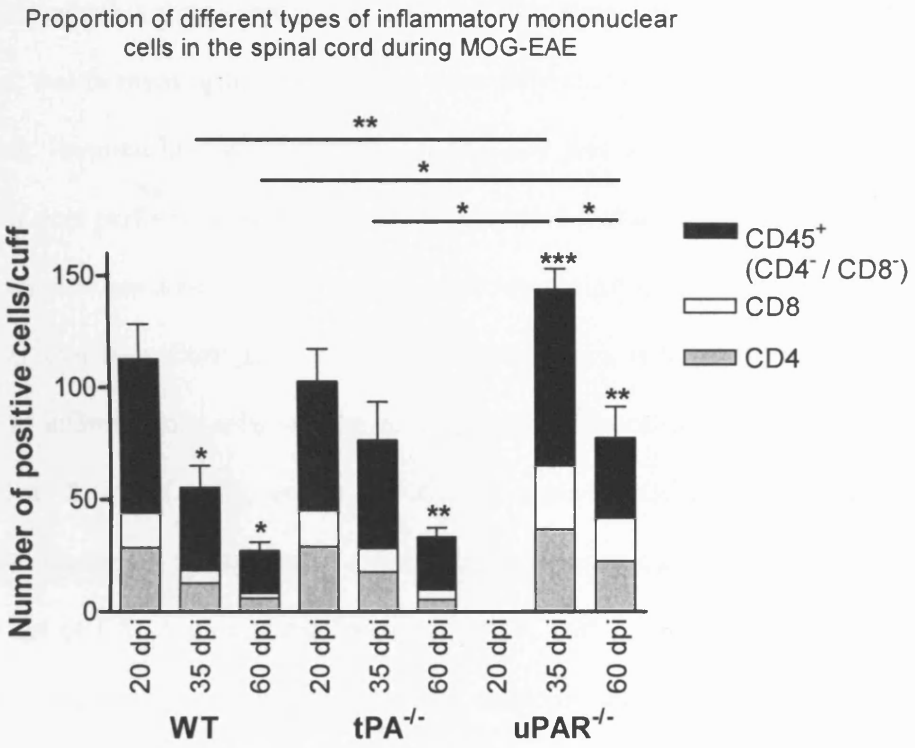

Figure 4.11. *Proportion of CD4$^+$, CD8$^+$ and CD45$^+$ (CD4$^-$/CD8$^-$) cells in perivascular cuffs.* The total number of CD45$^+$ cells were counted in three cuffs per section. On serial sections, the number of CD4$^+$ and CD8$^+$ cells were counted in corresponding perivascular cuffs. A total of three sections were counted per time point, per genotype. Results represent the mean ± SEM of CD45$^+$ cells. Statistical analyses for each genotype are versus 20 dpi and analyses between different genotypes are indicated by a bar. * $P < 0.05$, ** $P < 0.01$, *** $P < 0.001$.

4.2.6. Tight junctional proteins claudin-5 and occludin are unchanged before and during MOG-EAE disease.

Plasminogen activators are thought to play a role in the opening of the BBB through activation of MMPs and via interaction of tPA with LRP (Yepes *et al.*, 2003). Endothelial TJs have important roles in BBB regulation during pathological conditions. To investigate whether there were disturbances of TJs associated with increased BBB permeability, and to investigate whether there were differences between WT, $tPA^{-/-}$ and $uPAR^{-/-}$ mice, immunofluorescent staining for two key junctional proteins, claudin-5 and occludin was performed on sections from mice at different stages of MOG-EAE disease. Sections were double stained with an antibody against laminin, a component of blood vessel matrix. Changes in BBB permeability are thought to precede the infiltration of inflammatory cells and the development of clinical symptoms, thus mice were killed at 8 dpi of EAE, before any clinical signs of disease had developed. Additionally, sections were also taken from adjuvant injected control (AIC) mice and mice at 20 dpi of EAE with a clinical score of 3 or 4, with established inflammation. All blood vessels were examined in each section, and photomicrographs of representative areas were taken. Staining for claudin-5 and occludin in sections from AIC highlighted blood vessels and both proteins were closely localised with laminin in the vessel endothelial matrix (Figure 4.12). No differences were observed between the genotypes. In addition, there were no apparent differences between staining in sections from AIC and sections from mice at 8 and 20 dpi of EAE (Figures 4.13 A and B), and again no changes in patterns of staining between WT, $tPA^{-/-}$ and $uPAR^{-/-}$ mice. Thus the integrity of the TJs appeared intact pre-EAE disease onset, and at 20 dpi of MOG-EAE, in sections with a high presence of inflammatory mononuclear cells.

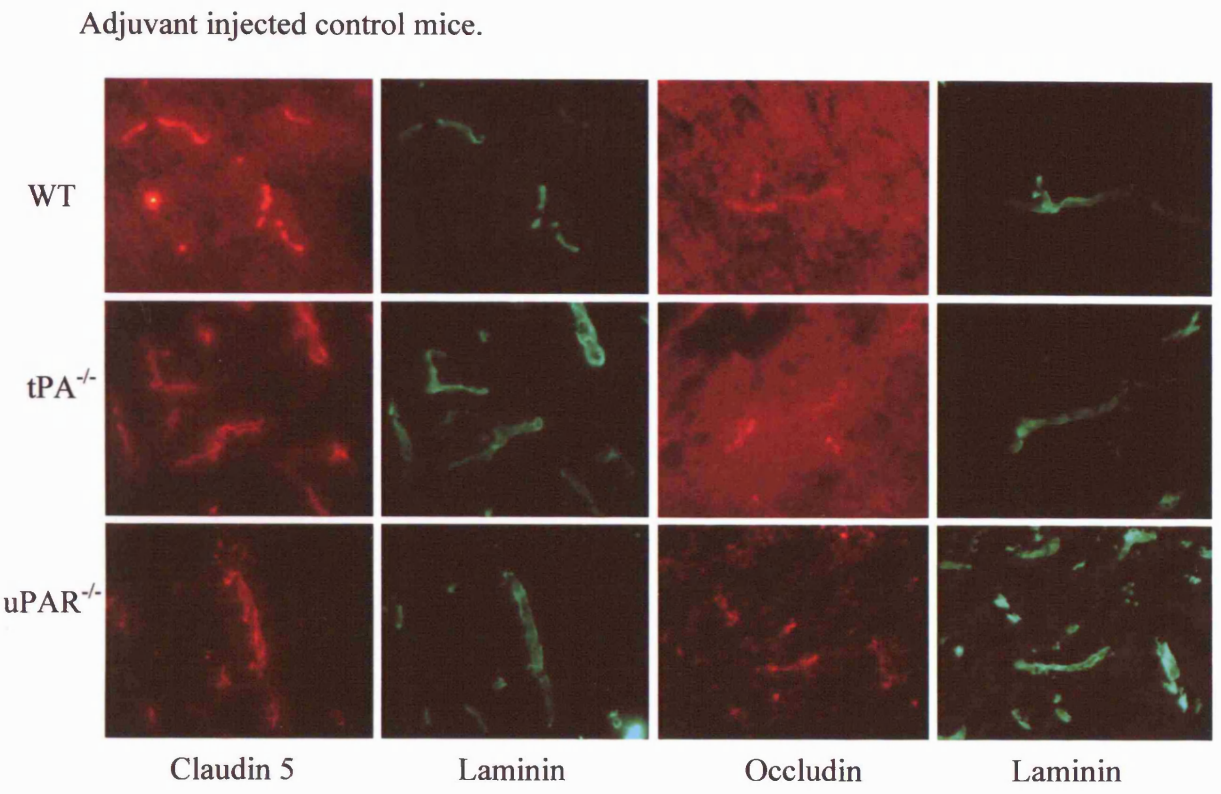

Figure 4.12. *Claudin 5 and occludin are co-localised with laminin at BBB tight junctions.* Frozen sections from adjuvant injected controls were sectioned and immunofluorescently stained for claudin 5 or occludin, and laminin. No differences were observed between the genotypes. Original magnification x 400.

A - MOG-EAE pre-disease onset; 8 dpi

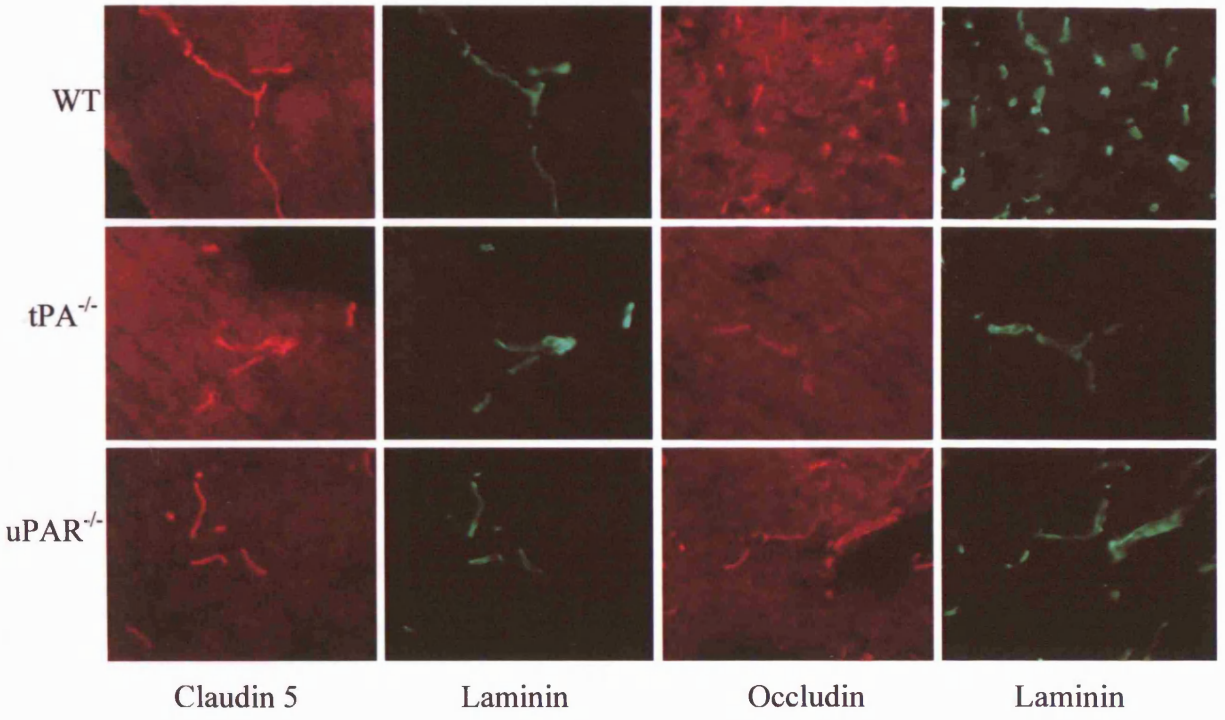

B - MOG-EAE post disease onset; 20 dpi.

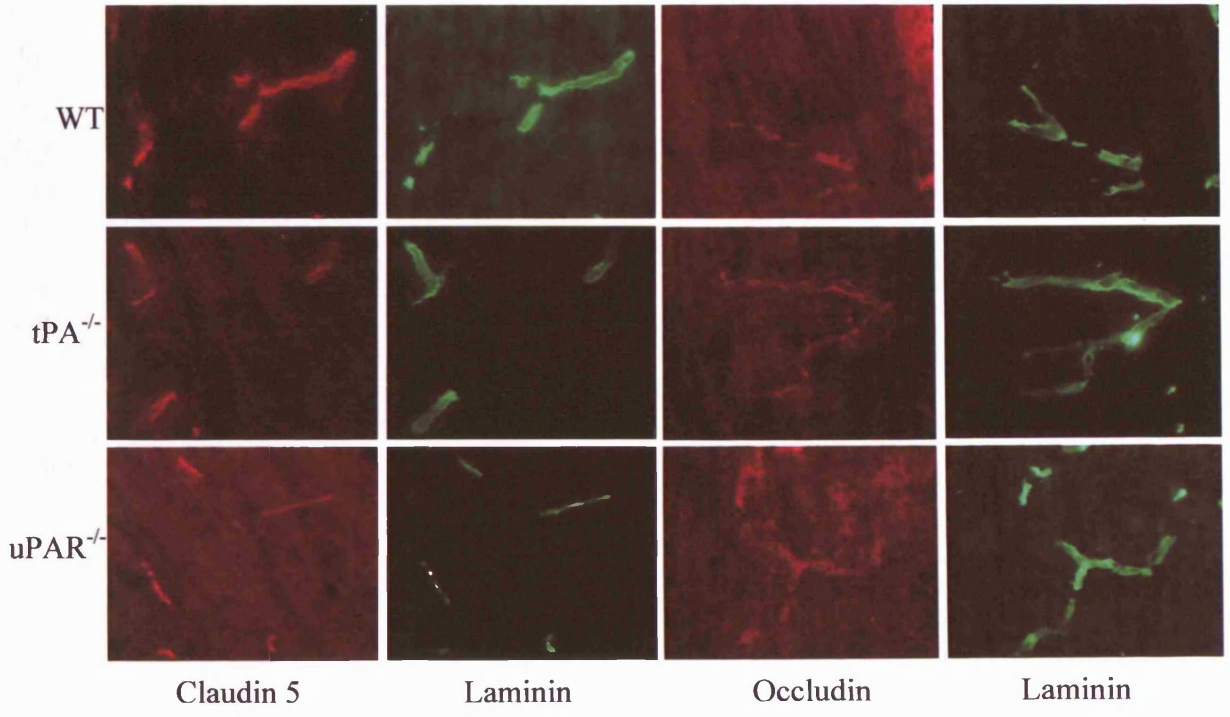

Figure 4.13. *Claudin 5 and occludin localisation at tight junctions does not change pre-or post MOG-EAE onset.* Frozen sections from EAE mice at 8 dpi **(A)**, pre EAE onset, and **(B)** post EAE onset at 20 dpi, were sectioned and immunofluorescently stained for claudin 5 or occludin, and laminin. No differences were observed between the genotypes and controls. Original magnification x 400.

4.2.7. Demyelination in MOG-EAE.

Staining with an antibody against MBP in representative sections of mouse spinal cord at specific time points during MOG-EAE development showed that demyelination was more pronounced in $tPA^{-/-}$ and $uPAR^{-/-}$ (Figure 4.14i E and F) mice than WT animals (Figure 4.14i D). The highest loss of myelin was seen at 60 dpi in $uPAR^{-/-}$ mice. Using densitometry scanning, the amount of light transmittance through sections stained with MBP was calculated to gain a semi-quantitative measure of myelin density. Four random fields per section were studied with three to four sections per group. The results were expressed as the amount of light transmittance through a stained portion of section normalised to a non-stained area of the slide. The density of myelin was decreased in WT and $tPA^{-/-}$ mice at 60 dpi of EAE, although this was not significant. Myelin density in $uPAR^{-/-}$ animals at 60 dpi was significantly reduced when compared to control animals (Figure 4.14ii; $P < 0.001$) and WT and $tPA^{-/-}$ mice at the same stage of disease ($P < 0.01$ and $P < 0.05$ respectively). Data at other time points of EAE showed no significant differences between genotypes.

(i) MBP

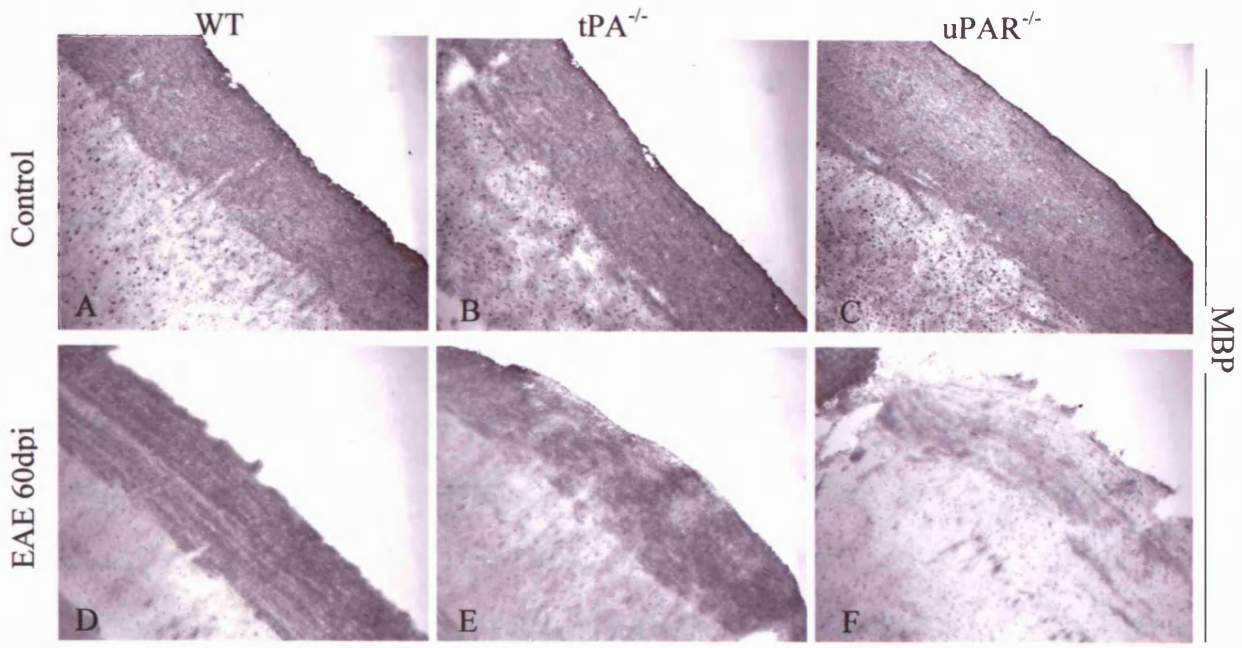

(ii)

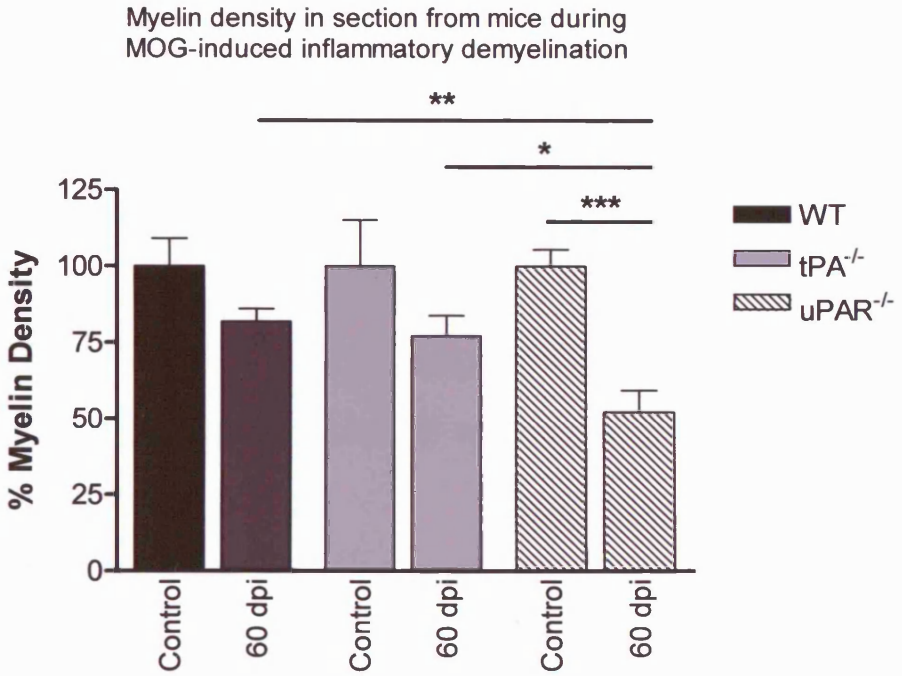

Figure 4.14. *Demyelination in MOG-EAE.* **(i).** Longitudinal frozen spinal cord sections from normal mice (A – C) and mice at 60 dpi onwards of EAE (D – F) were stained for myelin basic protein to assess the degree of demyelination in the CNS during EAE. MBP staining in control untreated mice, A – C and in EAE at 60 dpi, D – F. Original magnification x 100. **(ii).** Density of MBP staining was assessed using a Quantimet image analysis system, 4 random fields of myelin were assessed per slide, with three slides for each control and four slides for EAE groups. Results were normalised to untreated normal mice and are expressed as the mean ± SEM. Density of MBP staining in uPAR$^{-/-}$ mice at 60 dpi was significantly less than controls and WT animals at the same stage of disease. * $P < 0.05$, ** $P < 0.01$, *** $P < 0.001$.

4.2.8. Axonal pathology in MOG-EAE disease.

Levels of phosphorylated neurofilament have been documented to be increased in MS lesions, and other neurodegenerative disorders such as AD and ALS (Petzold, 2005). However, phosphorylated heavy chain neurofilaments (NfH), measured by ELISA are decreased in CREAE, and correlate with the degree of neurological deficit (Jackson *et al.,* 2005; Petzold *et al.,* 2003a; Pryce *et al.,* 2003). In control mice, immunohistochemical staining for phosphorylated neurofilament (SMI35) showed that SMI35 positive axons were clearly visible in the white matter of spinal cord sections (Figure 4.15i A – C). The appearance was uniform with long and straight axons packed in high density. In sections from MOG-EAE SMI35 staining revealed no obvious differences (Figure 4.15i D – E). Axons from 60 dpi of EAE showed slight changes in morphology, but these alterations were consistent in sections from WT, $tPA^{-/-}$ and $uPAR^{-/-}$ mice. There was no obvious increase or decrease in the number of axons stained for SMI35 between different genotypes and time points. To get a quantitative measure of phosphorylated neurofilament heavy chain an ELISA was performed using spinal cord protein extracts from MOG-EAE animals, in both the acute (20 dpi for $tPA^{-/-}$ and WT, 35 dpi for $uPAR^{-/-}$) and chronic phase (60 dpi.), and from normal control mice. No significant differences in levels of phosphorylated neurofilament NfH were observed between different time points of MOG-EAE and different genotypes of mice (Figure 4.15 ii).

Staining for non-phosphorylated neurofilament (SMI32) revealed very few immunopositive axons in sections from control mice (Figure 4.16i A - C), but large numbers of thickened SMI32 positive axons in sections from EAE mice, particularly at 60 dpi (Figure 4.16i D - F). Axonal pathology was assessed by counting the number of SMI32 positive axons in randomly selected areas of spinal cord white matter, from control and EAE mice at high magnification (x 400). Four areas were counted by two

independent observers per section with three sections per group to obtain a quantitative measure of axonal pathological changes (Trapp *et al.,* 1998) (Figure 4.16 ii). A statistically significant increase in SMI32 positive axons was found in $tPA^{-/-}$ mice at 20 dpi when compared to $tPA^{-/-}$ controls ($P < 0.05$). Furthermore, significant increases in SMI32 immunopositive axons were observed in all genotypes at 60 dpi when compared to relevant controls. $tPA^{-/-}$ and $uPAR^{-/-}$ mice had higher numbers of SMI32 positive axons when compared to WT mice at 60 dpi ($P < 0.001$ and $P < 0.01$ respectively).

(i) SMI35 – phosphorylated neurofilament

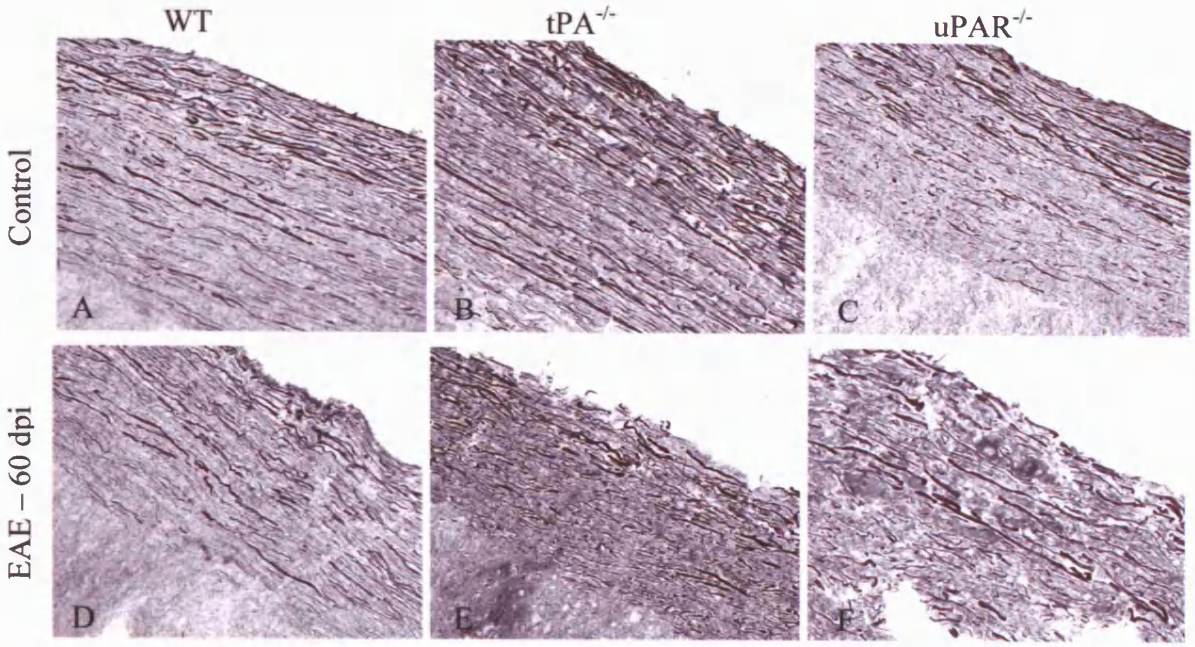

(ii)

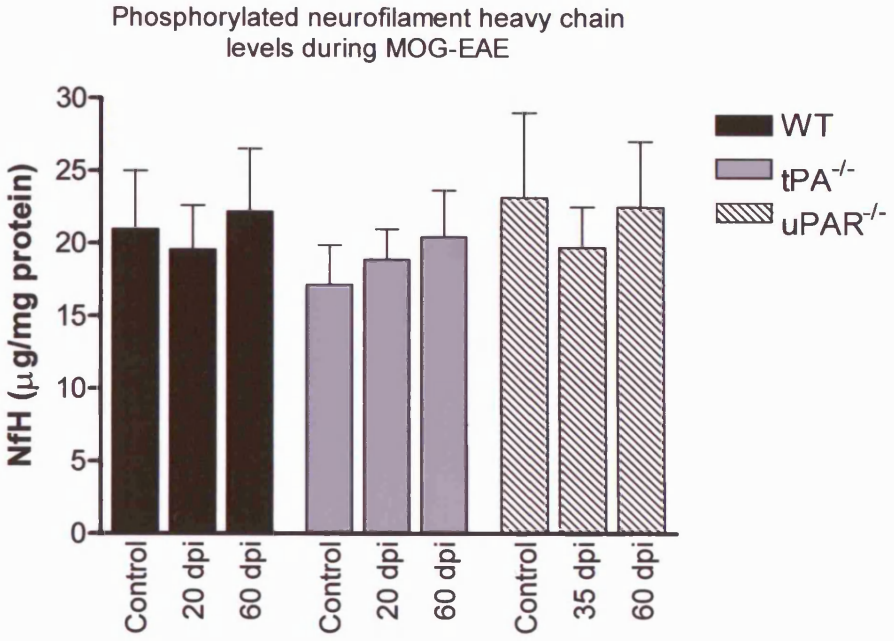

Figure 4.15. *Levels of phosphorylated neurofilament during MOG-EAE.* **(i)** Longitudinal frozen spinal cord sections from mice at 60 dpi were stained for SMI35 to assess changes in levels of phosphorylated neurofilament in the CNS during MOG-EAE. SMI35 staining in control untreated mice (A – C) and in EAE at 60 dpi (D – F). Original magnification x 100. **(ii)** A modified sandwich ELISA using antibodies against neurofilament was carried out on spinal cord homogenates from EAE and compared them with those from normal animals. n = 4 for each group, except for control WT and $tPA^{-/-}$ where n=8. Results are expressed as the mean NfH in µg per mg of protein ± SEM. There are no significant changes in levels of NfH in the spinal cords of WT, $tPA^{-/-}$ or $uPAR^{-/-}$ mice.

(i) SMI32 – non-phosphorylated neurofilament

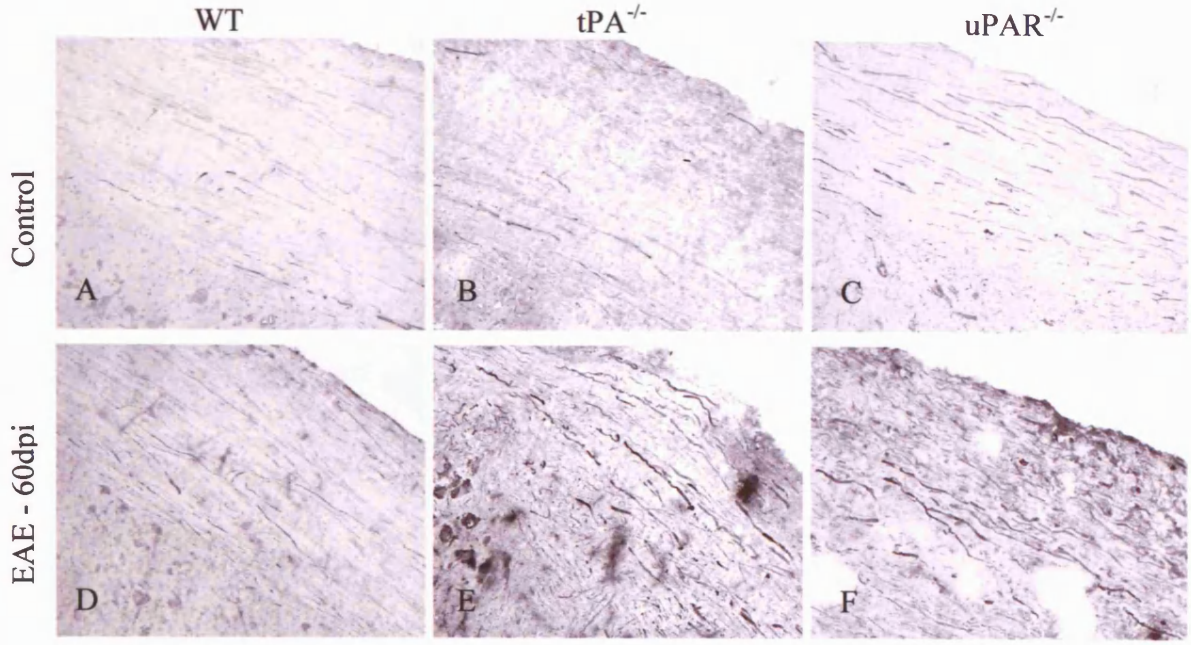

(ii)

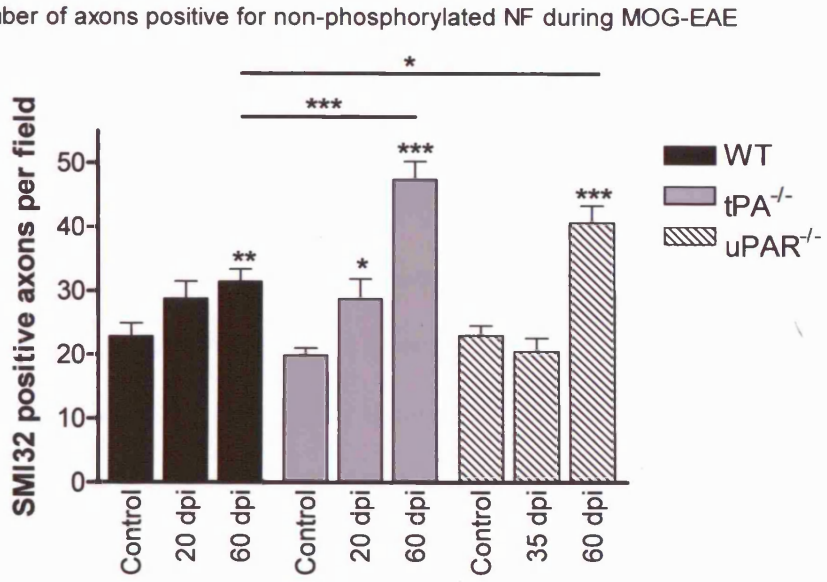

Figure 4.16. *Axonal pathology in MOG-EAE.* **(i)** Longitudinal frozen spinal cord sections from mice at 60 dpi onwards were stained for SMI32 to assess changes in axonal pathology in the CNS during EAE. SMI32 staining in control untreated mice (A – C) and in EAE at 60 dpi (D – F). Original magnification x 100. **(ii)** Four areas of white matter were counted by two observers per section with three sections per group. The number of SMI32 positive axons was increased in all genotypes at 60 dpi, significantly more so in $tPA^{-/-}$ and $uPAR^{-/-}$ mice. Results expressed as the mean ± SEM. * $P < 0.05$, ** $P < 0.01$, *** $P < 0.001$ versus relevant control and analyses between different genotypes are indicated by a bar.

4.3. Discussion.

Induction of EAE with MOG peptide produced variable results between the $tPA^{-/-}$, $uPAR^{-/-}$ and WT mice, with very different clinical pictures. A more severe and prolonged disease course was observed in $tPA^{-/-}$ mice characterised by an incomplete recovery and increased neurological deficit when compared to WT mice. In contrast, delayed onset and chronicity were major characteristics of EAE in $uPAR^{-/-}$ mice, coupled to persisting inflammatory cuffs of mononuclear cells, and a greater degree of demyelination. Adjuvant injected controls showed that clinical EAE disease results from an autoimmune response against MOG_{35-55} peptide and that Freund's adjuvant and *B. pertussis* toxin alone produce no CNS inflammation or demyelination.

We observed similar findings to Lu *et al.,* (2002), who also investigated the role of tPA in MOG-EAE using tPA deficient mice; with slight differences in the time of onset of disease, which could be accounted for by strain and interbreeding variations. The neurological signs in $tPA^{-/-}$ mice are reflected by a significantly higher clinical score and decreased motor activity, which was found in previous studies to be closely correlated with axonal damage (Pryce *et al.,* 2003). The significantly higher amount of non-phosphorylated neurofilament, SMI32, immunoreactivity in sections from $tPA^{-/-}$ mice also indicates that these animals had more axonal damage/dysfunction than WT mice. Non phosphorylated neurofilament is increased in MS tissue and is used as a marker for axonal integrity (Petzold *et al.,* 2003a; Trapp *et al.,* 1998). Whilst decreased neurofilament levels may not correlate directly to axonal loss at the early stages of disease but reflect a disruption of axonal integrity, neurofilament loss in the chronic phase of EAE has been shown to correlate with axonal degeneration (Petzold *et al.,* 2003a). As $tPA^{-/-}$ mice incur a higher degree of neurological deficit than the WT mice, tPA must be acting via a protective mechanism to aid in axonal survival. Additionally, WT mice could have a higher threshold for dephosphorylation of neurofilament and

axonal damage before degeneration occurs. Furthermore, as tPA has major roles in synaptic remodelling and plasticity in the brain (Seeds *et al.,* 1996), these results could also reflect a reduced ability of $tPA^{-/-}$ mice to remodel synaptic connections and functionally recover following neuronal/axonal damage. Remodelling of axonal connections has been shown to be an important contributing factor to recovery from targeted spinal cord EAE lesions in the rat (Kerschensteiner *et al.,* 2004). There is no apparent significant loss of myelin density in sections from $tPA^{-/-}$ mice indicating that axonal damage / degeneration can occur independently of demyelination. By activating latent TGF-β released from microglia and astrocytes, tPA can down-regulate NO release by microglia (Vincent *et al.,* 1998). Nitric oxide can form reactive nitrogen species, which can lead to oligodendrocyte damage (Mitrovic *et al.,* 1996), impairment of mitochondrial energy metabolism and ATP production, exacerbating demyelination and neurodegeneration (Bolanos *et al.,* 1995). Thus activation of TGF-β is another mechanism by which tPA could have protective effects during neuroinflammation.

The effect of lack of tPA on mice behaviour is controversial (Yepes and Lawrence, 2004), however the observation that normal $tPA^{-/-}$ mice were significantly more active than the WT counterparts is interesting in the light of the findings that neuroserpin deficiency leads to a decrease in locomotor activity in novel environments and in response to anxiety-like situations (Yepes and Lawrence, 2004). This suggests a role for the PA system on mouse behaviour and activity, possibly due to its involvement in long term potentiation, long term depression, learning and synaptic plasticity (Seeds *et al.,* 1996).

The delay in disease development in $uPAR^{-/-}$ mice, and in cell infiltration into the spinal cord reflects a reduced adhesion and migration of inflammatory mononuclear cells into the CNS coordinated by uPAR through its interactions with integrins and vitronectin (Blasi and Carmeliet P., 2002; Chapman, 1997). The importance of uPAR

has been documented in other *in vivo* models of infection or inflammation in uPAR$^{-/-}$ mice, (Gyetko *et al.,* 2000; Gyetko *et al.,* 2001; May *et al.,* 1998; Rijneveld *et al.,* 2002). Perivascular infiltration of mononuclear cells is indicative of the disease severity. The cuff count, cuff score and inflammatory histopathology in the CNS of uPAR$^{-/-}$ mice by 35 dpi, at the peak of disease, was comparable to that of WT and tPA$^{-/-}$ animals at 20 dpi, indicating that cells are migrating through the BBB, by other mechanisms, including the production of matrix metalloproteinases (MMPs) and upregulation of adhesion molecules (Sellebjerg and Sørensen, 2003). There were no changes in the numbers of different cell types between the WT and uPAR$^{-/-}$ mice at the peak/acute stages of disease, thus uPAR-mediated cell migration and adhesion appears to be important for all leucocytes. Persisting inflammation in the spinal cord of uPAR$^{-/-}$ mice, in addition to pronounced axonal impairment and demyelination with significant reduction in MBP, may account for chronicity of disease.

No changes were observed in the staining patterns for the tight junction associated proteins claudin-5 and occludin, thus cells migrating into the spinal cord do not appear to be travelling through this route. If leucocytes were travelling through the junctions it is highly likely that some disruption would be seen in the staining for these proteins. It is possible that cells were migrating by a transcellular pathway thus leaving the junctions intact, a more recent hypothesis which has been documented using brain endothelial cell lines (Etienne-Manneville *et al.,* 2000; Wolburg *et al.,* 2005). Although abnormalitites in staining for these proteins have been observed in MS tissue (Plumb *et al.,* 2000), this does not appear to be the case in this model of EAE. Staining for other junctional proteins could possibly have yielded different results. In one study investigating the patency of the BBB during EAE, a selective loss of claudin-3 was observed in blood vessels with associated presence of inflammatory cells, whilst staining for claudins 1 and 5, and ZO-1 was comparable with controls (Wolburg *et al.,*

2003), suggesting that this may not represent a primary pathological hallmark. Leucocytes could initially be passing through the endothelial cells but as inflammation increases, the number of cells and excessive amounts of proinflammatory cytokines could potentially lead to junctional protein disruption being associated with indirect secondary damage. However tPA has been documented to be involved in the opening of the BBB via interaction with MMP-9 and also with LRP. Infusion of tPA produces a dose-dependant increase in cerebrovascular permeability as measured by Evans Blue dye extravasation. This effect is inhibited by antibodies to LRP and by the LRP antagnoist RAP (Yepes *et al.,* 2003). Whilst it is clear that tPA increases BBB, permeability, it appears from this work that this is not due to a direct affect on tight junctions, but perhaps an effect at the basement membrane or endothelial cell level.

In this study, the role of tPA and uPAR in MOG-induced EAE, an animal model of inflammatory demyelination was investigated, in $tPA^{-/-}$ and $uPAR^{-/-}$ mice and their WT counterparts. In conclusion, both tPA and uPAR are implicated in the inflammation, demyelination and neurodegeneration characteristic of EAE, suggesting a major role for PA on modulating the course of neuroinflammatory disease. The effects of the PA system are unrelated to changes in BBB permeability via tight junction damage, however tPA appears to have a neuroprotective effect and uPAR mediated mononuclear cell migration appears to be important for development and progression of EAE.

5. Influence of the plasminogen activator system on fibrinolysis during EAE in tPA and uPAR deficient mice.

5.1. Introduction.

The plasma protein fibrin(ogen) is not normally present in the CNS, however under conditions of neuroinflammation, changes in the permeability of the BBB are accompanied by entry of serum proteins. As the plasminogen activator cascade is the key initiator of plasmin catalysed fibrin degradation, it was of interest to determine how changes in fibrinolysis, as a result of gene inactivation (tPA or uPAR) could be linked to the differences in clinical picture between the knockouts and WT mice. Impairment of fibrinolysis is a feature of MS tissue as a result of increased levels of PAI-1 and a subsequent decrease in tPA activity (Gveric *et al.,* 2003). Furthermore, fibrin deposition in a peripheral nerve injury model has been shown to hinder axonal regeneration, and contribute to demyelination and axonal degeneration (Akassoglou *et al.,* 2000).

To investigate the role of fibrinolysis in experimental neuroinflammation, levels of tPA, uPA, PAI-1 and plasminogen were measured in the different genotypes at different time points throughout the course of MOG-EAE disease. Additionally, the fibrinolytic capacity of EAE tissue was quantified and levels of fibrin(ogen) and fibrin D-dimer were assessed as a measure of plasminogen activity.

5.2. Results.

5.2.1. Presence of uPA, uPAR and PAI-1 positive cells in EAE perivascular cuffs.

Immunohistochemical analysis was performed on sections of spinal cords removed from mice during the acute phase of MOG-EAE disease and from normal non-injected control mice. Sections were stained with antibodies raised against uPA, uPAR and PAI-1. In sections from control mice there was very little staining for PAI-1, uPAR or uPA (Figure 5.1 A – C). Levels of PAI-1 were clearly increased in sections from MOG-EAE mice when compared to normal controls. PAI-1 was mainly located on

infiltrating inflammatory mononuclear cells in the perivascular cuffs observed in the sections of spinal cord from EAE mice, and additionally in some sections appeared to be produced locally within the spinal cord parenchyma. Staining patterns were similar in sections from WT and $tPA^{-/-}$ mice during MOG-EAE (Figure 5.1 D and G) however, increased PAI-1 staining was less obvious in $uPAR^{-/-}$ mice (Figure 5.1 J).

In the normal CNS there were no identifiable cells expressing uPAR (Figure 5.1 B). In spinal cord sections from WT EAE mice there was a dramatic increase in uPAR expressing cells (Figure 5.1 E) during the inflammatory stage of the disease, which were located in perivascular cuffs and areas of infiltration of inflammatory cells. In addition, an increase in uPAR staining was also observed in sections from $tPA^{-/-}$ EAE mice (Figure 5.1 H), however, not all infiltrating cells in these mice were uPAR positive (Figure 5.1 Hi). There was no uPAR staining in sections from $uPAR^{-/-}$ mice (Figure 5.1 K).

In sections from control mice there was some neuronal staining observed with the uPA antibody in the GM of spinal cord sections (Figure 5.1 C). However there was a marked increase in uPA staining in sections from EAE mice when compared to staining in sections from control mice (Figure 5.1 F, I and L). Cells positive for uPA could be identified in areas of inflammatory infiltration which were similar for WT, $tPA^{-/-}$ and $uPAR^{-/-}$ mice. uPA appeared to be located on inflammatory cells in the perivascular region and on cells migrating into the surrounding parenchyma.

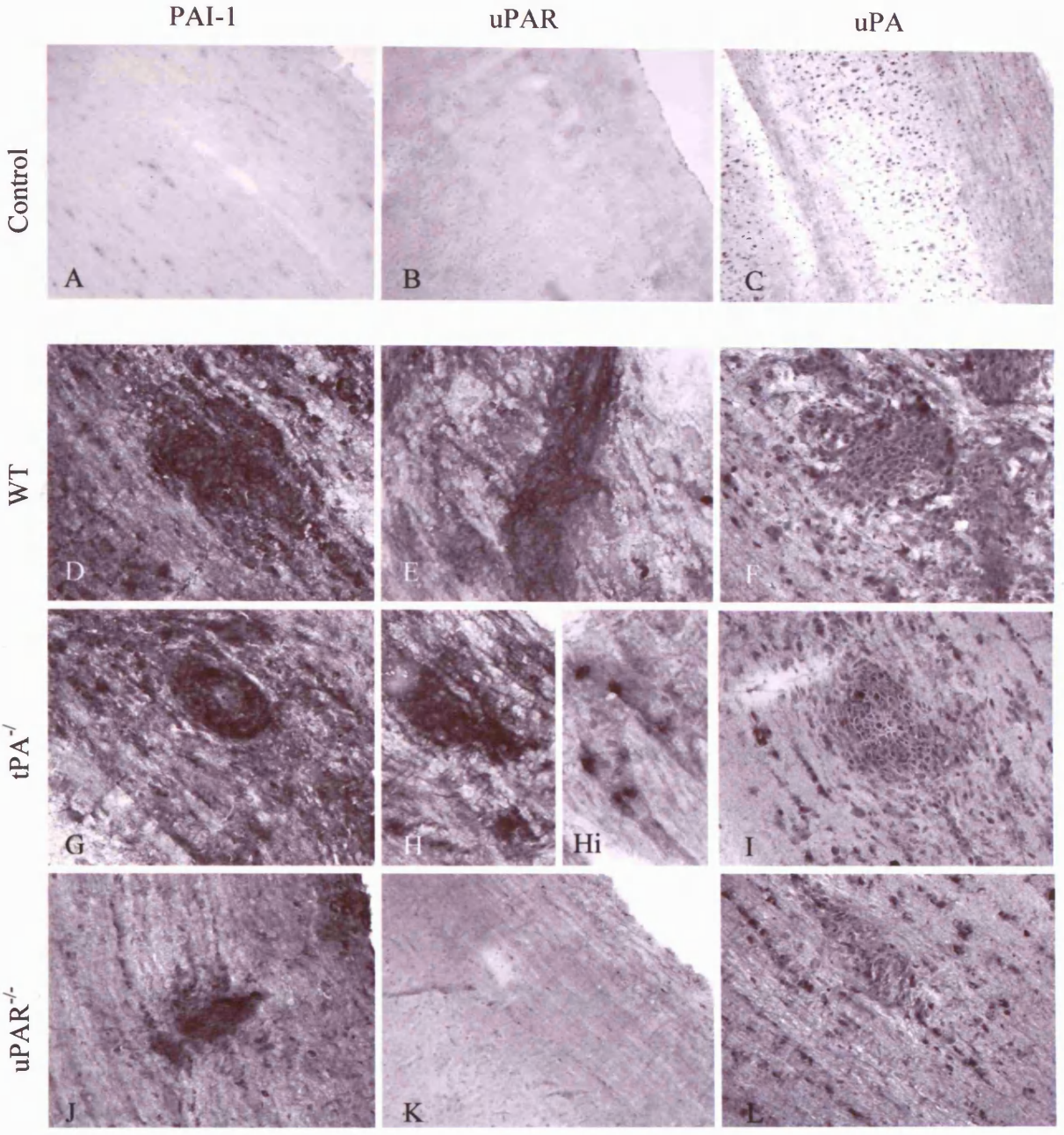

Figure 5.1. *PAI-1, uPAR and uPA staining in sections from MOG-EAE mice.* Spinal cords were removed from mice at the acute phase of EAE and cut longitudinally. Frozen sections were stained with antibodies raised against PAI-1, uPAR or uPA in sections from control (A - C), WT (D – F), $tPA^{-/-}$ (G - I) and $uPAR^{-/-}$ (J - L) mice. PAI-1, uPAR and uPA are increased in all mice during MOG-EAE and could be located on or surrounding infiltrating mononuclear cells in the spinal cord WM. No uPAR positive cells were observed in sections from $uPAR^{-/-}$ mice. Original magnification x 100 (A-C, K), x 400 (D – J, L).

5.2.2. Increased PAI-1 and uPA levels during MOG-EAE.

Levels of tPA and PAI-1 are increased in the CSF of MS patients (Akenami *et al.*, 1996; Akenami *et al.*, 1997) and PAI-1 antigen levels are also increased in MS brain tissue. Investigation into levels of tPA in MS and EAE tissue has lead to conflicting results (Ahmed *et al.*, 2001; Akenami *et al.*, 1999; Gveric *et al.*, 2001). To investigate how the levels of PAI-1, uPA and tPA changed during the course of MOG-EAE disease, ELISAs were performed on spinal cord protein extracts. Levels of PAI-1 showed marked fluctuations and were significantly higher ($P < 0.05$) at the peak of disease (20 dpi for $tPA^{-/-}$ and WT mice and 35 dpi for $uPAR^{-/-}$ animals) in all three genotypes (Figure 5.2 A - C). This was especially pronounced in $tPA^{-/-}$ mice in which the PAI-1 levels were approximately 10-fold higher in comparison with PAI levels from $uPAR^{-/-}$ and WT mice at 35 and 20 dpi respectively, and almost 100-fold higher than the appropriate control. An accumulation of uPA was observed during the acute (20 dpi and 35 dpi) and particularly chronic phase of EAE (60 dpi) in $tPA^{-/-}$ and $uPAR^{-/-}$ animals, which was not seen in WT mice (Figure 5.2 D - F). The increase in uPA was significant at 60 dpi in $tPA^{-/-}$ and $uPAR^{-/-}$ mice when compared to the relevant controls ($P < 0.05$). Levels of tPA did not change throughout the course of EAE disease in WT and $uPAR^{-/-}$ mice (Figure 5.3 A and B), and no tPA was detected in the spinal cords of $tPA^{-/-}$ mice. Ratios of tPA and uPA to PAI-1 are shown in Table 5.1. The ratio of tPA:PAI-1 was significantly decreased in WT mice at 20 dpi and $uPAR^{-/-}$ mice at 35 dpi of MOG-EAE ($P < 0.001$) when CNS inflammation was greatest, and at 60 dpi in both groups of mice ($P < 0.001$). Amount of uPA:PAI-1 was significantly decreased in WT, $tPA^{-/-}$ and $uPAR^{-/-}$ mice at the peak of disease ($P < 0.001$, $P < 0.001$ and $P < 0.05$ respectively). Additionally, the ratio of uPA:PAI-1 at 60 dpi in $tPA^{-/-}$ was also significantly lower than that in $tPA^{-/-}$ controls and WT and $uPAR^{-/-}$ mice at the same stage of EAE disease ($P < 0.01$, $P < 0.05$ and $P < 0.01$ respectively).

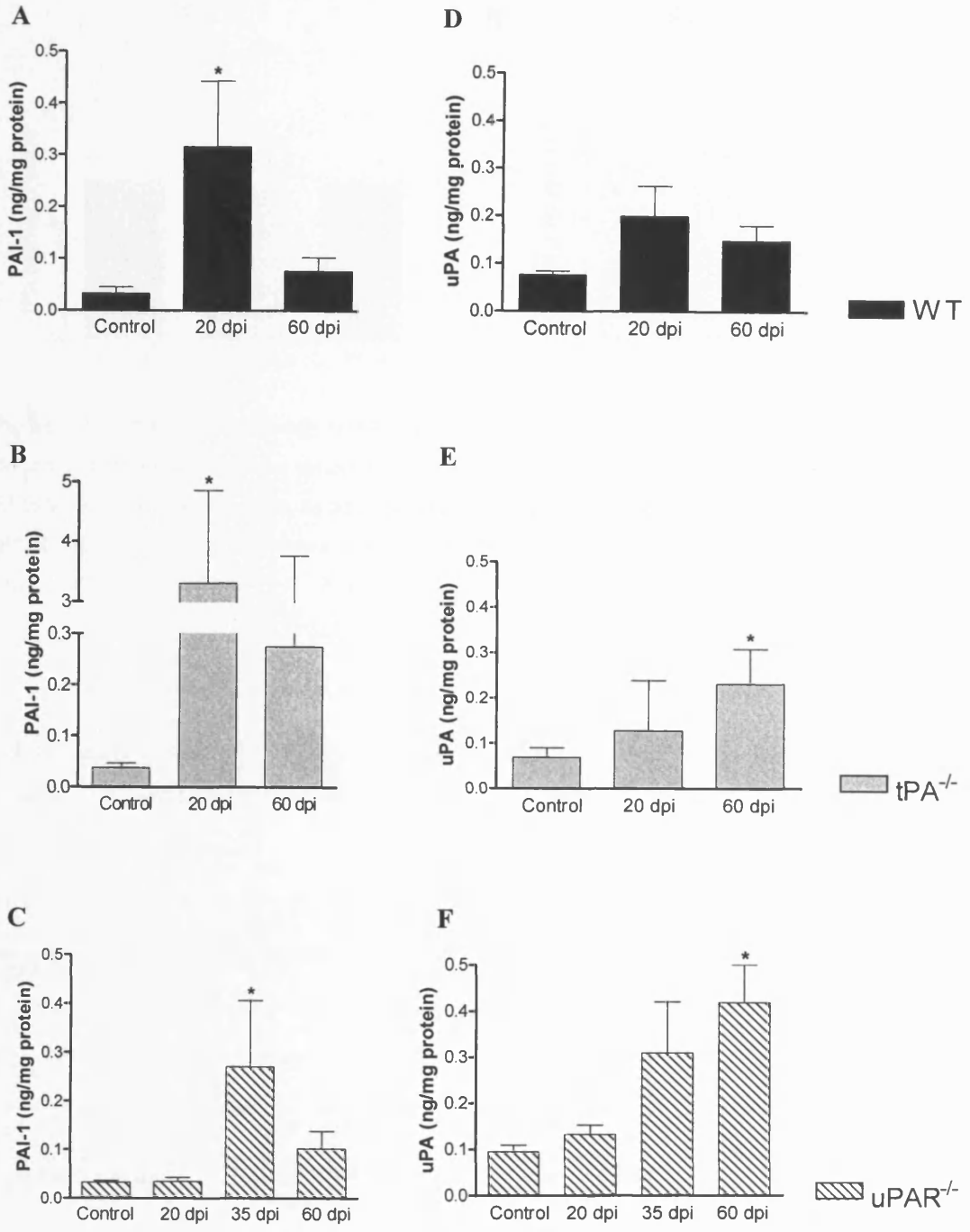

Figure 5.2. *Levels of PAI-1 and uPA during MOG-EAE in WT, tPA$^{-/-}$ and uPAR$^{-/-}$ mice.* Levels of PAI-1 (A – C) and uPA (D – F) antigen were determined in spinal cord homogenate samples from control and EAE mice by a modified sandwich ELISA. Results represent mean ng antigen / mg protein ± SEM. PAI-1 was significantly increased in WT, tPA$^{-/-}$ and uPAR$^{-/-}$ mice during the acute/peak phase of EAE (A - C). Levels of uPA were significantly higher that controls in tPA$^{-/-}$ and uPAR$^{-/-}$ mice at 60 dpi of MOG-EAE. n = 6 – 9 for WT, n = 6 or 7 for tPA$^{-/-}$ and n = 4 – 8 for uPAR$^{-/-}$. * $P < 0.05$ vs control.

Levels of tPA in the spinal cord during MOG-EAE

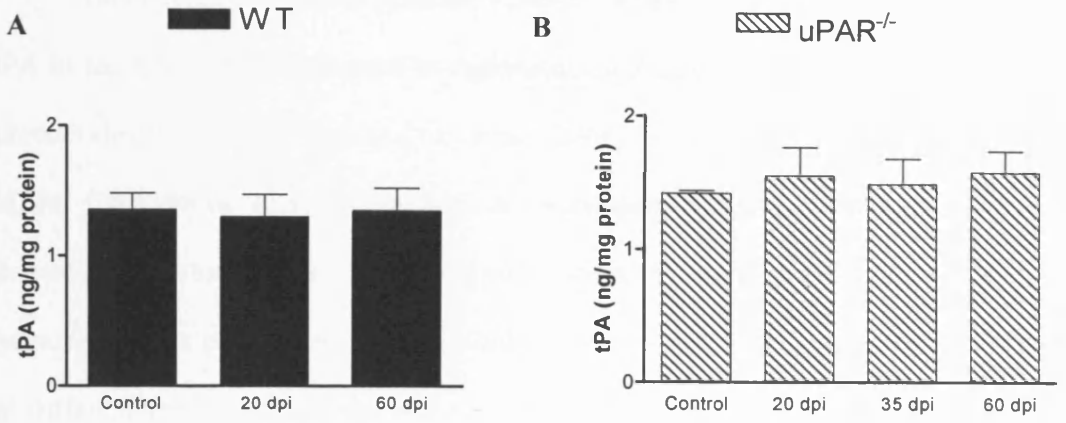

Figure 5.3. *Levels of tPA during MOG-EAE in WT and uPAR$^{-/-}$ mice.* Levels of tPA antigen were determined in spinal cord homogenate samples from control and EAE mice by a modified sandwich ELISA. Results represent mean ng antigen / mg protein ± SEM. There were no significant changes in tPA in WT or uPAR$^{-/-}$ mice during course of EAE. No tPA antigen was detected in samples from tPA$^{-/-}$ mice. n = 6 – 9 for WT and n = 4 – 8 for uPAR$^{-/-}$.

Ratio (ng/mg protein)	tPA:PAI-1	uPA:PAI-1
WT control	41.8 ± 4.0	2.4 ± 0.2
WT 20 dpi	4.1 ± 0.5 ***	0.6 ± 0.2 ***
WT 60 dpi	17.7 ± 2.3 ***	2.0 ± 0.4
tPA$^{-/-}$ control	-	1.8 ± 0.3
tPA$^{-/-}$ 20 dpi	-	0.0 ± 0.0 *** ¶
tPA$^{-/-}$ 60 dpi	-	0.8 ± 0.1 ** ¶ ¥
uPAR$^{-/-}$ control	44.1 ± 0.7	3.0 ± 0.4
uPAR$^{-/-}$ 20 dpi	45.4 ± 6.3	3.9 ± 0.6
uPAR$^{-/-}$ 35 dpi	5.5 ± 0.7 ***	1.1 ± 0.4 *
uPAR$^{-/-}$ 60 dpi	15.5 ± 1.6 ***	4.1 ± 0.8

Table 5.1. *Ratios of tPA and uPA to the inhibitor PAI-1 at different time points during MOG-EAE.* Results expressed as mean ± SEM, * $P < 0.05$, ** $P < 0.01$, *** $P < 0.001$ versus appropriate control, ¶ $P < 0.05$ tPA$^{-/-}$ versus WT at the same stage of disease, ¥ $P < 0.01$ tPA$^{-/-}$ versus uPAR$^{-/-}$ at the same stage of disease.

5.2.3. Neuroserpin is not upregulated during MOG-EAE disease.

Neuroserpin is a serine protease inhibitor (serpin), that reacts preferentially with tPA in the CNS. It is expressed in regions of the brain where either tPA message or protein are also found (Yepes and Lawrence, 2004). As PAI-1 is markedly upregulated in the CNS during experimental inflammatory demyelination, it was of interest to determine whether levels of neuroserpin were also altered. Western blotting for neuroserpin was performed on spinal cord protein extracts from control and EAE mice at different time points of the disease. No differences were observed in levels of neuroserpin between control and EAE mice, and additionally there were no differences between the genotypes (Figure 5.4).

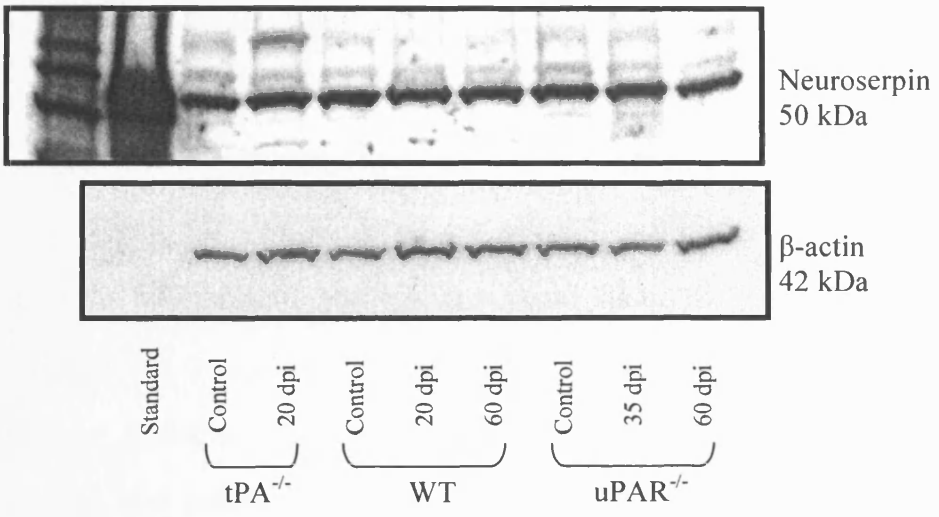

Figure 5.4. *Levels of neuroserpin do not change throughout the course of MOG-EAE disease.* Levels of neuroserpin were measured by Western blotting of spinal cord homogenate protein extract samples from control and EAE mice. Using an anti-neuroserpin antibody and a neuroserpin standard, no differences were observed between control and EAE samples. The blot was re-probed with anti-actin to ensure for equal protein loading onto the gel.

5.2.4. Plasminogen, fibrin(ogen) and fibrin D-dimer are significantly increased in tPA$^{-/-}$ mice during acute EAE.

Activity of tPA and uPA enzymes were likely to change as a result of increased PAI-1 levels. To investigate levels of plasminogen and plasmin activity, Western blotting was performed on spinal cord protein extracts from control and EAE WT, tPA$^{-/-}$ and uPAR$^{-/-}$ mice. Plasminogen migrated as an 85kDa band which corresponds to the cell-bound pre-activation form of plasminogen (lysine-plasminogen) (Figure 5.5 A). Using densitometry scanning, the highest amount of plasminogen was measured in tPA$^{-/-}$ mice at the peak of acute EAE (20 dpi) when compared to normal tPA$^{-/-}$ controls, and WT and uPAR$^{-/-}$ mice at the peak of disease ($P < 0.01$ and $P < 0.001$ respectively, Figure 5.5 B). Slight decreases in levels of plasminogen were observed in WT and uPAR$^{-/-}$ mice at 60 dpi of MOG-EAE, compared to levels in control mice and mice at the peak of disease, but these were not significantly different.

Using an antibody specific for fibrin(ogen), substantial extravasation and deposition of fibrin(ogen) was found surrounding perivascular cuffs in sections from EAE animals (Figure 5.6 D - F) when compared to fibrin(ogen) staining in sections from control mice (Figure 5.6 A – C). In WT and uPAR$^{-/-}$ mice fibrin deposits were confined to areas of inflammation, whereas in sections from tPA$^{-/-}$ mice, diffuse deposition was observed throughout the spinal cord parenchyma (Figure 5.6 E). Western blotting for fibrin(ogen) and the fibrin degradation product D-dimer was performed on spinal cord protein extracts from EAE and from control non-injected mice. This was to investigate the role of fibrin as a potential plasmin substrate in the progression of EAE. All mice were perfused before spinal cords were taken to remove any fibrinogen from the vascular sytem. Western blotting on spinal cord protein extracts showed that levels of fibrin D-dimer, a large molecular weight fibrin degradation product, changed throughout the course of MOG-EAE with a significant

increase during acute EAE (Figure 5.7 A). Similarly to plasminogen, the highest accumulation of fibrin D-dimer was observed in $tPA^{-/-}$ mice when compared to $tPA^{-/-}$ controls and WT animals at the same stage of disease development (Figure 5.7 B, $P < 0.05$). Statistical analysis revealed a strong positive correlation of PAI-1 with fibrin D-dimer ($r = 0.836$, $P < 0.001$), plasminogen levels ($r = 0.884$, $P < 0.001$) and clinical score ($r = 0.452$, $P < 0.01$).

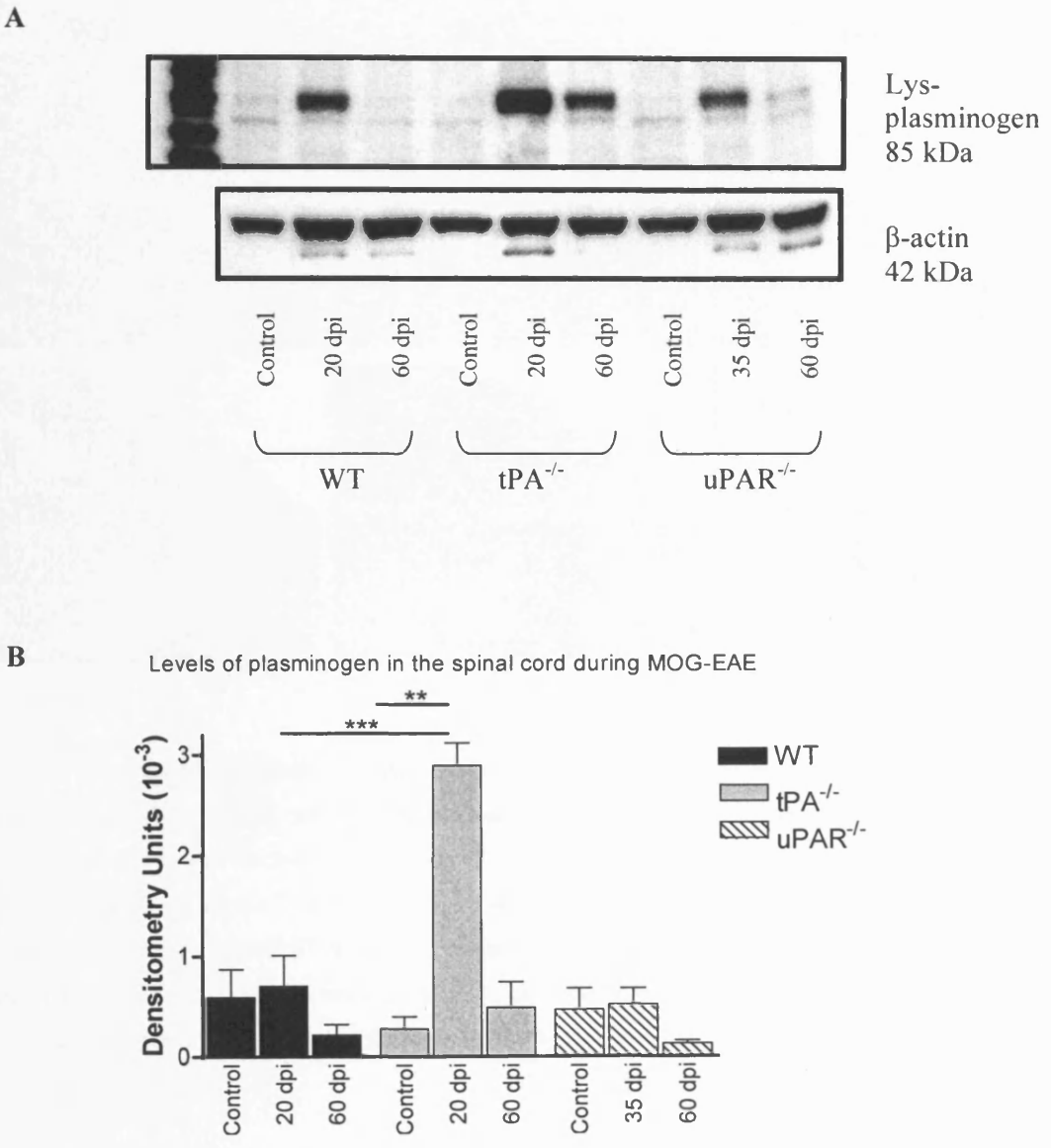

Figure 5.5. *Accummulation of plasminogen in tPA$^{-/-}$ mice during acute EAE.* Spinal cords from control and EAE mice were homogenised for protein extraction. **A.** Levels of plasminogen were detected by Western blotting and were quantitatively measured by densitometry scanning and results are shown as arbitrary densitometry units ± SEM. Blots were re-probed with anti-actin to ensure equal loading of proteins. **B.** Level of plasminogen were significantly increased during the acute phase of EAE in tPA$^{-/-}$ mice when compared to control mice and WT mice at the same stage of disease. n = 3, ** $P < 0.01$, *** $P < 0.001$.

Fibrin(ogen)

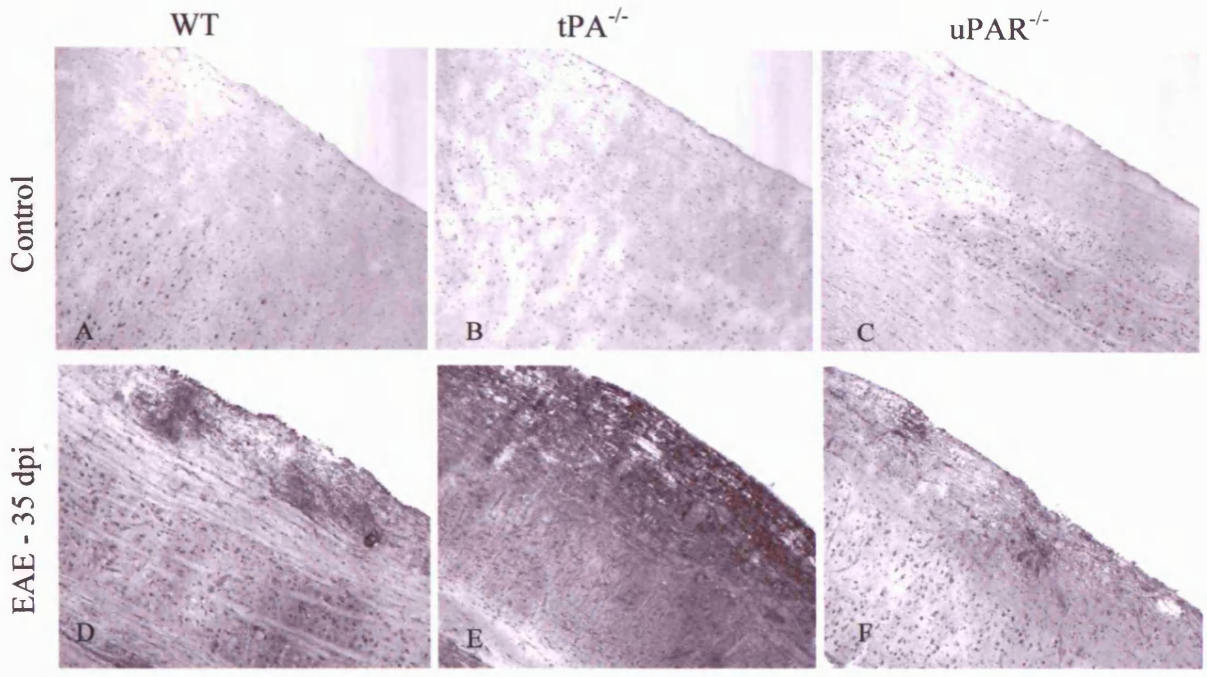

Figure 5.6. *Increased fibrin(ogen) staining during MOG-EAE in tPA$^{-/-}$ mice.* Spinal cords were removed from mice at 35 dpi of EAE and cut longitudinally. Frozen sections were stained with an antibody raised against fibrinogen in sections from WT, tPA$^{-/-}$ and uPAR$^{-/-}$ mice. There was an increase in fibrinogen staining in all EAE animals (D – F) when compared to the relevant controls (A – C), but particularly in sections from tPA$^{-/-}$ mice (E). Fibrinogen staining was particularly increased around cuffs in sections from WT and uPAR$^{-/-}$ mice (D and F), however a large amount of fibrin exudation in tPA$^{-/-}$ mice meant that it was also deposited throughout the spinal cord parenchyma. Original magnification x 100.

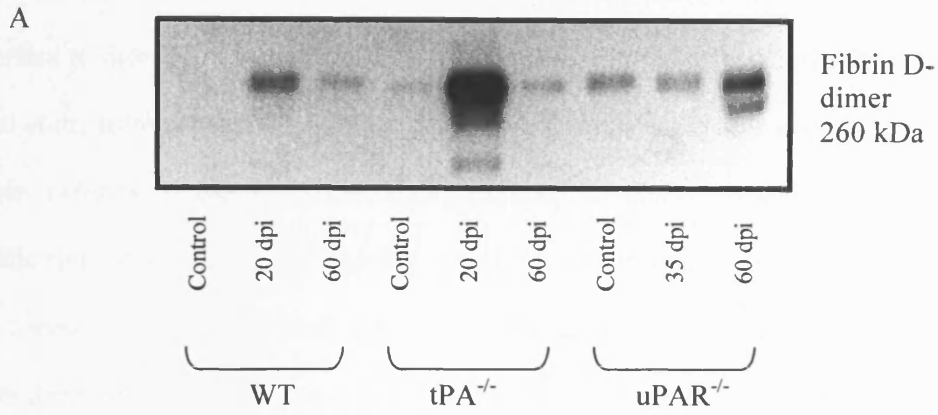

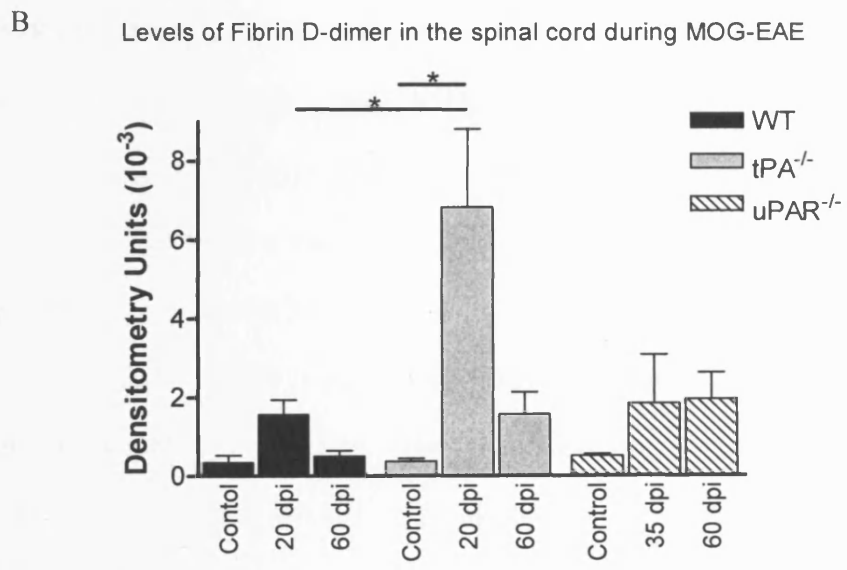

Figure 5.7. *Accummulation of fibrin D-dimer in tPA$^{-/-}$ mice during acute EAE.* Spinal cords from control and EAE mice were homogenised for protein extraction. **A.** Levels of fibrin were detected by Western blotting using an anti-fibrinogen antibody and were quantitatively measured by densitometry scanning. Results are shown as arbitrary densitometry units ± SEM. All animals were perfused before spinal cords were removed and fibrin detected is representative of the fibrin deposited in the nervous tissue. **B.** Levels of fibrin D-dimer were significantly increased during the acute phase of MOG-EAE in tPA$^{-/-}$ mice when compared to control mice, and WT and uPAR$^{-/-}$ mice at the same stage of disease. n = 4, * $P <$ 0.05.

5.2.5. Fibrinolysis in WT, tPA$^{-/-}$ and uPAR$^{-/-}$ animals during MOG-EAE.

As fibrin deposition is a known feature of MS (Claudio *et al.,* 1995), it was important to determine how the lack of tPA or uPAR would affect fibrin degradation in spinal cords from control and EAE animals. A clot lysis assay was used for spinal cord protein extracts to examine fibrinolytic capacity in control and knockout mice at specific time points during MOG-EAE. Over 5 h the fibrin clot degradation (measured as a decrease in OD at 405nm) was comparable in WT and uPAR$^{-/-}$ mice at all time points during EAE (Figure 5.8 A and C). In contrast there was no clot degradation in samples from tPA$^{-/-}$ mice during the first 5h of incubation (Figure 5.8 B). In order to establish whether other enzymes such as uPA can compensate for the lack of tPA, samples from tPA$^{-/-}$ mice were incubated up to 24h. A significantly higher clot degradation (75.4 % ± 10.0) was found in samples taken at 60 dpi of EAE in comparison to tPA$^{-/-}$ controls or samples taken at 20 dpi (31.38 % ± 11.69 and 28.9 % ± 13.0 respectively) ($P < 0.05$). Addition of tPA to sample buffer resulted in rapid clot degradation within the first hour of incubation, while omission of plasminogen in the sample buffer inhibited clot lysis.

Using fibrin overlay *in situ* zymography, the fibrinolytic capacity of sections of spinal cords could be investigated. The lysis of substrate was assessed by measuring lysis area and normalising this to total section area (Figure 5.9i). Sections from control uPAR$^{-/-}$ mice showed significantly less lysis of fibrin when compared to control WT mice ($P < 0.05$; Figure 5.9ii). Again there was no fibrinolysis in sections from tPA$^{-/-}$ animals (Figure 5.9ii) and sections from WT mice during acute and chronic phase of EAE showed significantly reduced fibrinolysis ($P < 0.05$). No differences in fibrinolysis between uPAR$^{-/-}$ control and EAE sections were observed. This data is in agreement with another study whereby all MS tissue, particularly acute lesion sites, showed a marked decrease in fibrinolysis (Gveric *et al.,* 2003).

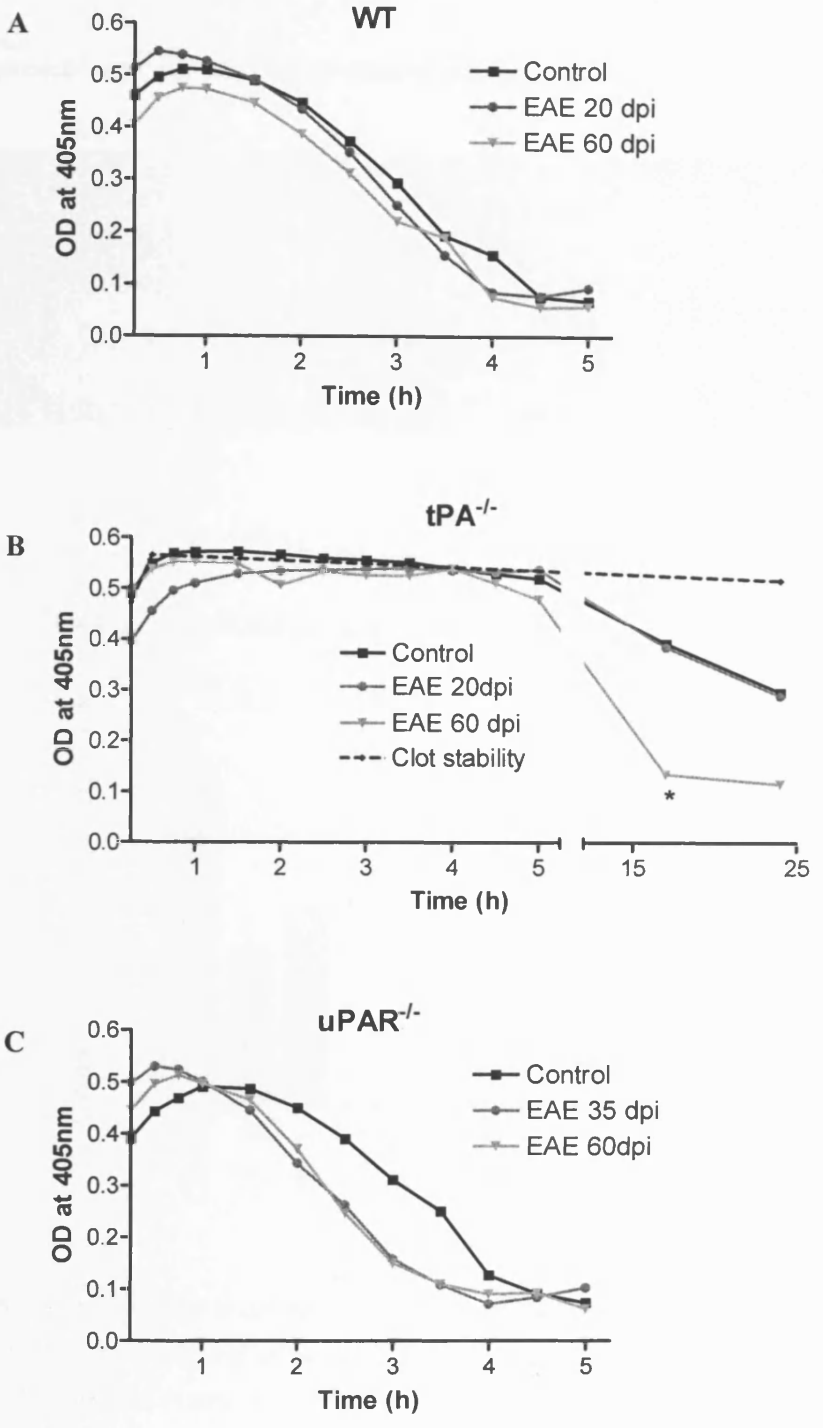

Figure 5.8. *Fibrinolysis in the mouse CNS.* Spinal cords from control and EAE mice at specific time points were homogenised for protein extraction. The fibrinolytic capacity was investigated using a clot lysis assay which measures the degradation of an *in vitro* formed clot using spectrophotometry. Results are presented as the mean clot degradation over time for **(A)** WT, **(B)** $tPA^{-/-}$ and **(C)** $uPAR^{-/-}$ mice. Samples from $tPA^{-/-}$ mice were incubated for 24 h to detect fibrinolysis initiated by uPA. $tPA^{-/-}$ mice at 60 dpi had a significantly faster clot degradation than either control or 20 dpi mice. n = 4,* $P < 0.05$.

Clot lysis *in situ* zymography

(i) – Representative sections from control mice

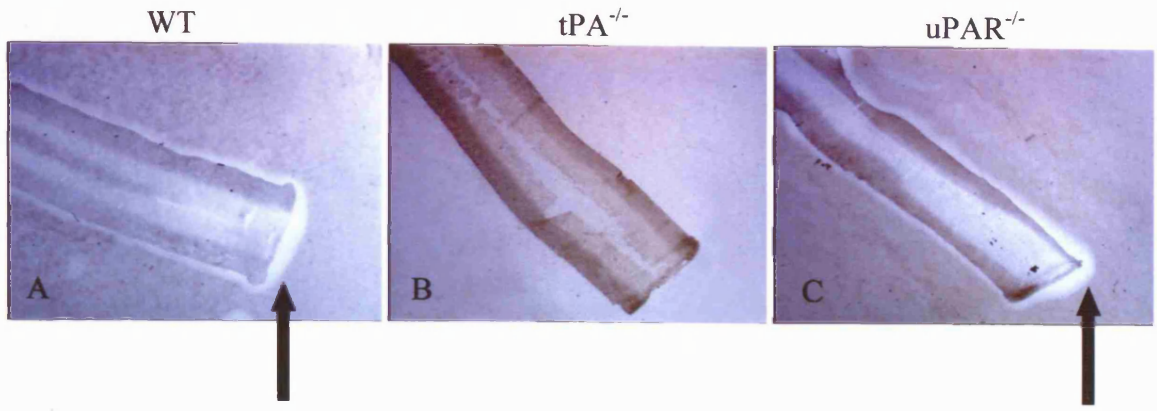

(ii)

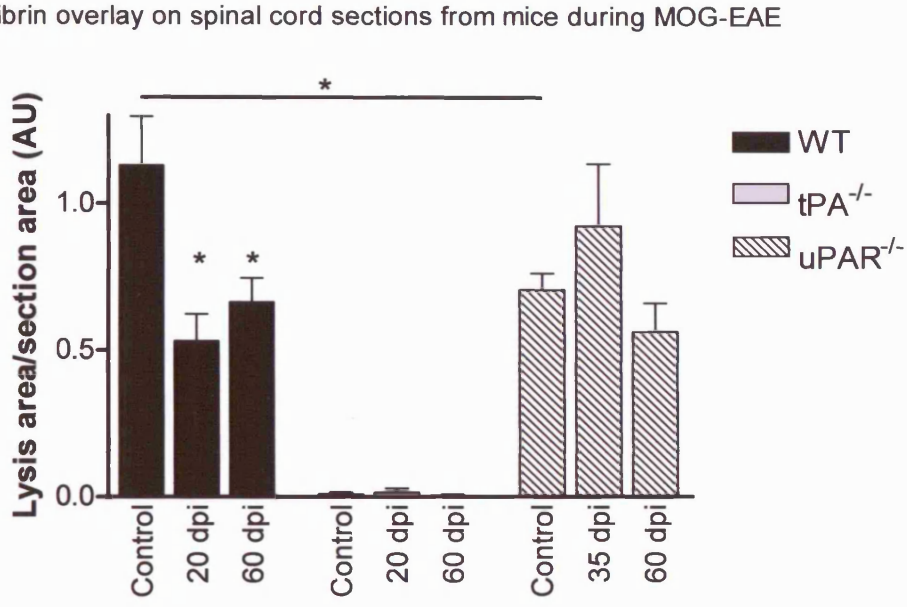

Figure 5.9. *Fibrin overlay in situ zymography of control and EAE spinal cords.* **(i)** Using frozen sections of spinal cord and overlaying an agarose solution of fibrinogen, plasminogen and thrombin, fibrin clot lysis can be measured *in situ*. Substrate lysis is identifed by a clear zone surrounding the tissue (arrows) which is not seen in sections from $tPA^{-/-}$ mice (A – C). The lysis of substrate was quantified using computer-assisted image analysis. The lysis area was normalised to the total section area, and results are presented as mean ± SEM. **(ii)** No fibrinolysis occurred in sections from $tPA^{-/-}$ mice. Spinal cord sections from WT EAE mice had a significantly reduced fibrinolytic capacity than control animals during the acute and chronic phases of disease, additionally, control WT mice had a significantly higher substrate lysis than control $uPAR^{-/-}$ mice. Statistical analysis versus relevant control and analyses between different genotypes are indicated by a bar, n = 3, * $P < 0.05$.

5.2.6. Fibrin(ogen) co-localised with non-phosphorylated neurofilament on axons in tPA$^{-/-}$ mice.

To investigate whether fibrin is deposited on axons and whether it can have an effect on axonal pathology, double fluorescent staining was carried out on perfused spinal cord sections from WT, tPA$^{-/-}$ and uPAR$^{-/-}$ mice. The two antibodies used were SMI32, for non-phosphorylated neurofilament, a measure of axonal integrity, and fibrinogen, FITC or a TRITC – labelled antibody respectively. Single staining with each antibody was used as a control. Single staining with SMI32 and fibrinogen (Figure 5.10 A and C) produced clear specific staining with no non-specific background (Figure 5.10 B and D). There were some fine axons stained with SMI32 in sections from normal tPA$^{-/-}$ control animals but no fibrinogen staining (Figure 5.10 E and F). Thick axons stained with SMI32 were detected in all EAE sections (Figure 5.10 G - I). Fibrin(ogen) staining was negligible in sections from WT and uPAR$^{-/-}$ EAE mice, but increased in sections from tPA$^{-/-}$ EAE mice (Figure 5.10 J – L). Double stained structures also positive for fibrinogen were largely seen in the tPA$^{-/-}$ animals (Figure 5.10 N), indicating fibrin deposition on damaged axons.

5.2.7. Altered Laminin expression during the course of MOG-EAE.

Fluorescent immunohistochemsitry and Western blotting for laminin were carried out to investigate the role of laminin as a potential plasmin substrate in the progression of MOG-EAE. Laminin is the known substrate of plasmin leading to neuronal death under conditions of excitotoxicity. Immunohistochemical staining for laminin in sections from EAE mice revealed blood vessel staining in WT and uPAR$^{-/-}$ mice, however in sections from tPA$^{-/-}$ mice, a high degree of laminin matrix was seen deposited through the spinal cord (Figure 5.11i A –C). Western Blotting on spinal cord protein extracts taken from acute (20 dpi for WT and tPA$^{-/-}$ mice, and 35 dpi for uPAR$^{-/-}$

mice) and chronic phase (60 dpi) of MOG-EAE and from control mice revealed an increase in laminin in $tPA^{-/-}$ mice at 20 dpi of EAE and in WT and $uPAR^{-/-}$ mice at 60 dpi of EAE (Figure 5.11ii)

Fibrin(ogen) and SMI32

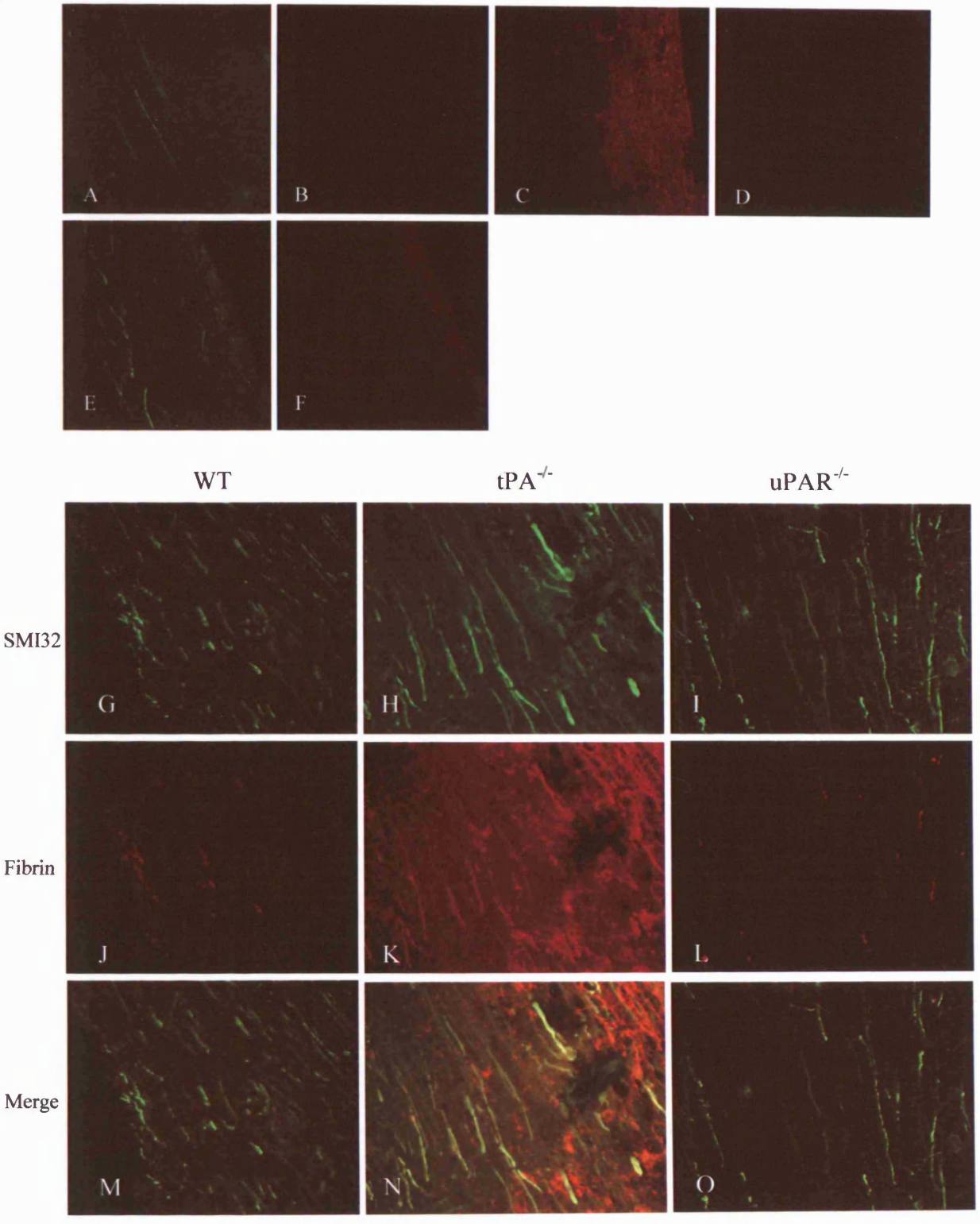

Figure 5.10. *Axons in tPA$^{-/-}$ EAE mice doubled stained with fibrin(ogen) and SMI32.* Spinal cords were removed from mice at 35 dpi for all animals and cut longitundinally. Frozen sections were stained with antibodies raised against non-phosphorylated neurofilament (SMI32) and fibrin(ogen) in sections from WT (G, J and M), tPA$^{-/-}$ (H, K and N) and uPAR$^{-/-}$ (I, L and O) mice. Fluorescent seconday antibodies were added to detect double stained cells. Controls include single staining with each antibody (A = SMI32 and C = Fibrinogen), and double staining in control tPA (E and F).

Laminin

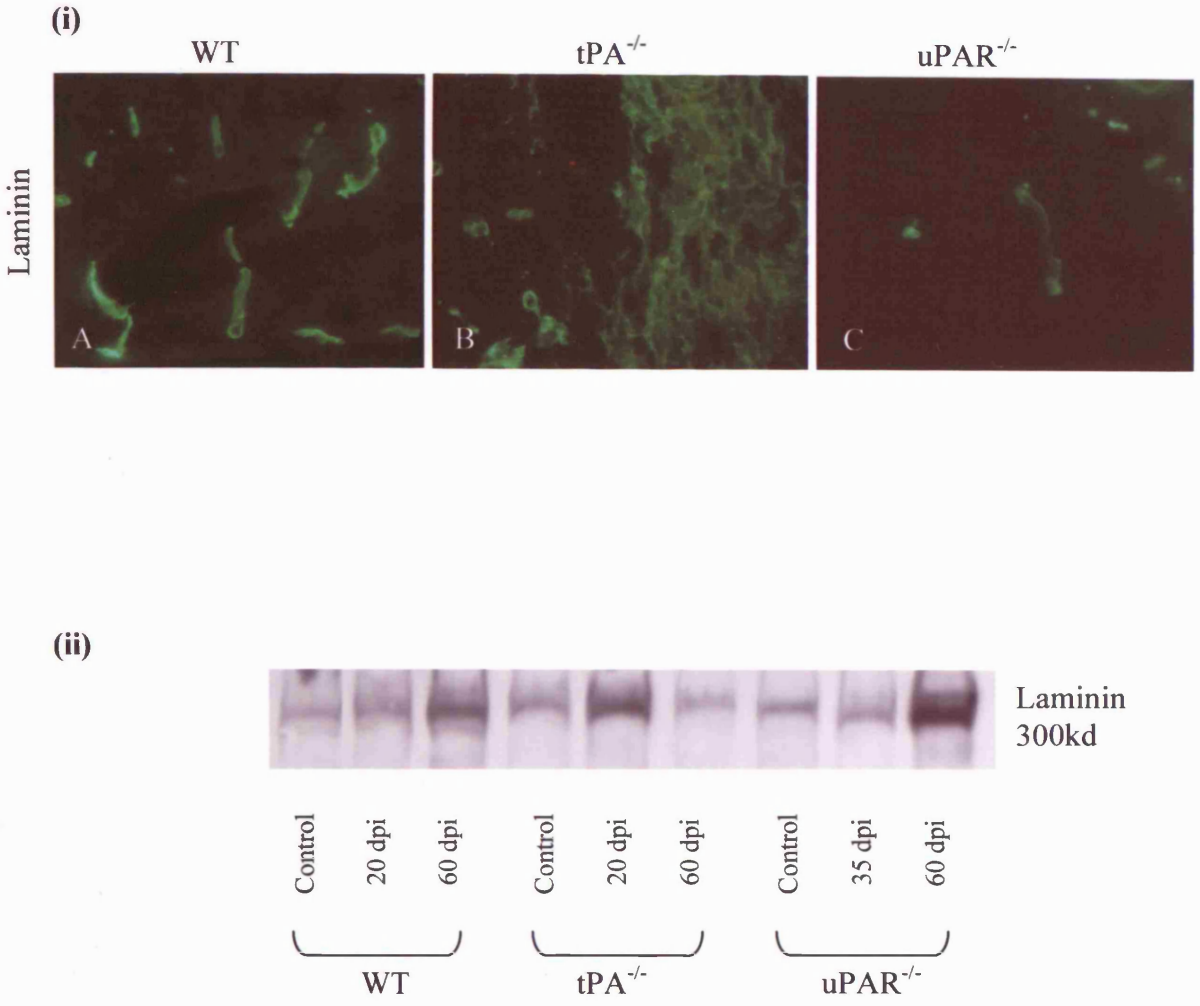

Figure 5.11. *Laminin protein in WT, tPA$^{-/-}$ and uPAR$^{-/-}$ mice during MOG-EAE.* Fluorescence immunohistochemistry and Western blotting for laminin were performed on spinal cord sections and protein extracts from control and EAE animals in the acute (20 dpi for tPA$^{-/-}$ and WT and 35 dpi for uPAR$^{-/-}$) and chronic (60 dpi) phase of disease using an anti-laminin antibody. **(i)** Immunofluorescence staining showed laminin ECM deposition in spinal cord sections from tPA$^{-/-}$ mice but not in sections from WT or uPAR$^{-/-}$ mice at 20 dpi of EAE. **(ii)** By Western blotting, an apparent increase in laminin was seen in the acute phase of tPA$^{-/-}$ mice and in the chronic phase of WT and uPAR$^{-/-}$ animals.

5.2.8. Altered expression of tPA receptors during the course of MOG-EAE.

Annexin II is a calcium-dependent phospholipid binding protein which is expressed at low levels in the adult CNS, but is upregulated in numerous pathological conditions. In endothelial cells and macrophages annexin II is expressed on the plasma membrane as a tetramer of two annexin II subunits linked by two p11 subunits. This provides a cell surface receptor for tPA and plasminogen interaction, resulting in an ~ 60 fold increase in plasmin generation, thus it has a direct effect on fibrinolysis. Annexin II has been implicated in tPA mediated activation of microglia (Siao and Tsirka, 2002), however in MS tissue, upregulation of annexin II and another tPA receptor, LRP, are correlated with an impairment of fibrinolysis and could indicate a compensatory mechanism in lesions to aid in fibrin degradation (Gveric *et al.*, 2005). LRP is a scavenger receptor which binds to a variety of biologically diverse ligands, including tPA and uPAR. LRP is expressed in the CNS by neuronal cells, microglia and astrocytes and consists of an extracellular ligand binding heavy chain (515 kDa) and a transmembrane light chain (85 kDa) (Herz, 2003). Whilst LRP regulates extracellular proteolysis by internalising proteases and protease:inhibitor complexes, it has also been linked to opening of the BBB through interaction with tPA (Yepes *et al.*, 2003). To investigate whether levels of these two tPA receptors changed throughout the course of MOG-EAE in WT, $tPA^{-/-}$ and $uPAR^{-/-}$ mice, Western blots were carried out on spinal cord protein extracts.

During MOG-EAE there was an increase in LRP at the acute stage of disease in WT, $tPA^{-/-}$ and $uPAR^{-/-}$ mice and at 60 dpi in $tPA^{-/-}$ and $uPAR^{-/-}$ mice (Figure 5.12 B). Annexin II (Figure 5.12 A) was also significantly increased during EAE, specifically in $tPA^{-/-}$ mice at 20 dpi and in WT mice at 60 dpi (Figure 5.12 D).

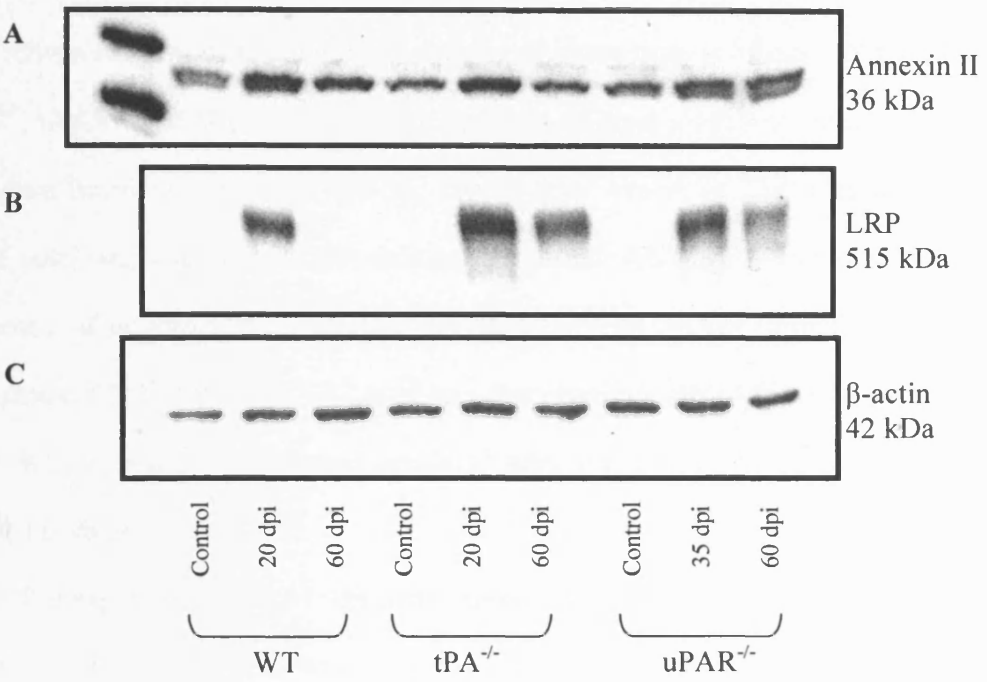

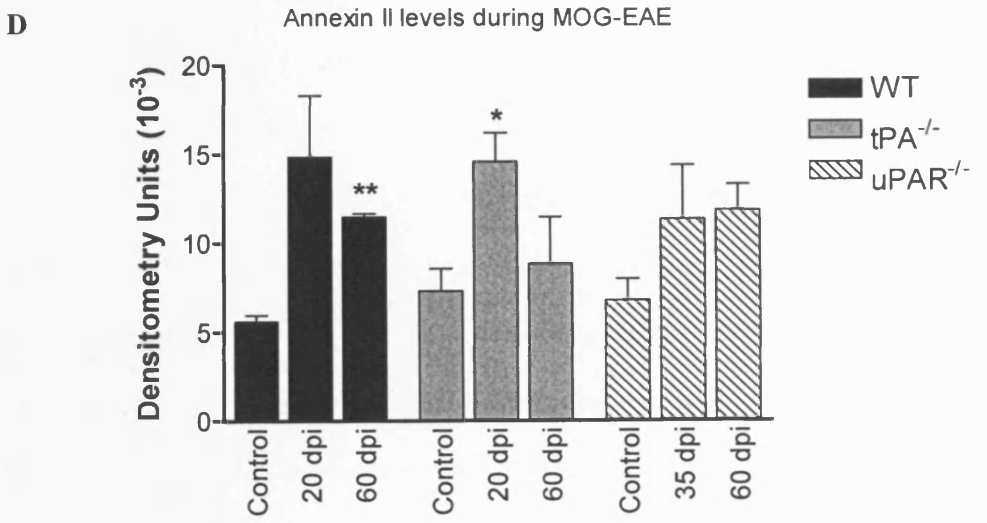

Figure 5.12. *Levels of the tPA receptors, Annexin II and LRP, during MOG-EAE.* Spinal cords from control and EAE mice were homogenised for protein extraction. Levels of (**A**) annexin II and (**B**) LRP were detected by Western blotting using an anti-annexin II and an anti-LRP heavy chain antibody. **C.** Blots were re-probed with anti-actin to ensure equal loading of proteins onto the gel. Levels of annexin II were quantitatively measured by densitometry scanning. **D.** Results are shown as arbitrary densitometry units ± SEM. Levels of annexin II and LRP were increased during MOG-EAE. Annexin II was significantly increased during the acute phase of MOG-EAE in $tPA^{-/-}$ mice when compared to control mice. n = 1 for LRP, n = 2 for annexin II, * $P < 0.05$, ** $P < 0.01$.

5.3. Discussion.

Given the very different clinical pictures resulting from induction of MOG-EAE in $tPA^{-/-}$, $uPAR^{-/-}$ and WT mice (Chapter 4), it was of great interest to investigate how the known functions of the PA system, i.e., its involvement in fibrinolysis, affected disease outcome. The effect of tPA deficiency on fibrinolysis in EAE was a significant impairment of *in vitro* clot degradation confirming tPA as the key fibrinolytic enzyme in the mouse CNS. Whilst $uPAR^{-/-}$ mice had comparable levels of fibrinolysis to those of the WT, significantly increased levels of uPA could account for the chronicity observed in these mice.

The expression of PAI-1, the main inhibitor of tPA and uPA, is upregulated by pro-inflammatory cytokines, such as interleukin-1 (IL-1) and tumour necrosis factor alpha (TNF-α) (Gabay and Kushner, 1999; Kasza *et al.*, 2001). The levels of PAI-1 in EAE spinal cord correlated strongly with clinical score, being highest at the peak of disease in all three genotypes. Additionally, cells positive for uPA, PAI-1 and uPAR, were located by immunohistochemistry to inflammatory perivascular cuffs. The approximate 10-fold increase in PAI-1 in $tPA^{-/-}$, compared to WT mice, during the acute phase of MOG-EAE, was sufficient to completely inhibit fibrinolysis initiated by uPA among other proteolytic enzymes, as reflected by the exceptionally high levels of fibrin D-dimer at this stage of disease. In addition, increased amounts of plasminogen in the spinal cord of $tPA^{-/-}$ mice at the peak of disease reflect its accumulation resulting from decreased activation of the zymogen into its active form plasmin. However as levels returned to normal, during the chronic stage of disease, increased uPA in $tPA^{-/-}$ spinal cord could account for higher turnover of plasminogen and the fibrinolysis. A higher degree of clot degradation was observed in $tPA^{-/-}$ mice at 60 dpi after 17 h incubation suggesting that in the chronic phase of disease there was a partial compensation by uPA, a slower acting enzyme, initiating fibrinolysis once levels of PAI-1 had decreased. In

addition to upregulation of uPA, increases in expression of the PA receptors annexin II and LRP could also represent endogenous compensatory mechanisms to increase local fibrinolysis. Binding of tPA to its receptors results in an ~ 60 fold increase in plasmin generation, thus by increasing annexin II and LRP, the efficiency of plasminogen activation is increased upon binding of tPA that is not complexed with PAI-1. In the same way, increased levels of annexin II and LRP are correlated with diminished fibrinolysis in MS tissue as increased formation of tPA:PAI-1 complexes reduces the capability of tPA receptors to generate plasmin (Gveric *et al.,* 2005). Although fibrin overlay shows a decrease in fibrinolysis in control uPAR$^{-/-}$ mice compared to control WT mice, this did not lead to a significant impairment of clot lysis nor an accumulation of fibrin, as tPA was present in sufficient amounts to compensate for this. Dewerchin *et al.,* (1996) have also documented decreased fibrin lysis in uPAR$^{-/-}$ mice by *in situ* zymography and concluded this was as a result of decreased uPA-mediated plasminogen activation. Western blotting did not detect an increase in plasminogen as a measure of decreased PA activity in uPAR$^{-/-}$ mice, however again, the tPA in these mice would account for the majority of plasminogen activation.

Levels of the CNS-specific tPA inhibitor neuroserpin did not change in the various genotypes throughout the course of MOG-EAE, suggesting a minimal role for neuroserpin in experimental neuroinflammation. These data agree with a study carried out in MS tissue whereby the decrease in fibrinolytic capacity of lesions was due to complex formation of tPA with PAI-1, not with neuroserpin (Gveric *et al.,* 2003). However in contrast to this study, which revealed a decrease in native neuroserpin, possibly a reflection of neuronal damage, no changes in levels of neuroserpin were found in spinal cord samples from EAE mice.

uPA, a stress-responsive proteinase upregulated in infiltrating inflammatory cells (Blasi and Carmeliet P., 2002; Gabay and Kushner, 1999), was found to be

significantly increased in the CNS in uPAR$^{-/-}$ mice in the chronic stages of EAE, compared to WT and tPA$^{-/-}$ animals. Accumulation of uPA could reflect the absence of a clearance mechanism in uPAR$^{-/-}$ animals, as endocytosis of uPA by uPAR, LRP and PAI-1 is a mechanism by which uPA is inactivated, cleared from the cell surface and degraded intracellularly (Irigoyen *et al.,* 1999). Furthermore, uPA may act independently of uPAR as uPA catalysed plasminogen activation during pericellular proteolysis is stimulated *in vitro* by cells that do not express uPAR (Longstaff *et al.,* 1999). Under normal conditions uPA is expressed at low levels and kept in balance by PAI-1. In uPAR$^{-/-}$ mice however, uPA is present at much higher concentrations than PAI-1 in chronic stage EAE and plasminogen is decreased at the same time point. Thus uncontrolled uPA-generated plasmin proteolysis could lead to myelin and neuronal damage in the CNS of these animals (Blasi and Carmeliet P., 2002), which would correlate with the greater demyelination and higher numbers of SMI32 positive axons detailed in Chapter 4. Plasmin and uPA are also able to cleave laminin (Chen and Strickland, 1997) and fibronectin (Gold *et al.,* 1992) respectively and possibly other axon-supporting ECM components. In addition, uPA-generated plasmin can activate MMPs (Carmeliet P. *et al.,* 1997), which are known to have detrimental effects under neuroinflammatory conditions (Cuzner and Opdenakker, 1999), particularly MMP-9 which can break down myelin. Furthermore, uPA can directly activate MMP-9 (Liu *et al.,* 2005), thus is a potential important pathogenic mechanism involved in inflammatory demyelination.

A key feature of neuroinflammation is increased BBB permeability and subsequent entry of fibrin into the CNS. Impairment of fibrinolysis due to increased PAI-1, as observed in MS tissue (Gveric *et al.,* 2003), and in the tPA$^{-/-}$ mice, leads to accumulation of fibrin which has important effects in the CNS, contributing to disease progression. Fibrin deposits frequently accompany inflammatory responses,

(Akassoglou and Strickland, 2002) and fibrin(ogen) has the ability to intensify inflammation, acting through signalling molecules, such as ICAM-1 (CD54) and Mac-1 (CD11b), to modulate cell adhesion and migration, (Flick *et al.,* 2004; Languino *et al.,* 1995) and increase expression of cytokines, including IL-1β (Perez *et al.,* 1999; Smiley *et al.,* 2001). Additionally, fibrin is a potent mediator and activator of macrophages, and stimulates them to secrete pro-inflammatory cytokines and chemokines (Akassoglou *et al.,* 2004). Low molecular weight degradation products of fibrin can enhance vascular permeability and have chemotactic activities (Sueishi *et al.,* 1981), thus potentially exacerbating BBB breakdown and promoting migration of leucocytes into the CNS. Genetic or pharmacological depletion of fibrin(ogen) in a tumour necrosis factor (TNF) transgenic mouse model of MS increases the lifespan of the animals as a result of decreased inflammation and a delay in demyelination (Akassoglou *et al.,* 2004). Previous studies have shown that fibrin deposition coincides with areas of demyelination (Kwon and Prineas, 1994), implicating a role for fibrin in regulating myelin breakdown (Akassoglou *et al.,* 2004). However fibrin deposition does not correlate well with demyelination in $tPA^{-/-}$ mice, although it correlates very well with a marker of neurofilament dephosphorylation, SMI32 (data from Chapter 4), indicating that in this study the effect of fibrin on axonal pathology is likely to be via a direct mechanism, rather than as a secondary result of demyelination.

Fibrin(ogen), which enters the CNS during the acute phase of disease, accumulated over time and was co-localised with SMI32 on axons in the spinal cords of $tPA^{-/-}$ mice. Lack of tPA and resultant fibrin deposition have been shown to exacerbate axonal damage in a model of peripheral nerve injury (Akassoglou *et al.,* 2000), suggesting similar conditions may influence inflammatory injury to CNS axons. Furthermore, inhibition of fibrin formation by attenuation of thrombin activity is neuroprotective in the injured optic nerve (Friedmann *et al.,* 2001). Following sciatic

nerve injury, it was revealed that fibrin can downregulate myelin gene expression in Schwann cells via the phosphorylation of extracellular signal regulated kinases 1 and 2 (Akassoglou *et al.,* 2002), which maintains Schwann cells in a proliferating, non-differentiated, non-myelinating form. Fibrin could have similar effects on oligodendrocytes, the myelinating cells of the CNS, thus inhibiting remyelination and functional recovery.

Laminin is a major functional component of basement membranes and is crucial for neuronal survival (Chen *et al.,* 2003; Indyk *et al.,* 2003; Jones *et al.,* 2003). It is a substrate for plasmin and its degradation is detrimental to neuronal survival in response to excitoxic challenge (Chen *et al.,* 2003). However, an increase in laminin was seen in $tPA^{-/-}$ mice during the acute phase of disease and during the chronic phase in WT and $uPAR^{-/-}$ animals. The expression of certain laminin isoforms are increased in response to IL-1 (Sixt *et al.,* 2003), thus this could represent an increase in laminin expression in response to pro-inflammatory cytokines during acute EAE. In addition, increases in laminin expression are seen in response to inflammation and certain laminin isoforms have roles assisting the adhesion and migration of T-cells (Sixt *et al.,* 2003). An increase in laminin in $uPAR^{-/-}$ mice could provide an alternative mechanism by which inflammatory cells can enter the CNS. In the PNS, laminin is a positive regulator of Schwann cell migration and differentiation and can induce myelination *in vitro* (Eldridge *et al.,* 1989). Following spinal cord injury, re-growth of axons is accompanied by an increase in extravascular laminin (Ma *et al.,* 2004), and during sciatic nerve regeneration, laminin expression is also increased (Akassoglou *et al.,* 2002). Thus similar mechanisms could be occuring the CNS, whereby laminin is increased as a safety mechanism, providing additional support to injured neurons, and providing a matrix along which oligodendrocyte precursors can migrate.

This study has suggested a major role for tPA in CNS fibrinolysis and highlighted the inhibitor PAI-1 as a potential target for disease modifying treatment. Similar to findings in MS tissue, fibrin removal in lesion sites appears to be important for a more favourable outcome. Investigation into the role of tPA and uPAR during neuroinflammation has revealed potential sites for therapeutic intervention such as the inhibition of uPAR-mediated cell migration and targeting PAI-1 to promote fibrinolysis.

6. Characterisation of EAE in PAI-1 deficient mice.

6.1. Introduction.

Mice deficient for PAI-1 were generated by homologous recombination in embryonic stem cells resulting in the deletion of the entire coding region of PAI-1 (Carmeliet P. *et al.,* 1993). These mice were then backcrossed for three generations onto the C57BL/6 background. Resulting offspring were of a different genetic background to the $tPA^{-/-}$ and $uPAR^{-/-}$ mice so had different wildtypes, which were genetically matched controls. Although these WT controls were genetically similar to $PAI\text{-}1^{-/-}$ mice, they were not derived from the same breeding pairs thus were not true WT littermates. Induction of MOG-EAE in $PAI\text{-}1^{-/-}$ and corresponding WT mice on the C57BL/6 background revealed a very low incidence of disease (36 % and 25 % respectively). As it was important to have a better comparison of knockouts with WT littermates, mice deficient for PAI-1 were backcrossed for 4 generations into the ABH strain of mice to increase EAE susceptibility. This yielded $PAI\text{-}1^{-/-}$ and appropriate WT littermates ($PAI\text{-}1^{+/+}$). These mice were susceptible to CREAE induction with spinal cord homogenate.

6.2. Results.

6.2.1. Clinical features of CREAE disease in $PAI\text{-}1^{-/-}$ and $PAI\text{-}1^{+/+}$ WT littermate mice.

Following immunisation with spinal cord, $PAI\text{-}1^{+/+}$ mice developed clinical signs of disease on day 13.9 ± 0.3 (Figure 6.1 A). Peak of EAE disease occurred on day 16.1 ± 0.3 with a mean maximal score of 2.7 ± 0.3 (Table 6.1). Clinical remission from EAE occurred between 25 and 30 dpi. Reimmunisation of mice can precipitate disease in the ABH strain or induce a relapse (Pryce *et al.,* 2003). This can be used as an additional priming agent when full susceptibility may not occur. Following re-immunisation on 28 dpi, $PAI\text{-}1^{+/+}$ mice suffered an induced relapse of disease beginning at 34 dpi, and mean clinical score at 40 dpi was 1.6 ± 0.4. Onset of CREAE in $PAI\text{-}1^{-/-}$

mice was significantly later than the PAI-$1^{+/+}$ at 16.2 ± 0.6 ($P < 0.001$) (Figure 6.1 A, Table 6.1). Peak of disease was also significantly delayed and occurred at 17.9 ± 0.5 ($P < 0.01$), with a significantly lower mean maximal score (1.5 ± 0.4; $P < 0.05$). Following re-immunisation at 28 dpi, no PAI-$1^{-/-}$ mice developed a clinical relapse, and mean score at 40 dpi was 0.2 ± 0.1, significantly lower than PAI-$1^{+/+}$ mice ($P < 0.05$). Incidence and time course of EAE onset is illustrated in figure 6.1 B. Whilst 77 % of PAI-$1^{+/+}$ mice developed EAE by 17 dpi, onset of EAE in PAI-$1^{-/-}$ mice was significantly later. In addition, incidence of EAE was lower, with 48% of PAI-$1^{-/-}$ mice developing clinical signs of EAE by 22 dpi.

Strain	EAE Incidence	Onset (dpi)	Peak of disease (dpi)	Mean Maximal Score	Mean Score at 40 dpi
PAI-$1^{+/+}$	20/26	13.9 ± 0.3	16.1 ± 0.3	2.7 ± 0.3	1.6 ± 0.4
PAI-$1^{-/-}$	11/23	16.2 ± 0.6***	17.9 ± 0.5**	1.5 ± 0.4*	0.2 ± 0.1*

Table 6.1. *Summary of the EAE data for PAI-$1^{-/-}$ and PAI-$1^{+/+}$ (WT) littermate mice.* All values shown as mean ± SEM, * $P < 0.05$, ** $P < 0.01$ and *** $P < 0.001$ compared to PAI-$1^{+/+}$.

Weights of all mice were monitored daily as significant weight loss precedes CREAE disease onset. Weights of PAI-$1^{-/-}$ mice at 11 dpi were significantly higher than the PAI-$1^{+/+}$ group ($P < 0.01$) before EAE onset (Figure 6.2). Furthermore, whilst PAI-$1^{-/-}$ mice that developed clinical disease suffered significant weight loss, as a group, this weight loss was not significant because 52 % failed to develop EAE disease. Weight loss in PAI-$1^{+/+}$ mice was observed from 13 dpi and by 17 dpi was significantly lower than weights at 11 dpi ($P < 0.01$). PAI-$1^{+/+}$ mice gained weight and by 21 dpi, had comparable weights to those before EAE onset. However, following re-immunisation of all mice at 28 dpi, weight loss was observed in PAI-$1^{+/+}$ mice before

onset of a relapse. AT 36 dpi, weights of PAI-$1^{+/+}$ mice were significantly lower than PAI-$1^{-/-}$ mice ($P < 0.001$).

6.2.2. Movement activity is significantly reduced following CREAE disease.

Movement activity of mice was performed to investigate motor dysfunction and the degree of neurological impairment (Pryce *et al.,* 2003). All data was normalised to the appropriate controls as control non-injected PAI-$1^{-/-}$ mice were slightly more active than control PAI-$1^{+/+}$ littermates. Following CREAE induction, all mice had a significant reduction in activity (Figure 6.3, $P < 0.05$). There was a 50 % reduction in activity of PAI-$1^{-/-}$ mice compared to PAI-$1^{-/-}$ control, and a 75 % reduction in activity of PAI-$1^{+/+}$ mice compared to the PAI-$1^{+/+}$ control group. Furthermore, PAI-$1^{+/+}$ littermates were significantly less active than PAI-$1^{-/-}$ mice at 35 dpi of EAE ($P < 0.05$). Mice which failed to develop clinical CREAE disease had comparable levels of activity to that of controls.

Baseline activity data Distanced travelled (cm) in 5 min	
ABH.PAI-$1^{+/+}$	ABH.PAI-$1^{-/-}$
577.6 ± 122.0	668.7 ± 94.9

Table 6.2. *Baseline activity data for control PAI-$1^{+/+}$ WT and PAI-$1^{-/-}$ mice.* Control PAI-$1^{-/-}$ mice were more active than control PAI-$1^{+/+}$ mice.

A

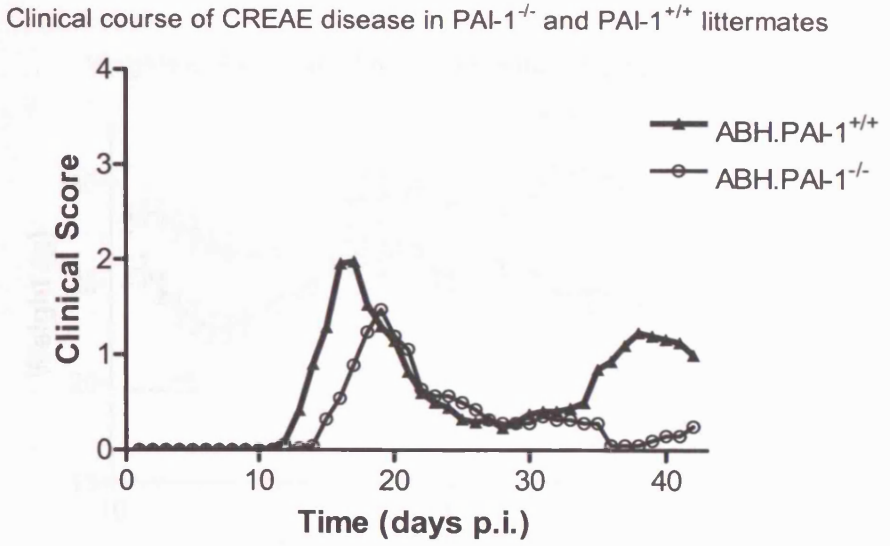

B

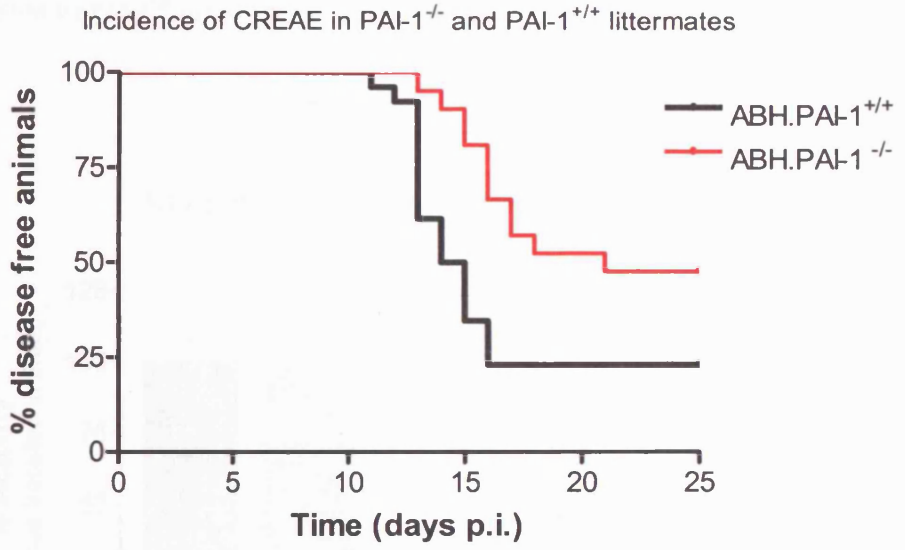

Figure 6.1. *Disease course, time of onset and incidence of CREAE in PAI$^{-/-}$ mice and PAI-1$^{+/+}$ littermates.* **A.** All mice were injected with spinal cord homogenate in IFA supplemented with *M. tuberculosis* and *M. butyricum* on day 0, 7 and 28. Mice were scored daily on a scale of 0 – 5 and the daily mean score was calculated for PAI-1$^{+/+}$ (n = 26) and PAI$^{-/-}$ (n = 23). **B.** 77% of PAI-1$^{+/+}$ mice showed signs of EAE disease by 17 dpi, however only 48% of PAI-1$^{-/-}$ mice developed clinical EAE signs by 22dpi.

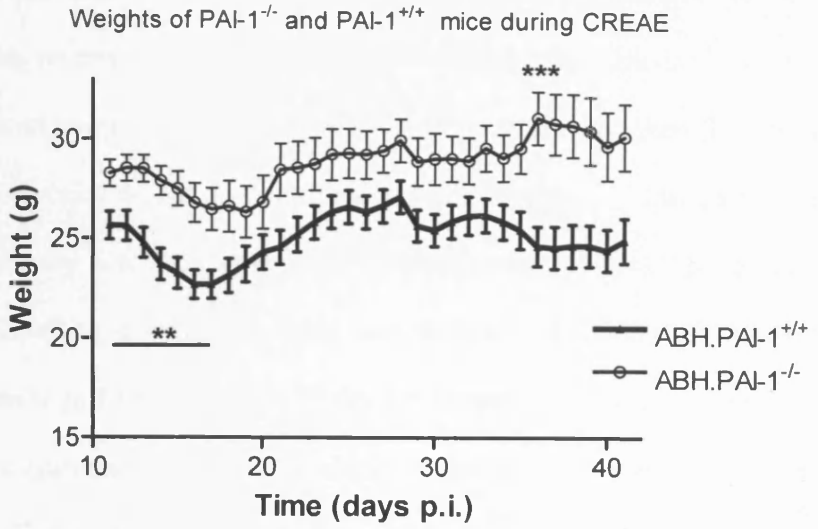

Figure 6.2. *Weights of PAI-1$^{-/-}$ and PAI-1$^{+/+}$ littermates during CREAE.* Following induction of EAE, mice were weighed daily to check for any significant weight loss. Data is expressed as the mean daily weights ± SEM for PAI-1$^{+/+}$ (n = 26) and PAI$^{-/-}$ (n = 23). ** $P < 0.01$ and *** $P < 0.001$.

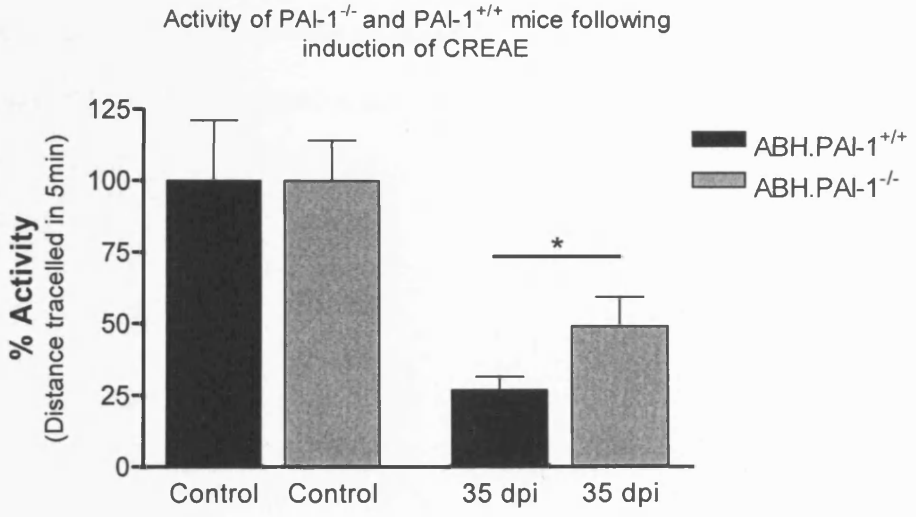

Figure 6.3. *Activity of PAI$^{-/-}$ mice and PAI-1$^{+/+}$ littermates before and after CREAE onset.* The motor function of control and EAE mice (35 dpi) was assessed using an open field activity chamber, and total distance travelled in 5 min was recorded for each mouse. The data represents the average activity of each group of mice normalised to the relevant control ± SEM. PAI-1$^{-/-}$ mice are more active than PAI-1$^{+/+}$ littermates at 35 dpi. n = 6 for control groups, n = 14 - 16 for EAE groups, * $P < 0.05$

6.2.3. Histological evaluation of spinal cords from CREAE mice.

Histological staining with haematoxylin and eosin of spinal cord sections, taken at 15, 20, 30 and 40 dpi, revealed differences in the degree of infiltration of inflammatory mononuclear cells into the CNS. No mononuclear cells were found in the spinal cords of control mice (Figure 6.4 A and B). Sections taken from mice at 15 dpi of CREAE revealed a high degree of inflammation in PAI-$1^{+/+}$ littermates (Figure 6.4 C and E), but very few cells were seen in sections from PAI-$1^{-/-}$ mice (Figure 6.4 D) indicating that disease onset may have been delayed compared to WT controls. At the peak of disease in PAI-$1^{-/-}$ mice at 20 dpi there were large number of perivascular cuffs in the spinal cord and comparable levels of inflammatory mononuclear cells to sections from PAI-$1^{+/+}$ mice (Figure 6.4 F). Sections from mice in disease remission at 30 dpi, revealed some evidence of ongoing inflammation in PAI-$1^{-/-}$ mice but very few infiltrating cells remained in spinal cords of PAI-$1^{+/+}$ mice (Figure 6.4 G and H), however at 40 dpi of CREAE, there was an increase in the number of inflammatory cells in the spinal cords of PAI-$1^{+/+}$ mice corresponding with disease relapse (Figure 6.4 I). The absence of mononuclear cells in sections from PAI-$1^{-/-}$ mice at 40 dpi (Figure 6.4 J) mirrored the clinical picture where animals remained in disease remission.

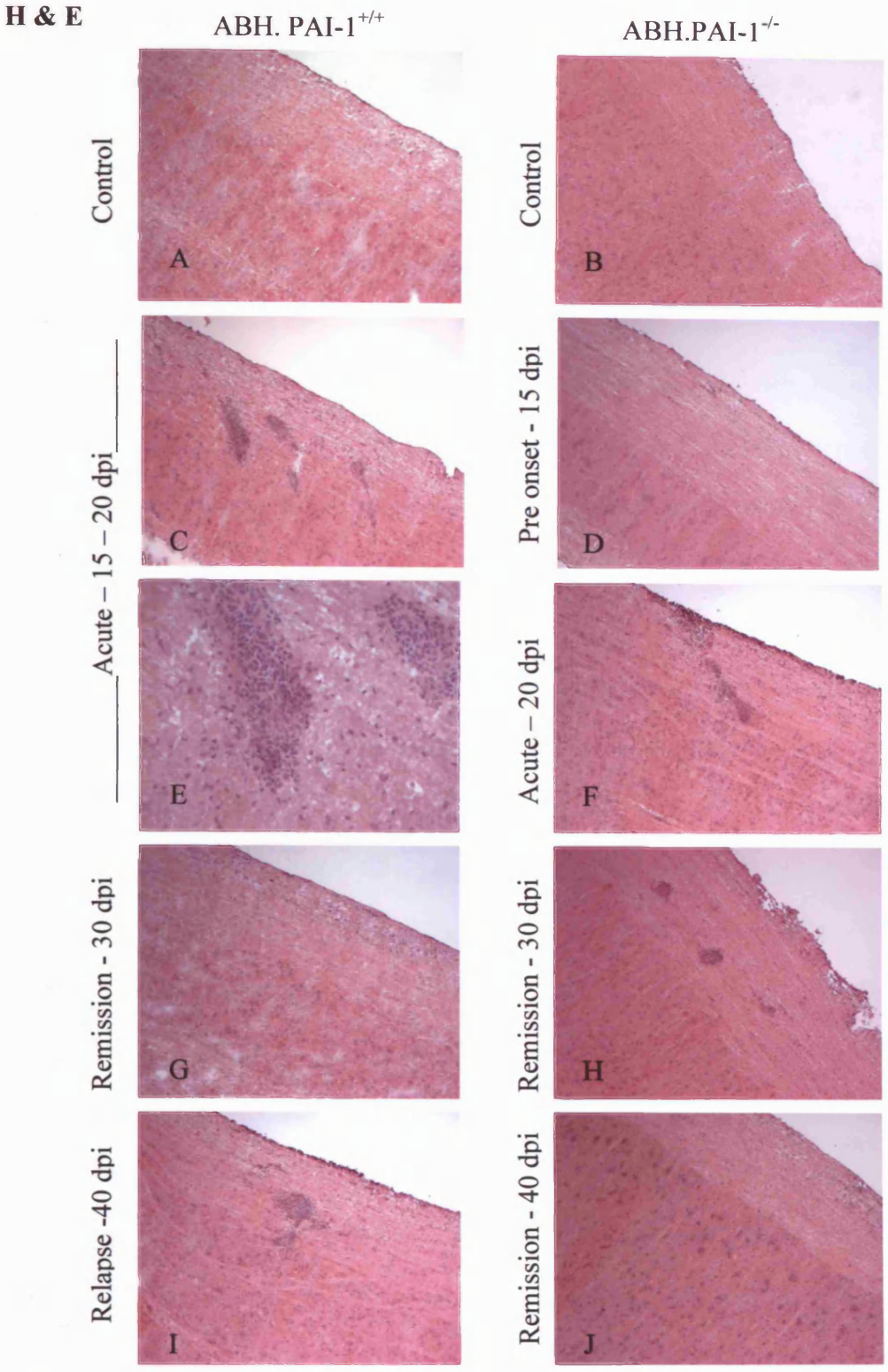

Figure 6.4. *Haematoxylin and eosin staining of spinal cord sections from PAI-1$^{-/-}$ and PAI-1$^{+/+}$ mice during acute and remission stages of CREAE.* Spinal cords were removed from mice at 15, 20, 30 and 40 dpi of CREAE and cut longitudinally. H & E was performed on frozen sections to detect nuclei distinct from other tissue components. Sections from control mice (A and B) and PAI-1$^{-/-}$ mice at 15 and 40 dpi (D and J) showed no clustering of nuclei indicative of cuffing. Perivascular cuffs were identifiable in sections from PAI-1$^{+/+}$ and PAI-1$^{-/-}$ mice during acute EAE (C, E and F) and in PAI-1$^{+/+}$ mice during relapse (I) indicative of inflammation. Samples from mice in remission (G and H) revealed some evidence of ongoing inflammation. Original magnification x 100 (A – D, F - J), x 400 (E).

6.2.4. Infiltration of macrophages, microglia and lymphocytes in CREAE.

Immunohistochemical staining was carried out on sections of spinal cords removed from mice during the acute phase of CREAE, 15 dpi for PAI-$1^{+/+}$ and 20 dpi for PAI-$1^{-/-}$, comparing CD45, F4/80, CD4 and CD8 staining on serial sections (Figure 6.5). No staining was observed in sections from control mice (not shown). Staining on serial sections for CD45, F4/80, CD4 and CD8 and showed that both macrophages/microglia and lymphocytes were present in large numbers in perivascular cuffs in PAI-$1^{-/-}$ mice and PAI-$1^{+/+}$ littermates. Additionally, microglia and macrophages contributed to a high proportion of CD45 positive cells observed infiltrating into the CNS. A high number of perivascular cuffs were observed in PAI-$1^{-/-}$ and PAI-$1^{+/+}$ mice at the peak of disease (15 dpi for PAI-$1^{+/+}$ and 20 dpi for knockouts) which corresponded to high clinical disease scores (Figures 6.5 A and G). Although there were similar numbers of CD45 positive cells surrounding blood vessels in sections from both genotypes (Figure 6.5 B and H), there were less microglia/macrophages in the perivascular cuffs in PAI-$1^{-/-}$ mice when compared to sections from PAI-$1^{+/+}$ (Figure 6.5 E and K). No CD4 or CD8 positive cells are present in sections from control mice (not shown). Immunohistochemical analysis of CD4 and CD8 positive lymphocytes on serial sections of EAE spinal cord revealed the presence of both of these cell types in the inflammatory infiltrates of perivascular cuffs. Numbers of these cells were comparable between PAI-$1^{-/-}$ mice and PAI-$1^{+/+}$ littermates during active disease, however in both groups of mice, the numbers of $CD4^+$ cells (Figure 6.5 C and I) were greater than the number of $CD8^+$ lymphocytes (Figure 6.5 F and L), consistent with previous findings (Allen *et al.*, 1993; Baker *et al.*, 1990).

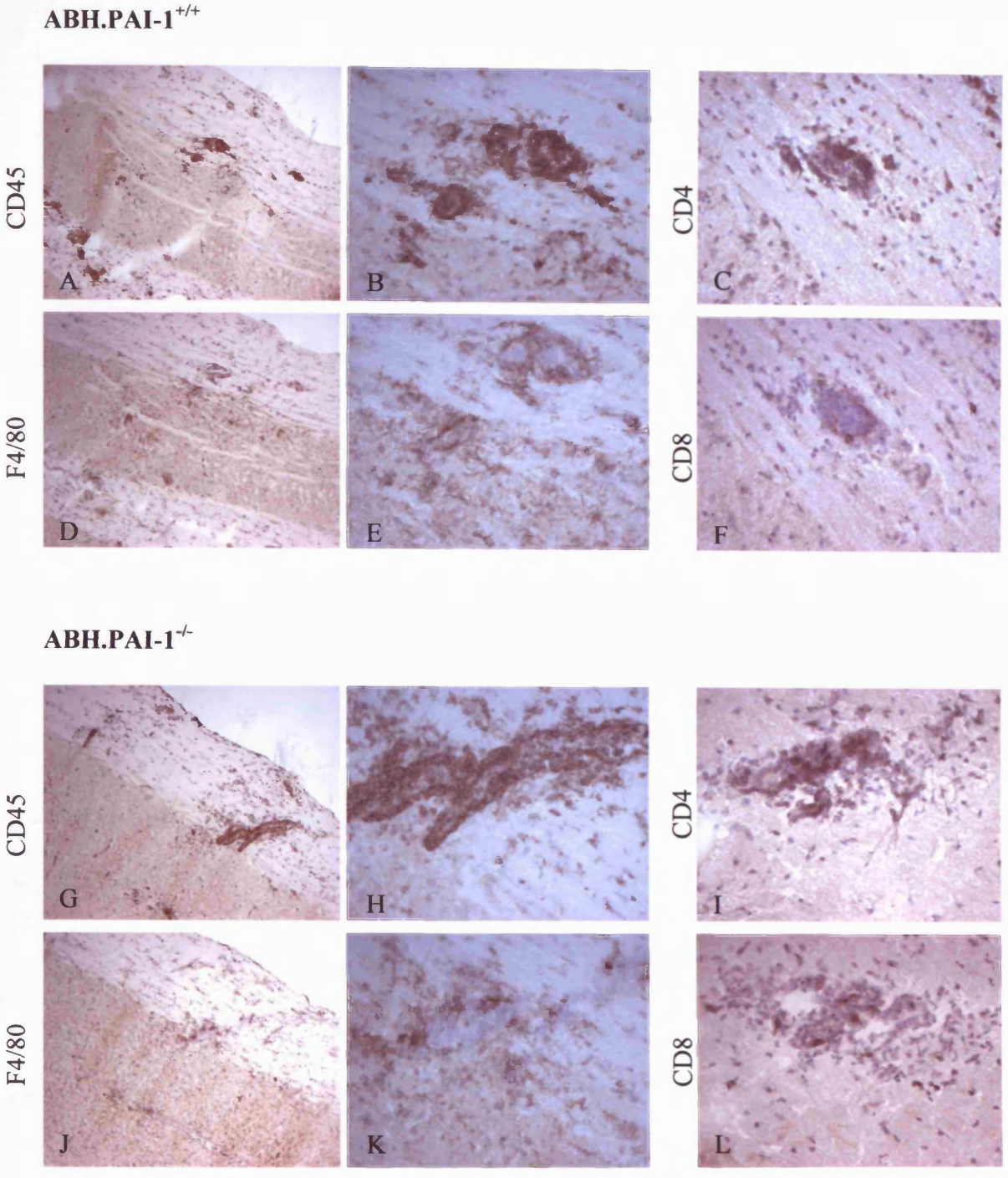

Figure 6.5. *CD45, F4/80, CD4 and CD8 staining in PAI-1$^{+/+}$ and knockout mice during acute CREAE.* Spinal cords were removed at the acute stage of CREAE and cut longitudinally. Frozen sections were stained with an antibody against CD45 (A, B, G and H), F4/80 (D, E, J and K), CD4 (C and I) or CD8 (F and L) and counterstained with Mayer's haematoxylin to assess the infiltration/migration of inflammatory mononuclear cells. In control animals there were no mononuclear cells in the spinal cord tissue (not shown). CD45 (A and G) and F4/80 (D and J) showed very similar patterns of staining. Perivascular cuffs containing CD4$^+$ and CD8$^+$ cells were evident in PAI-1$^{-/-}$ and PAI-1$^{+/+}$ mice at the peak of EAE disease, but no differences were observed between the two genotypes. In all corresponding serial sections there were more CD4$^+$ cells (C and I) than CD8$^+$ lymphocytes (F and L) Original magnification; x 100 (A, D, G, and J), x 400 (B, C, E, F, H, I, K and L).

6.2.5. Demyelination after induction of CREAE in PAI-1$^{-/-}$ mice and PAI-1$^{+/+}$ littermates.

Staining with an antibody against MBP in representative sections of mouse spinal cord at different time points during CREAE progression was used to assess demyelination. In control mice myelin staining was dense and complete in the white matter of the spinal cord (Figure 6.6 A and D) and no differences were observed between PAI-1$^{+/+}$ and PAI-1$^{-/-}$ mice. In sections from EAE mice during the peak of disease (15 dpi for PAI-1$^{+/+}$ and 20 dpi for PAI-1$^{-/-}$ mice), the appearance of myelin density was altered with the presence of perivascular cuffs, which contained macrophages, and hence active demyelination (Figure 6.6 B, C, E and F). Following disease remission at 30 dpi there were obvious patches of demyelination in the white matter appearing as changes in myelin density (Figure 6.6 G and I). At 40 dpi of CREAE, PAI-1$^{-/-}$ mice were still in disease remission and had normal appearing myelin staining (Figure 6.6 J), whilst PAI-1$^{+/+}$ littermates were relapsing, and had further evidence of demyelination in the spinal cord, specifically in areas of perivascular inflammation (Figure 6.6 H and Hi).

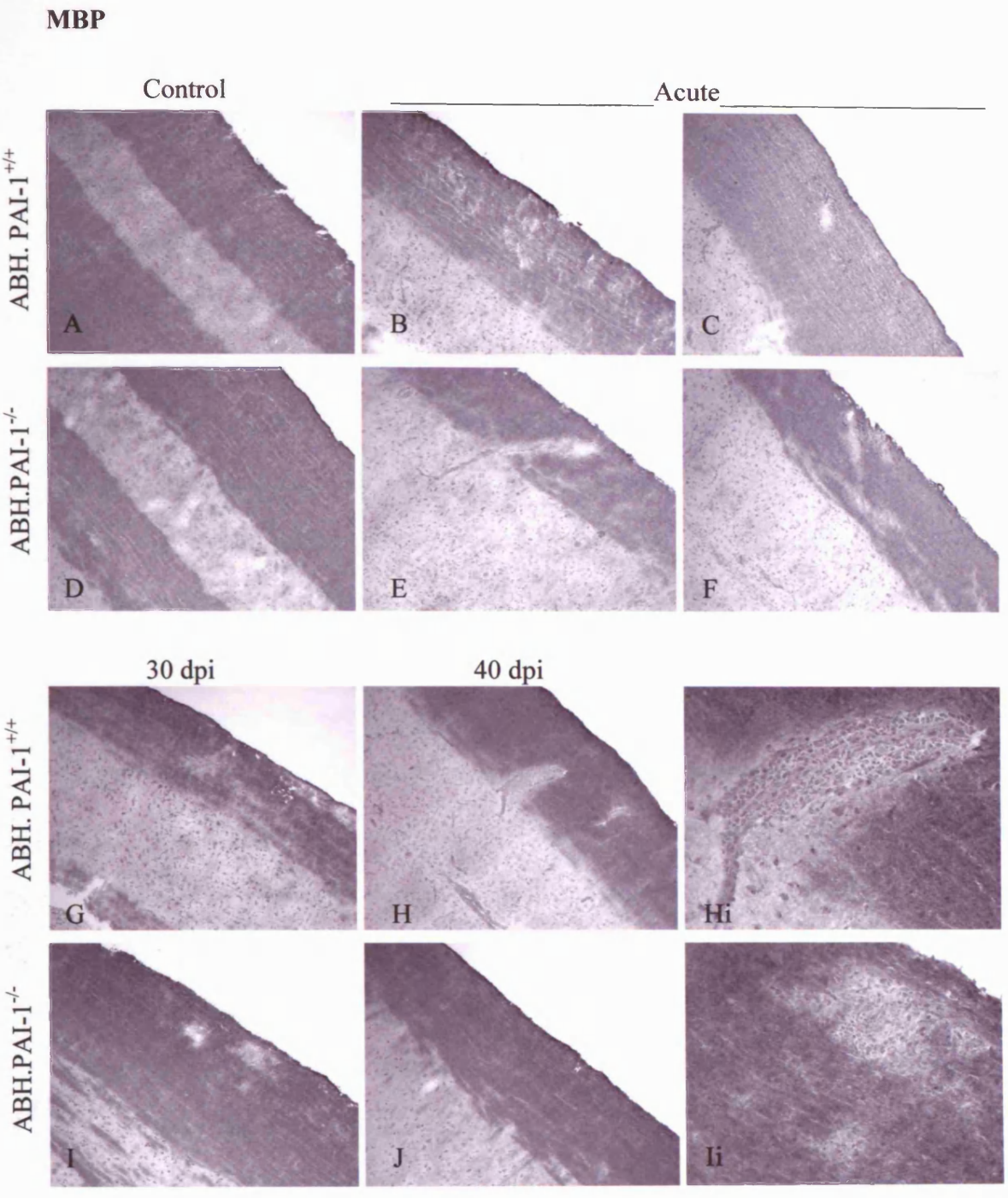

Figure 6.6. *MBP staining in PAI-1$^{+/+}$ and knockout mice during acute, remission and relapse stages of CREAE.* Spinal cords were removed at different stages of EAE and cut longitudinally. Frozen sections were stained with an antibody against MBP to assess the degree and location of demyelination. MBP staining in control (A and D) and EAE mice (B, C, E, F, G - I). Loss of myelin appeared to be restricted to areas of perivascular cuffing. Hi and Ii are high magnification images of H and I respectively. Original magnification; x 100 (A – H, I and J), x 400 (Hi and Ii).

6.2.6. Axonal pathology in CREAE in PAI-1$^{-/-}$ mice and PAI-1$^{+/+}$ littermates.

Changes in axonal pathology were assessed by staining for phosphorylated (SMI35) and non-phosphorylated (SMI32) neurofilaments on sections from 30 and 40 dpi of CREAE. There was no obvious increase or decrease in the number of axons stained for SMI35 between different genotypes and time points (Figure 6.7i). In control mice, SMI35 positive axons were clearly visible in the white matter of spinal cord sections (Figure 6.7i A and D). The appearance was uniform with long and straight axons packed in high density. In sections from PAI-1$^{+/+}$ and PAI-1$^{-/-}$ CREAE mice, there were slight changes in axonal appearance; with some thickened, non-uniform axons visible surrounding perivascular cuffs (Figure 6.7i B and E). In areas of infiltration there was a paucity of axons (Figure 6.7i B and E) consistent with the lack of myelin in these areas (Figure 6.6 B and E). This suggests that the infiltrating inflammatory cells may have changed the path of axons around the lesion. Following remission of clinical EAE disease, axons appeared most normal in sections from PAI-1$^{-/-}$ mice, with some larger thicker axons still present (Figure 6.7i F). However in PAI-1$^{+/+}$ littermate mice, with on-going inflammation, varicose axons were still visible, with the appearance of bulbs or ovoids indicating possible axonal transection (Figure 6.7i C). In sections from control PAI-1$^{-/-}$ and PAI-1$^{+/+}$ mice there were very few axons stained for SMI32 (Figure 6.7ii G and J). Following induction of CREAE at disease remission, 30 dpi, there was an increase in the number of axons stained for SMI32 (Figure 6.7ii H and K), although there were no apparent differences between the two genotypes. However at 40 dpi of CREAE, there were much higher numbers of axons stained for SMI32 in sections from PAI-1$^{+/+}$ WT mice, which were undergoing disease relapse, than in sections from PAI-1$^{-/-}$ mice, still in clinical remission (Figure 6.7ii I and L).

(i) SMI35 – phosphorylated neurofilament

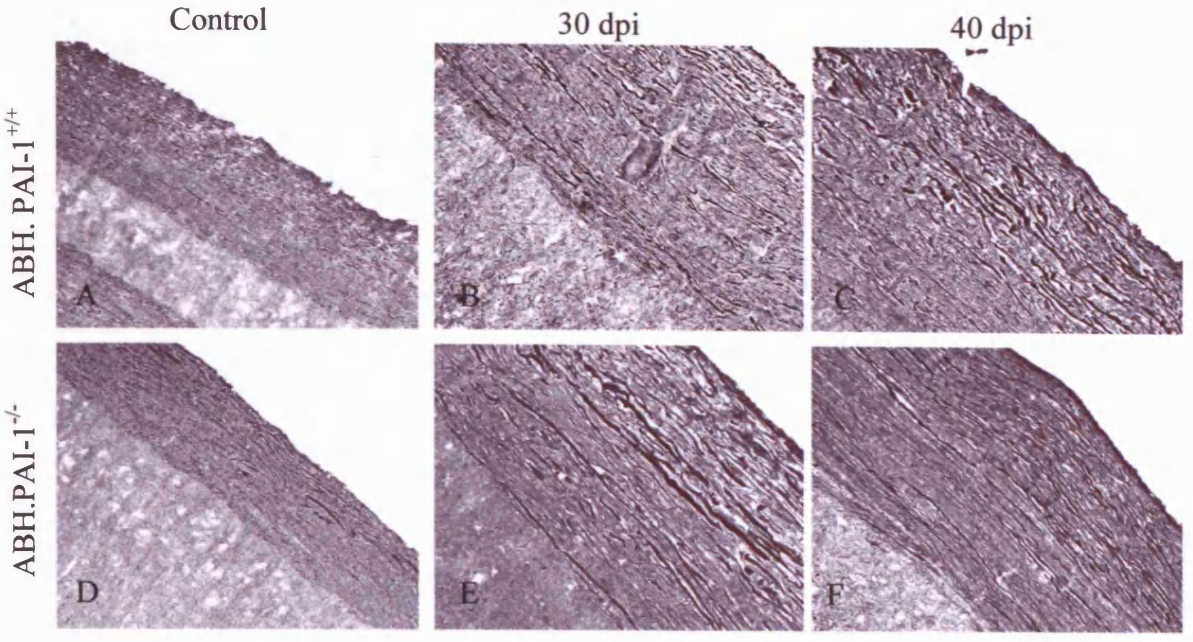

(ii) SMI32 – non-phosphorylated neurofilament

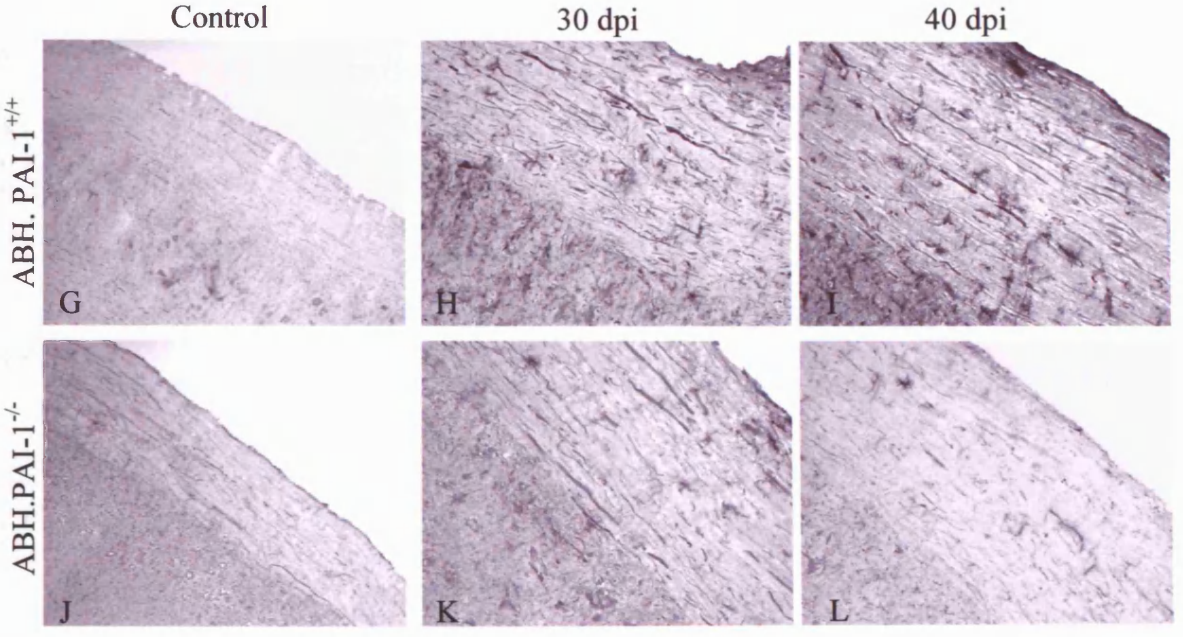

Figure 6.7. *Levels of phosphorylated and non-phosphorylated neurofilament during CREAE in PAI-1$^{-/-}$ and PAI-1$^{+/+}$ littermates.* Longitudinal spinal cord sections from control animals and mice in the remission and relapse stages of EAE were stained for **(i)** SMI35 and **(ii)** SMI32 to assess changes in levels of phosphorylated and non-phosphorylated neurofilament in the CNS. SMI35 in control mice (A and D) and in EAE (B, C, E and F). SMI32 in control mice (G and I) and at 30 and 40 dpi of CREAE (H, I, K and J). Original magnification x100 (A, D, G and J), x 200 (B, C, E, F, H, I, K and L).

6.2.7. *Levels of tPA, uPA and PAI-1 in PAI-1$^{-/-}$ and PAI-1$^{+/+}$ mice during CREAE.*

To investigate how the levels of tPA, uPA and PAI-1 change during the course of CREAE disease, in the absence of PAI-1, ELISAs were performed on spinal cord protein extracts. Levels of tPA did not change throughout the course of CREAE disease in PAI-1$^{+/+}$ littermate mice (Figure 6.8 A). However in samples from PAI-1$^{-/-}$ mice, levels of tPA were significantly increased at all stages of CREAE, when compared to PAI-1$^{-/-}$ controls, particularly during the acute and remission phases ($P < 0.01$; Figure 6.8 B). uPA protein did not change significantly during the acute phase of CREAE in either PAI-1$^{-/-}$ or PAI-1$^{+/+}$ WT mice, however levels were significantly increased during disease remission in PAI-1$^{-/-}$ mice at 30 dpi ($P < 0.05$) and during disease relapse in samples from PAI-1$^{+/+}$ littermates ($P < 0.01$) (Figure 6.8 C and D). As predicated no PAI-1 protein was detected by ELISA in samples from PAI-1$^{-/-}$ mice, however in WT littermates, PAI-1 was increased during the acute and relapse stages of CREAE, corresponding to inflammation ($P < 0.05$) (Figure 6.8 E). To investigate what these changes meant in the *in vivo* situation, calculating ratios of enzyme to inhibitor are useful (Table 6.3). Under physiological conditions, in control PAI-1$^{+/+}$ mice the ratio of tPA to PAI-1 was approximately 36:1, and the ratio of uPA to PAI-1 was approximately 5:1. This ensured that at all times enzyme was present in much greater amounts than inhibitor. Ratios of tPA and uPA enzyme to inhibitor during the acute phase of CREAE, at 15 dpi fell dramatically when compared to controls ($P < 0.05$ and $P < 0.01$ respectively). This would indicate that levels of PAI-1 were higher than uPA or tPA during the inflammatory stages of the disease, thus inhibiting the majority of plasminogen activation by these enzymes during acute EAE. Ratios were not significantly different during remission at 30 dpi, and were much nearer physiological levels. Interestingly, ratio levels of tPA and uPA enzyme to inhibitor fell significantly again during disease relapse at 40 dpi ($P < 0.05$). Ratios in PAI-1$^{-/-}$ mice could not be

calculated as there was no PAI-1, thus it could be assumed that the majority of tPA and uPA detected are free, un-complexed enzymes.

Ratio (ng/mg)	Control	Acute 20 dpi	Remission 30 dpi	Relapse 40 dpi
tPA:PAI-1	36.1 ± 19.2	2.0 ± 0.2*	41.6 ± 4.2	0.5 ± 0.1*
uPA:PAI-1	4.5 ± 0.6	0.2 ± 0.4**	15.4 ± 7.8	0.2 ± 0.0*

Table 6.3. *Ratios of tPA and uPA to the inhibitor PAI-1 during different phases of CREAE in PAI-1$^{+/+}$ WT mice.* Results expressed as mean ± SEM, * $P < 0.05$, ** $P < 0.01$ versus control.

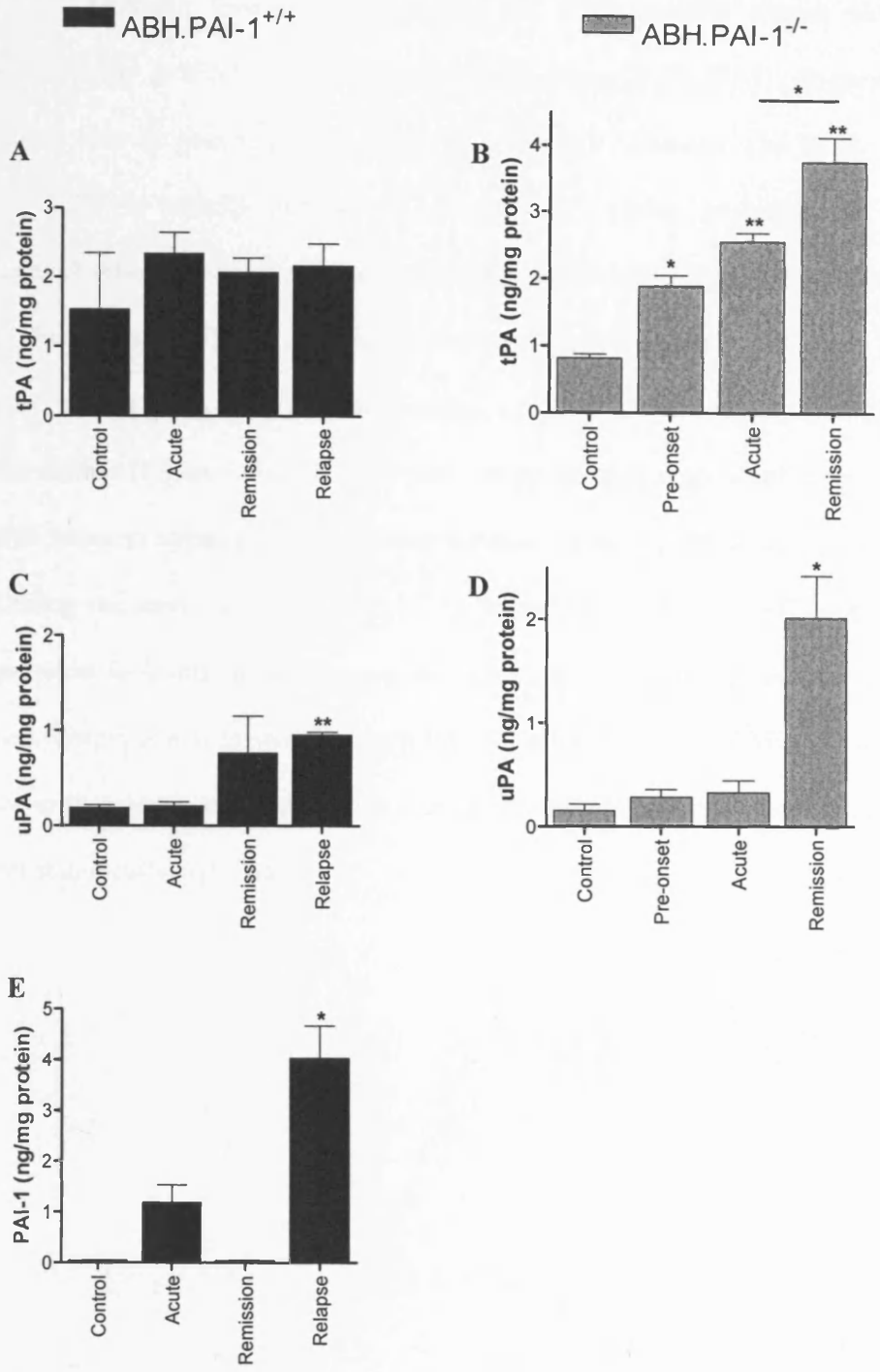

Figure 6.8. *Levels of tPA, uPA and PAI-1 in ABH backcross mice during CREAE.* Levels of tPA (A and B), uPA (C and D) and PAI-1 (E) were measured in spinal cord homogenate protein extracts from control animals and mice at different stages of CREAE. tPA and uPA were increased in samples from PAI-$1^{-/-}$ mice, particularly during disease remission. No PAI-1 was detected in samples from PAI-$1^{-/-}$ mice. uPA and PAI-1 were significantly increased in PAI-$1^{+/+}$ mice during EAE relapse. All data presented as mean ± SEM, n = 3 per time point. * $P < 0.05$, ** $P < 0.01$, versus control unless indicated by a bar.

6.2.8. Levels of neuroserpin during CREAE disease.

Although levels of neuroserpin, the CNS specific serpin, did not change significantly in $tPA^{-/-}$, $uPAR^{-/-}$ and WT mice during MOG-EAE (Chapter 5), differing results may be obtained in mice following CREAE induction with SCH. Additionally, as PAI-1 is usually upregulated in the CNS during experimental inflammatory demyelination, it was of interest to determine whether levels of neuroserpin were altered in the absence of PAI-1. Western blotting for neuroserpin was carried out on spinal cord protein extracts from normal control and CREAE mice at different time points of the disease (Figure 6.9). A higher, but not statistically significant level of neuroserpin was found in spinal cords from control $PAI\text{-}1^{-/-}$ mice compared to $PAI\text{-}1^{+/+}$ littermates. During the acute phase of CREAE in both $PAI\text{-}1^{+/+}$ and $PAI\text{-}1^{-/-}$ mice there was a decrease in levels of neuroserpin, however this was not significant. A decrease in neuroserpin levels in samples from $PAI\text{-}1^{-/-}$ mice during CREAE remission were also lower than levels in samples from control, pre-onset and acute mice, but again this was not statistically significant.

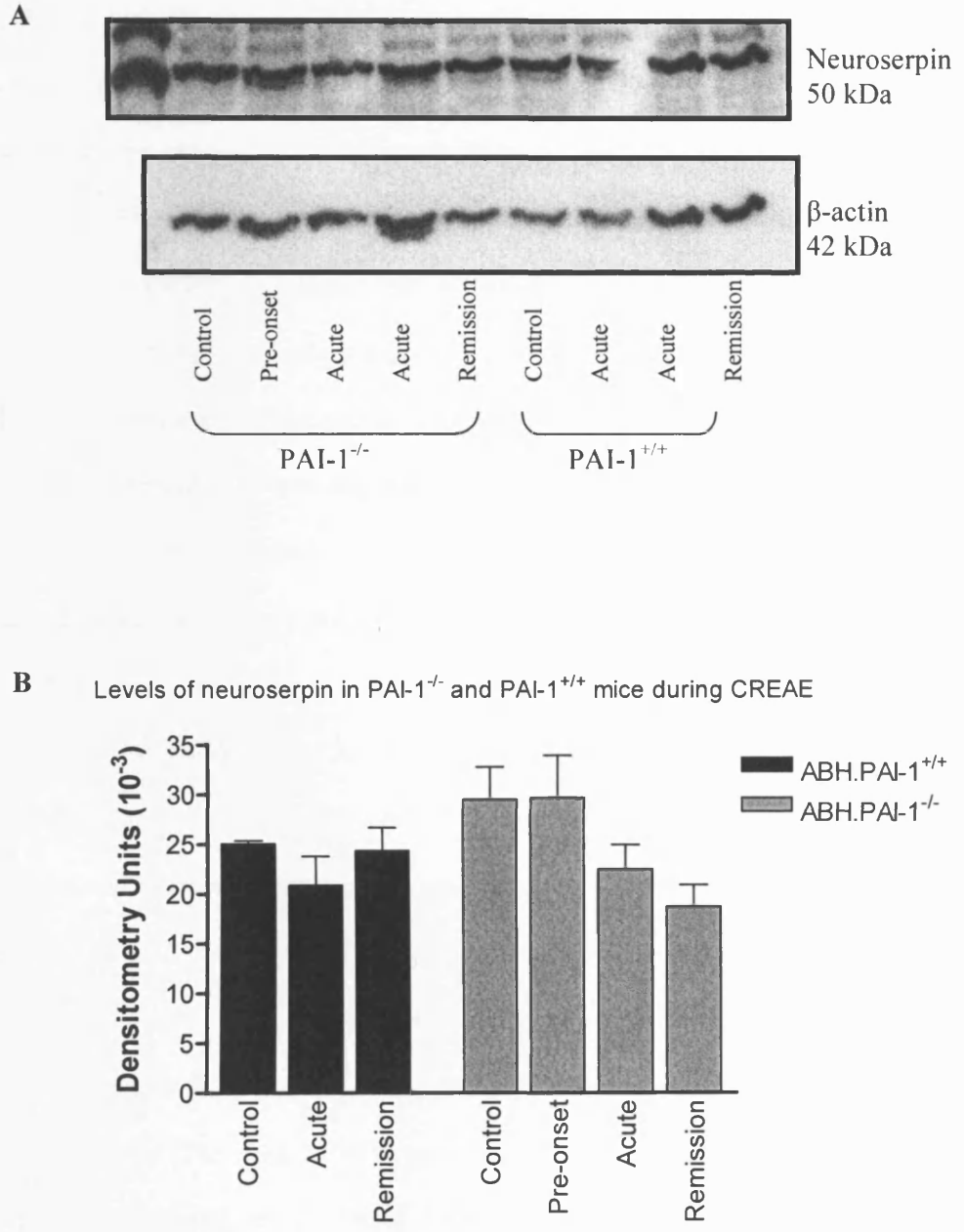

Figure 6.9. *Levels of neuroserpin do not change significantly throughout the course of CREAE disease.* Spinal cords from control and CREAE mice were homogenised for protein extraction. **A.** Levels of neuroserpin were detected by Western blotting and were quantitatively measured by densitometry scanning and results are shown as arbitrary densitometry units ± SEM. **B.** Using an anti-neuroserpin antibody, no significant differences were observed between control and EAE samples. The blot was re-probed with anti-actin to control for protein loading onto the gel. n = 3.

6.2.9. Plasminogen, fibrin(ogen) and fibrin D-dimer are significantly increased during CREAE.

Activity of tPA and uPA was likely to change as a result of lack of PAI-1 in the knockouts. To investigate levels of plasminogen and plasmin activity, Western blotting was performed on spinal cord protein extracts from control and CREAE PAI-$1^{+/+}$ and PAI-$1^{-/-}$ mice. Plasminogen migrated as an 85kDa band which corresponds to the cell-bound pre-activation form of plasminogen (lysine-plasminogen) (Figure 6.10 A). Using densitometry scanning, the highest amount of plasminogen was measured in PAI-$1^{-/-}$ mice before the onset of CREAE (15 dpi) when compared to $PAI^{-/-}$ controls (Figure 6.10 B, $P < 0.05$). Increases in levels of plasminogen were observed in PAI-$1^{+/+}$ and PAI-$1^{-/-}$ mice at the acute and remission phases of CREAE (15 dpi, 20 dpi and 30 dpi), compared to levels in control mice but these were not significant. However during relapse at 40 dpi, PAI-$1^{+/+}$ mice had a significant increase in plasminogen when compared to levels in PAI-$1^{+/+}$ control mice ($P < 0.01$).

Using an antibody specific for fibrin(ogen), extravasation and deposition of fibrin(ogen) was assessed in sections of spinal cord from PAI-$1^{-/-}$ and PAI-$1^{+/+}$ WT mice before and after induction of CREAE, during different time points of disease progression. In control mice there was no fibrin(ogen) in the CNS of either PAI-$1^{+/+}$ or PAI-$1^{-/-}$ mice (Figure 6.11i A and D). An increase in staining for fibrin(ogen) was seen in all sections from EAE mice. Fibrin(ogen) was particularly high in sections from the acute phase of EAE (15 dpi for PAI-$1^{+/+}$ and 20 dpi for PAI-$1^{-/-}$) and fibrin deposits were located to areas of inflammatory infiltration (Figure 6.11i B and E). In sections from PAI-$1^{+/+}$ mice more diffuse deposition was observed throughout the spinal cord parenchyma (Figure 6.11i B). During CREAE disease remission in PAI-$1^{-/-}$ mice, staining for fibrin(ogen) was reduced and was limited to small areas of heightened BBB permeability (Figure 6.11i F). At 40 dpi of CREAE, when PAI-$1^{-/-}$ mice were still in

disease remission, PAI-$1^{+/+}$ mice were relapsing with accompanying increases in BBB permeability and fibrin(ogen) deposition (Figure 6.11i C).

Western blotting for fibrin(ogen) and the fibrin degradation product D-dimer was performed on spinal cord protein extracts from CREAE and from control non-injected mice (Figure 6.11ii). This was to investigate the role of fibrin as a potential plasmin substrate in the progression of CREAE. All mice were perfused before spinal cords were taken to remove any fibrinogen from the vascular sytem, thus fibrin detected is representative of that deposited in the nervous tissue. Western blotting on spinal cord protein extracts showed that levels of fibrin D-dimer, a large molecular weight fibrin degradation product, change throughout the course of CREAE. In PAI-$1^{-/-}$ mice a significant increase in fibrin was observed at 15 dpi which was before clinical signs of EAE disease had developed in this genotype, (Figure 6.11iii, $P < 0.01$ versus PAI-$1^{-/-}$ controls). However levels of fibrin D-dimer at other stages of CREAE disease in PAI-$1^{-/-}$ mice were not significantly different to controls. A significant increase in fibrin D-dimer was observed during acute and relapse (15 and 40 dpi) phases of CREAE in samples from PAI-$1^{+/+}$ mice when compared to controls (Figure 6.11iii, $P < 0.05$ and $P < 0.05$ respectively). The highest levels of fibrin D-dimer were observed in samples from PAI-$1^{+/+}$ mice during CREAE relapse, and this was significantly higher than the highest levels found in samples from PAI-$1^{-/-}$ mice at 15 dpi ($P < 0.01$). Statistical analysis revealed a strong correlation of PAI-1 with fibrin D-dimer ($r = 0.836$, $P < 0.01$), and plasminogen levels ($r = 0.884$, $P < 0.01$). In addition there was a significant negative correlation between plasminogen and tPA ($r = -0.556$, $P < 0.05$).

A

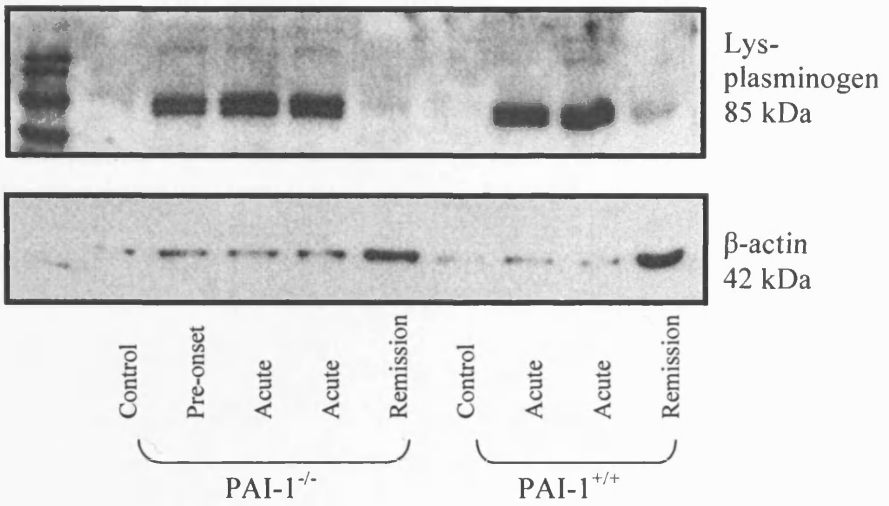

B

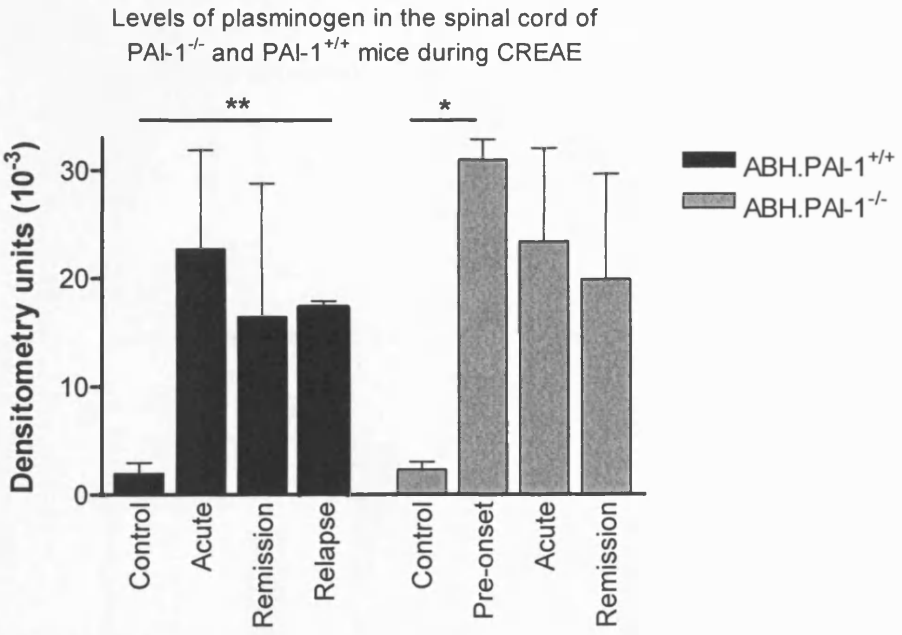

Figure 6.10. *Increased levels of plasminogen in PAI-1$^{+/+}$ and PAI-1$^{-/-}$ mice during CREAE.* Spinal cords from control and EAE mice were homogenised for protein extraction. **A.** Levels of plasminogen were detected by Western blotting and were quantitatively measured by densitometry scanning and results are shown as arbitrary densitometry units ± SEM. Blots were re-probed with anti-actin to control for loading of proteins onto the gel. **B.** Levels of plasminogen were increased pre onset of EAE in PAI$^{-/-}$ mice, and during the acute phase of EAE in both PAI-1$^{-/-}$ and PAI-1$^{+/+}$ mice. n = 3, * $P < 0.05$, ** $P < 0.01$.

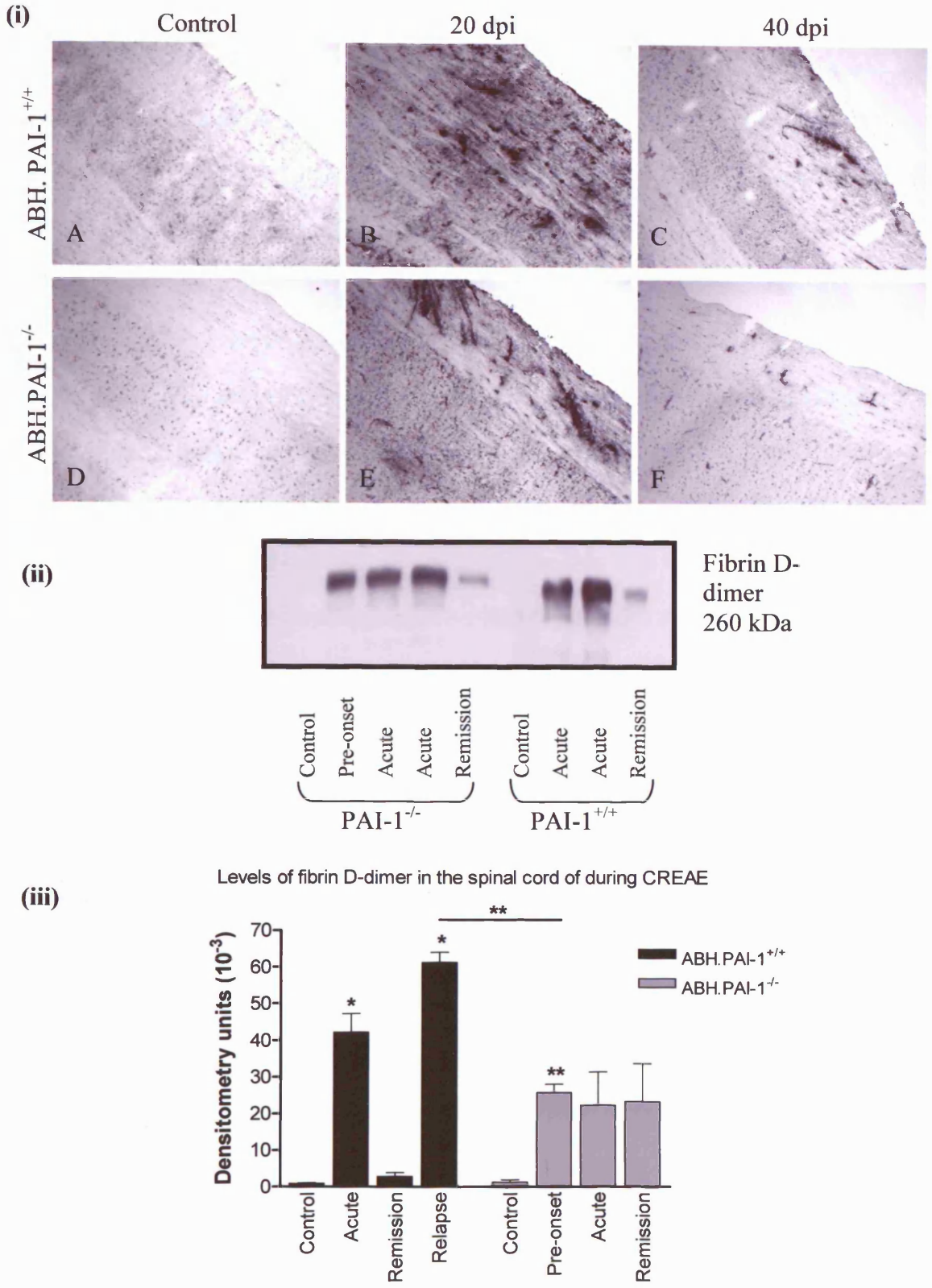

Figure 6.11. *Fibrin(ogen) deposition in the spinal cords of PAI-1$^{-/-}$ and PAI-1$^{+/+}$ mice during CREAE.* **(i)** Spinal cords were removed from mice during different stages of EAE and cut longitundinally. Frozen sections were stained with an antibody raised against fibrin(ogen) in sections from PAI-1$^{+/+}$ (A – C) and PAI-1$^{-/-}$ (D – F) mice. Original magnification x100. **(ii)** Levels of fibrin were detected by Western blotting using an anti-fibrin(ogen) antibody and **(iii)** were quantitatively measured by densitometry scanning. Results are shown as arbitrary densitometry units ± SEM. n = 3, * $P < 0.05$, ** $P < 0.01$ versus appropriate control and analysis between genotypes is indicated by a bar.

6.2.10. Fibrinolysis in PAI-1$^{-/-}$ mice and PAI-1$^{+/+}$ littermates during CREAE.

As fibrin deposition is a known feature of MS (Claudio *et al.*, 1995), it was important to determine how the lack of PAI-1 would affect fibrin degradation in spinal cords from control and CREAE animals. A clot lysis assay was used for spinal cord protein extracts to examine fibrinolytic capacity in control and knockout mice at specific time points during CREAE. Over 5 h the fibrin clot degradation (measured as a decrease in OD at 405nm) was comparable in PAI-1$^{+/+}$ and PAI-1$^{-/-}$ control mice. (Figure 6.12 A and B). In samples from PAI-1$^{+/+}$ mice during acute and relapse stages of CREAE, clot lysis was significantly impaired ($P < 0.01$). In control PAI-1$^{+/+}$ mice, fibrin clot degradation was complete at 2 h, however in samples from PAI-1$^{+/+}$ mice during the acute phase of CREAE, clot lysis was not complete till 4 h. Furthermore, samples from PAI-1$^{+/+}$ WT mice during CREAE relapse failed to degrade the *in vitro* formed clot within the 5 h time frame of the experiment. Protein extract samples from PAI-1$^{+/+}$ mice in remission, did appear to have a slower rate of fibrinolysis, however this was not significant. Samples from PAI-1$^{-/-}$ mice during acute and remission stages of CREAE had comparable clot lysis to PAI-1$^{-/-}$ controls (Figure 6.12 B), however, at 15 dpi, before clinical signs had developed in these mice, clot lysis at 2 h was significantly slower compared to control mice, however was complete within 3.5 h. Addition of tPA to sample buffer resulted in rapid clot degradation within the first hour of incubation, while omission of plasminogen in the sample buffer inhibited clot lysis.

Using fibrin overlay *in situ* zymography, the fibrinolytic capacity of sections of spinal cords could be investigated. The lysis of substrate was assessed by measuring lysis area and normalising this to total section area. Sections from PAI-1$^{+/+}$ mice showed no significant differences in fibrin lysis at any stage of CREAE when compared to controls, although there was a slight decrease in sections from mice during acute CREAE (Figure 6.13). There was a very low level of fibrin(ogen) lysis in sections from

control PAI-$1^{-/-}$ mice, and fibrinolysis was increased significantly in sections from mice at all stages of CREAE. Lysis of fibrin substrate was increased in sections from PAI-$1^{-/-}$ mice pre EAE onset ($P < 0.05$) and in sections from mice during the acute phase of CREAE at 20 dpi ($P < 0.05$). Although during CREAE remission in PAI-$1^{-/-}$ mice, levels of fibrinolysis had decreased, they were still significantly higher than PAI-$1^{-/-}$ control ($P < 0.01$).

Fibrinolysis in the spinal cords of PAI-$1^{-/-}$ and PAI-$1^{+/+}$ mice during CREAE

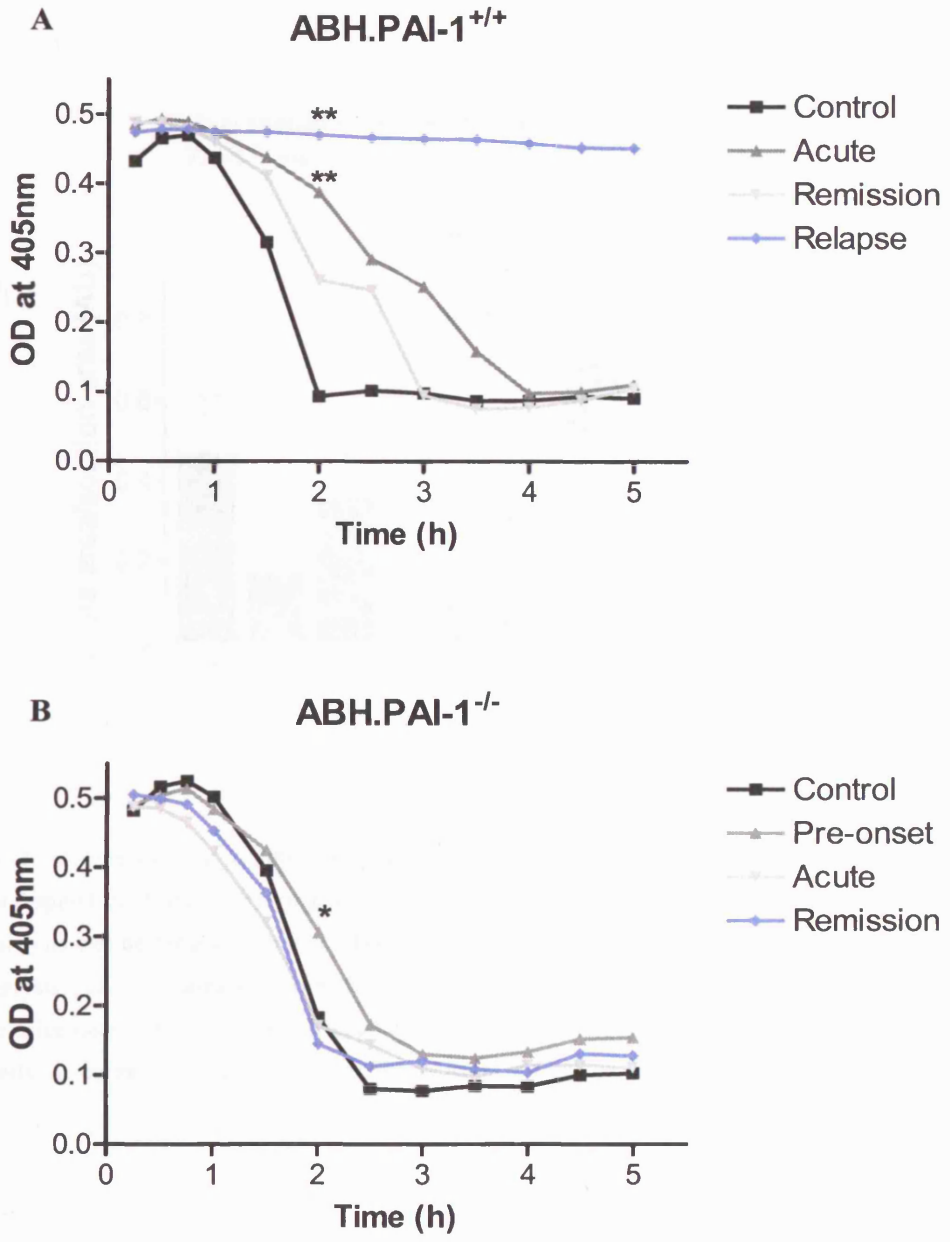

Figure 6.12. *Clot lysis in PAI-$1^{-/-}$ and wildtype littermates before and during CREAE disease onset.* Spinal cords from control and EAE mice at specific time points were homogenised for protein extraction. The fibrinolytic capacity was investigated using a clot lysis assay which measures the degradation of an *in vitro* formed clot using spectrophotometry. Results are presented as the mean clot degradation over time for PAI-$1^{+/+}$ **(A)** and PAI-$1^{-/-}$ **(B)** mice. Clot lysis in samples from acute and relapse stages of EAE in PAI-$1^{+/+}$ mice were significanly slower than control. Furthermore, pre EAE onset, fibrinolysis was impaired in PAI-$1^{-/-}$ mice. n = 3, * $P < 0.05$, ** $P < 0.01$.

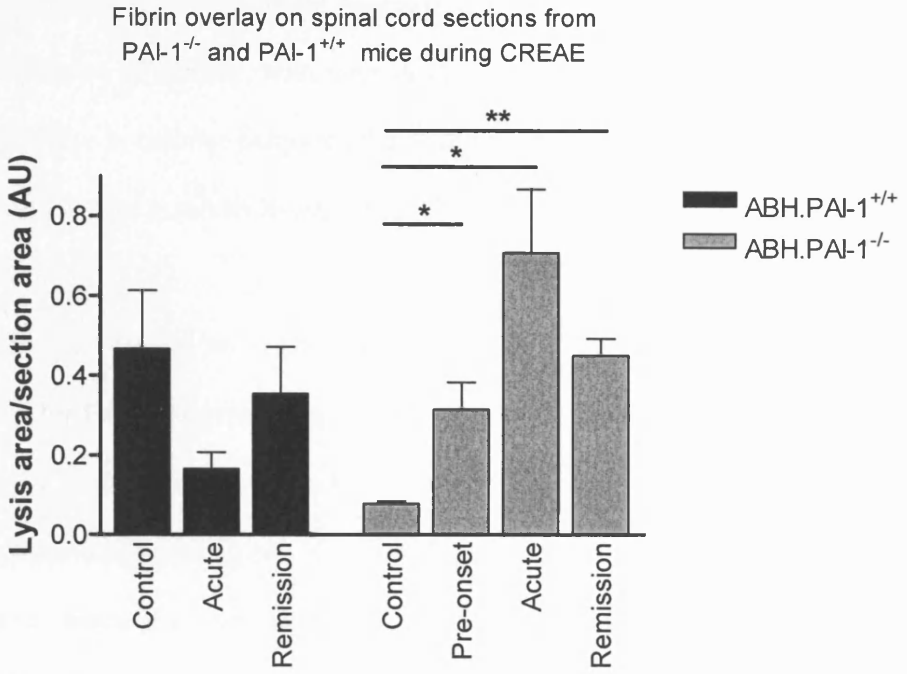

Figure 6.13. *Fibrin overlay in situ zymography of control and CREAE spinal cords.* Using frozen sections of spinal cord and overlaying an agarose solution of fibrinogen, plasminogen and thrombin, fibrin clot lysis can be measured *in situ*. The lysis of substrate was quantified using computer-assisted image analysis. The lysis area was normalised to the total section area. The fibrinolytic capacity in WT littermate mice does not significantly change throughout the course of CREAE. However, fibrinolysis significantly increases in spinal cord sections from PAI-$1^{-/-}$ EAE mice. n = 4, * $P < 0.05$, ** $P < 0.01$.

6.3. Discussion

Induction of CREAE in PAI-$1^{-/-}$ and PAI-$1^{+/+}$ mice on the ABH background led to a less severe clinical course of disease, and less marked pathophysiological features than in $tPA^{-/-}$ and $uPAR^{-/-}$ mice. PAI-$1^{+/+}$ littermates had a very similar disease to mice of the pure ABH strain with significant inflammation, impairment of fibrinolysis, and evidence of demyelination and axonal degeneration. CREAE in PAI-$1^{-/-}$ mice resulted in a lower incidence of disease, with mice developing signs of EAE significantly later than WTs. A delay in cellular entry into the CNS accompanied by a higher capacity for fibrinolysis resulted in a milder disease in PAI-$1^{-/-}$ mice with no clinical relapses and less axonal damage.

The delayed disease onset and inflammation in the spinal cord of PAI-$1^{-/-}$ mice support a role for PAI-1 in promoting cell adhesion and migration. A key modulatory effect of PAI-1 is its capacity to bind the adhesive glycoprotein, vitronectin (VN), a component of the ECM (Hertig and Rondeau, 2004). The VN meshwork is detected in the blood vessel walls of active MS lesions (Gveric *et al.,* 2001; Sobel *et al.,* 1995). In solution, VN-bound PAI-1 is twice as stable as unbound PAI-1, and the half life can exceed 24 h (Binder *et al.,* 2002). PAI-1 acts as a "molecular switch" interfering with the adhesive uPAR-VN link, leading to detachment of cells from the substrate (Deng *et al.,* 1996) and by promoting detachment of uPAR bearing cells from VN, PAI-1 increases cellular migration on this matrix (Waltz *et al.,* 1997). Thus in PAI-$1^{-/-}$ mice, there would be no interference with the adhesive uPAR-VN link, so detachment and migration of cells into the CNS is interrupted. The effect of PAI-1 on cell migration is particularly evident in cancer whereby high levels of this inhibitor are associated with tumour metastasis and a poor prognosis (Dellas and Loskutoff, 2005). Furthermore, in an antigen-induced mouse model of rheumatoid arthritis, PAI-1 deficiency attenuated joint inflammation, thus proving that PAI-1 has an important role in inflammation

through promoting leucocyte adhesion and migration (Van Ness *et al.*, 2002). This effect was also due to increased synovial fibrinolysis and a reduced accumulation of fibrin.

In ABH.PAI-$1^{+/+}$ littermates, a significant impairment of fibrinolysis was observed during acute and relapse stages of CREAE, associated with increased PAI-1 and decreased plasminogen activation, leading to lys-plasminogen and fibrin D-dimer accumulation. These finding are very similar to those observed in ABH mice, detailed in Chapter 3. An increase in SMI32 staining and a decrease in motor activity point to a significant degree of axonal damage and neurological impairment in the PAI-$1^{+/+}$ littermates, when compared to the PAI-$1^{-/-}$ mice. Again these findings correlated particularly well with fibrin accumulation, indicating a role for fibrin on axonal pathology (Akassoglou *et al.*, 2000; East *et al.*, 2005). Furthermore, decreased fibrin deposition provides a more favourable environment for regeneration (Akassoglou *et al.*, 2000; Akassoglou *et al.*, 2002).

Lack of PAI-1 in the knockout mice may ensure that fibrin entering through the BBB in CREAE is quickly removed, due to the absence of the key fibrinolytic inhibitor. The clot lysis assay and fibrin overlay *in situ* zymography showed that fibrinolysis was much more efficient in PAI-$1^{-/-}$ mice than in the PAI-$1^{+/+}$ littermates, and actually increased during CREAE disease, due to raised levels of plasminogen activators. Even though CREAE disease was clinically silent at 40 dpi in PAI-$1^{-/-}$ mice, significant accumulation of tPA and uPA during remission showed that there was still some ongoing pathology, underlying these changes. Accumulation of tPA and uPA in PAI-$1^{-/-}$ mice, not seen in PAI-$1^{+/+}$ mice, could represent a regulatory effect of PAI-1 on these enzymes. This could be at the gene expression, mRNA level or protein level. Additionally, PAI-1 is responsible for termination of tPA and uPA activity by their removal from the circulation through interaction with LRP and subsequent cellular

internalisation (Strickland and Ranganathan, 2003). Lack of PAI-1 means that this key clearance mechanism is lacking, thus ineffective elimination could explain the high levels of PAs in this genotype. Such high levels of these plasminogen activators, in the absence of an inhibitor could have potentially detrimental effects. Via plasmin, tPA and uPA have the ability to activate MMPs, which are known to degrade the BBB, and exacerbate myelin breakdown in MS. Additionally, tPA can mediate microglial activation (Rogove *et al.,* 1999), and play a key role in neuronal cell death following excitotoxic injury through proteolytic degradation of laminin (Chen and Strickland, 1997; Tsirka *et al.,* 1995; Tsirka *et al.,* 1997a). However as there was little evidence of neurodegeneration in PAI-$1^{-/-}$ mice, it appears that tPA and uPA were not acting via these potentially damaging mechanisms. Alternatively, other PA inhibitors could be compensating for loss of PAI-1. Neuroserpin, the CNS-specific tPA inhibitor was not upregulated during CREAE, however levels of this protein did decrease at 20 and 30 dpi in PAI-$1^{-/-}$ mice, which could correspond to increased complex formation of neuroserpin with tPA. Furthermore, PAI-2, which is synthesised by monocytes and macrophages in response to TNF-α (Dobrovolsky and Titaeva, 2002; Irigoyen *et al.,* 1999), could play a role in inhibiting excessive PA activity. It was not logistically possibly to continue with this experiment beyond 40 days due to low n-numbers rendering the data statistically non-viable. Although if the CREAE experiment had been continued, it is possible that with continuing increases in tPA and uPA, there might have been some further evidence of demyelination and axonal degeneration. In uPAR$^{-/-}$ mice, high levels of uPA during disease chronicity lead to a high degree of myelin loss and an increase in neuronal damage (Chapters 4 and 5).

Mice deficient for PAI-$1^{-/-}$ did not undergo a clinical relapse following re-immunisation. Thus, fibrinolysis appears to have a major influence in neuroinflammation, possibly by contributing to disease relapse. Inefficient fibrin

removal in PAI-$1^{+/+}$ littermate mice during CREAE could contribute to exacerbation of disease and clinical relapse as fibrin is known to have a key role in inflammation. Fibrin(ogen) participates in a variety of cellular responses associated with inflammation through binding with different types of integrin and non-integrin receptors. Binding to $\alpha_5\beta_1$, $\alpha_M\beta_2$ (Mac-1 or CD11b/CD18) and $\alpha_V\beta_3$, which are expressed on leucocytes, macrophages and monocytes, can lead to different effects depending on the cell type and the intracellular signalling pathways elicited (Adams *et al.,* 2004). Through interaction with ICAM-1, fibrin(ogen) binding to vascular cell receptors can initiate increased leucocyte adhesion to endothelium and leucocyte transendothelial migration (Languino *et al.,* 1995). Additionally the fibrin(ogen):ICAM-1 complex can lead to an anti-apoptotic state of cells through activation of the MAP kinase pathway (Pluskota and D'Souza, 2000). Apoptosis of T-cells is thought to be an important contributory factor to disease remission during EAE and MS (Pender and Rist, 2001), and suppression of T-cell apoptosis in EAE increases the severity of the disease (Okuda *et al.,* 2002). Akassoglou *et al.,* (2004) demonstrated that fibrin can exacerbate inflammation in a model of MS. Genetically or pharmacologically fibrin depleted mice demonstrated reduced neuroinflammation, decreased demyelination and as a result a lengthened lifespan compared to wildtype or vehicle injected animals (Akassoglou *et al.,* 2004). Additionally it was found that fibrinogen can stimulate secretion of pro-inflammatory cytokines and chemokines, and is a potent stimulator of macrophage activation (Akassoglou *et al.,* 2004). As fibrin is capable of modulating inflammation via a number of different mechanisms, it is clear that removal of this plasma protein, by enhancing fibrinolysis, can produce extremely beneficial results.

In summary, inhibition of PAI-1 could be therapeutically beneficial in treating MS. This would provide a dual palliative approach whereby leucocyte migration and inflammation are reduced, allowing efficient removal of fibrin, which could potentially

decrease axonal/neuronal damage, and reduce frequency of disease relapses in MS patients.

7. Synaptic and dendritic proteins as markers of axonal pathology in EAE.

7.1. Introduction.

Many studies have focused on the degree and timing of axonal injury in MS (Bjartmar and Trapp, 2001), and by using various axonal/neuronal markers, such as APP and SMI32, neuronal injury and degeneration can be assessed (discussed in section 1.5) (Ferguson *et al.*, 1997; Trapp *et al.*, 1998). Recently a study by Zhu and collegues (Zhu *et al.*, 2003) discovered that various synaptic and dendritic proteins may provide useful markers and tools to investigate early changes during inflammatory demyelination. Additionally, as dendrites are very susceptible to excitotoxicity (Hasbani *et al.*, 2001), dendritic markers can provide clues about the role of excessive glutamate in neuroinflammation. Excitotoxicity is thought to be one of the underlying pathogenic mechanisms involved in EAE and MS (Groom *et al.*, 2003). Additionally, tPA is known to play a role in excitotoxicity through enhancement of NMDA receptor signalling, possibly by cleavage of the NR1 subunit of the NMDA receptor (Nicole *et al.*, 2001; Vivien *et al.*, 2003). It was therefore of interest to investigate how these synaptic and dendritic proteins changed in $tPA^{-/-}$, $uPAR^{-/-}$, $PAI\text{-}1^{-/-}$ and their respective WT mice throughout the course of EAE disease. This would allow further investigation into these proteins as markers for changes in synaptic and dendritic pathology in relation to measures of neuronal damage. Although MAP-2, synaptophysin, GAP-43 and PSD-95 have been investigated previously in acute Lewis rat EAE (Zhu *et al.*, 2003), this model is largely monophasic and inflammatory in nature, lacking clear demyelination and axonal pathology (Ahmed *et al.*, 2001). Therefore levels of these proteins were investigated in the MOG-EAE and ABH chronic relapsing EAE model. The SCH-induced CREAE model shows more notable nerve pathology than the Lewis rat model (Baker *et al.*, 1990; Jackson *et al.*, 2005), as animals in the chronic phase of disease fail to relapse, but have accumulating neurological deficit and axonal pathology (Pryce *et al.*, 2003).

7.2 Results.

7.2.1. Expression of PSD-95 in the spinal cord during EAE.

Immunohistochemical staining for the synaptic protein PSD-95 revealed some neuronal structures in the GM of control spinal cord sections, but very little staining in WM (Figure 7.1 A – C and Figure 7.2 A and D). Following induction of MOG-EAE there was an increase in PSD-95 staining in the WM of sections from WT, $tPA^{-/-}$ and $uPAR^{-/-}$ mice at the acute stage of disease (20 dpi for WT and $tPA^{-/-}$ and 35 dpi for $uPAR^{-/-}$ mice). Following SCH induced CREAE there was also an increase in PSD-95 staining in the WM of sections from ABH.PAI-$1^{+/+}$ and ABH.PAI-$1^{-/-}$ mice at the acute stage of disease (15 dpi for PAI-$1^{+/+}$ and 20 dpi for PAI-$1^{-/-}$ mice). PSD-95 was specifically localised in EAE tissue and the antibody against this protein reproducibly stained axons running through or around perivascular cuffs (Figure 7.1 D – L and Figure 7.2 B, C, E – G and J). . During the chronic phase of MOG-EAE at 60 dpi, there was little PSD-95 staining in sections from WT and $tPA^{-/-}$ mice (Figure 7.1 M and N), but there were still some axons stained surrounding perivascular cuffs in sections from $uPAR^{-/-}$ mice as a result of on-going inflammation (Figure 7.1 O). During the remission phase of CREAE at 30 dpi, there was little PSD-95 staining in sections from PAI-$1^{+/+}$ mice (Figure 7.2 H) consistent with the relative lack of mononuclear cell infiltration, but there were still some axons stained surrounding perivascular cuffs in sections from $PAI^{-/-}$ mice in perivascular cuffs underlying ongoing inflammation (Figure 7.2 K). At 40 dpi in PAI-$1^{+/+}$ mice undergoing a relapse, there was a further increase in PSD-95 staining on axons in the perivascular cuffs, however there was no axons visible in sections from PAI-$1^{-/-}$ mice (Figure 7.2 I and L), which were not relapsing at the time of sampling.

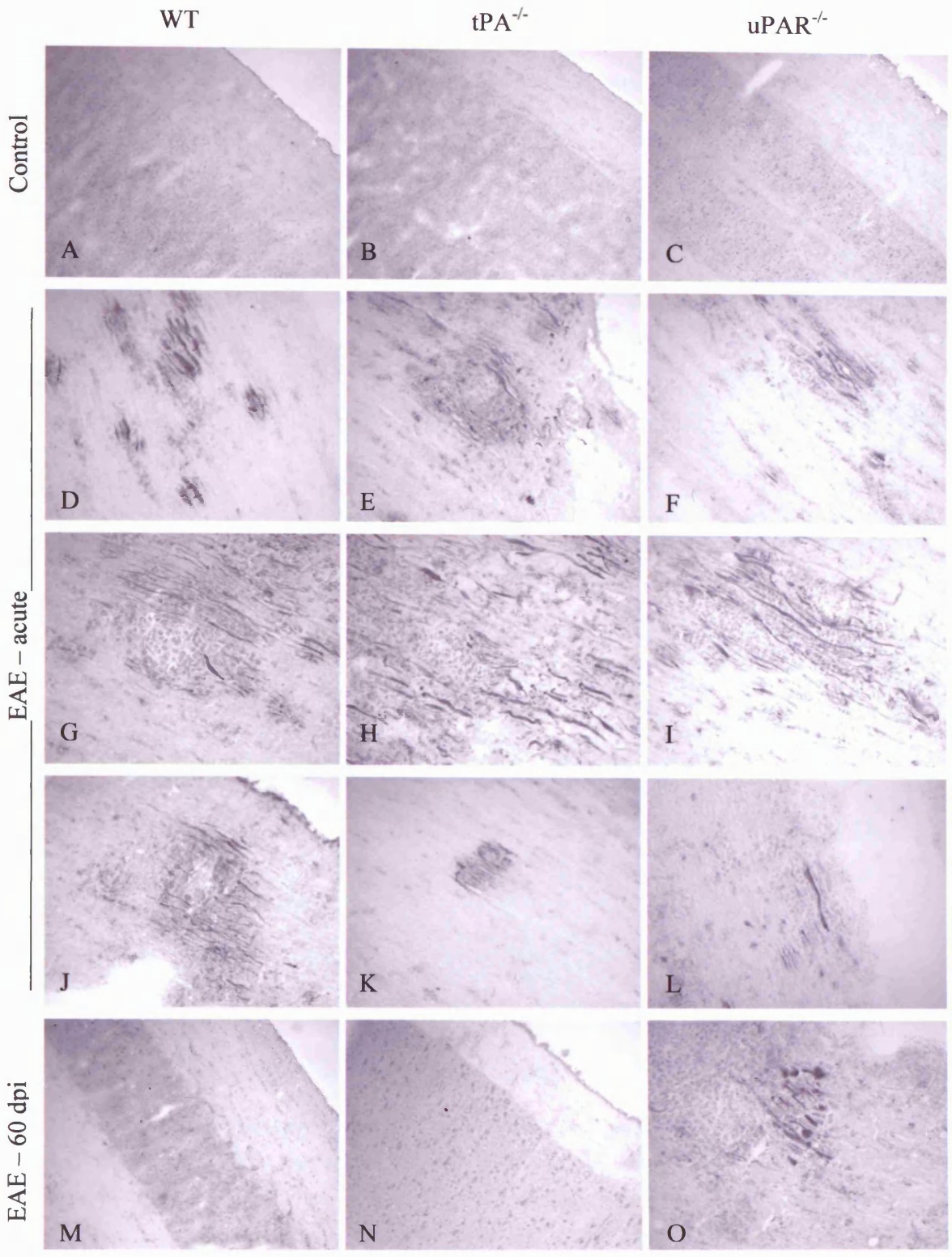

Figure 7.1. *PSD-95 is localised to axons in perivascular cuffs in MOG-EAE tissue.* Spinal cords removed from control and EAE mice were sectioned longitudinally. Frozen sections were stained with an antibody against PSD-95. Staining in sections from control mice revealed very little PSD-95 positive structures (A – C), however in sections from EAE mice (D – O), axons within perivascular infiltration were consistently strongly immunopositive for PSD-95. There were no differences between the genotypes. Original magnification x100 (A – C, M and N) and x 200 (D – L and O).

PSD-95

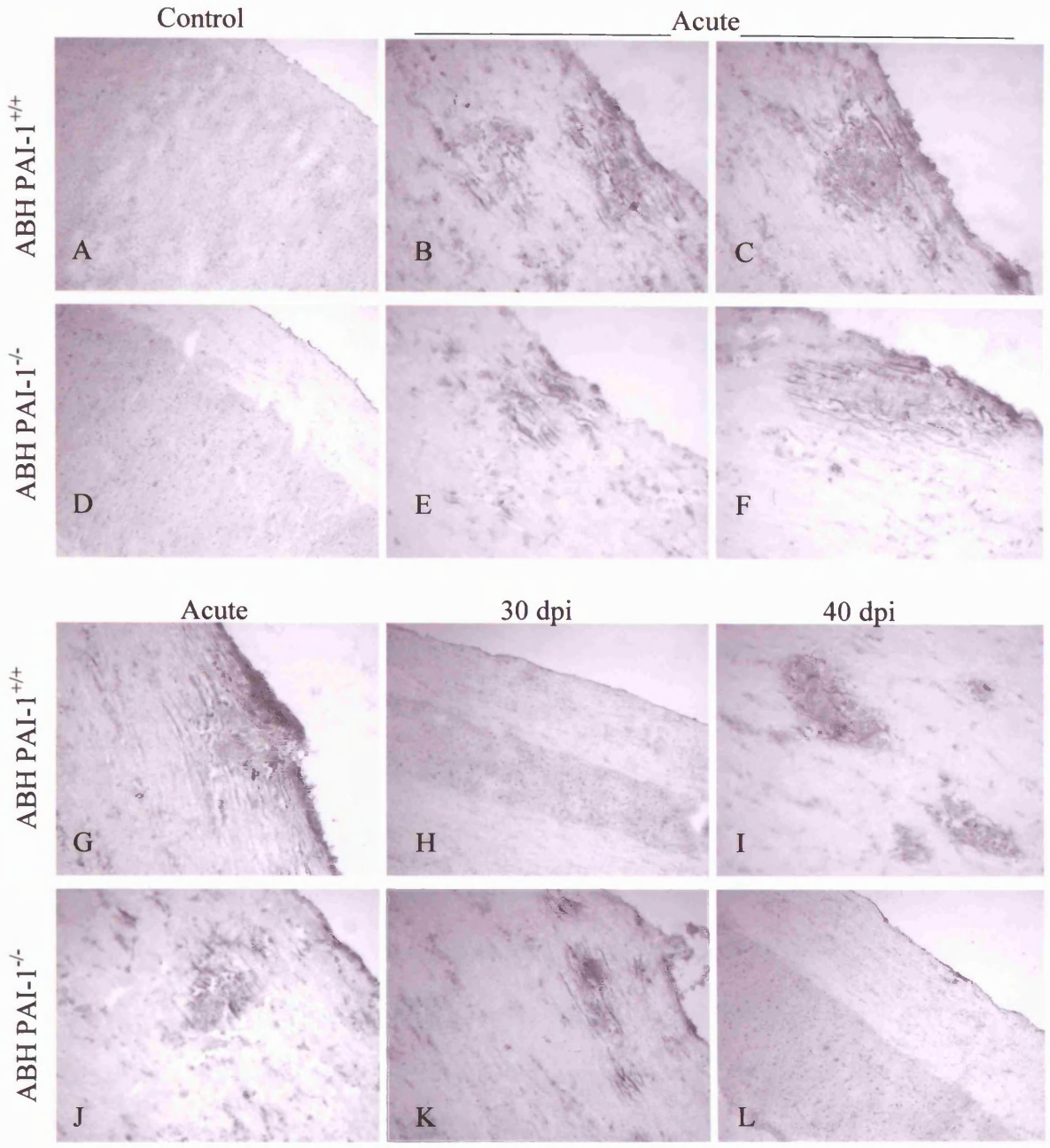

Figure 7.2. *PSD-95 is localised to axons in perivascular cuffs in CREAE tissue*. Spinal cords removed from control and CREAE mice were sectioned longitudinally. Frozen sections were stained with an antibody against PSD-95. Staining in sections from control mice revealed very little PSD-95 positive structures (A and D), however in sections from CREAE mice (B, C, E, F, G – L), axons within perivascular cuffs were consistently strongly immunopositive for PSD-95. There were no differences between the genotypes. Original magnification x100 (A, D, H and L) and x 200 (B, C, E, F, G, I - K).

7.2.2. Expression of MAP-2 in the spinal cord during EAE.

Western blotting for MAP-2 was performed using spinal cord protein extracts from normal control ABH mice, and mice during acute, remission and chronic stages of CREAE in ABH mice (at 20, 30 and 80 dpi respectively) (Figure 7.3 A). MAP-2 protein was decreased significantly during the acute phase of CREAE at 20 dpi ($P < 0.01$), however during disease remission at 30 dpi, levels of MAP-2 were not significantly different from controls but were significantly higher than levels at 20 dpi ($P < 0.01$; Figure 7.3 B). During the chronic stage of EAE, at 80 dpi, MAP-2 was lost again, and levels in the spinal cord were significantly lower than those in the CNS of control ABH mice ($P < 0.05$).

Immunocytochemistry for MAP-2 on spinal cord sections from control WT, $tPA^{-/-}$ and $uPAR^{-/-}$ mice on a C57BL/6 background showed staining of neuronal cell bodies in the GM, similarly in the different genotypes (Figure 7.4 A – F). In sections from the acute phase of MOG-EAE, there was a reduction in density of staining, with fewer neuronal cell bodies (Figure 7.4 G –L), particularly in sections from $tPA^{-/-}$ mice (Figure 7.4 H). At 60 dpi of MOG-EAE, there was more staining in sections from $uPAR^{-/-}$ mice and WT mice when compared to that in sections from $tPA^{-/-}$ mice (Figure 7.4 J – L). Additionally there were hypertrophic neuronal cell bodies in the grey matter in sections from $tPA^{-/-}$ and $uPAR^{-/-}$ mice, which were not observed in WT spinal cord sections. Western blotting on spinal cord protein extracts was used to quantitatively measure levels of MAP-2 in the CNS at different time points of MOG-EAE disease in the different genotypes (Figure 7.5 A). Levels of MAP-2 protein were comparable in control WT, $tPA^{-/-}$ and $uPAR^{-/-}$ mice. Following MOG-EAE induction, MAP-2 was significantly decreased in WT and $tPA^{-/-}$ mice at 20 dpi ($P < 0.01$), such that no MAP-2 could be detected in samples from mice at this time point (Figure 7.5 B). At 35 dpi, the peak of disease in $uPAR^{-/-}$ mice, levels of MAP-2 were also decreased, although this

was not significantly different when compared to relevant controls. At 60 dpi, MAP-2 levels had recovered slightly in WT and $tPA^{-/-}$ mice, however the amount of MAP-2 protein was still significantly lower than those of control ($P < 0.01$). No MAP-2 was detected in the spinal cords of $uPAR^{-/-}$ mice at 60 dpi, ($P < 0.01$ versus control). No significant differences were observed between the different genotypes at any of the time points.

Staining for MAP-2 protein in sections of spinal cord from ABH.PAI-$1^{-/-}$ and ABH.PAI-$1^{+/+}$ control mice also revealed neuronal cell bodies in the GM (Figure 7.6i A and D). Following induction of CREAE, staining for MAP-2 was reduced particularly in sections from PAI-$1^{+/+}$ mice at the peak of disease (15 dpi) and during relapse (40 dpi) (Figure 7.6i B and C). At 20 and 40 dpi, staining for MAP-2 in sections from PAI-$1^{-/-}$ mice did not appear significantly different to that in controls (Figure 7.6i E and F). Western blotting on spinal cord protein extracts was used to quantitatively measure levels of MAP-2 in the CNS at different time points of CREAE disease in the different genotypes (Figure 7.6 ii). Levels of MAP-2 protein were comparable in control PAI-$1^{+/+}$ and $PAI^{-/-}$ mice (Figure 7.6 ii). At 15 dpi of CREAE, when PAI-$1^{+/+}$ mice were in the peak acute phase of disease there was a decrease in MAP-2 in these mice although this was not significant. There were no changes in MAP-2 in PAI-$1^{-/-}$ mice before disease onset, although during acute CREAE, there appeared to be a decrease but this failed to reach statistical significance. When both groups of mice were in disease remission, there was a subsequent increase in MAP-2 to levels that were comparable to controls. Following disease relapse in PAI-$1^{+/+}$ mice there was a significant decrease in MAP-2 when compared to PAI-$1^{+/+}$ controls ($P < 0.05$).

MAP-2

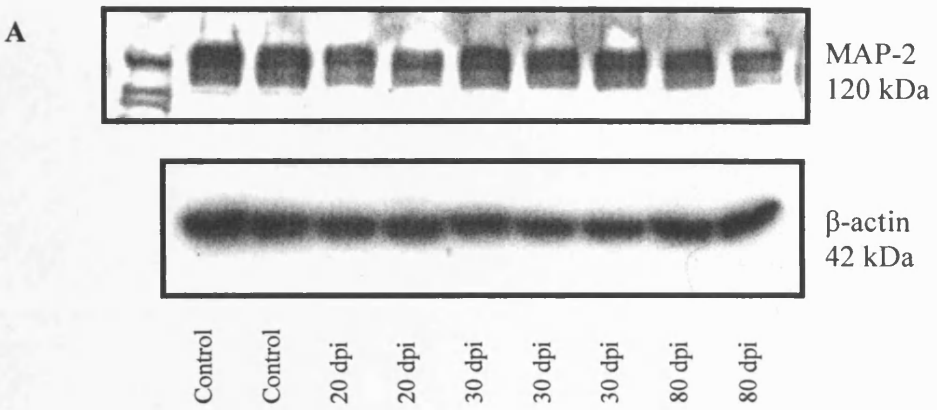

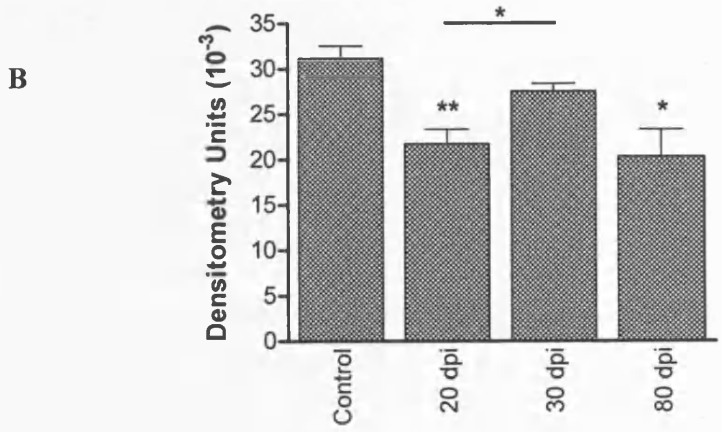

Figure 7.3. *Western blotting of MAP-2 during SCH-CREAE in ABH mice.* **A.** Western blotting for MAP2 was performed on spinal cord protein extracts from normal non-injected and EAE animals using an anti-MAP-2 antibody. Blots were quantitatively measured by densitometry scanning and were re-probed with anti-actin to control for loading of proteins onto the gel. **B.** MAP-2 was significantly decreased during acute and chronic stages of CREAE. Results are expressed as the mean ± SEM, n = 3 - 5. * $P < 0.05$, ** $P < 0.01$ versus control unless indicated by a bar

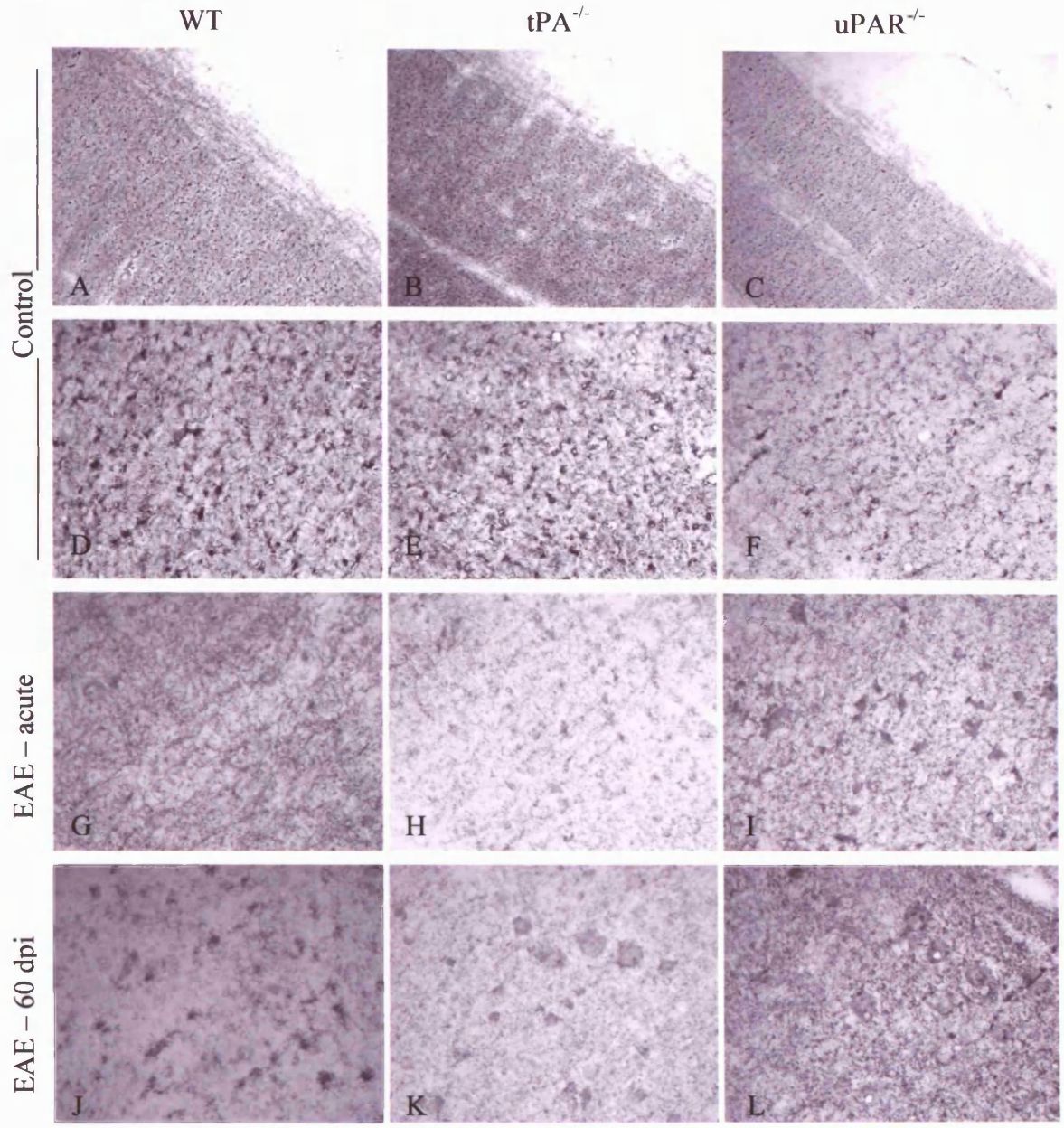

Figure 7.4. *MAP-2 staining is reduced in sections from MOG-EAE mice.* Spinal cords removed from control and EAE mice were sectioned longitudinally. Frozen sections were stained with an antibody against MAP-2. Staining in sections from control mice revealed MAP-2 positive structures in the grey matter of spinal cords (A – F). In sections from EAE mice (G – L), staining was reduced, particularly in sections from $tPA^{-/-}$ mice. Original magnification x100 (A – C) and x 400 (D – L).

MAP-2

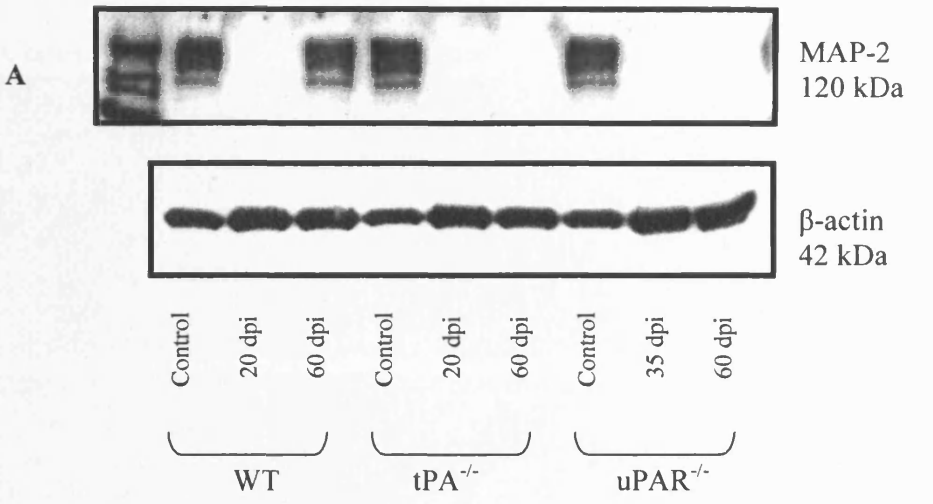

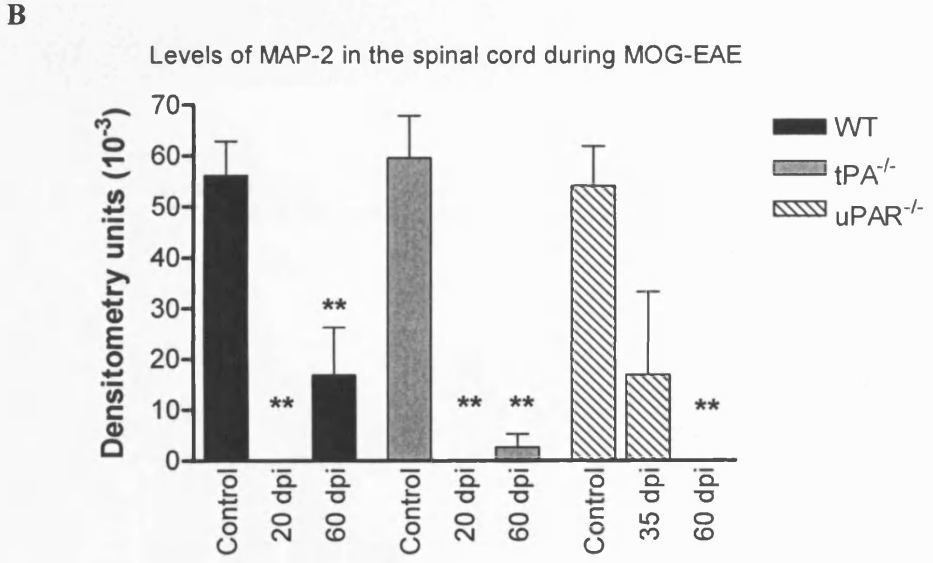

Figure 7.5. *Levels of MAP-2 during MOG-EAE.* **A.** Western blotting for MAP2 was performed on spinal cord protein extracts from normal non-injected and EAE animals using an anti-MAP-2 antibody. Blots were quantitatively measured by densitometry scanning and were re-probed with anti-actin to control for loading of proteins onto the gel. **B.** A significant loss of MAP-2 was seen in the acute phase of EAE particularly in WT and $tPA^{-/-}$ mice. Levels of MAP-2 recovered slightly in WT and $tPA^{-/-}$ animals by 60 dpi but not in $uPAR^{-/-}$ mice. Results are expressed as the mean ± SEM, n = 3 – 5, ** $P < 0.01$.

MAP-2

(i) Immunohistochemistry

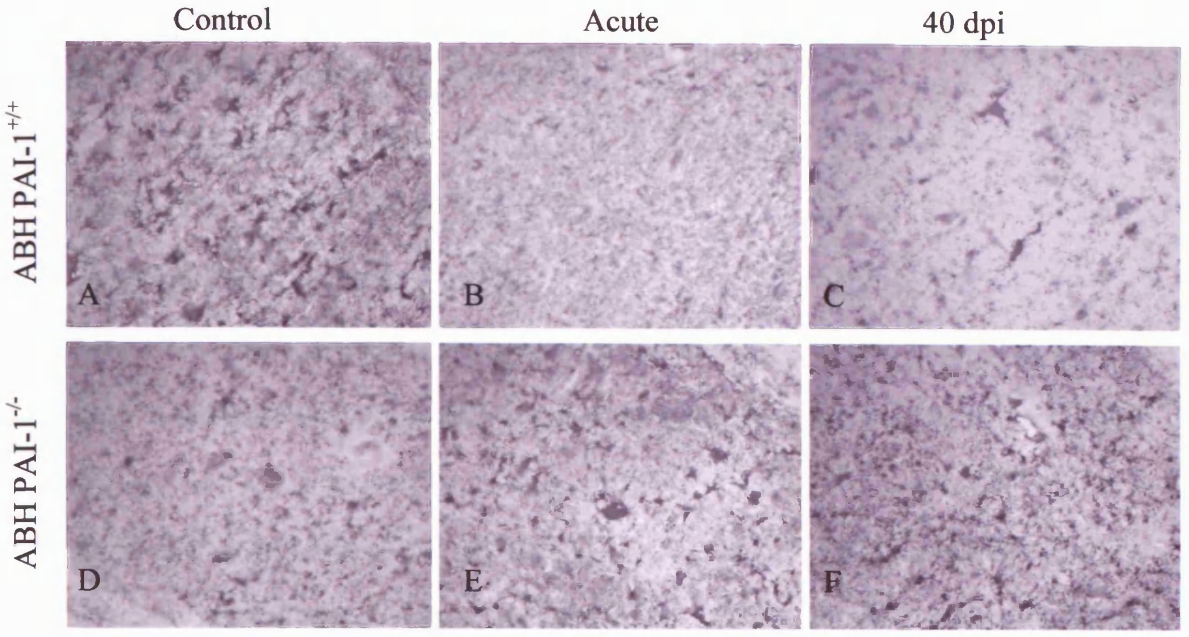

(ii) Western blotting

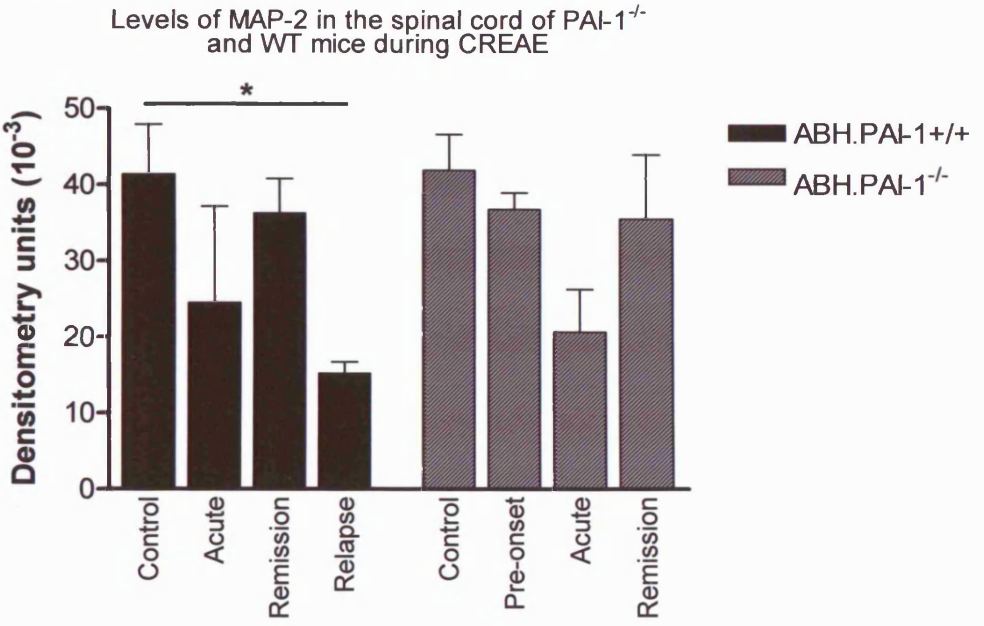

Figure 7.6. *Levels of MAP-2 during SCH-CREAE in ABH.PAI-1$^{-/-}$ and PAI-1$^{+/+}$ mice.* **(i)** Spinal cords removed from control (A and D) and EAE (B, C, E and F) mice were sectioned longitudinally. Frozen sections were stained with an antibody against MAP-2. In sections from CREAE mice, GM staining was reduced at 20 and 40 dpi in sections from *PAI-1$^{+/+}$* mice. Original magnification x 400. **(ii)** Western blotting for MAP2 was performed on spinal cord protein extracts from control and EAE animals. Blots were quantitatively measured by densitometry scanning. A loss of MAP-2 was seen in the acute phase of CREAE in both PAI-1$^{-/-}$ and *PAI-1$^{+/+}$* mice. Levels of MAP-2 in recovered to near those of controls during disease remission, however MAP-2 was significanlty decreased during relapse in *PAI-1$^{+/+}$* mice. Results are expressed as the mean ± SEM, n = 3. * $P < 0.05$.

7.2.3. Expression of synaptophysin in the spinal cord during EAE.

Western blotting for synaptophysin (Figure 7.7 A) revealed that there was a decrease in all samples from ABH mice during CREAE; however none of these changes were statistically significant (Figure 7.7 B).

Immunohistochemical staining for synaptophysin in sections from control C57BL/6 mice stained mostly GM in the spinal cord (Figure 7.8 A – F), with some immunopositive neuronal cell bodies. In sections from WT, $tPA^{-/-}$ and $uPAR^{-/-}$ mice, on the C57BL/6 background, at the acute and chronic stages of MOG-EAE disease there were no apparent differences between staining in the genotypes at different time points (Figure 7.8 G – L), although in sections from $tPA^{-/-}$ and $uPAR^{-/-}$ mice at 60 dpi, there were noticeable changes in the morphology of neuronal bodies, which appeared enlarged and hypertrophic when compared to those in sections from WT mice (Figure 7.8 J – L). Whilst Western blotting for synaptophysin revealed slight fluctuations in levels of the protein at different time points of MOG-EAE disease (Figure 7.9 A), there were no significant increases or decreases during MOG-EAE compared with controls, nor between the different genotypes (Figure 7.9 B).

Synaptophysin staining in sections from control ABH.PAI-$1^{+/+}$ and ABH.PAI-$1^{-/-}$ mice stained GM neuronal cell bodies in the spinal cord (Figure 7.10i A and D). In sections from PAI-$1^{+/+}$ and PAI-$1^{-/-}$ mice at the acute, remission and relapse stages of CREAE disease there were no apparent differences between staining in the different genotypes at the different time points (Figure 7.10i B, C, E and F). Western blotting for synaptophysin revealed no significant differences during CREAE compared with controls, nor between the different genotypes (Figure 7.10 ii).

Synaptophysin

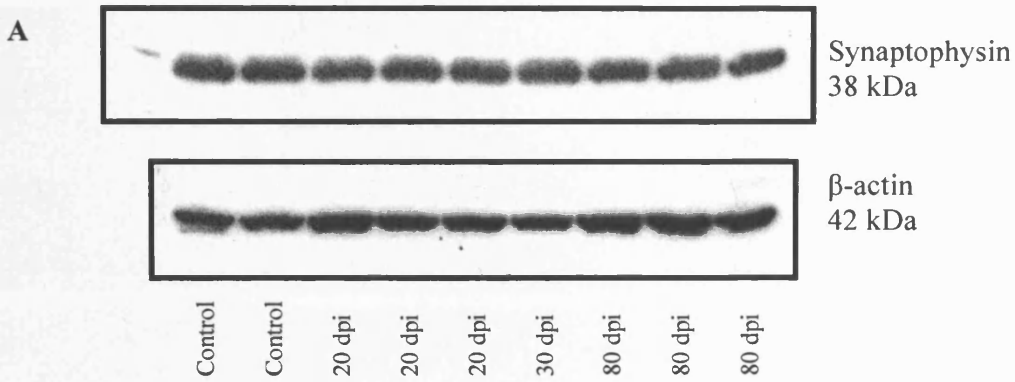

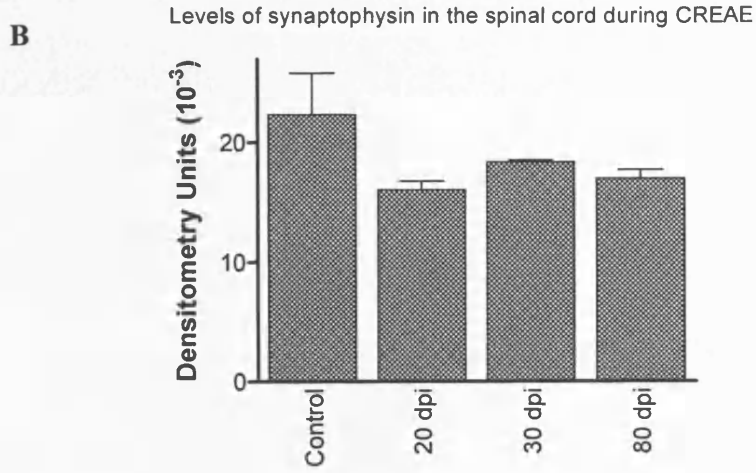

Figure 7.7. *Western blotting of synaptophysin during SCH-CREAE in ABH mice.* **A.** Western blotting for synaptophysin was performed on spinal cord protein extracts from normal non-injected and CREAE animals using an anti-synaptophysin antibody. Blots were quantitatively measured by densitometry scanning and were re-probed with anti-actin to control for loading of proteins onto the gel. **B.** Synaptophysin protein did not change significantly throughout the course of CREAE disease. Results are expressed as the mean ± SEM, n = 3 - 5.

Synaptophysin

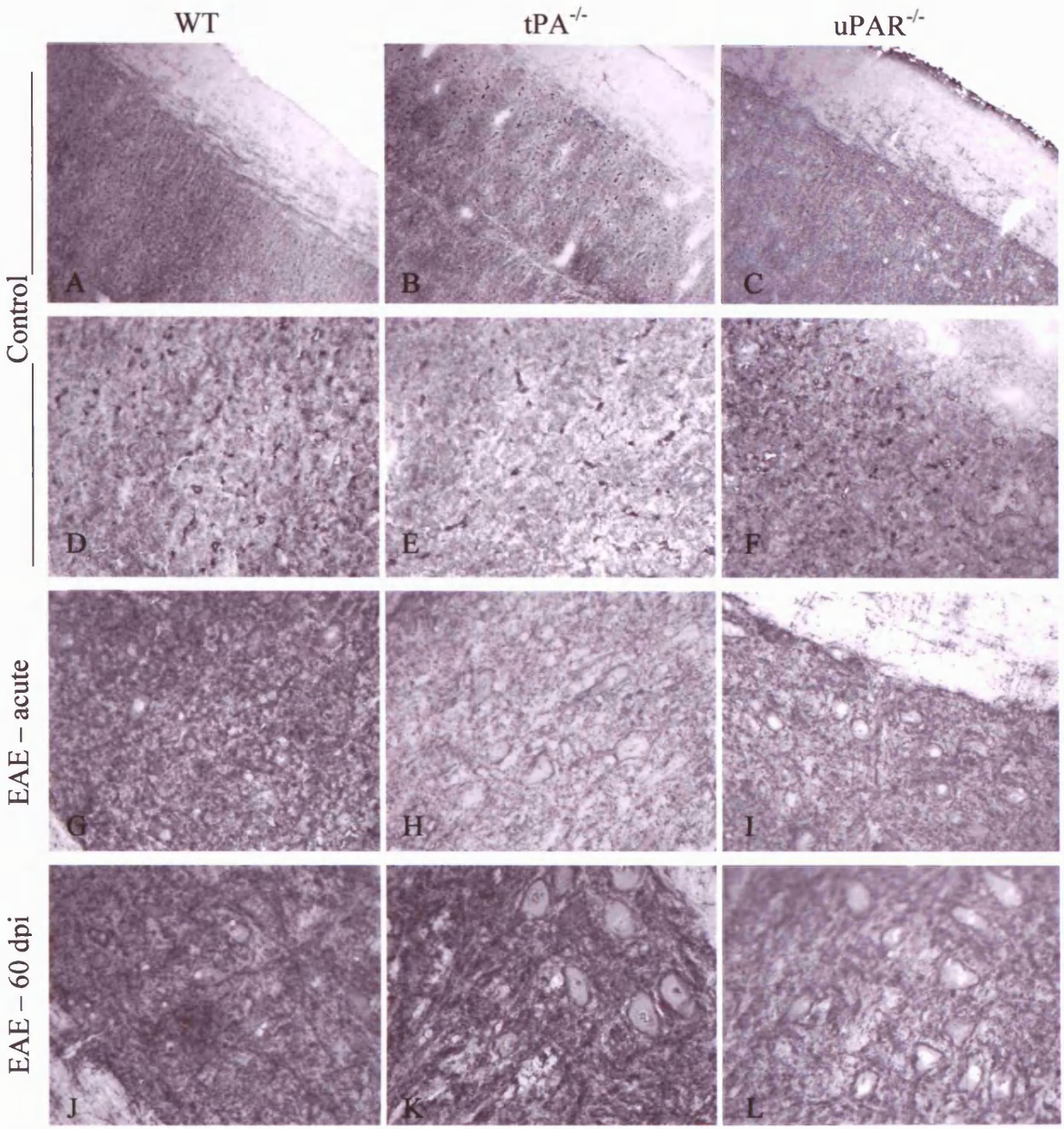

Figure 7.8. *Synaptophysin staining in sections from MOG-EAE mice*. Spinal cords removed from control and EAE mice were sectioned longitudinally. Frozen sections were stained with an antibody against synaptophysin. Staining in sections from control mice revealed synaptophysin positive structures, localised in the grey matter (A – F). In sections from EAE mice (G – L), there were changes in the morphology of cells with neuronal bodies appearing hypertrophic in $tPA^{-/-}$ and $uPAR^{-/-}$ mice. Original magnification x100 (A – C) and x 400 (D – L).

Synaptophysin

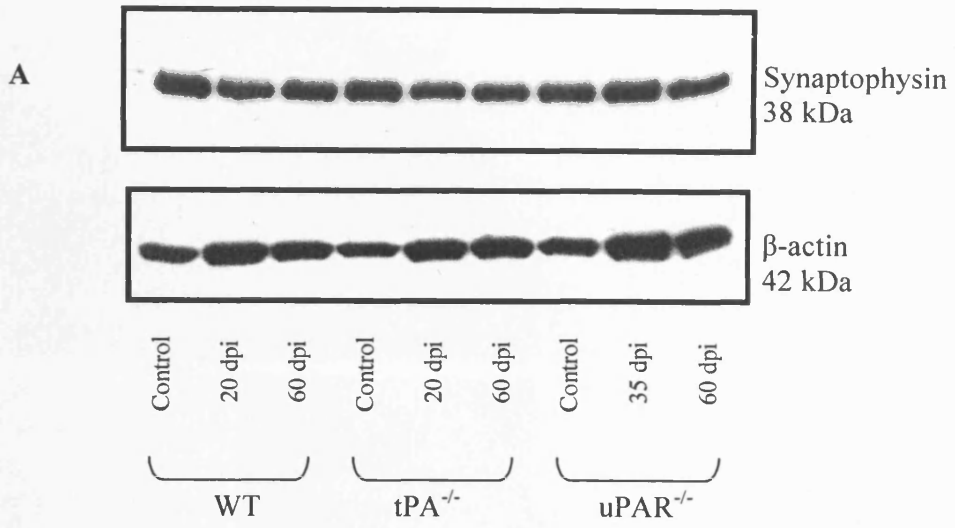

B

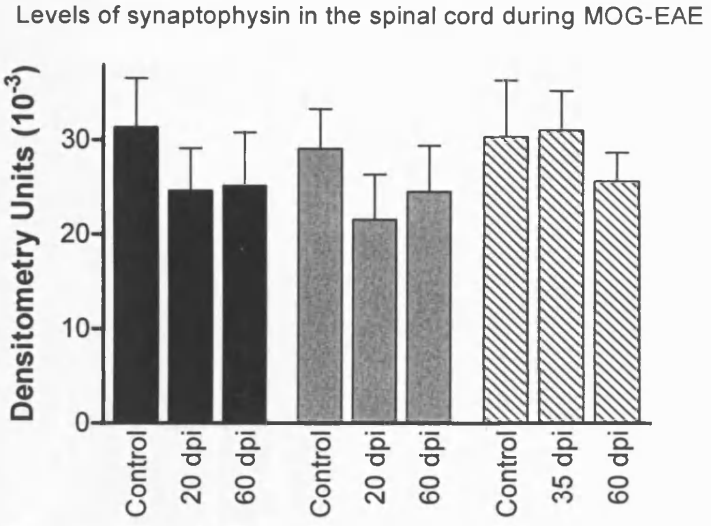

Figure 7.9. *Levels of synaptophysin during MOG-EAE.* **A.** Western blotting for synaptophysin was performed on spinal cord protein extracts from normal non-injected and EAE animals using an anti-synaptophysin antibody. Blots were quantitatively measured by densitometry scanning and were re-probed with anti-actin to control for loading of proteins onto the gel. **B.** No significant differences were seen in synaptophysin levels in WT, $tPA^{-/-}$ or $uPAR^{-/-}$ mice following induction of MOG-EAE. Results are expressed as the mean ± SEM, n = 3.

Synaptophysin

(i) Immunohistochemistry

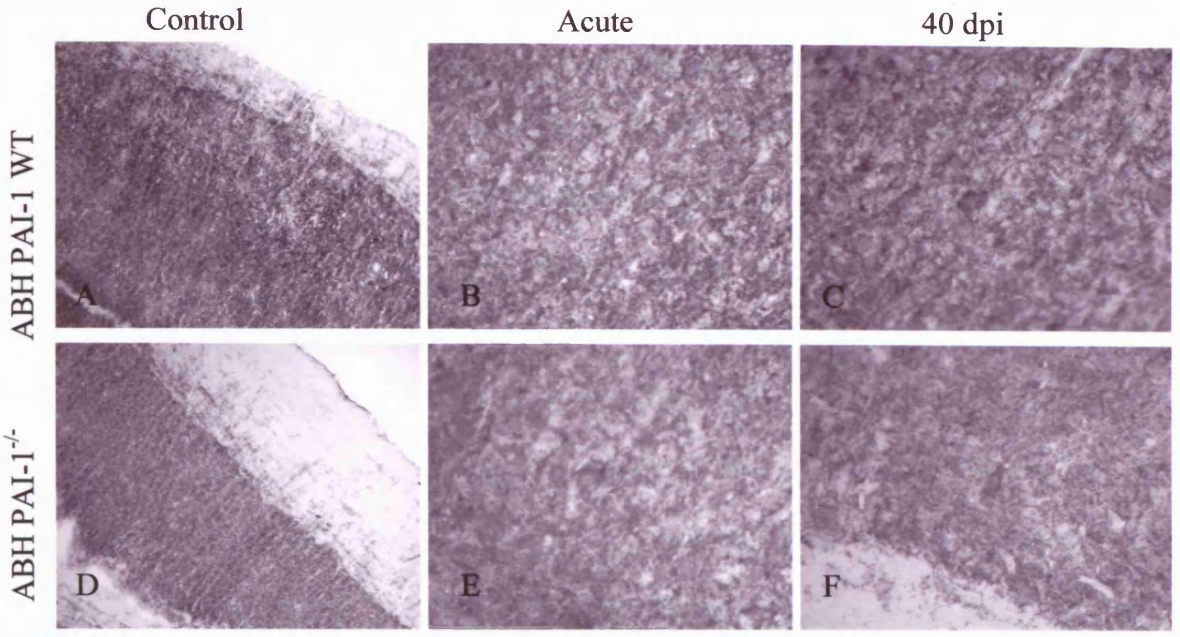

(ii) Western blotting

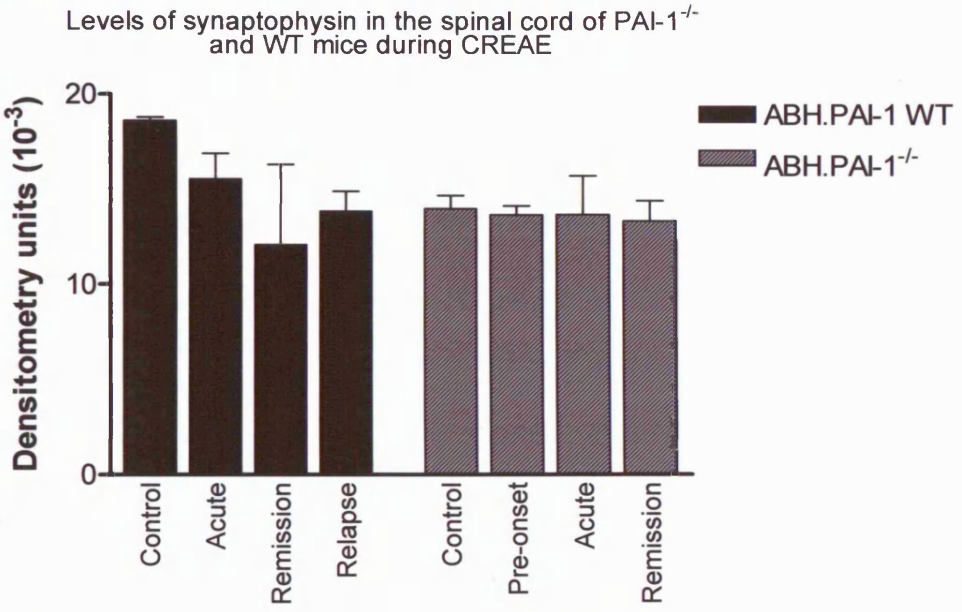

Figure 7.10. *Levels of synaptophysin during SCH-CREAE in ABH PAI-1$^{-/-}$ and WT mice.* **(i)** Spinal cords removed from control and EAE mice were sectioned longitudinally. Frozen sections were stained with an antibody against synaptophysin. There were no obvious changes in synaptophysin staining and no apparent differences between the genotypes. Original magnification x100 (A and D) and x 400 (B, C, E and F). **(ii)** Western blotting for synaptophysin was performed on spinal cord protein extracts from normal non-injected and CREAE animals using an anti-synaptophysin antibody. Blots were quantitatively measured by densitometry scanning. No significant differences were seen in synaptophysin levels in the acute, remission or relapse stages of CREAE disease. Results are expressed as the mean ± SEM, n = 3.

7.2.4. Expression of GAP-43 in the spinal cord during EAE.

GAP-43 protein decreased over time in ABH mice as CREAE disease progressed (Figure 7.11 A and B). During the acute and remission phases of disease, at 20 and 30 dpi respectively, GAP-43 was significantly decreased ($P < 0.05$) when compared to control. During remission, levels of GAP-43 were slightly lower than those during acute CREAE, however this was not significant. A highly significant decrease of GAP-43 was observed in samples from the spinal cords of mice at 80 dpi of CREAE, the chronic phase ($P < 0.001$). Additionally, this was also significantly lower than levels of GAP-43 during disease remission ($P < 0.05$).

There was a high density of immunohistochemical staining for GAP-43 in sections from control C57BL/6 mice, which could be largely located to axons in the WM of the spinal cord (Figure 7.12 A – F). During acute EAE, at 20 dpi for WT and $tPA^{-/-}$ and 35 dpi for $uPAR^{-/-}$ mice, there was a decrease in GAP-43 staining in the spinal cord (Figure 7.12 G – I), however it did not appear that there were any differences between the genotypes. Furthermore at 60 dpi, there were no apparent differences in GAP-43 staining between the genotypes (Figure 7.12 J – L). To quantitatively measure levels of GAP-43, Western blotting was performed on spinal cord homogenates (Figure 7.13 A). GAP-43 was significantly decreased in samples from WT and $tPA^{-/-}$ mice at 20 dpi of MOG-EAE when compared to the relevant controls (Figure 7.13 B; $P < 0.05$). In WT mice at 60 dpi, levels of GAP-43 returned to amounts that were comparable to those of controls; however there was still a significant decrease in GAP-43 in $tPA^{-/-}$ mice at 60 dpi which was significantly lower ($P < 0.05$) than levels in $tPA^{-/-}$ controls and significantly lower ($P < 0.05$) than levels in WT mice at 60 dpi. Although there were decreases in the level of GAP-43 in samples from $uPAR^{-/-}$ mice at 35 and 60 dpi of EAE, these were not statistically significantly different to $uPAR^{-/-}$ controls.

Staining for GAP-43 in spinal cords from control and CREAE ABH.PAI-$1^{+/+}$ and ABH.PAI-$1^{-/-}$ mice revealed no striking differences at different time points between the genotypes (Figure 7.14i A and D). There was a high density of immunohistochemical staining in all sections, which was located to axons in the WM of the spinal cord. During acute CREAE at 15 dpi for PAI-$1^{+/+}$ and 20 dpi for PAI-$1^{-/-}$, there were apparent decreases in GAP-43 staining, particularly surrounding perivascular cuffs (Figure 7.14i B and E). At 40 dpi, there was evidence of increased GAP-43 expression in PAI-$1^{-/-}$ mice, however GAP-43 staining in PAI-$1^{+/+}$ mice was still reduced compared to that in sections from control mice (Figure 7.14i C and F). To quantitatively measure levels of GAP-43, Western blotting was performed on spinal cord homogenates. GAP-43 was lower in samples from control PAI-$1^{-/-}$ mice than control PAI-$1^{+/+}$ mice, however this was not statistically significant (Figure 7.14 ii). There were no significant changes in levels of GAP-43 in PAI-$1^{+/+}$ littermates at any stage during CREAE, although the trend suggested a decrease during acute and relapse stages with a slight recovery during disease remission. In samples from PAI-$1^{-/-}$ mice there was increases in GAP-43 pre-CREAE disease onset (15 dpi) and during disease remission. During the acute phase of disease there was a decrease in GAP-43 protein, which was similar to levels in control mice, but significantly lower than levels in mice from CREAE remission ($P < 0.05$).

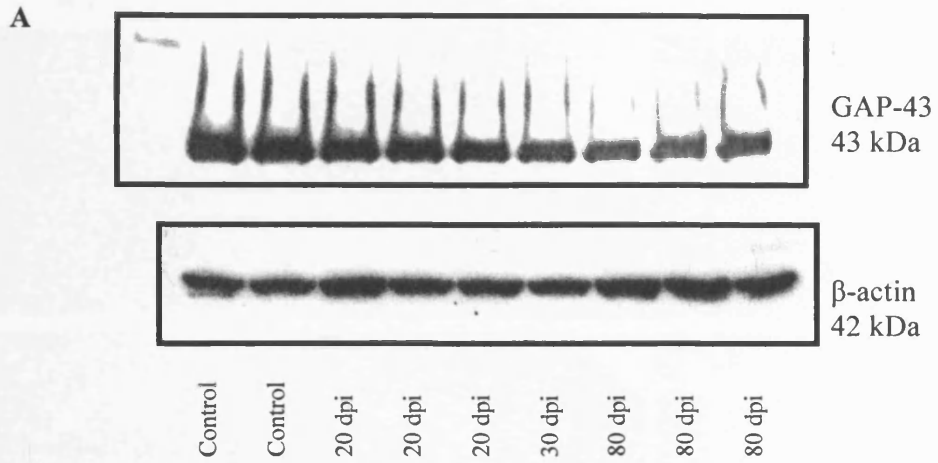

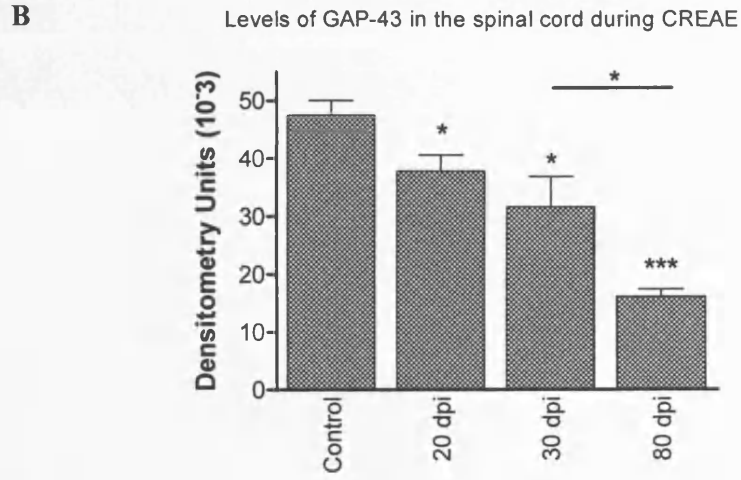

Figure 7.11. *Western blotting of GAP-43 during SCH-CREAE in ABH mice.* **A.** Western blotting for GAP-43 was performed on spinal cord protein extracts from normal non-injected and CREAE animals using an anti-GAP-43 antibody. Blots were quantitatively measured by densitometry scanning and were re-probed with anti-actin to control for loading of proteins onto the gel. **B.** Levels of GAP-43 decreased over time as EAE progressed and levels during the chronic stages of CREAE were approximately a third of that of control mice. Results are expressed and the mean ± SEM, n = 3 - 5. * $P < 0.05$, *** $P < 0.001$ versus control unless indicated by a bar.

GAP-43

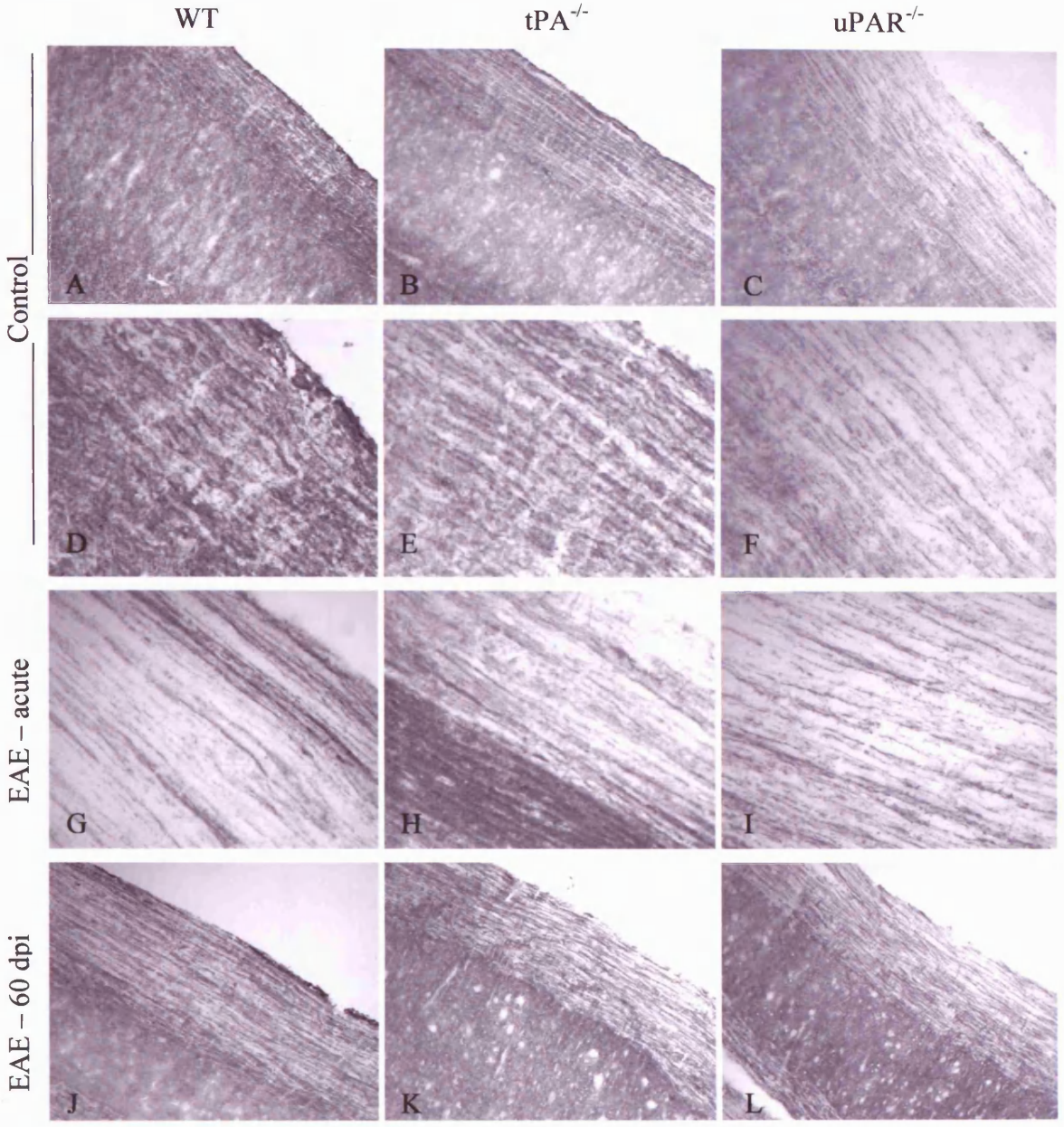

Figure 7.12. *GAP-43 staining in sections from MOG-EAE mice*. Spinal cords removed from control and EAE mice were sectioned longitudinally. Frozen sections were stained with an antibody against GAP-43. Staining in sections from control mice revealed GAP-43 positive structures, particularly in white matter (A – F), however in sections from EAE mice, staining was reduced, although no apparent differences were obvious between the different genotypes. Original magnification x100 (A – C, J - L) and x 400 (D – I).

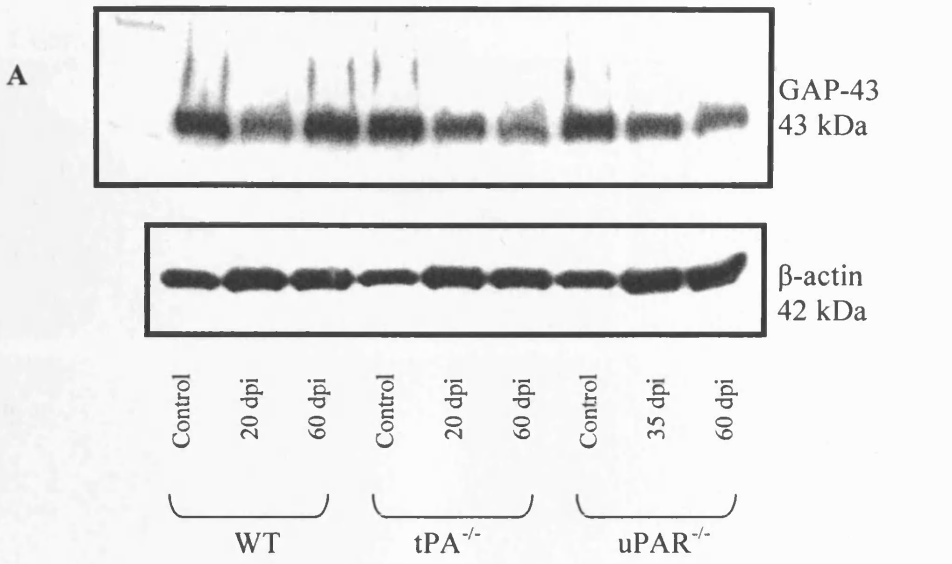

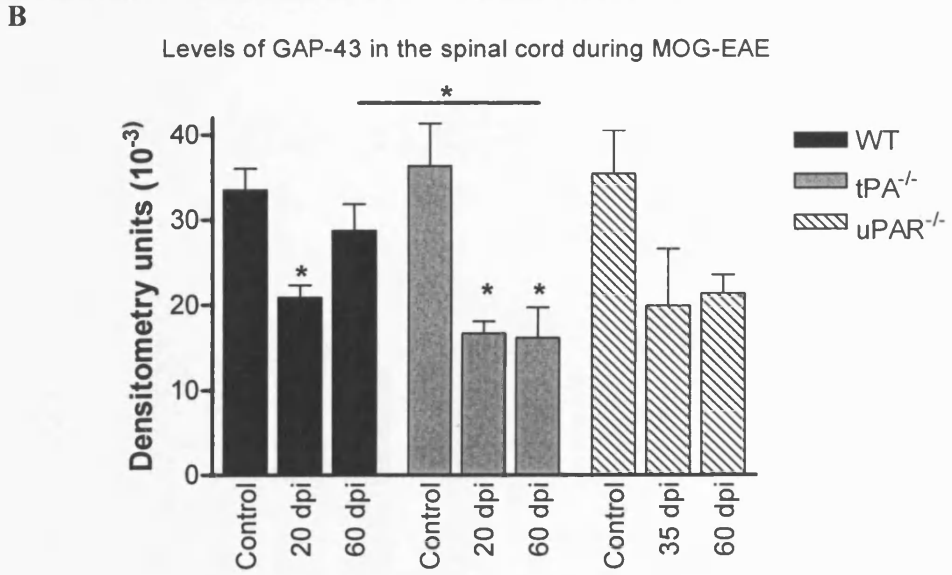

Figure 7.13. *Levels of GAP-43 during MOG-EAE.* **A.** Western blotting for GAP-43 was performed on spinal cord protein extracts from normal non-injected and EAE animals using an anti-GAP-43 antibody. Blots were quantitatively measured by densitometry scanning and were re-probed with anti-actin to control for loading of proteins onto the gel. **B.** A significant loss of GAP-43 was seen in the acute phase of EAE in all three groups of mice. In WT mice at 60 dpi, levels of GAP-43 recovered to those of control mice however $tPA^{-/-}$ and $uPAR^{-/-}$ mice had sustained GAP-43 loss by 60 dpi. Results are expressed and the mean ± SEM, n = 3 - 5. * $P < 0.05$ against appropriate control unless indicated by a bar.

GAP-43

(i) Immunohistochemistry

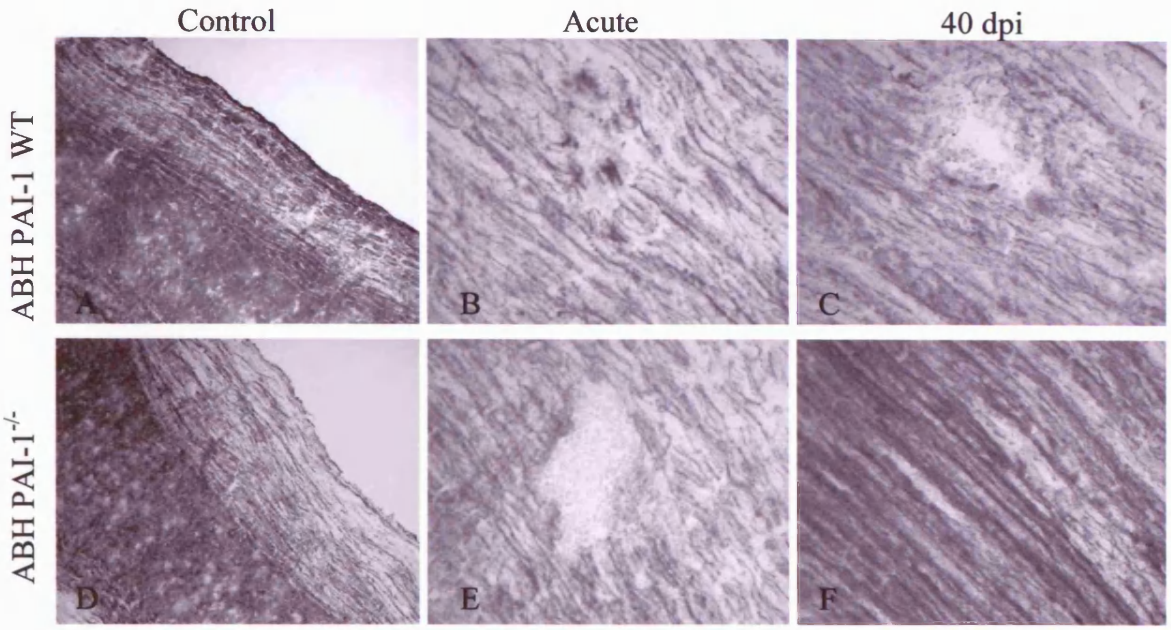

(ii) Western blotting

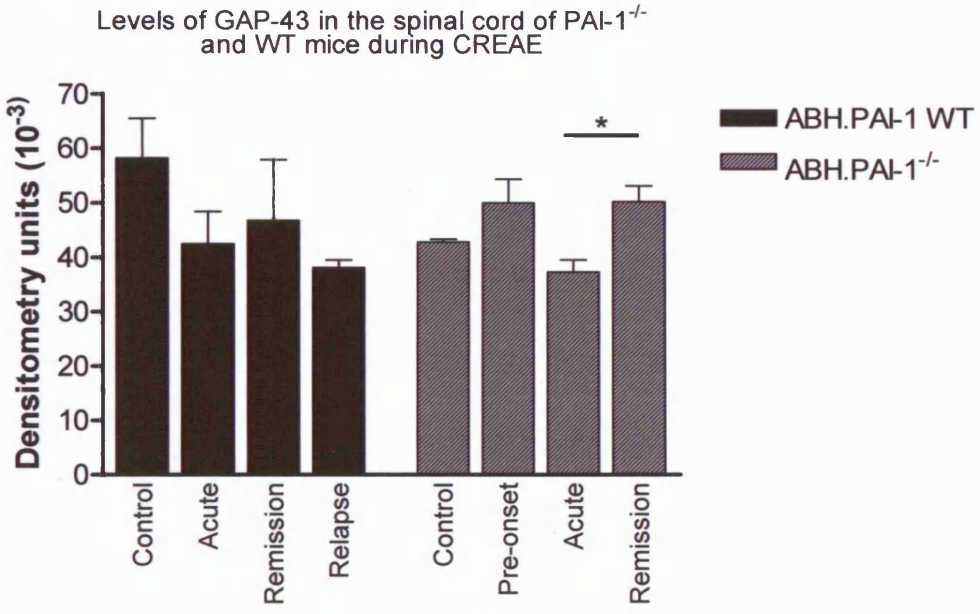

Figure 7.14. *Levels of GAP-43 during SCH-CREAE in ABH PAI-1$^{-/-}$ and PAI-1$^{+/+}$ WT mice.* **(i)** Spinal cords removed from control and EAE mice were sectioned longitudinally. Frozen sections were stained with an antibody against GAP-43. In sections from CREAE mice, WM staining was slightly reduced, although no apparent differences were obvious between the different genotypes. Original magnification x100 (A and D) and x 400 (B, C, E and F). **(ii)** Western blotting for GAP-43 was performed on spinal cord protein extracts from normal non-injected and EAE animals. Blots were quantitatively measured by densitometry scanning. Levels of GAP-43 decreased during acute and relapse stages of CREAE. A significanlt increase in GAP-43 was seen following disease remission in PAI-1$^{-/-}$ mice compared to levels during the acute phase of CREAE. Results are expressed and the mean ± SEM, n = 3. * $P < 0.05$.

7.3. Discussion.

Expression of different synaptic and dendritic proteins has provided very useful tools to investigate axonal, neuronal and dendritic pathology in the CNS during EAE. During neuroinflammation notable changes were observed in axonal and dendritic proteins, which are primarily located in the white matter (WM), whilst grey matter (GM) synapses were relatively unaffected. Dendrites appear to be the one of the first structures affected by the inflammatory attack. Although this is initially reversible, a more permanent loss of dendritic proteins was observed following chronic disease. The capacity for axonal regeneration and plasticity decreased as EAE disease progressed, possibly reflecting neuronal loss and degeneration.

Specific upregulation of PSD-95 on axons in lesion areas indicates a role for this protein in WM axonal functioning, in addition to its role at the post-synaptic density. In contrast, no striking changes in the staining pattern for PSD-95 in the GM were observed here in MOG-EAE or CREAE tissue. Previous work has revealed a physiological role for PSD-95 showing that this protein can play a decisive role in controlling synaptic strength and activity-dependant plasticity (Beique and Andrade, 2003; Migaud *et al.,* 1998), thus upregulation of PSD-95 could be a mechanism to increase plasticity and remodelling around lesion areas. However Zhu *et al.,* (2003) found a clear decrease in PSD-95 staining in the GM and WM of rat EAE spinal cord sections, which reportedly represented excessive NMDA receptor activation under excitotoxic conditions. One key difference in these experiments was the way in which the sections were prepared. In order to gain a semi-quantitative measurement of PSD-95 levels Western blotting would need to be carried out, but the antibody used here was not suitable for this application. Upregulation of PSD-95 could also reflect potentially damaging effects of this protein. PSD-95 promotes functional localisation of NMDA receptors by clustering at synapses, increasing their stability and glutamate signalling

(Kim and Sheng, 2004). Additionally PSD-95 couples NMDA receptors to neuronal nitric oxide synthase (nNOS), and excessive NO can have detrimental effects on axonal conductance (Kapoor *et al.,* 2003).

PSD-95, in addition to clustering of NMDA receptors, also induces clustering of Kv1 type potassium channels (Jugloff *et al.,* 2000). Specific redistribution of Kv1 potassium channels on neurons is a feature of axons in MS lesions and is observed during remyelination (Jugloff *et al.,* 2000). Injured axons have increased expression of Kv1 channels, and their distribution is changed to a more dispersed pattern along demyelinated axons (Nashmi and Fehlings, 2001). Specific expression of PSD-95 on axons in the area of perivascular cuffs during EAE could represent a mechanism for clustering of K^+ channels, thus stabilising them by reducing their rate of internalisation/endocytosis (Jugloff *et al.,* 2000). In this way PSD-95 might aid in neuronal functioning by helping the axon maintain an action potential. However whilst this might help in the short term as an endogenous response to demyelination and axonal damage, K^+ in the long term can be potentially harmful. Increased activity of K^+ channels holds the membrane potential close to the equilibrium potential of K^+ and results in axonal conduction block (Nashmi and Fehlings, 2001), and 4-aminopyridine (4-AP) a broad K^+ channel blocker, has shown therapeutic potential in EAE and is currently in clinical trials for treatment of MS (Nashmi and Fehlings, 2001). Thus disruption of the PSD-95 interaction with K^+ channels could provide a potentially therapeutic effect. Furthermore perturbation of the PSD-95-NMDA receptor link has proved to be beneficial in a model of ischaemic brain injury, by preventing downstream neurotoxic signalling (Aarts *et al.,* 2002).

GAP-43 is a major constituent of the growth cone where it modulates the formation of new connections as well as in guiding the growth of axons. It is expressed by developing or regenerating axons and can serve as a marker for axonal sprouting thus

is considered to be an intrinsic determinant of the growth state of neurons (Benowitz and Routtenberg, 1997). GAP-43 expression is important for re-connectivity following a targeted EAE lesion in the spinal cord (Kerschensteiner *et al.,* 2004). A decrease in GAP-43 over time in ABH mice during CREAE indicates that the environment was not conducive for regeneration or repair. From previous work, it is clear that ABH mice at 80 dpi of CREAE have substantial neuronal loss (Jackson *et al.,* 2005; Pryce *et al.,* 2003), thus significant loss of GAP-43 may also represented a decrease in plasticity and regeneration of axons. In the MOG-EAE model, a significant decrease in GAP-43 was only seen in $tPA^{-/-}$ mice at 60 dpi. Akassoglou *et al.,* (2002) found that fibrin deposition and depletion did not affect axonal sprouting and elongation (as measured by GAP-43), and that the inhibitory effect of fibrin was on regeneration of the nerve. However in the CNS under neuroinflammatory conditions, GAP-43 expression was reduced in $tPA^{-/-}$ mice correlating with fibrin deposition and SMI32 staining, which could indicate that fibrin was creating a hostile environment for axonal sprouting and regeneration. Local reorganisation of synaptic connections can occur spontaneously in the CNS after injury (Kerschensteiner *et al.,* 2004). As tPA plays a key role in synaptic plasticity (Seeds *et al.,* 1996), decreased GAP-43 in $tPA^{-/-}$ mice could represent a decrease in levels of remodelling around lesion areas.

Demyelination would usually be associated with a reduced effect of myelin inhibition on neurite outgrowth in and around lesion areas by molecules such a Nogo-A, leading to an increase in GAP-43 expression (Kerschensteiner *et al.,* 2004; Pot *et al.,* 2002). However, the negative correlation that should exist between GAP-43 and myelin did not appear in this study. This was probably as a result of significant axonal damage and degeneration, reducing the numbers of axons capable of sprouting new processes for reconnection and plasticity surrounding lesion areas.

Dendrites are particularly susceptible to excitotoxic damage as they receive most of the synaptic inputs (Harris and Kater, 1994; Zhu *et al.,* 2003). The dendritic marker MAP-2 was primarily located in the grey matter of sections in neuronal cell bodies whilst white matter dendrites were not clearly visible. Although some MAP-2 was lost in the GM, it is more likely that the loss seen in Western blotting was that lost in the WM and dendritic tree as this was the site of inflammation, demyelination and axonal damage. This suggests that excitotoxic mechanisms are playing a role in dendritic pathology in the MOG and CREAE models of neuroinflammation. However as there was no significant difference between the genotypes, it is unlikely that the PA system has a direct effect here on NMDA receptor function and signalling. Although MAP-2 loss may be induced by excitotoxicity (Zhu *et al.,* 2003), it remains to be determined whether fibrin, and exposure to other neurotoxic factors such as inflammatory cytokines, reactive oxygen species or proteases could also result in a decrease of this protein.

Similar to findings by Zhu *et al.,* (2003), decreased levels of MAP-2 correlated with inflammation, and subsequently increased following disease recovery/remission. In ABH mice, loss of MAP-2 at 80 dpi, where mice had significant neurological deficit and movement impairment (Jackson *et al.,* 2005; Pryce *et al.,* 2003), eludes to a more permanent loss of MAP-2 as a result of dendritic degeneration. Frequent episodes of CNS inflammatory demyelinating attacks result in cumulative synaptic damage and transmission failure in WM dendrites and could possibly contribute to the movement dysfunction in EAE (Zhu *et al.,* 2003). Additionally loss of MAP-2 may be an early indicator of neuronal dysfunction, and may precede neurodegeneration (Matesic and Lin, 1994). The total loss of MAP-2 protein in WT, $tPA^{-/-}$ and $uPAR^{-/-}$ mice detected by Western blotting was a somewhat puzzling observation. This could not represent a total loss of spinal cord MAP-2 as the mice wouldn't be able to survive. Additionally

staining for MAP2 was still seen in spinal cord sections by immunohistochemistry. However it could represent loss of the particular epitope of MAP-2 which the antibody detects. MAP-2 also contributes to dendritic remodelling and postsynaptic alterations that occur after specific lesions, and increased MAP-2 immunoreactivity during CREAE remission could be associated with axonal sprouting (Johnson and Jope, 1992).

No changes in levels of synaptophysin indicate that induction of CREAE or MOG-EAE does not significantly affect neurons at the synaptic level. Since most synapses are present in the GM, this is not entirely surprising as most EAE pathology is observed in the WM. These results contrast with findings by Zhu *et al.,* (2003) who found a significant loss of synaptophysin, and another synaptic marker synapsin 1, with more significant reductions in the GM than WM. Although no changes were observed in mice during MOG-EAE, staining with the synaptophysin antibody in sections did reveal some hypertrophic neuronal cell bodies particularly in sections from $tPA^{-/-}$ mice. Upon closer examination these cells showed signs of nuclei condensation, a sign of apoptosis, thus this could be a possible indicator of neuronal apoptosis.

In summary, whilst there is no definitive marker for axonal and neuronal degeneration, the synaptic and dendritic proteins investigated here could provide useful information on pathological changes in MS. This work supports the findings that neuronal/axonal dysfunction occurs early on during EAE, and is not just a feature of chronicity (Onuki *et al.,* 2001). Additionally synaptic proteins are relatively unchanged revealing that CNS pathology in EAE mice affects preferentially the WM axons, with relative sparing of the GM and synaptic functioning. Finally, in the midst of looking for better, more accurate predicators of disease outcome, a potential therapeutic target has been revealed in PSD-95.

8. Conclusions and Future work.

8.1. Conclusions.

The findings from the studies in this thesis have highlighted that manipulation of the PA system can affect outcome of neuroinflammatory disease. CREAE-induction in the ABH mouse has been previously characterised as a robust model of inflammatory demyelination. Investigation into the involvement of the PA system using this model revealed some important pathological similarities to MS, with increased PAI-1 synthesis and impairment of fibrinolysis as key features of disease. Fibrin deposition was associated with inflammation and persisted over time correlating with chronicity and neuronal degeneration. Additionally, analysis of dendritic proteins supported evidence that neuronal / axonal dysfunction occurs early in EAE disease, and is not just a feature of chronicity.

Induction of EAE with MOG peptide in $tPA^{-/-}$ mice led to a more severe clinical disease than wildtype mice thus revealing a protective and beneficial role for this enzyme during neuroinflammation. This contrasts with ischaemia and excitotoxicity where tPA has a detrimental effect on outcome. After further investigation, the protective role of tPA seems to occur through its ability to initiate plasmin-catalysed removal of CNS and axonal fibrin deposits. This also highlights the potentially damaging influence of fibrin, which could have a direct effect on axonal pathology, in addition to indirect actions via exacerbation of inflammation.

EAE induction in $uPAR^{-/-}$ and $PAI\text{-}1^{-/-}$ revealed an involvement of these molecules in regulating cell migration and adhesion of leucocytes. Any interference of this unique system interrupts cell migration in the CNS, and delays disease onset. Another feature of EAE disease in $PAI\text{-}1^{-/-}$ mice was an enhanced fibrinolytic potential, which contributed to a reduction in disease severity and improved outcome in these mice.

In conclusion, all three of these components of the PA cascade are implicated in the inflammation, demyelination and neurodegeneration characteristic of EAE and are capable of modulating clinical progression. Investigation into the role of tPA, uPAR and PAI-1 during neuroinflammation has revealed potential sites for therapeutic intervention. This study has suggested a major role for tPA in CNS fibrinolysis and highlighted the inhibitor PAI-1 as a potential target for disease modifying treatment. Interruption of the uPAR-PAI-1-VN link could prove to be another method of targeting and reducing cell migration into the CNS. Inhibition of PAI-1 could be therapeutically beneficial in treating MS. This would provide a dual palliative approach whereby leucocyte migration and inflammation are reduced, allowing efficient removal of fibrin, which could potentially decrease axonal/neuronal damage, and reduce frequency of disease relapses in MS patients.

8.2. Future work.

The work presented here is a step towards elucidating the role of the PA system during neuroinflammation, and highlights potential sites for therapeutic intervention. Additional experimental studies are needed to fully clarify to role of fibrin on axonal pathology and to further investigate the findings from this work.

Previous work by Inoue *et al.,* (1996) and Akassoglou *et al.,* (2004) has found that pharmacological and genetic depletion of fibrin is beneficial under experimental neuroinflammatory conditions. Additionally, removal of fibrin by ancrod aids neuronal regeneration and demyelination in a model of peripheral nerve injury (Akassoglou *et al.,* 2000). This has not however been investigated in the MOG or CREAE model, nor has it been looked at in $tPA^{-/-}$ mice. Treating $tPA^{-/-}$ mice with ancrod would determine whether removing fibrin could rescue these mice from the more severe disease and what effect it would have in CREAE in ABH mice.

To confirm the localisation and deposition of fibrin on axons in lesions, electron microscopial studies are required. Investigation into whether fibrin(ogen), fibrin or FDPs has a direct or indirect toxic effect on neurons and whether is it capable of activating microglia in the same way that it can activate macrophages (Akassoglou *et al.,* 2004) could be done by *in vitro* studies. Adding fibrin to microglial cultures would assess its affect on microglial activation, and adding the conditioned medium to neuronal cultures would assess a potential indirect toxic effect. Additionally by using these techniques in cultures derived from the different knockout mice, it could be revealed whether neurons from $tPA^{-/-}$ mice are more susceptible to fibrin induced toxicity. Furthermore, it would be of interest to determine whether fibrin(ogen), fibrin matrix or FDPs affect the migration and remyelinating properties of oligodendrocyte precursors cells as in the PNS with Schwann cells (Akassoglou *et al.,* 2002).

To further investigate the mechanisms involved in uPAR mediated cell migration, and to determine which cell types are particularly affected by lack of uPAR, a series of experiments could be carried out. Using a transfer EAE protocol, encephalitogenic T cells from $uPAR^{-/-}$ mice, either from sensitised animals or propagated *in vitro*, could be injected into WT recipients. This would determine whether uPAR was affecting T lymphocyte migration/adhesion into the CNS and if this accounted for the differences in clinical pictures observed between the WT and $uPAR^{-/-}$ mice. It would be interesting to see if cells from $uPAR^{-/-}$ mice injected into WT mice would produce a disease similar to that in $uPAR^{-/-}$ mice and whether T-cells from WT mice, would produce a WT-like disease course in $uPAR^{-/-}$ mice. Additionally cell migration and adhesion assays could be carried out to determine which cells are affected by the absence of uPAR or PAI-1. For example T-lymphocytes, peritoneal macrophages, and microglia could be isolated from the different genotypes and the cell migration capabilities of these different cells compared.

The plasminogen activator system is linked with the MMP cascade as plasmin can activate several of the enzymes. In the absence of tPA, with a reduction in plasminogen activation there could potentially be a reduction in MMP-3 activation. Furthermore, in PAI-$1^{-/-}$ mice, there is a higher degree of plasminogen activation, possibly leading to excessive MMP activation, which could ultimately have detrimental effects during inflammatory demyelination. Investigation into levels of different MMP enzymes, particularly MMPs 3, 7 and 9 in the different knockout mice would determine how the link between these two systems is changed during EAE in the different knockout mice. This could be done by western blotting, using non-reducing conditions to identify native and complexed enzymes. Additionally, activity assays could be carried out to further characterise this.

To clarify and expand on the findings in the PAI-$1^{-/-}$ mice, there are several experiments that could be carried out. Firstly a tPA activity assay could be performed in order to confirm that increased tPA during EAE is reflected by an increase in activity due the absence of PAI-1. Furthermore, by investigating levels of PAI-2, it could be determined whether this serpin is compensating for lack of PAI-1. This could be done by Western blotting. Additionally levels of the plasmin inhibitor, α_2-AP could be investigated, to establish whether enhanced tPA activity is controlled at the level of plasmin activity.

Investigations into the staining for other TJ proteins including claudin-3 would clarify whether these junctions are kept intact during CREAE and MOG-EAE, or if the proteins already examined, i.e. claudin-5 and occludin, are specifically unaffected during infiltration of inflammatory mononuclear cells into the CNS. Additionally, the localisation and expression of these proteins during CREAE in ABH mice have not previously been investigated. This would also enable more detailed investigation to how these proteins change over time, as EAE progresses, and would aid in determining

whether TJ disruption, if it occurs, happens during the primary inflammatory attack, or whether it occurs following secondary damage. Looking at staining for ZO-1, a TJ accessory protein might provide additional information on mechanisms of TJ disruption, as ZO-1 is a ligand for MMP-9 (Harkness *et al.,* 2000).

Further characterisation of the findings with PSD-95 is necessary to confirm the axonal localisation. Double staining of PSD-95 with SMI-32 or myelin would allow identification of which subset of axons in the perivascular cuff region are stained. PSD-95 might only be upregulated on demyelinated, damaged axons. Additionally, Western blotting and densitometry analysis would enable a semi-quantitative analysis of the levels of PSD-95 and how they change over the course of EAE disease progression. Glutamate antagonists acting at the NMDA receptors have been shown to be beneficial in EAE, however are associated with severe side effects in the clinic (Paul and Bolton, 2002). Thus new and different ways to disrupt NMDA receptor mediated neurotoxicity without interfering with normal receptor functioning are being sought. An interesting experiment would be to disrupt the PSD-95-NMDA receptor link by injection with a specific peptide to see how this would affect onset and development of EAE disease. This strategy has been shown to be protective in a model of ischaemia (Aarts *et al.,* 2002), and could be beneficial in treating neuroinflammatory conditions.

9. References

Aarts M, Liu Y, Liu L, Besshoh S, Arundine M, Gurd JW, Wang YT, Salter MW, Tymianski M (2002) Treatment of ischemic brain damage by perturbing NMDA receptor- PSD-95 protein interactions. Science 298: 846-850.

Aarts MM, Tymianski M (2003) Novel treatment of excitotoxicity: targeted disruption of intracellular signalling from glutamate receptors. Biochem Pharmacol 66: 877-886.

Abdul-Majid KB, Wefer J, Stadelmann C, Stefferl A, Lassmann H, Olsson T, Harris RA (2003) Comparing the pathogenesis of experimental autoimmune encephalomyelitis in CD4-/- and CD8-/- DBA/1 mice defines qualitative roles of different T cell subsets. J Neuroimmunol 141: 10-19.

Abe Y, Nakamura H, Yoshino O, Oya T, Kimura T (2003) Decreased neural damage after spinal cord injury in tPA-deficient mice. J Neurotrauma 20: 43-57.

Achiron A, Miron S, Lavie V, Margalit R, Biegon A (2000) Dexanabinol (HU-211) effect on experimental autoimmune encephalomyelitis: implications for the treatment of acute relapses of multiple sclerosis. J Neuroimmunol 102: 26-31.

Adams C (1989) A Colour Atlas of Multiple Sclerosis & other myelin disorders. Wolfe Medical Publications Ltd.

Adams RA, Passino M, Sachs BD, Nuriel T, Akassoglou K (2004) Fibrin mechanisms and functions in nervous system pathology. Mol Interv 4: 163-176.

Ahmed Z, Baker D, Cuzner ML (2003) Interleukin-12 induces mild experimental allergic encephalomyelitis following local nervous system injury in the Lewis rat. J Neuroimmunol 140: 109-117.

Ahmed Z, Gveric D, Pryce G, Baker D, Leonard JP, Diemel LT, Cuzner ML (2001) Myelin/axonal pathology in interleukin-12 induced serial relapses of experimental allergic encephalomyelitis in the Lewis rat. Am J Pathol 158: 2127-2138.

Akassoglou K, Adams RA, Bauer J, Mercado P, Tseveleki V, Lassmann H, Probert L, Strickland S (2004) Fibrin depletion decreases inflammation and delays the onset of demyelination in a tumour necrosis factor transgenic mouse model for multiple sclerosis. Proc Natl Acad Sci USA 101: 6698-6703.

Akassoglou K, Kombrinck KW, Degen JL, Strickland S (2000) Tissue plasminogen activator-mediated fibrinolysis protects against axonal degeneration and demyelination after sciatic nerve injury. J Cell Biol 149: 1157-1166.

Akassoglou K, Strickland S (2002) Nervous system pathology: the fibrin perspective. Biol Chem 383: 37-45.

Akassoglou K, Wei-Ming Y, Akpinar P, Strickland S (2002) Fibrin inhibits peripheral nerve remyelination by regulating schwann cell differentiation. Neuron 33: 861-875.

Akenami FO, Koskiniemi M, Farkkila M, Vaheri A (1997) Cerebrospinal fluid plasminogen activator inhibitor-1 in patients with neurological disease. J Clin Pathol 50: 157-160.

Akenami FO, Siren V, Koskiniemi M, Siimes MA, Teravainen H, Vaheri A (1996) Cerebrospinal fluid activity of tissue plasminogen activator in patients with neurological dieseases. J Clin Pathol 49: 577-580.

Akenami FO, Siren V, Wessman M, Koskiniemi M, Vaheri A (1999) Tissue plasminogen activator gene expression in multiple sclerosis brain tissue. J Neurol Sci 165: 71-76.

Al-Chalabi A, Miller CJ (2003) Neurofilaments and neurological disease. BioEssays 24: 346-355.

Allen SJ, Baker D, O'Neill JK, Davison AN, Turk JL (1993) Isolation and characterization of cells infiltrating the spinal cord during the course of chronic relapsing experimental allergic encephalomyelitis in the Biozzi AB/H mouse. Cell Immunol 146: 335-350.

Aloisi F (2001) Immune functions of microglia. Glia 36: 165-179.

Amor S, Baker D, Groome N, Turk JL (1993) Identification of a major encephalitogenic epitope of proteolipid protein (residues 56 - 70) for the induction of experimental allergic encephalomyelitis in biozzi AB/H and nonobese diabetic mice. J Immunol 150: 5666-5672.

Amor S, Groom N, Linington C, Morris MM, Dornmair K, Gardinier MV, Matthieu JM, Baker D (1994) Identification of epitopes of myelin oligodendrocyte glycoprotein for the induction of experimental allergic encephalomyelitis in SJL and Biozzi AB/H mice. J Immunol 153: 4349-4356.

Andersson M, Alvarez-Cermeno J, Bernardi G, Cogato I, Fredman P, Frederiksen J, Gallo P, Grimaldi LM, Gronning M, et al (1994) Cerebrospinal fluid in the diagnosis of multiple sclerosis: a concensus report. J Neurol Neurosurg Psychiatry 57: 897-902.

Arnason BG, Toscas A, Dayal A, Qu Z, Noronha A (1997) Role of interferons in demyelinating disease. J Neural Transm Suppl 49: 117-123.

Bajramovic JJ, Lassmann H, van Noort JM (1997) Expression of αB-crstallin in glial cells during lesional development in multiple sclerosis. J Neuroimmunol 78: 143.

Baker D, O'Neill JK, Gschmeissner SE, Wilcox CE, Butter C, Turk JL (1990) Induction of chronic relapsing experimental allergic encephalomyelitis in Biozzi mice. J Neuroimmunol 28: 261-270.

Balabanov R, Lisak D, Beaumont T, Lisak RP, Dore-Duffy P (2001) Expression of urokinase plasminogen activator receptor on monocytes from patients with relapsing-remitting multiple sclerosis: Effect of glatiramer acetate (copolymer 1). Clin Diag Lab Immunol 8: 1196-1203.

Bar-Or A, Nuttall RK, Duddy M, Alter A, Kim HJ, Ifergan I, Pennington CJ, Bourgoin P, Edwards DR, Yong VW (2003) Analyses of all matrix metalloproteinase members in leukocytes emphasize monocytes as major inflammatory mediators in multiple sclerosis. Brain 126: 2738-2749.

Barnett MH, Prineas JW (2004) Relapsing and remitting multiple sclerosis: pathology of the newly forming lesion. Ann Neurol 55: 458-468.

Bebo BF, Schuster JC, Vandenbark AA, Offner H (1998) Gender differences in experimental autoimmune encephalomyelitis develop during the induction of the immune response to encephalitogenic peptides. J Neurosci Res 52: 420-426.

Bechtold DA, Kapoor R, Smith KJ (2004) Axonal protection using flecainide in experimental autoimmune encephalomyelitis. Ann Neurol 55: 607-616.

Beique JC, Andrade R (2003) PSD-95 regulates synaptic transmission and plasticity in rat cerebral cortex. J Physiol 546: 859-867.

Benowitz LI, Routtenberg A (1997) GAP-43: an intrinsic determinant of neuronal development and plasticity. Trends Neurosci 20: 84-91.

Bernard CC, Carnegie PR (1975) Experimental allergic encephalomyelitis in mice: immunologic response to mouse spinal cord and myelin basic proteins. J Immunol 114: 1537-1540.

Bernard CC, Johns TG, Slavin AJ, Ichikawa M, Ewing C, Liu J, Bettadapura J (1997) Myelin oligodendrocyte glycoprotein: a novel candidate autoantigen in multiple sclerosis. J Mol Med 75: 77-88.

Beschorner R, Schluesener HJ, Nguyen TD, Magdolen V, Luther T, Pedel I, Mattern R, Meyermann R, Schwab JM (2000) Lesion-associated accumulation of uPAR/CD87-expressing infiltrating granulocytes, activated microglial cells/macrophages and upregulation by endothelial cells following TBI and FCI in humans. Neuropathol Appl Neurobiol 26: 522-527.

Bianchi E, Bender JR, Blasi F, Pardi R (1997) Through and beyond the wall: late steps in leukocyte transendothelial migration. Immunol Today 18: 586-591.

Binder BR, Christ G, Gruber F, Grubic N, Hufnagl P, Krebs M, Mihaly J, Prager GW (2002) Plasminogen activator inhibitor-1: physiological and pathophysiological roles. News Physiol Sci 17: 56-61.

Bitsch A, Schuchardt J, Bunkowski S, Kuhlmann T, Brück W (2000) Acute axonal injury in multiple sclerosis. Correlation with demyelination and inflammation. Brain 123: 1174-1183.

Bjartmar C, Trapp BD (2001) Axonal and neuronal degeneration in multiple sclerosis: mechanisms and functional consequences. Curr Opin Neurol 14: 271-278.

Bjartmar C, Wujek JR, Trapp BD (2003) Axonal loss in the pathology of MS: consequences for understanding the progressive phase of the disease. J Neurol Sci 206: 165-171.

Blakemore WF (1973) Demyelination of the superior cerebellar peduncle in the mouse induced by cuprizone. J Neurol Sci 20: 63-72.

Blakemore WF (1978) Observations on remyelination in the rabbit spinal cord following demyelination induced by lysolecithin. Neuropathol Appl Neurobiol 4: 47-59.

Blakemore WF (1982) Ethidium bromide induced demyelination in the spinal cord of the cat. Neuropathol Appl Neurobiol 8: 365-375.

Blasi F (1997) uPA, uPAR, PAI-1: key intersection of proteolytic, adhesive and chemotactic highways. Immunol Today 18: 415-417.

Blasi F, Carmeliet P. (2002) uPAR: a versatile signalling orchestrator. Nat Rev Mol Cell Biol 3: 932-943.

Bo L, Mork S, Kong PA, Nyland H, Pardo CA, Trapp BD (1994) Detection of MHC class II-antigens on macrophages and microglia, but not on astrocytes and endothelia in active multiple sclerosis lesions. J Neuroimmunol 51: 135-146.

Bolanos JP, Heales SJ, Land JM, Clark JB (1995) Effect of peroxynitrite on the mitochondrial respiratory chain: differential susceptibility of neurones and astrocytes in primary culture. J Neurochem **64**: 1965-1972.

Bolton C, Paul C (1997) MK-801 limits neurovascular dysfunction during experimental allergic encephalomyelitis. J Pharmacol Exp Ther 282: 397-402.

Bolton SJ, Anthony DC, Perry VH (1998) Loss of the tight junction proteins occludin and zonula occludens-1 from cerebral endothelium during neutrophil-induced bllod-brain barrier breakdown in vivo. Neuroscience 86: 1245-1257.

Brosnan CF, Bornstein MB, Bloom BR (1981) The effects of macrophage depletion on the clinical and pathologic expression of experimental allergic encephalomyleitis. J Immunol 126: 614-620.

Brown KA (2001) Factors modifying the migration of lymphocytes across the blood-brain barrier. Int Immunopharmacol 1: 2062.

Brundula V, Rewcastle NB, Metz LM, Bernard CC, Yong VW (2002) Targeting leukocyte MMPs and transmigration: minocycline as a potential therapy for multiple sclerosis. Brain 125: 1297-1308.

Bu G, Warshawsky I, Schwartz AL (1994) Cellular receptors for the plasminogen activators. Blood 83: 3427-3436.

Busso N, Péclat V, Van Ness K, Kolodziesczyk E, Degen J, Bugge TH, So A (1998) Exacerbation of antigen-induced arthritis in urokinase-deficient mice. J Clin Invest 102: 41-50.

Butter C, Baker D, O'Neill JK, Turk JL (1991) Mononuclear cell trafficking and plasma protein extravasation into the CNS during chronic relapsing experimental allergic encephalomyelitis in Biozzi AB/H mice. J Neurol Sci 104: 9-12.

Cammer W, Bloom BR, Norton WT, Gordon S (1978) Degradation of basic protein in myelin by neutral proteases secreted by stimulated macrophages: a possible mechanism of inflammatory demyelination. Proc Natl Acad Sci USA 75: 1554-1558.

Cannella B, Raine CS (1995) The adhesion molecule and cytokine profile of multiple sclerosis lesions. Ann Neurol 37: 424-435.

Carmeliet P., Bouché A, De Clercq C, Janssen S, Pollefeyt S, Wyns S, Mulligan RC, Collen D (1995) Biological effects of disruption of the tissue-type plasminogen activator, urokinase-type plasminogen activator, and plasminogen activator inhibitor-1 genes in mice. Ann N Y Acad Sci 17: 367-381.

Carmeliet P., Kieckens L, Schoonjans L, Ream B, Van Nuffelen A, Prendergast G, Cole M, Bronson R, Collen D, Mulligan RC (1993) Plasminogen activator inhibitor-1 gene-deficient mice. I. Generation by homologous recombination and characterisation. J Clin Invest 92: 2746-2755.

Carmeliet P., Moons L., Lijnen H.R., Baes M, Lemaitre V, Tipping P, Drew A, Eeckhout Y, Shapiro S, Lupu F, Collen D (1997) Urokinase-generated plasmin activates matrix metalloproteinases during aneurysm formation. Nat Genet 17: 439-444.

Carmeliet P., Schoonjans L, Kieckens L, Ream B, Degen J, Bronson R, De Vos R, van den Oord JJ, Collen D, Mulligan RC (1994) Physiological consequences of loss of plasminogen activator gene function in mice. Nature 368: 419-424.

Carson MJ (2002) Microglia as liaisons between immune and central nervous systems: Functional implications in multiple sclerosis. Glia 40: 218-231.

Castellino FJ, Ploplis VA (2005) Structure and function of the plasminogen/plasmin system. Thromb Haemost 93: 647-654.

Chapman HA (1997) Plasminogen activators, integrins, and the coordinated regulation of cell adhesion and migration. Curr Opin Cell Biol 9: 714-724.

Chavarria A, Alcocer-Varela J (2004) Is damage in central nervous system due to inflammation? Autoimmunity Rev 3: 251-260.

Chen Z, Strickland S (1997) Neuronal death in the hippocampus is promoted by plasmin catalysed degradation of laminin. Cell 91: 917-925.

Chen ZL, Indyk JA, Strickland S (2003) The hippocampal laminin matrix is dynamic and critical for neuronal survival. Mol Biol Cell 14: 2665-2676.

Choong PFM, Nadesapillai APW (2003) Urokinase plasminogen activator system. A multifunctional role in tumour progression and metastasis. Clin Orthop 415: S46-S58.

Cinelli P, Madani R, Tsuzuki N, Vallet P, Arras M, Zhao CN, Osterwalder T, Rülicke T, Sonderegger P (2001) Neuroserpin, a neuroprotective factor in focal ischaemia. Mol Cell Neurosci 18: 443-457.

Claudio L, Raine CS, Brosnan CF (1995) Evidence of persistent blood-brain barrier abnormalities in chronic progressive multiple sclerosis. Acta Neuropathol 30: 228-238.

Clements JM, Cossins JA, Wells GM, Corkill DJ, Helfrich K, Wood LM, Pigott R, Stabler G, Ward GA, Gearing AJ, Miller KM (1997) Matrix metalloproteinase expression during experimental autoimmune encephalomyelitis and effects of a combined matrix metalloproteinase and tumour necrosis factor-alpha inhibitor. J Neuroimmunol 74: 85-94.

Cobbold SP, Jayasuriya A, Nash A, Prospero TD, Waldmann H (1984) Therapy with monoclonal antibodies by elimination of T-cell subsets *in vivo*. Letters to Nature 312: 548-551.

Coleman MP, Perry VH (2002) Axon Pathology in neurological disease: a neglected therapeutic target. Trends Neurosci 25: 532-537.

Coles AJ, Cox A, Le PE, Jones J, Trip SA, Deans J, Seaman S, Miller DH, Hale G, Waldmann H, Compston DA (2005) The window of therapeutic opportunity in multiple sclerosis Evidence from monoclonal antibody therapy. J Neurol.

Compston A, Coles A (2002) Multiple sclerosis. Lancet 359: 1221-1231.

Compston A, Ebers G, Lassmann H, McDonald I, Matthews B, Wekerle H (1998) McAlpine's Multiple Sclerosis. Churchill Livingstone.

Conlon P, Oksenberg JR, Zhang J, Steinman L (1999) The immunobiology of multiple sclerosis: an autoimmune disease of the central nervous system. Neurobiol disease 6: 149-166.

Cua DJ, Hinton DR, Stohlman SA (1995) Self-antigen-induced Th2 responses in experimental allergic encephalomyelitis (EAE)-resistant mice. Th2-mediated suppression of autoimmune disease. J Immunol 155: 4052-4059.

Cuzner ML, Gveric D, Strand C, Loughlin AJ, Paemen L, Opdenakker G., Newcombe J (1996) The expression of tissue-type plasminogen activator, matrix metalloproteases and endogenous inhibitors in the central nervous system in multiple sclerosis: Comparison of stages in lesion evolution. J Neuropathol Exp Neurol 55: 1194-1204.

Cuzner ML, Norton WT (1996) Biochemistry of demyelination. Brain Pathol 6: 231-242.

Cuzner ML, Opdenakker G (1999) Plasminogen activators and matrix metalloproteases, mediators of extracellular proteolysis in inflammatory demyelination of the central nervous system. J Neuroimmunol 94: 1-14.

Cuzner ML, Woodroofe MN (2002) Inflammatory demyelination and axonopathy in the central nervous system. In: Immune and inflammatory responses in nervous system (Rothwell NJ, Loddick S, eds), pp 127-144. Oxford: Open University Press.

Dal Canto MC, Kim BS, Miller SD, Melvold RW (1996) Theiler's murine encephalomyelitis virus (TMEV) - induced demyelination: a model for human multiple sclerosis. Methods 10: 453-461.

De Vries HE, Blom-Roosemalen MCM, Van Oosten M, De Boer AG, Van Berkel TJC, Breimer DD, Kuiper J (1996) The influence of cytokines on the integrity of the blood-brain barrier in vitro. J Neuroimmunol 64: 37-43.

Declerck PJ, Verstreken M, Collen D (1995) Immunoassay of murine t-PA, u-PA and PAI-1 using monoclonal antibodies raised in gene-inactivated mice. Thromb Haemost 74: 1305-1309.

Dellas C, Loskutoff DJ (2005) Historical analysis of PAI-1 from its discovery to its potential role in cell motility and disease. Thromb Haemost 93: 631-640.

Deng G, Curriden SA, Wang S, Rosenberg S, Loskutoff DJ (1996) Is plasminogen activator inhibitor-1 the molecular switch that governs urokinase receptor-mediated cell adhesion and release? J Cell Biol 134: 1563-1571.

Descamps FJ, Van den Steen PE, Nelissen I, Van Damme J, Opdenakker G. (2003) Remnant epitopes generate autoimmunity: from rheumatoid arthritis and multiple sclerosis to diabetes. Adv Exp Med Biol 535: 69-77.

Dewerchin M, Van Nuffelen A, Wallays G, Bouché A, Moons L, Carmeliet P. (1996) Generation and characterisation of urokinase receptor-deficient mice. J Clin Invest 97: 870-878.

Dhib-Jalbut S (2003) Glatiramer acetate (Copaxone) therapy for multiple sclerosis. Pharm Therap 98: 245-255.

Diemel LT, Copelman CA, Cuzner ML (1998) Macrophages in CNS remyelination: friend or foe? Neurochem Res 23: 341-347.

Dietzmann K, von Bossanyi P, Krause D, Wittig H, Mawrin C, Kirches E (2000) Expression of the plasminogen activator system and the inhibitors PAI-1 and PAI-2 in posttraumatic lesions of the CNS and brain injuries following dramatic circulatory arrests: an immunohistochemical study. Pathol Res Pract 196: 15-21.

Dobrovolsky AB, Titaeva EV (2002) The fibrinolysis system: regulation of activity and physiologic functions of its main components. Biochemistry (Mosc) 67: 99-108.

Dubois B, Masure S, Hurtenbach U, Paemen L, Heremans H, Oord J, Sciot R, Meinhardt T, Hammerling G, Opdenakker G, Arnold B (2002) Resistance of young gelatinase B-deficient mice to experimental autoimmune encephalomyelitis and necrotizing tail lesions. J Clin Invest 104: 1507-1515.

East E, Baker D, Pryce G, Lijnen HR, Cuzner ML, Gveric D (2005) A role for the plasminogen activator system in inflammation and neurodegeneration in the central nervous system during experimental allergic encephalomyelitis. Am J Pathol 167: 545-554.

Eldridge CF, Bunge MB, Bunge RP (1989) Differentiation of axons related Schwann cells *in vitro*: II. Control of myelin formation by basal lamina. J Neurosci 9: 625-638.

Engelhardt B, Ransohoff RM (2005) The ins and outs of T-lymphocyte trafficking to the CNS: anatomical sites and molecular mechanisms. Trends Immunol 26: 485-495.

Estreicher A, Muhlhauser J, Carpentier JL, Orci L, Vassalli JD (1990) The receptor for urokinase type plasminogen activator polarises expression of the protease to the leading edge of migrating monocytes and promotes degradation of enzyme inhibitor complexes. J Cell Biol 111: 783-792.

Etienne-Manneville S, Manneville J-B, Adamson P, Wilbourn B, Greenwood J, Couraud P-O (2000) ICAM-1-coupled cytoskeletal rearrangements and transendothelial lymphocyte migration involve intracellular calcium signalling in brain endothelial cell lines. J Immunol 165: 3375-3383.

Fallis RJ, Raine CS, McFarlin DE (1989) Chronic relapsing experimental allergic encephalomyelitis in SJL mice following the adoptive tranfer of an epitope-specific T cell line. J Neuroimmunol 22: 93-105.

Fauser S, Deininger MH, Kremsner PG, Magdolen V, Luther T, Meyermann R, Schluesener HJ (2000) Lesion associated expression of urokinase-type plasminogen activator receptor (uPAR, CD87) in human cerebral malaria. J Neuroimmunol 111: 234-240.

Fazakerley JK (2004) Semliki forest virus infection of laboratory mice: a model to study the pathogenesis of viral encephalitis. Arch Virol Suppl 179-190.

Ferguson B, Matyszak MK, Esiri MM, Perry VH (1997) Axonal damage in acute multiple sclerosis lesions. Brain 120: 393-399.

Flavin MP, Zhao G, Ho LT (2000) Microglial tissue plasminogen activator (tPA) triggers neuronal apoptosis in vitro. Glia 29: 347-354.

Flick MJ, Du X, Witte DP, Jiroušková M, Soloviev DA, Busuttil SJ, Plow EF, Degen J (2004) Leukocyte engagement of fibrin(ogen) via the integrin receptor αMβ2/Mac-1 is critical for host inflammatory response *in vitro*. J Clin Invest 113: 1596-1606.

Friedmann I, Yoles E, Schwartz M (2001) Thrombin attenuation is neuroprotective in the injured rat optic nerve. J Neurochem 76: 641-649.

Fritz RB, McFarlin DE (1989) Encephalitogenic epitopes of myelin basic protein. Chem Immunol 46: 101-125.

Gabay C, Kushner I (1999) Acute-phase proteins and other systemic responses to inflammation. N Engl J Med 340: 448-454.

Gale CR, Martyn CN (1995) Migrant studies in multiple sclerosis. Prog Neurobiol 47: 448.

GAMES, Transatlantic Multiple Sclerosis Genetics Cooperative (2003) A meta-analysis of whole genome linkage screens in multiple sclerosis. J Neuroimmunol 143: 39-46.

Garcia-Monco JC, Coleman JP, Benach JP (2002) Soluble urokinase receptor (uPAR,CD87) is present in serum and cerebrospinal fluid in patients with neurological diseases. J Neuroimmunol 129: 216-223.

Gijbels K, Masure S, Carton H, Opdenakker G. (1992) Gelatinase in the cerebrospinal of patients with multiple sclerosis and other inflammatory neurological disorders. J Neuroimmunol 41: 29-34.

Gijbels P, Proost P, Masure S, Carton H, Billiau A, Opdenakker G. (1993) Gelatinase B is present in the cerebrospinal fluid during experimental autoimmune encephalomyelitis and cleaves myelin basic protein. J Neurosci Res 36: 432-440.

Gilgun-Sherki Y, Panet H, Holdengreber V, Mosberg-Galili R, Offen D (2003a) Axonal damage is reduced following glatiramer acetate treatment in C57/bl mice with chronic-induced experimental auoimmune encephalomyelitis. Neurosci Res 47: 201-207.

Gilgun-Sherki Y, Panet H, Melamed E, Offen D (2003b) Riluzole supresses experimental autoimmune encephalomyelitis: implications for the treatment of multiple sclerosis. Brain Res 989: 196-204.

Glabinski AR, Tani M, Tuohy VK, Ransohoff RM (1997) Murine experimental autoimmune encephalomyelitis: a model of immune- mediated inflammation and multiple sclerosis. Methods Enzymol 288: 182-190.

Gold LI, Rostagno A, Frangione B, Passalaris T (1992) Localization of the cleavage sites on fibronectin following digestion by urokinase. J Cell Biol 50: 441-452.

Goverman J, Woods A, Larson L, Weiner LP, Hood L, Zaller DM (1993) Transgenic mice that express a myelin basic protein-specific T cell receptor develop spontaneous autoimmunity. Cell 72: 551-560.

Grant P, Pant HC (2000) Neurofilament protein synthesis and phosphorylation. J Neurocytol 29: 843-872.

Groom AJ, Smith T, Turski L (2003) Multiple sclerosis and glutamate. Ann N Y Acad Sci 993: 229-275.

Gualandris A, Jones TE, Strickland S, Tsirka SE (1996) Membrane depolarisation induces calcium-dependent secretion of tissue plasminogen activator. J Neurosci 16: 2220-2225.

Gveric D, Hanemaaijer R, Newcombe J, van Lent NA, Sier CF, Cuzner ML (2001) Plasminogen activators in multiple sclerosis lesions: implications for the inflammatory response and axonal damage. Brain 124: 1978-1988.

Gveric D, Herrera BM, Cuzner ML (2003) Impaired fibrinolysis in multiple sclerosis: a role for tissue plasminogen activator inhibitors. Brain 126: 1590-1598.

Gveric D, Herrera BM, Cuzner ML (2005) tPA receptors and the fibrinolytic response in multiple sclerosis lesions. Am J Pathol 166.

Gyetko MR, Sud S, Kendall T, Fuller JA, Newstead MW, Standiford TJ (2000) Urokinase receptor-deficient mice have impaired neutrophil recruitment in response to pulmonary *Psuedomonas aeruginosa* infection. J Immunol 165: 1513-1519.

Gyetko MR, Sud S, Sonstein J, Polak T, Sud A, Curtis JL (2001) Antigen-driven lymphocyte recruitement to the lung is diminished in the absence of urokinase-type plasminogen activator (uPA) receptor, but is independent of uPA. J Immunol 167: 5539-5542.

Haines JL, Ter-Minassian M, Bazyk A, Gusella JF, Kim DJ, Terwedow H, Pericak-Vance MA, Rimmler JB, Haynes CS, Roses AD, Lee A, Shaner B, Menold M, Seboun E, Fitoussi RP, Gartioux C, Reyes C, Ribierre F, Gyapay G, Weissenbach J, Hauser SL, Goodkin DE, Lincoln R, Usuku K, Oksenberg JR, et al (1996) A complete genomic screen for multiple sclerosis underscores a role for the major histocompatibility comples. The Multiple sclerosis genetics group. Nat Genet 13: 377-378.

Harkness KA, Adamson P, Sussman JD, vies-Jones GA, Greenwood J, Woodroofe MN (2000) Dexamethasone regulation of matrix metalloproteinase expression in CNS vascular endothelium. Brain 123 (Pt 4): 698-709.

Harris KM, Kater SB (1994) Dendritic spines: cellular specializations imparting both stability and flexibility to synaptic function. Annu Rev Neurosci 17: 341-371.

Hasbani MJ, Schlief ML, Fisher DA, Goldberg MP (2001) Dendritic spines lost during glutamate receptor activation reemerge at original sites of synaptic contact. J Neurosci 21: 2393-2403.

Hastings GA, Coleman TA, Haudenschild CC, Stefansson S, Smith EP, Barthlow R, Cherry S, Sandkvist M, Lawrence DA (1997) Neuroserpin, a brain-associated inhibitor of tissue plasminogen activator is localised primarily in neurons. J Biol Chem 272: 33062-33067.

Hemmer B, Archelos JJ, Hartung HP (2002) New concepts in the immunopathogenesis of multiple sclerosis. Nat Rev Neurosci 3: 291-301.

Hertig A, Rondeau E (2004) Plasminogen activator inhibitor type 1: two faces of the same coin. Curr Opin Nephr Hyper 13: 39-44.

Herz J (2003) LRP: a bright beacon at the blood-brain barrier. J Clin Invest 112: 1483-1485.

Hewson AK, Smith T, Leonard JP, Cuzner ML (1995) Suppression of experimental allergic encephalomyelitis in the Lewis rat by the matrix metalloproteinase inhibitor ro31-9790. Inflamm Res 44: 345-349.

Hickey W (2001) Basic principles of immunological surveillance of the normal central nervous system. Glia 36: 118-124.

Hofstetter HH, Shive CL, Forshuber TG (2002) Pertussis toxin modulates the immune response to neuroantigens injected in incomplete Freund's adjuvant: induction of Th1 cells and experimental autoimmune encephalomyleitis in the presence of high frequencies of Th2 cells. J Immunol 169: 117-125.

Huber JD, Egleton RD, Davis TP (2001) Molecular physiology and pathophysiology of tight junctions in the blood-brain barrier. Trends Neurosci 24: 719-725.

Huber K (2001) Plasminogen activator inhibitor type-1 (part one): basic mechanisms, regulation and role for thromboembolic disease. J Thromb Thrombolysis 11: 183-193.

Huitinga I, van Rooijen N, De Groot CJ, Uitdehaag BM, Dijkstra CD (1990) Suppression of experimental allergic encephalomyelitis in Lewis rats after elimination of macrophages. J Exp Med 172: 1025-1033.

Huseby ES, Liggitt D, Brabb T, Schnabel B, Ohlen C, Goverman J (2001) A pathological role for myelin-specific CD8 + T cells in a model of multiple sclerosis. J Exp Med 194: 669-676.

Hynd MR, Scott HL, Dodd PR (2004) Glutamate-mediated excitotoxicity and neurodegeneration in Alzheimer's disease. Neurochem Int 45: 583-595.

Imitola J, Chitnis T, Khoury SJ (2005) Cytokines in multiple sclerosis: from bench to bedside. Pharmacol Ther 106: 163-177.

Indyk JA, Chen ZL, Tsirka SE, Strickland S (2003) Laminin chain expression suggests that laminin-10 is a major isoform in the mouse hippocampus and is degraded by the tissue plasminogen activator/plasmin protease cascade during excitotoxic injury. Neuroscience 116: 359-371.

Inoue A, Koh CS, Shimada K, Yanagisawa N, Yoshimura K (1996) Suppression of cell-transferred experimental autoimmune encephalomyelitis in defibrinated Lewis rats. J Neuroimmunol 71: 131-137.

Inoue A, Koh CS, Yamazaki M, Yanagisawa N, Ishihara Y, Kim BS (1997) Fibrin deposition in the central nervous system correlates with the degree of Theiler's murine encephalomyelitis virus-induced demyelinating disease. J Neuroimmunol 77: 185-194.

Irigoyen JP, Muñoz-Cánoves P, Montero L, Koziczak M, Nagamine Y (1999) The plasminogen activator system: biology and regulation. Cell Mol Life Sci 56: 104-132.

Jackson SJ, Pryce G, Diemel LT, Cuzner ML, Baker D (2005) Cannabinoid-receptor 1 null mice are susceptible to neurofilament damage and caspase 3 activation. Neuroscience 134: 261-268.

Janeway CA, Travers P, Walpot M, Sholmchik M (2001) Immunobiology. New York: Garland Publishing.

Johnson GV, Jope RS (1992) The role of microtubule-associated protein 2 (MAP-2) in neuronal growth, plasticity, and degeneration. J Neurosci Res 33: 505-512.

Jones JCR, Dehart GW, Gonzales M, Goldfinger LE (2003) Laminins: an overview. Microsc Res Tech 51: 211-213.

Jugloff DG, Khanna R, Schlichter LC, Jones OT (2000) Internalization of the Kv1.4 potassium channel is suppressed by clustering interactions with PSD-95. J Biol Chem 275: 1357-1364.

Kamath S, Lip GY (2003) Fibrinogen: biochemistry, epidemiology and determinants. QJM 96: 711-729.

Kapoor R, Davies M, Blaker PA, Hall SM, Smith KJ (2003) Blockers of sodium and calcium entry protect axons from nitric oxide-mediated degeneration. Ann Neurol 53: 174-180.

Kasza A, Kowanetz M, Poslednik K, Witek B, Kordula T, Koj A (2001) Epidermal growth factor and pro-inflammatory cytokines regulate the expression of components of the plasminogen activator system in U373-MG astrocytoma cells. Cytokine 16: 187-190.

Kellar-Wood HF, Wood NW, Holmans P, Clayton D, Robertson N, Compstom DA (1995) Multiple sclerosis and the HLA-D region: linkage and association studies. J Neuroimmunol 58: 183-190.

Kermode AG, Thompson AJ, Tofts P, MacManus DG, Kendall BE, Kingsley DP, Moseley IF, Rudge P, McDonald WI (1990) Breakdown of the blood-brain barrier precedes symptoms and other MRI signs of new lesions in multiple sclerosis. Pathogenic and clinical implications. Brain 113: 1477-1489.

Kerschensteiner M, Bareyre FM, Buddebuerg BS, Merkler D, Stadelmann C, Brück W, Misgeld T, Schwab ME (2004) Remodelling of axonal connections contributes to recovery in an animal model of multiple sclerosis. J Exp Med 200: 1027-1038.

Killestein J, Kalkers NF, Polman CH (2005) Glutamate inhibition in MS: the neuroprotective properties of riluzole. J Neurol Sci 233: 113-115.

Kim E, Sheng M (2004) PDZ domain proteins of synapses. Nat Rev Neurosci 5: 771-781.

Kirk J, Plumb J, Mirakhur M, McQuaid S (2003) Tight junctional abnormality in multiple sclerosis white matter affects all calibres of vessel and is associated with blood-brain barrier leakage and active demyelination. J Pathol 201: 319-327.

Koenig W (2003) Fibrin(ogen) in cardiovascular disease: an update. Thromb Haemost 89: 601-609.

Koenig W, Rothenbacher D, Hoffmeister A, Griesshamer M, Brenner H (2001) Plasma fibrin D-dimer levels and risk of stable coronary artery disease: results of a large case-control study. Arterioscler Thromb Vasc Biol 21: 1701-1705.

Koh CS, Gausas J, Paterson PY (1993) Neurovascular permeability and fibrin deposition in the central neuraxis of Lewis rats with cell-transferred experimental allergic encephalomyelitis in relationship to clinical and histopathological features of the disease. J Neuroimmunol 47: 141-145.

Kopeikina LT, Kamper EF, Koutsoukos V, Bassiakos Y, Stavridis I (1997) Imbalance of tissue-type plasminogen activator (t-PA) and its specific inhibitor (PAI-1) in patients with rheumatoid arthritis associated with disease activity. Clin Rheumatol 16: 254-260.

Kornek B, Storch MK, Weissert R, Wallstroem E, Stefferl A, Olsson T, Linington C, Schmidbauer M, Lassmann H (2000) Multiple sclerosis and chronic autoimmune encephalomyelitis: a comparative quantitative study of axonal injury in active, inactive, and remyelinated lesions. Am J Pathol 157: 267-276.

Kreutzberg GW (1996) Microglia: a sensor for pathological events in the CNS. Trends Neurosci 19: 312-318.

Kwon EE, Prineas JW (1994) Blood-brain barrier abnormalities in longstanding multiple sclerosis lesions. An immunohistochemical study. J Neuropathol Exp Neurol 53: 625-636.

Lafaille JJ, Van de Keere F, Hsu AL, Baron JL, Haas W, Raine CS, Tonegawa S (1997) Myelin basic protein-specific T helper 2 (Th2) cells cause experimental autoimmune encephalomyelitis in immunodeficient hosts rather than protect them from the disease. J Exp Med 186: 307-312.

Languino LR, Duperray A, Joganic KJ, Fornaro M, Thornton GB, Altieri DC (1995) Regulation of leukocyte-endothelium interaction and leukocyte transendothelial migration by intracellular adhesion molecule 1-fibrinogen recognition. Proc Natl Acad Sci USA 92: 1505-1509.

Lassmann H (1998) Neuropathology in multiple sclerosis: new concepts. Mult Scler 4: 93-98.

Ledeen RW, Chakraborty G (1998) Cytokines, signal transduction, and inflammatory demyelination: Review and hypothesis. Neurochem Res 23: 277-289.

Lee JM, Schneider HA (1962) Critical relationship between constituents of the antigen-adjuvant emulsion affecting experimental allergic encephalomyelitis in a completely susceptible mouse genotype. J Exp Med 115: 157-168.

Lee SJ, Benveniste EN (1999) Adhesion molecule expression and regulation on cells of the central nervous system. J Neuroimmunol 98: 77-88.

Lehmann PV, Forsthuber T, Miller A, Sercarz EE (1992) Spreading of T-cell autoimmunity to cryptic determinants of an autoantigen. Nature 358: 155-157.

Lehrich JR, Arnason BG, Hochberg FH (1976) Demyelinative myelopathy in mice induced by the DA virus. J Neurol Sci 29: 149-160.

Leppert D, Ford J, Stabler G, Grygar C, Lienert C, Huber S, Miller KM, Hauser SL, Kappos L (2003) Matrix metalloproteinase-9 (gelatinase B) is selectively elevated in CSF during relapses aand stable phases of multiple sclerosis. Brain 121: 2327-2334.

Leppert D, Waubant E, Galardy R, Bunnet NW, Hauser SL (1992) T cell gelatinases mediate basement membrane transmigration in vitro. J Immunol 154: 4379-4389.

Levine S, Sowinski R (1973) Experimental allergic encephalomyelitis in inbred and outbred mice. J Immunol 110: 139-143.

Li H, Cuzner ML, Newcombe J (1996) Microglia-derived macrophages in early multiple sclerosis plaques. Neuropathol Appl Neurobiol 22: 207-215.

Li H, Newcombe J, Groome NP, Cuzner ML (1993) Characterization and distribution of phagocytic macrophages in multiple sclerosis plaques. Neuropathol Appl Neurobiol 19: 214-223.

Lijnen H.R. (2002) Matrix metalloproteinases and cellular fibrinolytic activity. Biochemistry (Mosc) 67: 92-98.

Lijnen HR, Hoef BV, Lupu F, Moons L, Carmeliet P, Collen D (1998) Function of the Plasminogen/Plasmin and Matrix Metalloproteinase Systems After Vascular Injury in Mice With Targeted Inactivation of Fibrinolytic System Genes. Arterioscler Thromb Vasc Biol 18: 1035-1045.

Lindberg RL, De Groot CJ, Montagne L, Freitag P, Van der Valk P, Kappos L, Leppert D (2001) The expression profile of matrix metalloproteinases (MMPs) and their inhibitors (TIMPs) in lesions and normal appearing white matter of multiple sclerosis. Brain 124: 1743-1753.

Lipton HL, Dal Canto MC (1979) Susceptibility of inbred mice to chronic central nervous system infection by Theiler's murine encephalomyelitis. Infect Immun 26: 369-374.

Liu Z, Li N, Diaz LA, Shipley M, Senior RM, Werb Z (2005) Synergy between a plasminogen cascade and MMP-9 in autoimmune disease. J Clin Invest 115: 879-887.

Lo EH, Wang X, Cuzner ML (2002) Extracellular proteolysis in brain injury and inflammation: role for plasminogen activators and matrix metalloproteinases. J Neurosci Res 69: 1-9.

Longstaff C, Merton RE, Fabregas P, Felez J (1999) Characterization of cell-associated plasminogen activation catalyzed by urokine-type plasminogen activator, but independent of urokinase receptor (uPAR, CD87). Hem Thromb Vasc Biol 93: 3839-3846.

Lorentzen JC, Issazadeh S, Storch M, Mustafa MI, Lassman H, Linington C, Klareskog L, Olsson T (1995) Protracted, relapsing and demyelinating experimental autoimmune encephalomyelitis in DA rats immunized with syngeneic spinal cord and incomplete Freund's adjuvant. J Neuroimmunol 63: 193-205.

Loskutoff DJ, Curriden SA, Hu G, Deng G (1999) Regulation of cell adhesion by PAI-1. APMIS 107: 54-61.

Lowry OH, Rosenbrough NJ, Farr AL, Randall RJ (1951) Protein measurement with the Folin phenol reagent. J Biol Chem 193: 265-275.

Lu W, Bhasin M, Tsirka SE (2002) Involvement of tissue plasminogen activator in onset and effector phases of experimental allergic encephalomyelitis. J Neurosci 22: 10781-10789.

Lu X, Rong Y, Baudry M (2000) Calpain-mediated degradation of PSD-95 in developing and adult rat brain. Neurosci Lett 286: 149-153.

Lucchinetti C, Brück W, Parisi J, Scheithauer B, Rodriguez M, Lassmann H (2000) Heterogeneity of multiple sclerosis lesion: implications for the pathogenesis of demyelination. Ann Neurol 47: 707-717.

Ma M, Wei P, Wei T, Ransohoff RM, Jakeman LB (2004) Enhanced axonal growth into a spinal cord contusion injury site in a strain of mouse (129X1/SvJ) with a diminished inflammatory response. J Comp Neurol 474: 469-486.

Martino G, Adorini L, Rieckmann P, Hillert J, Kallmann B, Comi G, Filippi M (2002) Inflammation in multiple sclerosis: the good, the bad, and the complex. Lancet Neurol 1: 499-509.

Masliah E, Alford M, DeTeresa R, Mallory M, Hansen L (1996) Deficient glutamate transport is associated with neurodegeneration in Alzheimer's disease. Ann Neurol 40: 759-766.

Masliah E, Mallory M, Alford M, DeTeresa R, Hansen LA, McKeel DW, Jr., Morris JC (2001) Altered expression of synaptic proteins occurs early during progression of Alzheimer's disease. Neurology 56: 127-129.

Matesic DF, Lin RCS (1994) Microtubule-associated protein as an early indicator of ischemia-induced neurodegeneration in the gerbil forebrain. J Neurochem 63: 1012-1020.

Matsumoto Y, Ohmori K, Fujiwara M (1992) Immune regulation by brain cells in the central nervous system: microglia but not astrocytes present myelin basic protein to encephalitogenic T cells under in vivo-mimicking conditions. Immunology 76: 209-216.

Matute C, Alberdi E, Domercq M, Perez-Cerda F, Perez-Samartin A, Sanchez-Gomez MV (2001) The link between excitotoxic oligodendroglial death and demyelinating diseases. Trends Neurosci 24: 224-230.

May AE, Kanse SM, Lund LR, Gisler RH, Imhof BA, Preissner KT (1998) Urokinase receptor (CD87) regulates leukocyte recruitment via β2 integrins in vivo. J Exp Med 188: 1029-1037.

McCarthy KM, Skare IB, Stankewich MC, Furuse M, Tsukita S, Rogers RA, Lynch RD, Schneeberger EE (1996) Occludin is a functional component of the tight junction. J Cell Sci 109: 2287-2298.

Melchor JP, Pawlak R, Strickland S (2003) The tissue plasminogen activator-plasminogen proteolytic cascade accelerates amyloid-β (Aβ) degradation and inhibits Aβ-induced neurodegeneration. J Neurosci 23: 8867-8871.

Mendel I, Kerlero de Rosbo N, Ben-Nun A (1995) A myelin oligodendrocyte glycoprotein peptide induces typical chronic experimental autoimmune encephalomyelitis in H-2b mice: fine specificty and T cell receptor V beta expression of encephalitogenic T cells. Eur J Immunol 25: 1951-1959.

Migaud M, Charlesworth P, Dempster M, Webster LC, Watabe AM, Makhinson M, He Y, Ramsay MF, Morris RG, Morrison JH, O'Dell TJ, Grant SG (1998) Enhanced long-term potentiation and impaired learning in mice with mutant postsynaptic density-95 protein. Nature 396: 433-439.

Miller CCJ, Ackerley S, Brownless J, Grierson AJ, Jacobsen NJO, Thornhill P (2002) Axonal transport of neurofilaments in normal and disease states. Cell Mol Life Sci 59: 323-330.

Miller DH, Khan OA, Sheremata WA, Blumhardt LD, Rice GP, Libonati MA, Willmer-Hulme AJ, Dalton CM, Miszkiel KA, O'Connor PW (2003) A controlled trial of Natalizumab for relapsing multiple sclerosis. N Engl J Med 348: 15-23.

Mitrovic B, Parkinson J, Merrill JE (1996) An *in vitro* model of oligodendrocyte destruction by nitric oxide and its relevance to multiple sclerosis. Methods 10: 501-513.

Mori T, Wang X, Kline AE, Siao CJ, Dixon CE, Tsirka SE, Lo EH (2001) Reduced cortical injury and edema in tissue plasminogen activator knockout mice after brain trauma. Neuroreport 12: 4117-4120.

Mullay-Eberhard HJ, Miescher PA (1976) Textbook of immunopathology. New York: Grune and Stratton.

Myöhänen H, Vaheri A (2004) Regulation and interactions in the activation of cell-associated plasminogen. Cell Mol Life Sci 61: 2840-2858.

Nashmi R, Fehlings MG (2001) Mechanisms of axonal dysfunction after spinal cord injury: with an emphasis on the role of voltage-gated potassium channels. Brain Res Brain Res Rev 38: 165-191.

Neumann H (2003) Molecular mechanisms of axonal damage in inflammatory central nervous system diseases. Curr Opin Neurol 16: 267-273.

Neumann H, Medana IM, Bauer J, Lassmann H (2002) Cytotoxic T lymphocytes in autoimmune and degenerative CNS diseases. Trends Neurosci 25: 313-319.

Nicole O, Docagne F, Ali C, Margaill I, Carmeliet P, MacKenzie ET, Vivien D, Buisson A (2001) The proteolytic activity of tissue-plasminogen activator enhances NMDA receptor-mediated signaling. Nat Med 7: 59-64.

Nitta T, Hata M, Gotoh S, Seo Y, Sasaki H, Hashimoto N, Furuse M, Tsukita S (2003) Size-selective loosening of the blood-brain barrier in claudin-5-deficient mice. J Cell Biol 161: 653-660.

Nygardas PT, Hinkkanen AE (2002) Up-regulation of MMP-8 and MMP-9 activity in the BALB/c mouse spinal cord correlates with the severity of experimental autoimmune encephalomyelitis. Clin Exp Immunol 128: 245-254.

Nykjaer A, Conese M, Christensen EI, Olsen D, Cremona O, Gliemann J, Blasi F (1997) Recycling of the urokinase receptor upon internalisation of the uPA:serpin complexes. EMBO J 16: 2610-2620.

O'Neill JK, Baker D, Davison AN, Allen SJ, Butter C, Waldmann H, Turk JL (1993) Control of immune-mediated disease of the central nervous system with monoclonal (CD4-specific) antibodies. J Neuroimmunol 45: 1-14.

Okuda Y, Okuda M, Bernard CC (2002) Gender does not influence the susceptibility of C57BL/6 mice to develop chronic experimental autoimmune encephalomyelitis induced by myelin oligodendrocyte glycoprotein. Immunol Lett 81: 25-29.

Oleszak EL, Zaczynska E, Bhattacharjee M, Butunoi C, Legido A, Katsetos CD (1998) Inducible nitric oxide synthase and nitrotyrosine are found in monocytes/macrophages and/or astrocytes in acute, but not in chronic, multiple sclerosis. Clin Diagn Lab Immunol 5: 438-445.

Onuki M, Ayers MM, Bernard CC, Orian JM (2001) Axonal degeneration is an early pathological feature in autoimmune-mediated demyelination in mice. Microsc Res Tech 52: 731-739.

Owens T (2003) The enigma of multiple sclerosis: inflammation and neurodegeneration cause heterogeneous dysfuction and damage. Curr Opin Neurol 16: 267-273.

Papenfuss TL, Rogers CJ, Gienapp I, Yurrita M, McClain M, Damico N, Valo.J., Song F, Whitacre CC (2004) Sex differences in experimental autoimmune encephalomyelitis in multiple murine strains. J Neuroimmunol 150: 59-69.

Paterson PY (1960) Transfer of allergic encephalomyelitis in rats by means of lymph node cells. J Exp Med 111: 119-136.

Paterson PY (1976) Experimental allergic encephalomyelitis: a role of fibrin deposition in immunopathogenesis of inflammation in rats. Fed Proc 35: 2428-2435.

Paul C, Bolton C (2002) Modulation of blood-brain barrier dysfunction and neurological deficits during acute experimental allergic encephalomyelitis by the N-methyl-D-aspartate receptor antagonist memantine. J Pharmacol Exp Ther 302: 50-57.

Pender MP, Rist MJ (2001) Apoptosis of inflammatory cells in immune control of the nervous system: role of glia. Glia 36: 137-144.

Perez RL, Ritzenhaler JD, Roman J (1999) Transcriptional regulation of the interleukin-1β promoter via fibrinogen engagement of the CD18 intergin receptor. Am J Respir Cell Mol Biol 20: 1059-1066.

Petty MA, Lo EH (2002) Junctional complexes of the blood-brain barrier: permeability changes in neuroinflammation. Prog Neurobiol 68: 311-323.

Petzold A (2005) Neurofilament phosphoforms: surrogate markers for axonal injury, degeneration and loss. J Neurol Sci 233: 183-198.

Petzold A, Baker D, Pryce G, Keir G, Thompson EJ, Giovannoni G (2003a) Quantification of neurodegeneration by measurement of brain-specific proteins. J Neuroimmunol 138: 45-48.

Petzold A, Keir G, Green AJE, Giovannoni G, Thompson EJ (2003b) A specific ELISA for measuring neurofilament heavy chain phosphoforms. J Immunol Methods 9369: 1-12.

Pitt D, Werner P, Raine CS (2000) Glutamate excitotoxicity in a model of multiple sclerosis. Nat Med 6: 67-70.

Ploplis VA, Castellino FJ (2002) Gene targeting of components of the fibrinolytic system. Thromb Haemost 87: 22-31.

Plumb J, McQuaid S, Mirakhur M, Kirk J (2000) Abnormal endothelial tight junctions in active lesions and normal-appearing white matter in multiple sclerosis. Brain Pathol 12: 154-169.

Pluskota E, D'Souza SE (2000) Fibrinogen interactions with ICAM-1 (CD54) regulate endothelial cell survival. FEBS 267: 4693-4704.

Pot C, Simonen M, Weinmann O, Schnell L, Christ F, Stoeckle S, Berger P, Rulicke T, Suter U, Schwab ME (2002) Nogo-A expressed in Schwann cells impairs axonal regeneration after peripheral nerve injury. J Cell Biol 159: 29-35.

Pryce G, Ahmed Z, Hankey DJ, Jackson SJ, Croxford JL, Pocock JM, Ledent C, Petzold A, Thompson AJ, Giovannoni G, Cuzner ML, Baker D (2003) Cannabinoids inhibit neurodegeneration in models of multiple sclerosis. Brain 126: 2191-2202.

Pryce G, Male D, Campbell I, Greenwood J (1997) Factors controlling T-cell migration across rat cerebral endothelium in vitro. J Neuroimmunol 75: 84-94.

Pryce G, O'Neill JK, Croxford JL, Amor S, Hankey DJ, East E, Giovannoni G, Baker D (2005) Autoimmune tolerance eliminates relapses but fails to halt progression in a model of multiple sclerosis. J Neuroimmunol 165: 41-52.

Qian Z, Gilbert ME, Colicos MA, Kandel ER, Kuhl D (1993) Tissue-plasminogen activator is induced as an immediate-early gene during seizure, kindling and long-term potentiation. Nature 361: 453-457.

Raine CS, Barnett LB, Brown A, Behar T, McFarlin DE (1980) Neuropathology of experimental allergic encephalomyelitis in inbred strain of mice. Lab Invest 43: 150-157.

Rijneveld AW, Levi M, Florquin S, Speelman P, Carmeliet P., van der Poll T (2002) Urokinase receptor is necessary for adequate host defence against Pneumococcal pneumonia. J Immunol 168: 3507-3511.

Rivers TM, Sprunt DH, Berry GP (1933) Observations on attempts to produce acute disseminated encephalomyelitis in monkeys. J Exp Med 58: 39-53.

Rogove AD, Siao C, Keyt B, Strickland S, Tsirka SE (1999) Activation of microglia reveals a non-proteolytic cytokine function for tissue plasminogen activator in the central nervous system. J Cell Sci 112 (Pt 22): 4007-4016.

Rosenberg GA (2002) Matrix metalloproteinases in neuroinflammation. Glia 39: 279-291.

Saitou M, Furuse M, Sasaki H, Schulzke J-D, Fromm M, Takano H, Noda T, Tsukita S (2002) Complex phenotype of mice lacking occludin, a component of tight junction strands. Mol Biol Cell 11: 4131-4142.

Sappino AP, Madani R, Huarte J, Belin D, Kiss JZ, Wohlwend A, Vassalli JD (1993) Extracellular proteolysis in the adult murine brain. J Clin Invest 92: 679-685.

Schroeter M, Stoll G, Weissert R, Hartung HP, Lassmann H, Jander S (2003) CD8+ phagocyte recruitment in rat experimental autoimmune encephalomyelitits. Am J Pathol 163: 1517-1524.

Sedgewick JD, Riminton DS, Cyster JG, Körner H (2000) Tumor necrosis factor: a master-regulator of leukocyte movement. Immunol Today 21: 110-113.

Seeds NW, Friedman G, Hayden S, Thewke D, Haffke S, McGuire P, Krystosek A (1996) Plasminogen activators and their interaction with the extracellular matrix in neural development, plasticity and regeneration. Seminars in the Neurosciences 8: 405-412.

Sellebjerg F, Sørensen TL (2003) Chemokines and matrix metalloproteinase-9 in leukoctye recruitment to the central nervous system. Brain Res Bull 61: 347-355.

Siao C, Tsirka SE (2002) Tissue plasminogen activator mediates microglial activation via its finger domain through annexin II. J Neurosci 22: 3352-3358.

Siao CJ, Fernandez SR, Tsirka SE (2003) Cell type-specific roles for tissue plasminogen activator released by neurons or microglia after excitotoxic injury. J Neurosci 23: 3234-3242.

Siconolfi LB, Seeds NW (2001a) Induction of the plasminogen activator system accompanies peripheral nerve regeneration after sciatic nerve crush. J Neurosci 21: 4336-4347.

Siconolfi LB, Seeds NW (2001b) Mice lacking tPA, uPA, or plasminogen genes showed delayed functional recovery after sciatic nerve crush. J Neurosci 21: 4348-4355.

Siva A, Kesselring J, Thompson AJ (1999) Frontiers in multiple sclerosis. London: Martin Dunitz Ltd.

Sixt M, Engelhardt B, Pausch F, Hallmann R, Wendler O, Sorokin LM (2003) Endothelial cell laminin isoforms, laminins 8 and 10, play decisive roles in T cell recruitment across the blood-brain barrier in experimental autoimmune encephalomyelitis. J Cell Biol 153: 933-945.

Smiley ST, King JA, Hancock WW (2001) Fibrinogen stimulates macrophage chemokine secretion through toll-like receptor 4. J Immunol 167: 2887-2894.

Smith KJ, Lassmann H (2002) The role of nitric oxide in multiple sclerosis. Lancet Neurol 1: 232-241.

Smith KJ, Kapoor R, Hall SM, Davies M (2001) Electrically active axons degenerate when exposed to nitric oxide. Ann Neurol 49: 470-476.

Smith T, Groom A, Zhu B, Turski L (2000) Autoimmune encephalomyelitis ameliorated by AMPA antagonists. Nat Med 6: 62-66.

Sobel RA, Chen M, Maeda A, Hinojoza JR (1995) Vitronectin and integrin vitronectin receptor localization in multiple sclerosis lesions. J Neuropathol Exp Neurol 54: 202-213.

Soldan SS, varez Retuerto AI, Sicotte NL, Voskuhl RR (2003) Immune modulation in multiple sclerosis patients treated with the pregnancy hormone estriol. J Immunol 171: 6267-6274.

Srinivasan R, Sailasuta N, Hurd R, Nelson S, Pelletier D (2005) Evidence of elevated glutamate in multiple sclerosis using magnetic resonance spectroscopy at 3 T. Brain 128: 1016-1025.

Steinman L (1996) Multiple sclerosis: a coordinated immunological attack against myelin in the central nervous system. Cell 85: 299-302.

Steinman L (2001) Myelin-specific CD8 T cells in the pathogenesis of experimental allergic encephalitis and multiple sclerosis. J Exp Med 194: F27-F30.

Stepaniak JA, Gould KE, Sun D, Swanborg RH (1995) A comparitive study of experimental autoimmune encephalomyelitis in Lewis and Da rats. J Immunol 155: 2762-2769.

Strickland DK, Ranganathan S (2003) Diverse role of LDL receptor-related protein in the clearance of proteases and in signaling. J Thromb Haemost 1: 1663-1670.

Sueishi K, Nanno S, Tanaka K (1981) Permeability enhancing and chemotactic activities of lower molecular weight degradation products of human fibrinogen. Thromb Haemost 45: 90-94.

Sun D, Whitaker JN, Huang Z, Liu D, Coleclough C, Wekerle H, Raine CS (2001) Myelin antigen-specific CD8+ T cells are encephalitogenic and produce severe disease in C57BL/6 mice. J Immunol 166: 7579-7587.

Tabrizi P, Wang L, Seeds NW, McComb G, Yamada S, Griffin JH, Carmeliet P., Weiss MH, Zlokovic BV (1999) Tissue plasminogen activator (tPA) deficiency exacerbates cerebrovascular fibrin deposition and brain injury in a murine stroke model. Arterioscler Thromb Vasc Biol 19: 2801-2806.

Tarui T, Mazar AP, Cines DB, Takada Y (2001) Urokinase-type plasminogen activator receptor (CD87) is a ligand for integrins and mediates cell-cell interaction. J Biol Chem 276: 3983-3990.

Teesalu T, Hinkkanen AE, Vaheri A (2001) Coordinated induction of extracellular proteolysis systems during experimental autoimmune encephalomyelitis in mice. Am J Pathol 159: 2227-2237.

Teesalu T, Kulla A, Asser T, Koskiniemi M, Vaheri A (2002) Tissue plasminogen activator as a key effector in neurobiology and neuropathology. Biochem Soc Trans 30: 183-189.

Tepass U (2003) Claudin complexities at the apical junctional complex. Nat Cell Biol 5: 595-597.

Trapp BD, Peterson J, Ransohoff RM, Rudick R, Mörk S, Bö L (1998) Axonal transection in the lesions of multiple sclerosis. N Engl J Med 338: 278-285.

Traynelis SF, Lipton SA (2001) Is tissue plasminogen activator a threat to neurons? Nat Med 7: 17-18.

Tsirka SE, Bugge TH, Degen JL, Strickland S (1997a) Neuronal death in the central nervous system demonstrates a non-fibrin substrate for plasmin. Proc Natl Acad Sci USA 94: 9779-9781.

Tsirka SE, Gualandris A, Amaral DG, Strickland S (1995) Excitotoxin-induced neuronal degeneration and seizure are mediated by tissue plasminogen activator. Nature 377: 340-344.

Tsirka SE, Rogove AD, Bugge TH, Degen JL, Strickland S (1997b) An extracellular proteolytic cascade promotes neuronal degeneration in the mouse hippocampus. J Neurosci 17: 543-552.

Tucker HM, Kihiko M, Caldwell JN, Wright S, Kawarabayashi T, Price D, Walker D, Scheff S, McGillis JP, Rydel RE, Estus S (2000) The plasmin system is induced by and degrades amyloid-β aggregates. J Neurosci 20: 3937-3946.

Tucker HM, Kihiko-Ehmann M, Estus S (2002) Urokinase-type plasminogen activator inhibits amyloid-beta neurotoxicity and fibrillogenesis via plasminogen. Neurosci Res 70: 249-255.

Tuohy VK, Sobel RA, Lees MB (1988) Myelin proteolipid protein-induced experimental allergic encephalomyelitis. Variations of disease expression in different strains of mice. J Immunol 140: 1868-1873.

Urano T, Takada Y, Ihara H, Takada A (1996) Re-examination of the extent of the activation of Lys(78) plasminogen by tissue plasminogen activator in the presence of polymerised fibrin. Haemostasis 26: 220-227.

Valtorta F, Pennuto M, Bonanomi D, Benfenati F (2004) Synaptophysin: leading actor or walk-on role in synaptic vesicle exocytosis? BioEssays 26: 445-453.

Van Ness K, Chobaz-Péclat V, Castellucci M, So A, Busso N (2002) Plasminogen activator inhibitor type-1 deficiency attenuates murine antigen-induced arthritis. Rheumatology 41: 136-141.

van Noort JM, van Sechel AC, Bajramovic JJ, El Ouagmiri M, Polman CH, Lassmann H, Ravid R (1995) The small heat shock protein αB-crystallin as candidate autoantigen in multiple sclerosis. Nature 375: 798.

van-Horssen J, Bo L, Vos CM, Virtanen I, De Vries HE (2005) Basement membrane proteins in multiple sclerosis-associated inflammatory cuffs: potential role in influx and transport of leukocytes. J Neuropathol Exp Neurol 64: 722-729.

Vanderlugt CL, Miller SD (2002) Epitope spreading in immune-mediated diseases: implications for immunotherapy. Nat Rev Immunol 2: 85-95.

Vartiainen N, Tikka T, Keinanen R, Chan PH, Koistinaho J (1999) Glutamatergic receptors regulate expression, phosphorylation and accumulation of neurofilaments in spinal cord neurons. Neuroscience 93: 1123-1133.

Vincent VAM, Lowik CWGM, Verheijen JH, De Bart ACW, Tilders FJH, Van Dam A (1998) Role of astrocyte-derived tissue-type plasminogen activator in the regulation of endotoxin-stimulated nitric oxide producation by microglial cells. Glia 22: 130-137.

Vivien D, Monréal MF, Nicole O, Buisson A (2003) Tissue plasminogen activator and NMDA receptor cleavage. Nat Med 9: 371-373.

Voskuhl RR, Pitchekian-Halabi H, MacKenzie-Graham A, McFarland HF, Raine CS (1996) Gender differences in autoimmune demyelination in the mouse: implications for multiple sclerosis. Ann Neurol 39: 724-733.

Wakefield AJ, More LJ, Difford J, McLaughlin JE (1994) Immunohistochemical study of vascular injury in acute multiple sclerosis. J Clin Pathol 47: 129-133.

Waldner H, Whitters MJ, Sobel RA, Collins M, Kuchroo VK (2000) Fulminant spontaneous autoimmunity of the central nervous system in mice transgenic for the myelin proteolipid protein-specific T cell receptor. Proc Natl Acad Sci U S A 97: 3412-3417.

Walker DG, Lue LF, Beach TG (2002) Increased expression of the urokinase plasminogen-activator receptor in amyloid β peptide-treated human brain microglia and in AD brains. Brain Res 926: 69-79.

Walters CE, Pryce G, Hankey DJ, Sebti SM, Hamilton AD, Baker D, Greenwood J, Adamson P (2002) Inhibitors of Rho GTPases with protein prenyltransferase inhibitors prevents leukocyte recruitment to the central nervous system and attentuates clinical signs of disease in an animal model of multiple sclerosis. J Immunol 168: 4087-4094.

Waltz DA, Natkin LR, Fujita RM, Wei Y, Chapman HA (1997) Plasmin and plasminogen activator inhibitor type 1 promote cellular motility by regulating the interaction between the urokinase receptor and vitronectin. J Clin Invest 100: 58-67.

Wang L, Ho CL, Sun D, Liem RK, Brown A (2000) Rapid movement of axonal neurofilaments interrupted by prolonged pauses. Nat Cell Biol 2: 137-141.

Wang YF, Tsirka SE, Strickland S, Stieg PE, Soriano SG, Lipton SA (1998) Tissue plasminogen activator (tPA) increases neuronal damage after focal cerebral ischaemia in wild type and tPA-deficient mice. Nat Med 4: 148-150.

Washington RA, Becher B, Balabanov R, Antel J, Dore-Duffy P (1996) Expression of the activation marker urokinase plasminogen activator receptor in cultured human central nervous system microglia. J Neurosci Res 45: 392-399.

Werner P, Pitt D, Raine CS (2000) Glutamate excitotoxicity - a mechanism for axonal damage and oligodendrocyte death in multiple sclerosis. J Neural Transm Suppl 60: 375-385.

Werner P, Pitt D, Raine CS (2001) Multiple sclerosis: altered glutamate homeostasis in lesions correlates with oligodendrocyte and axonal damage. Ann Neurol 50: 169-180.

Willer CJ, Dyment DA, Risch NJ, Sadovnick AD, Ebers GC, Canadian Collaborative Study Group (2003) Twin concordance and sibling recurrence rates in multiple sclerosis. Proc Natl Acad Sci USA 100: 12877-12882.

Wolburg H, Wolburg-Buchholz K, Engelhardt B (2005) Diapedesis of mononuclear cells across cerebral venules during experimental autoimmune encephalomyelitis leaves tight junctions intact. Acta Neuropathol (Berl) 109: 181-190.

Wolburg H, Wolburg-Buchholz K, Kraus J, Rascher-Eggstein G, Liebner S, Hamm S, Duffner F, Grote EH, Risau W, Engelhardt B (2003) Localization of claudin-3 in tight junctions of the blood-brain barrier is selectively lost during experimental autoimmune encephalomyelitis and human glioblastoma multiforme. Acta Neuropathol (Berl) 105: 586-592.

Woodruff RH, Franklin RJ (1999) Demyelination and remyelination of the caudal cerebellar peduncle of adult rats following stereotaxic injections of lysolecithin, ethidium bromide, and complement/anti-galactocerebroside: a comparitive study. Glia 25: 216-228.

Wujek JR, Bjartmar C, Richer E, Ransohoff RM, Yu M, Tuohy VK, Trapp BD (2002) Axon loss in the spinal cord determines permanent neurological disability in an animal model of multiple sclerosis. J Neuropathol Exp Neurol 61: 23-32.

Yepes M, Lawrence DA (2004) Tissue-type plasminogen activator and neuroserpin: a well-balanced act in the nervous system? Trends Cardiovasc Med 14: 173-180.

Yepes M, Sandkvist M, Moore EG, Bugge TH, Strickland S, Lawrence DA (2003) Tissue plasminogen activator induces opening of the blood-brain barrier via the LDL receptor-related protein. J Clin Invest 112: 1533-1540.

Yepes M, Sandkvist M, Wong MKK, Coleman TA, Smith EP, Cohan SL, Lawrence DA (2000) Neuroserpin reduces cerebral infarct volume and protects neurons from ischaemia-induced apoptosis. Blood 96: 569-576.

Young IR, Hall AS, Pallis CA, Legg NJ, Bydder GM, Steiner RE (1981) Nuclear magnetic resonance imaging of the brain in multiple sclerosis. Lancet 2: 1063-1066.

Zameer A, Hoffman SA (2003) Increased ICAM-1 and VCAM-1 expression in the brains of autoimmune mice. J Neuroimmunol 142: 67-74.

Zamvil SS, Steinman L (2003) Diverse targets for intervention during inflammatory and neurodegenerative phases of multiple sclerosis. Neuron 38: 685-688.

Zhang S-C, Fedoroff S (1996) Neuron-microglia interactions in vitro. Acta Neuropathol 91: 385-395.

Zhu B, Luo L, Moore GRW, Paty DW, Cynader MS (2003) Dendritic and synaptic pathology in experimental autoimmune encephalomyelitis. Am J Pathol 162: 1639-1650.